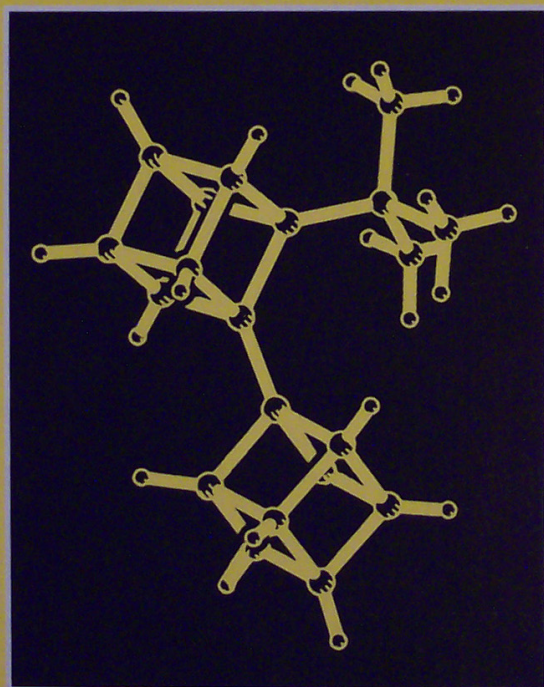


Chemistry of Energetic Materials



Edited by

*George A. Olah
David R. Squire*

RetroSynthetic
RetroSynthetic



Richard S. Miller

Dr. Richard S. Miller is recognized both as a scientist and as a manager in the Office of Naval Research. His contributions to this field well illustrate the role and value of federal support in nurturing innovative science. Dick Miller is a model for the perfect federal science manager: technically brilliant, adroit in assembling novel yet balanced programs, and most of all entirely dedicated to the welfare of the scientists and graduate students whose research fulfills his mission. As a result of Dr. Miller's efforts, the Navy has benefited from tremendous new knowledge of energetic materials.

The articles in this volume provide an overview of the field where Dr. Miller has had such a great influence. The contributions in this critical and rapidly growing area of science have profoundly benefited the advancement of knowledge as well as our national defense. The quality of the contributions herein and the eminence of the investigators clearly testifies that the study of energetic materials is no longer only of great practical significance but has also achieved high standing as an area of fundamental scholarly research.

We dedicate this volume to Dick Miller as a scientist, a faithful provider of federal funding for science, and a brilliant manager of technology for our future Navy.

F. E. Saalfeld
Director Office of
Naval Research

Chemistry of Energetic Materials

Edited by

George A. Olah

*Loker Hydrocarbon Research Institute
Department of Chemistry
University of Southern California
Los Angeles, California*

David R. Squire

*Defense Sciences Office
DARPA
Arlington, Virginia*

This book is printed on acid-free paper. (∞)

No Rights Reserved.

All parts of this publication may be reproduced or transmitted in any form or by any means, electronic or mechanical, including photocopy, recording, or any information storage and retrieval system.

Library of Congress Cataloging-in-Publication Data

Chemistry of energetic materials / [edited by] George A. Olah, David R. Squire

p. cm.

Includes index.

ISBN 0-12-525440-7

1. Combustion. 2. Thermodynamics. 3. Explosives.
4. Propellants. I. Olah, George A. (George Andrew), date
II. Squire, David R.

QD516.C538 1991

541.3'61--dc20

91-12536

CIP

PRINTED IN THE UNITED STATES OF AMERICA

91 92 93 94 9 8 7 6 5 4 3 2 1

Contents

Contributors vii

Preface ix

1. **The Structural Investigation of Energetic Materials** **1**
Richard D. Gilardi and Jerome Karle
 - I. Introduction 1
 - II. Pressure and Impulse 2
 - III. Energetic Materials Database 3
 - IV. Bending Angles in Nitramines 6
 - V. Nitroolefins 11
 - VI. Cubane and Substituents 16
 - VII. Conclusions 22
 - References 23

2. **Studies of Initial Dissociation Processes in 1,3,3-Trinitroazetidine by Photofragmentation Translational Spectroscopy** **27**
Deon S. Anex, John C. Allman, and Yuan T. Lee
 - I. Introduction and Overview 27
 - II. The Thermal Decomposition of TNAZ 33
 - III. Analysis and Discussion 42
 - IV. Summary 53
 - References/Endnotes 54

3. **Studies of Molecular Dissociation by Means of Ultrafast Absorption and Emission Spectroscopy and Picosecond X-Ray Diffraction** **55**
Peter M. Rentzepis and B. Van Wonerghem
 - I. Introduction 55
 - II. Photodissociation of Haloaromatics 56
 - III. Picosecond X-Ray Diffraction 69
 - References 75

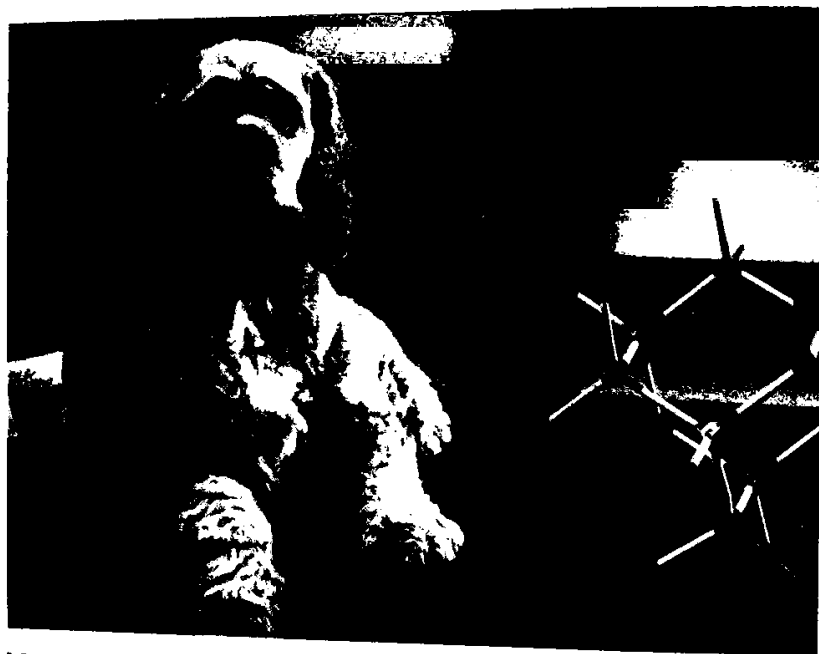
4. **Computer-Aided Design of Monopropellants** **77**
Peter Politzer, Jane S. Murray, M. Edward Grice, and Per Sjoberg
 - I. Introduction 77

II. Theoretical Background	78	
III. Application of Specific Impulse Formula		80
IV. Calculated Specific Impulse Values	81	
V. Perspectives	91	
VI. Summary	92	
References	92	
5. Polycyclic Amine Chemistry		95
<i>Arnold T. Nielsen</i>		
I. Introduction	95	
II. Approaches to Synthesis of Caged Nitramine Explosives		97
III. Polyazaadamantanes	100	
IV. Polyazawurtzitanes	104	
V. Polyazaisowurtzitanes	110	
VI. Summary	119	
References	120	
6. Metallocarboranes of the Lanthanide and Alkaline-Earth Metals: Potential High Energy Fuel Additives		125
<i>Rajesh Khattar, Mark J. Manning, and M. Frederick Hawthorne</i>		
I. Lanthanide Element Metallocarboranes	125	
II. Preparation and Characterization of Bis-Dicarbollide Complexes of Sm and Yb	129	
III. Alkaline-Earth Element Metallocarboranes		131
References	136	
7. Methods for Preparing Energetic Nitro-Compounds: Nitration with Superacid Systems, Nitronium Salts, and Related Complexes		139
<i>George A. Olah</i>		
I. Introduction	139	
II. Protic-Acid-Catalyzed Nitration		140
III. Lewis-Acid-Catalyzed Nitration		152
IV. Nitration with Nitronium Salts		158
V. Transfer Nitration	186	
VI. Demetallative Nitration	191	
References	198	
<i>Index</i>		205

Contributors

Numbers in parentheses indicate the pages on which the authors' contributions begin.

- John C. Allman (27), Materials and Chemical Sciences Division, Lawrence Berkeley Laboratory and Department of Chemistry, University of California, Berkeley, California 94720
- Deon S. Anex (27), Materials and Chemical Sciences Division, Lawrence Berkeley Laboratory and Department of Chemistry, University of California, Berkeley, California 94720
- Richard D. Gilardi (1), Naval Research Laboratory, Washington, D.C. 20375
- M. Edward Grice (77), Department of Chemistry, University of New Orleans, New Orleans, Louisiana 70418
- M. Frederick Hawthorne (125), Department of Chemistry and Biochemistry, University of California, Los Angeles, California 90024
- Jerome Karle (1), Naval Research Laboratory, Washington, D.C. 20375
- Rajesh Khattar (125), Department of Chemistry and Biochemistry, University of California, Los Angeles, California 90024
- Yuan T. Lee (27), Materials and Chemical Sciences Division, Lawrence Berkeley Laboratory and Department of Chemistry, University of California, Berkeley, California 94720
- Mark J. Manning (125), Department of Chemistry and Biochemistry, University of California, Los Angeles, California 90024
- Jane S. Murray (77), Department of Chemistry, University of New Orleans, New Orleans, Louisiana 70418
- Arnold T. Nielsen (95), Chemistry Division, Research Department, Naval Weapons Center, China Lake, California 93555
- George A. Olah (139), Loker Hydrocarbon Research Institute, and Department of Chemistry, University of Southern California, Los Angeles, California 90089
- Peter Politzer (77), Department of Chemistry, University of New Orleans, New Orleans, Louisiana 70418
- Peter M. Rentzepis (55), Department of Chemistry, University of California, Irvine, California 92717
- Per Sjöberg (77), Nobel Chemicals, Division Nobelkrut, S-691 85, Karlskoga, Sweden
- B. Van Wanterghem (55), Department of Chemistry, University of California, Irvine, California 92717



Mookie, the Olahs' cocker spaniel enlightens this otherwise blank page.
(Photo by Mark Sassaman.)

Preface

The field of energetic materials has long been considered primarily for its practical aspects and it is only recently that the modern fundamental science phenomena began to emerge. This has been particularly true in academic science, where fundamental acceptance and progress in the field has only recently developed. Energetic materials, however, have been of great practical importance from the time of the discovery of gunpowder to modern day explosives and rocket fuels. These materials have had a profound, if not always positive, effect on history. However the significance of their peaceful uses, ranging from the use of explosives in mining and road building to applications such as missile propulsion systems, should not be overshadowed by their potential destructive power. The ultimate use of the knowledge gleaned by this research is not a question for debate here.

Research on energetic materials extends from bulk synthesis, to engineering and materials science, to the microscopic study of molecular dynamics and structure (i.e., the molecular level understanding of these systems). In order to understand the combustion of energetic materials, the detailed chemistry of the decomposition processes must be understood. The nature of the individual reaction steps, the dynamics of the dissociation, and the energy released during combustion reactions must be recognized. Thus, the study of energetic materials spans many disciplines. Chemistry, as the science that can lead to such materials, is at the focal point. Indeed, an ever-extending array of new energetic compounds is continually being synthesized. Historically, nitro derivatives played a special role as the most commonly used compounds. Energetic nitro compounds range from C-nitro derivatives such as trinitrotoluene (TNT), to O-nitro compounds such as trinitroglycerol, to N-nitro compounds such as HMX and RDX. Nitrogen oxides continue to be significant oxidants.

Any study of energetic materials must clearly start with the characterization of structure. R. D. Gilardi and J. Karle discuss in the first chapter the structural investigation of energetic materials by the use of single crystal x-ray crystallography. In conjunction with their colleagues at the Naval Research Laboratory, they have over the years advanced these studies in a remarkable way and in the process obtained a unique collation of the structural data of more than 500 energetic compounds of great significance. Their chapter centers on the structural study of the most recent significant classes of compounds. In addition to facilitating an understanding of the relationship of structure to function (such as density), this structural work also plays a valuable role in the development of new and improved materials by facilitating synthesis of promising new types of substances, as well as characterizing those already synthesized. It is even possible now, on occasion, to make

x
reasonable suggestions based on structural aspects for the feasibility of certain contemplated syntheses.

The understanding of the chemical dynamics of initial dissociation processes is also of fundamental importance. Y. T. Lee and his colleagues discuss in Chapter 2 their study by photofragmentation translational spectroscopy of the significant model system 1,3,3-trinitroazetidene, a cyclic nitroalkyl nitramine related to the energetic cyclic nitramines HMX and RDX. Although a significant portion of the combustion of energetic materials is related to condensed phase reactions, the understanding of the chemistry of isolated species is also pertinent. Of particular interest is the understanding of the primary decomposition steps. In photofragmentation translational spectroscopy, the compound studied is expanded from a nozzle into a vacuum and the expansion is collimated to form a molecular beam. The molecular beam is then crossed with the output of a pulsed CO₂ laser, which excites the molecule of interest above the dissociation threshold; this infrared multiphoton excitation induces dissociation of the molecule. This method has also been applied previously to the study of the initial steps in RDX decomposition. Molecular beam studies provide a useful complement to bulk phase decomposition studies. The characterization of the initial steps in the decomposition allows a better understanding of the results of bulk phase studies with regard to secondary reactions and the role of the condensed state. Molecular beam studies also contribute significantly to the theoretical understanding of combustion processes.

P. M. Rentzepis and B. Van Wanterghem discuss in Chapter 3 the kinetics and mechanism of dissociation of molecules by means of ultrafast absorption and emission spectroscopy. The spectra of the intermediate states and species are obtained in real time and the formation and decay of these species measured. The development of picosecond x-ray spectroscopy (PXR), a new field that enables the recording of the evolution of the structure of intermediates during the course of chemical reactions, is also presented. Application of these new pioneering methods to the study of energetic systems will widen our understanding and knowledge of the fundamentals of molecular dissociation processes.

In Chapter 4, P. Politzer and colleagues discuss the computer-aided design of monopropellants. They center their discussion on methods that calculate the specific impulse I , of energetic oxidizers (i.e., monopropellants), a characteristic essential to the design of new efficient high-performance propellants. An energetic molecule develops thrust (or recoil force) due to the discharge of gaseous products when it undergoes combustion. The specific impulse I , is the integral of the thrust, per unit weight of the material, over the time of the combustion. It is widely used as a means of characterizing and evaluating propellants and is viewed as the key measure in their performance evaluation. Theoretical techniques allowing the calculation of specific impulse values of known and potential energetic molecules are thus of obvious great significance.

The remaining three chapters deal with the synthesis of energetic (and potentially energetic) materials. A. T. Nielsen in Chapter 5 gives an account of the

synthesis of some exciting new and potentially useful polycyclic caged amines. After discussing general approaches to the synthesis of caged nitramine explosives, he presents the chemistry which led to the synthesis of three significant new classes of caged polycyclic amines, the polyazaadamantanes, polyazawurtzitanes, and polyazaisowurtzitanes.

R. Khattar and colleagues in Chapter 6 discuss the synthetic and structural chemistry of the metallacarboranes of the lanthanide and alkaline-earth metals. These potentially high-energy fuel additives represent a significant addition to the broad class of metallacarboranes. Their fascinating structural aspects are also of much interest.

G. A. Olah in Chapter 7 reviews some of the most useful methods in preparing nitro compounds (i.e., electrophilic nitrations with superacid systems, nitronium salts, and related Friedel-Crafts type complexes). Polynitro compounds were traditionally and still are the most widely used explosives [e.g., nitroglycerol, trinitrotoluene (TNT), and *N*-nitramines (RDX and HMX)]. Methods of preparing nitro compounds thus remain a key part of the synthesis of energetic materials.

The study of energetic materials is emerging from a field primarily directed toward practical interests to an advanced area of fundamental research, where state-of-the-art methods and theory are used side by side with modern synthetic methods. That two of the contributors to this volume are Nobel laureates and five are members of the National Academy of Sciences speaks well for the maturing nature of the field and the related degree of scientific sophistication. Obviously a volume of this size cannot give a comprehensive review of the entire field of the chemistry of energetic materials. It offers, however, a good perspective of the present day research in both the structural-physicochemical as well as preparative aspects of the field. The contributions herein should give all practitioners of the field, whether in academia, industry, or governmental laboratories, a good overview of some of the frontlines of the field. It is also hoped that the book will stimulate young scientists and engineers to take interest in the field of energetic materials. It is after all the future generation of practitioners who will take over and build on the present effort to advance the chemistry of energetic materials to new levels of understanding and improved applications.

The U.S. Navy has traditionally, through its own research at the renowned Naval Research Laboratory and its sponsorship of outside research administered by the Office of Naval Research, contributed greatly to the development of the field of energetic materials. One of its most devoted and knowledgeable science administrators, Dr. Richard Miller, was to a great extent responsible for fostering this process and this volume is dedicated to him.

George A. Olah
David R. Squire

1

The Structural Investigation of Energetic Materials

Richard D. Gilardi and Jerome Karle

I. Introduction

Structure determination in the context of this chapter means the determination of the atomic arrangements in materials in the crystalline state. There are a number of aspects to structural analyses. They may be used to identify substances since they can be performed without previous knowledge of chemical composition. It is possible to determine from structural analyses the connectedness, conformation, configuration (or absolute configuration under special experimental circumstances), packing, solvent interactions, and average thermal motion associated with the substances of interest. With careful experimentation in properly chosen cases, electron density distributions can also be evaluated.

Applications of this type of information in a variety of scientific disciplines are evident. Some examples of areas of science that can be benefited are synthetic organic chemistry, natural products chemistry, pharmaceutical chemistry, the study of rearrangement reactions, reaction mechanisms, ion transport through biological membranes, and biomolecular engineering. In addition to facilitating an understanding of the relationship of structure to function, structural information plays a valuable role in the development of new and improved materials. It is in this latter context that the work described in this article was mainly carried out. The predominant purpose was to facilitate the synthesis of improved or new types of substances, characterize those already synthesized, and on occasion, make some suggestions concerning the feasibility of certain contemplated syntheses.

One consequence of the extensive research activity in structural analysis has been the development of a computerized X-ray crystal structure

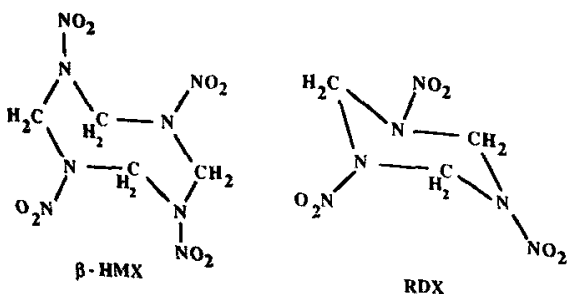
database, known as the Cambridge Structural Database [1], containing parameters from over 82,000 organic chemical structures (as of January 1991). It can be searched by computer to provide information for use in studies of the relation of structure to activity and the design of substances with desired properties (e.g., the design of drugs). The investigation of the structures of a large number of energetic materials has provided information for an extensive database for such substances [2]. It has served as a useful source of information for making predictions concerning the possible success in the synthesis of new materials.

II. Pressure and Impulse

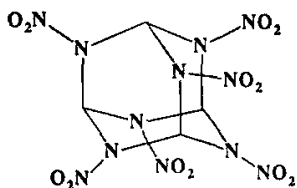
Density plays an important role in the behavior of energetic materials. The pressure in explosions and the impulse produced by the same compound when used as a propellant are related. The shockwave pressure behind the detonation front is proportional to the density squared [3] times the specific impulse [4]. The specific impulse itself depends on the volume of gas produced and the heat of combustion *per gram of propellant* which leads to a further complex dependence on density [5]. Thus, the overall dependency of the detonation pressure on the density is greater than quadratic. Two examples of dense energetic materials are the widely used β -HMX and RDX [6,7], shown in Fig. 1.

In addition to density, strain also offers the opportunity for higher energy release. Any gain, however, from molecular strain would be lost if the packing of the molecules was not dense. An example of a synthetic goal is a highly strained molecule that packs densely and contains a large number of energetic groups.

Fig. 1. Structural diagrams of β -HMX (density = 1.90 g/cc) and RDX (density = 1.81 g/cc), two well-studied dense energetic compounds widely used as explosives and as components of solid rocket fuels.

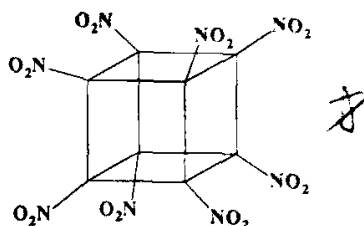


Hexanitrohexa-aza-adamantane



Predicted Density = 2.0-2.2 g/cc

Octanitrocubane



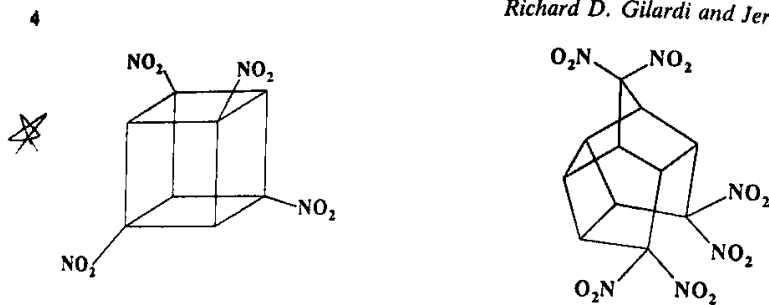
Predicted Density = 2.0-2.1 g/cc

Fig. 2. Two major high-energy targets for synthetic chemists.

It is possible to conceive of molecules that contain a large number of substituted groups and make predictions regarding their density in the crystalline state [8]. To achieve better results, it is necessary to consider a number of packing models for various crystallographic space groups [9]. Two substances that have among the highest predicted densities are the substituted adamantane and cubane shown in Fig. 2. The cubane nucleus has, in addition, its inherent strain energy. 1,3,5,7-Tetranitrocubane has been synthesized [10] and has a density of 1.814 g/cc in the crystalline state. To date, three nitro-substituted cubanes have been synthesized, the di-, tri-, and tetra-nitrocubanes, which have densities proportional to the number of nitro substituents, namely, 1.66, 1.74 and 1.81 g/cc, respectively [11].

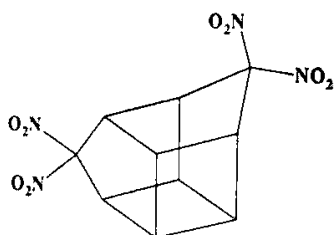
III. Energetic Materials Database

A virtue of developing a database of energetic materials is its use in the prediction of target structures that have potentially desirable features. The large number of crystal structure analyses of energetic materials that have been performed in recent years has provided much useful information. Examples are structural parameters associated with the NO₂ group, two NO₂ groups on the same carbon atom, and cage compounds having a variety of substituents. Illustrations of some types of compounds that make up the current database consisting of about 300 compounds are shown in Fig. 3. An application of the database is the calculation of the structure of the hypothetical molecule, octanitrocubane. The predicted distances and angles are consistent with those in the database and the nitro groups are in

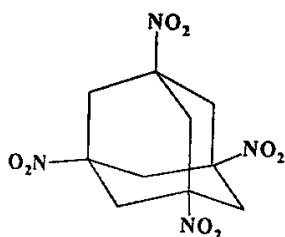


1,3,5,7-Tetranitrocubane

A Hexanitropentacycloundecane



A Tetranitrobishomocubane



1,3,5,7 Tetranitroadamantane

Fig. 3. Structures of four recently synthesized energetic cage compounds (Refs. [10,12,13,14]).

a conformation that is associated with an energy minimum. The calculation of the energy minimum was made with MM2 [15] modified by adding structural parameters and appropriate bending and stretching force constants (e.g., nitro and nitramine groups). The shortest nonbonded approaches in the hypothetical model of octanitrocubane are shown in Table I, and a drawing of the minimum energy model is given in Fig. 4. Hexanitrohexaazaadamantane (HNZADA) has been calculated by use of the modified MM2 program to have much less electrostatic repulsion than octanitrocubane, which has eight strong dipoles pointing outward

Table I. Shortest Nonbonded Approaches in an Energy-Minimized Octanitrocubane Model

Type	No. of Occurrences	Distance (Å)	vdW Contact (Å)
N...O	8		
O...O	4	2.98	2.90
O...C	8	3.08	2.80
O...C	8	3.02	3.10
O...C	8	3.06	3.10

appropriate
 article
 authors' interest
 in this case that
 in all cases
 1,3,5,7
 1,3,5,7
 1,3,5,7

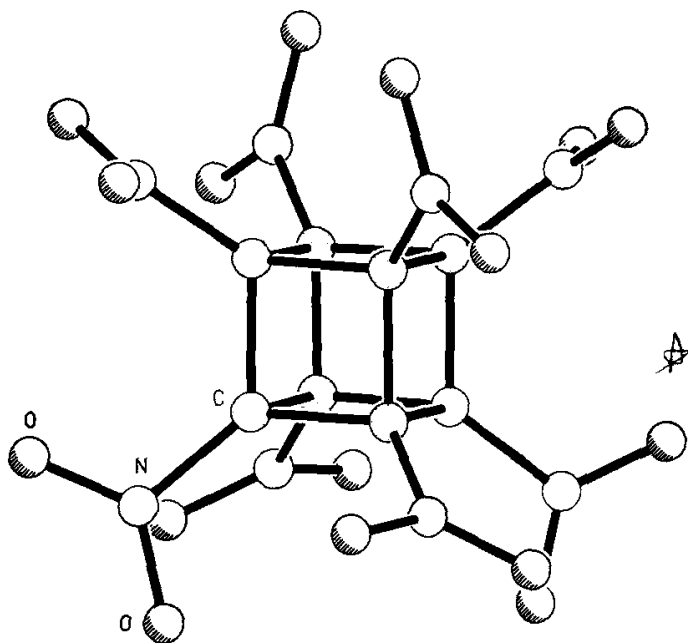


Fig. 4. An energy-minimized model of the hypothetical molecule, octanitrocubane.

from a common center. HNZADA has six N—NO₂ dipoles pointing outward, but also has four CH dipoles pointing inward, interposed between the nitro groups, which is electrostatically favorable. Quantum mechanical calculations on the similar nitramines, HMX and RDX [16,17], indicate that the CH dipoles will be much stronger (and thus more stabilizing) than ordinary aliphatic CH, due to the electron-withdrawing nature of the many nitramine groups.

A substituted triazaadamantane, 2,4,10-trinitro-2,4,10-triazaadamantane, was made a few years ago by Nielsen [18]. Its synthesis showed that a methine (CH) surrounded by nitramines in an adamantane cage is chemically stable, a matter that had previously been the subject of debate. There are four such groupings in HNZADA. Otherwise, the local connections are much the same as in HMX and RDX. Molecular mechanics model-building shows that the nitramines are no more crowded than in HMX and RDX, so there is reason to expect that this target molecule will not be especially sensitive or readily subject to chemical deterioration.

An extension of the hypothetical HNZADA is the nonanitrazo-target cage compound shown in Fig. 5. This hypothetical compound has the same

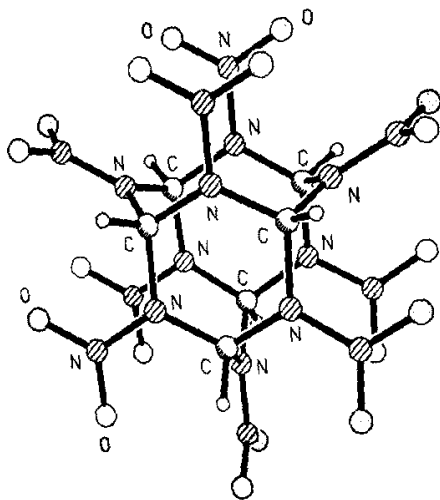


Fig. 5. A model of a nonanitrazo-target compound proposed by one of the authors (R.G.). The rings which make up the nonaaza cage all resemble the simpler compounds RDX and HMX.

atomic ratios and groupings as HNZADA. On the assumption that HNZADA and this nonanitrazo-compound can be synthesized, it would be of interest to compare their physical and chemical properties. This is one example of a large variety of paths that may be followed in the development of energetic compounds that have improved characteristics.

IV. Bending Angles in Nitramines

Nitramines are potentially high density materials and are among the types of substances that have been targeted for synthesis. It has been found from the database that amino groups in nitramines are rather flexible. The distribution of the out-of-plane bending angles for the amino group (the angle between the N-N vector and the C-N-C plane) is illustrated in Fig. 6. The histogram for the amino bend ranges from 0 to 60°; though dominated by small [0-20°] angles of bending, one example has been seen at 59°. Nitro groups, by comparison, are much less flexible, as may also be seen in Fig. 6. The relevant angle for nitro groups is that between the N-N vector and the O-N-O plane.

An example of a large amino bend (44.6°) is shown by monoketo RDX [19] illustrated in Fig. 7. The carbonyl group has the effect of flattening the

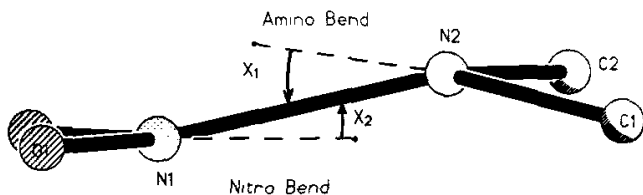
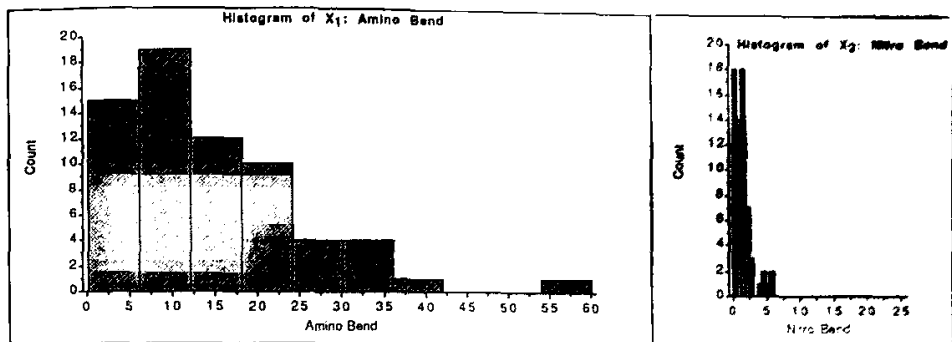
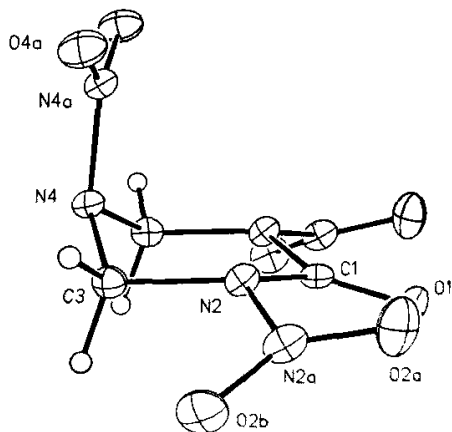


Fig. 6. Frequency distributions for two out-of-plane deformations of the nitramino group.

Fig. 7. The structure of 1,3,5-trinitro-2-oxo-1,3,5-triazacyclohexane. The presence of a carbonyl group flattens the chair-shaped ring and the two nitramines adjacent to it. The third nitramine displays one of the largest out-of-plane bends yet observed in a nitramine; the N-N bond is bent 44.6° from the adjacent CNC plane.



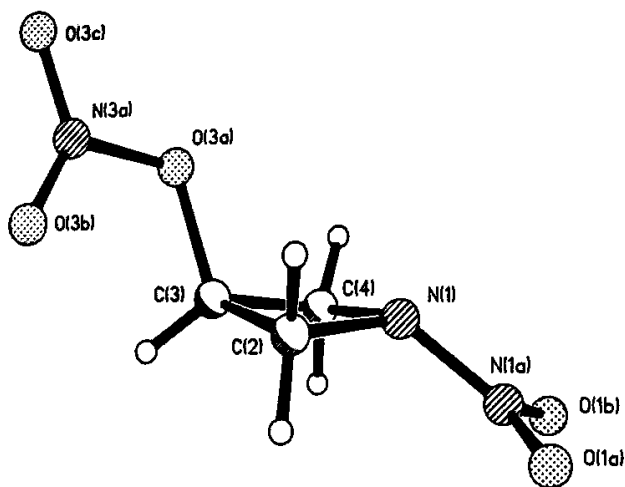


Fig. 8. The structure of 1-nitro-3-nitratoazetidine. The nitramine is part of a four-membered ring, and the N-N bond is bent out of the adjacent CNC plane by 39.6° .

chair-shaped ring and the two nitramine groups near it. Weak forces can produce relatively large changes in the amino bend since the energies are not much different for the in-plane and out-of-plane configurations. For example, an *ab initio* study of dimethylnitramine indicated that only 400 cal/mol were required to bend the nitro group 40° out of the C-N-C plane [20]. The amino bend in 1-nitro-3-nitratoazetidine [21], illustrated in Fig. 8, is 39.6° . In a nitroaziridine compound [22], the amino bend is 59° from the plane of the 3-membered ring (see Fig. 9)

A quantum chemical calculation [23] (using the program MNDO) on trinitroazetidine (see Fig. 10) also indicated that a sizeable out-of-plane amino bend (30°) was the minimum energy conformation. This observation stimulated another MNDO calculation [24] on a simple model compound, dimethylnitramine shown in Fig. 11. Although the MNDO minimum energy conformation for this molecule is planar, it was found that the amino bend could be bent $\pm 20^\circ$ from this plane with almost no energy increase ($\Delta E \leq 0.1$ kcal/mol). This predicted low-energy range agrees well with the distribution of crystallographic values.

It is of interest to note here that a correlation exists between the C-N-C angle and the out-of-plane amino bend (see Fig. 12). There is also an indication of a trend toward increasing values of the N-N bond distance with increasing values of the out-of-plane amino bend, although individual values are widely distributed as shown in Fig. 13.

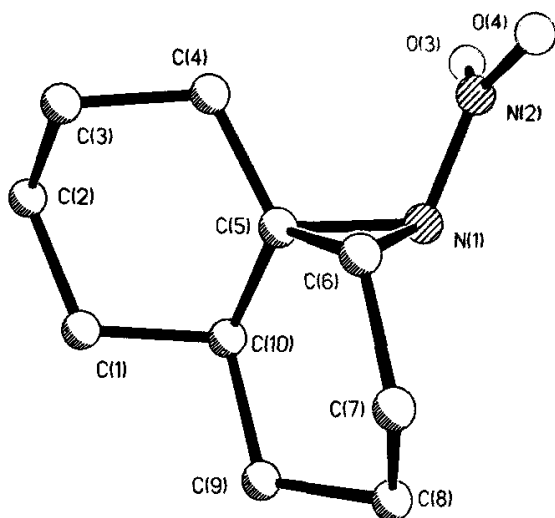
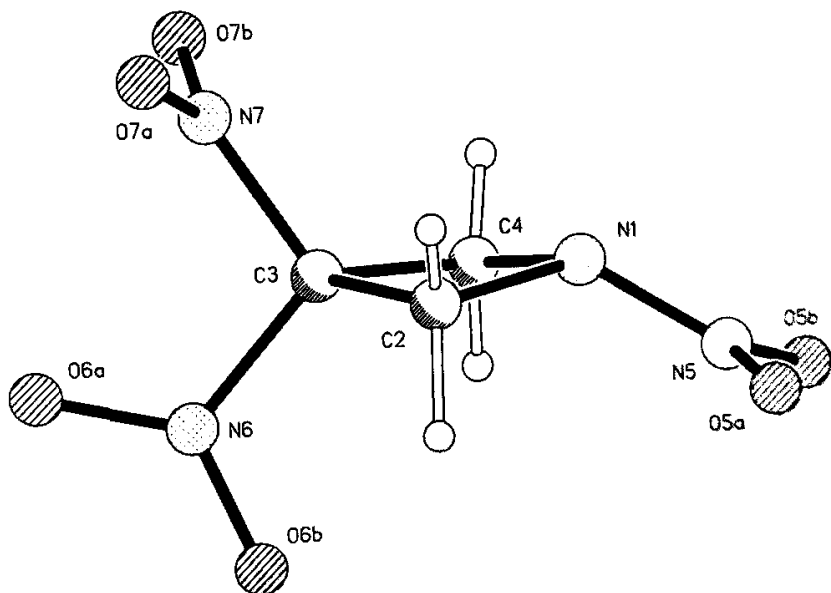


Fig. 9. The only reported example of a nitramine incorporated into a three-membered aziridine ring (only a portion of the full molecule is shown here); the amino bend is 59° , which is the highest yet reported.

Fig. 10. The molecular structure of 1,3,3-trinitroazetidine as observed in the crystal.



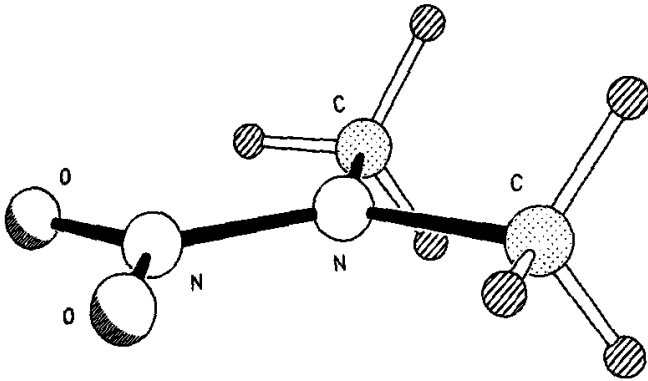
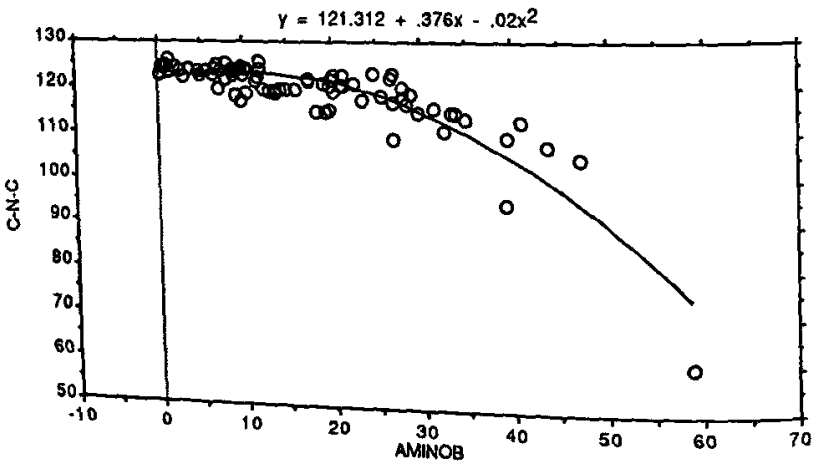


Fig. 11. The dimethylnitramine molecule.

Fig. 12. A scattergram display of the amino C-N-C bond angle and the amino bend (in degrees, see Fig. 6 for definition) of the nitramino group, as observed in more than 60 X-ray structural determinations. The curved line represents the best fit to the data by a second-degree polynomial function.



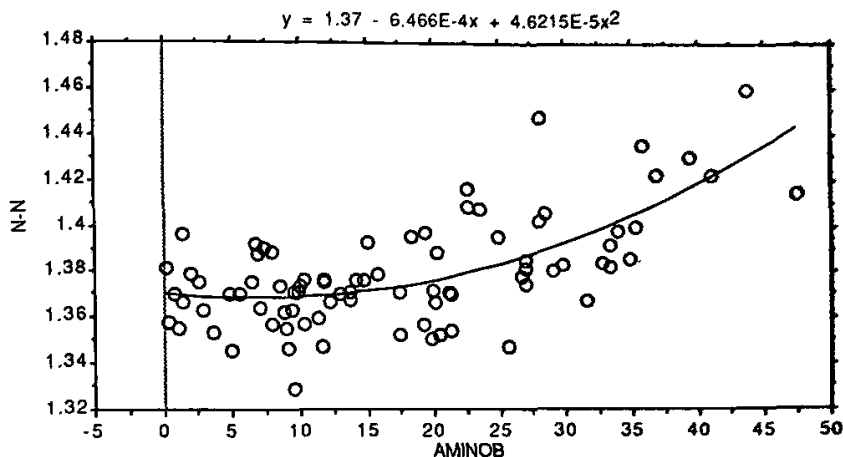


Fig. 13. A scattergram display of the N-N distance (in Å) and the amino bend (°) of the nitramino group.

V. Nitroolefins

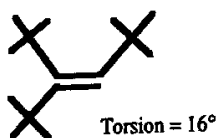
There have been a number of investigations involving the study of nitroolefins as useful intermediates in the synthesis of energetic materials. A characteristic of many of them is a large twist about the double bond. Interest in the structural characteristics that accompany the rotation motivates a discussion of details. As would be expected, the rotation out of the normal planar conformation is associated with spatial crowding. Figure 14 illustrates some of the largest out-of-plane rotations that have been measured and, in one case, calculated for crowded ethylenes [25].

In 1,1-dinitro-2,2-di(dimethylamino)ethylene [26] (Fig. 15) there is a torsion of the N1-C1-N2 plane about the C1-C2 double bond of 51.4° relative to the N3-C2-N4 plane. The C1-C2 distance is 1.434(3) Å, which is considerably longer than a typical isolated double bond length (~1.33 Å) [27].

The ease with which internal rotation can take place is generally much greater for single than double bonds. Does the crowding stretch the doublebonded C-C distance making it closer to the single-bonded distance and thus facilitate the out-of-plane twist? The C-C distance will be examined in the twisted molecules to determine whether a correlation exists between the torsion angle and the C-C distance.

A quite useful precursor in the synthesis of twisted diaminodinitroolefins is 1,1-diiodo-2,2-dinitroethylene [26] whose structure is shown in

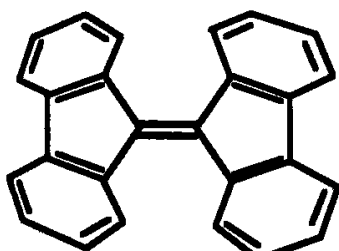
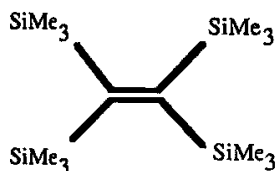
Severely Twisted Olefins



Tri-t-butyl ethylene



Tetra-t-butyl ethylene

Unknown! Torsion calc'd to be 45° Torsion = 43° 

Tetra-trimethylsilyl ethylene

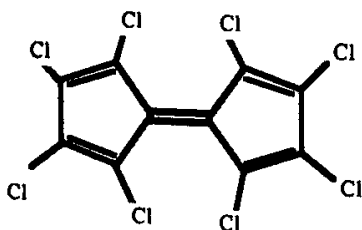
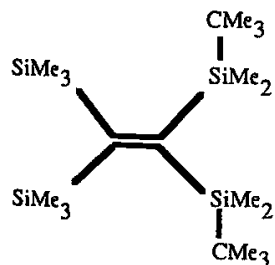
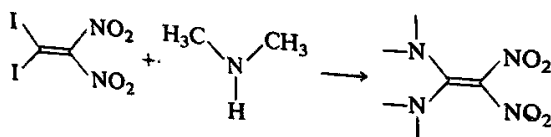
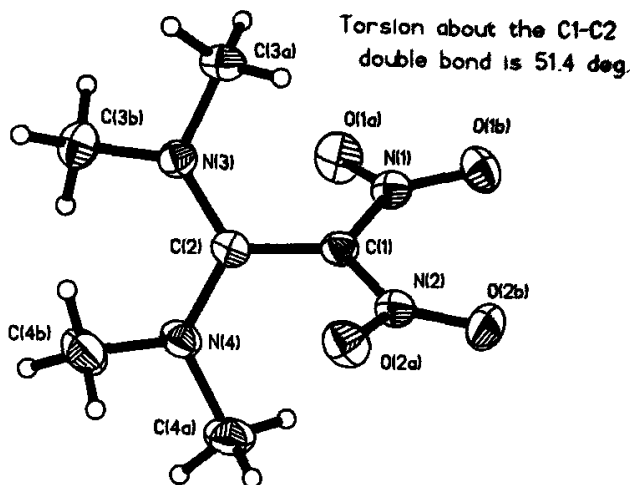
Torsion = 29.5° Torsion = 41° Torsion = 49.5°

Fig. 14. Some examples of observed and calculated twists in olefins.

Fig. 16. The reaction that leads to the synthesis of 1,1-dinitro-2,2-di(dimethylamino)ethylene is

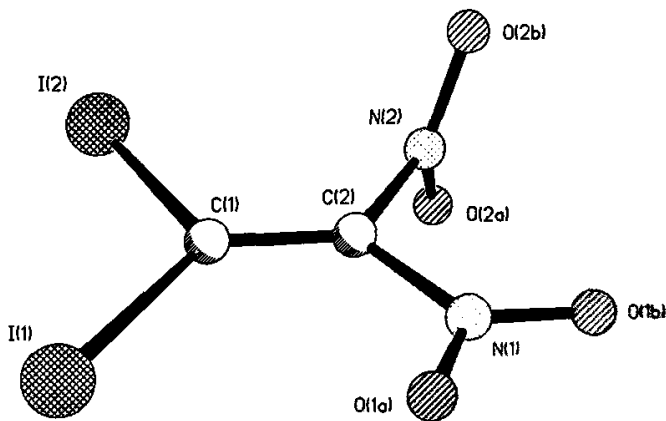




1,1-Dinitro-2,2-di(dimethylamino) Ethylene

Fig. 15. The molecular structure of 1,1-dinitro-2,2-di(dimethylamino)ethylene. The C1-C2 bond is formally a double bond but is lengthened from the normal value (~ 1.33 Å) to a value of 1.434(3) Å. [A digit in parentheses following a reported value is the estimated standard deviation (esd) in the final digit(s) of the reported parameter and represents the error to be expected in repeated determinations of that parameter due to random measurement errors in the X-ray intensities.]

Fig. 16. The structure of 1,1-diiodo-2,2-dinitroethylene. The N2 nitro group is rotated ca. 85° from the best plane of the rest of the atoms (which are essentially coplanar).



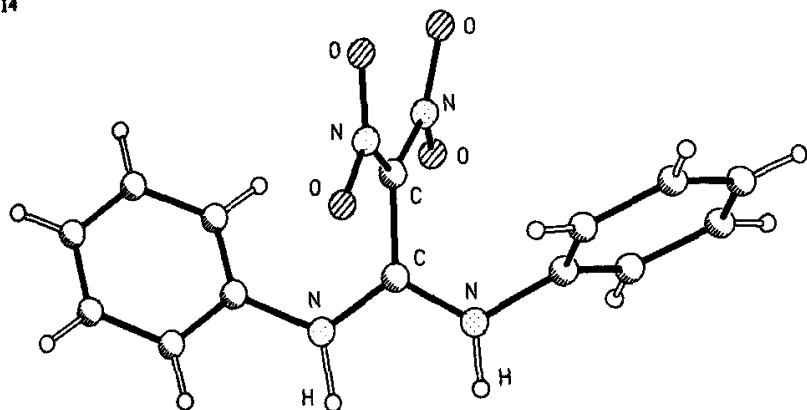
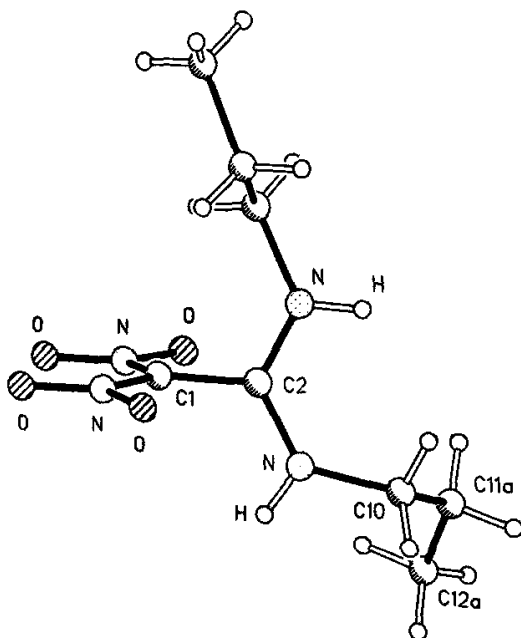


Fig. 17. The molecular structure of 1,1-dinitro-2,2-di(phenylamino)ethylene. The C1-C2 bond is lengthened to a value of 1.451(8) Å.

Fig. 18. The molecular structure of 1,1-dinitro-2,2-di(*n*-propyl)ethylene. The C1-C2 bond is lengthened to a value of 1.464(13) Å. One propyl chain [C10-C11a-C12a] is disordered in the crystal, and only the major conformation is shown here.



Note that the diiodo compound in Fig. 16 is not symmetric. The plane of one NO_2 group is essentially perpendicular to that of the other.

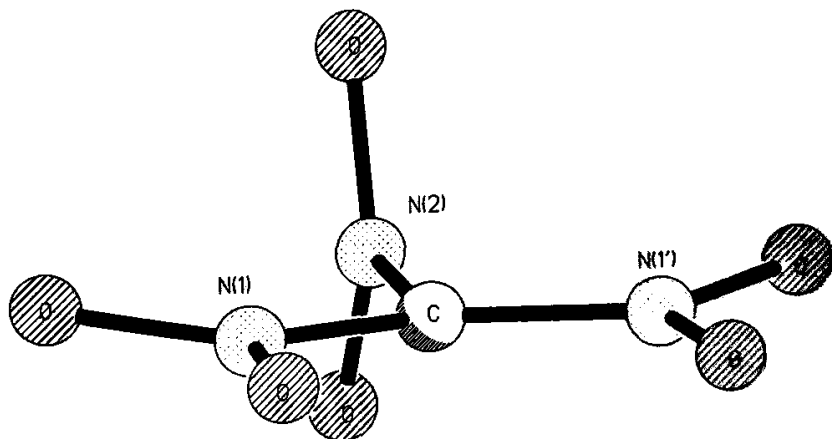
An illustration of the molecule, 1,1-dinitro-2,2-diphenylaminoethylene [26] is seen in Fig. 17. It is apparent that this molecule could be synthesized from 1,1-diiodo-2,2-dinitroethylene and aniline. The dinitro plane is twisted 71° from the N-C-N plane at the amino end of the double bond. The phenyl groups are twisted 40 and 60° from the N-C-N plane.

A structural determination of 1,1-dinitro-2,2-dipropylaminoethylene [26] reveals a considerable twist of 87.1° about the C-C double bond (see Fig. 18). In this case, the C-C distance has increased by almost 0.12 \AA over the normal value.

An extension of the C-N (nitro) bond length by approximately 0.08 \AA is associated with a large out-of-plane twist in *t*-butylammonium trinitromethanide [28]. Figure 19 depicts the negatively charged trinitromethanide moiety. In this anion, the carbon atom and two of the nitro groups are essentially coplanar; the third nitro group is perpendicular to the plane of the other atoms. In the last two examples, the changes in the bond lengths are considerable.

As a final example, the steps in the synthesis [26] of a highly energetic compound which proceeds via a twisted olefin are indicated. The synthesis is once again initiated by the use of 1,1-diiodo-2,2-dinitroethylene and

Fig. 19. The structure of the anion in the *t*-butylammonium trinitromethanide salt. Two of the nitro distances are equal ($1.367(2) \text{ \AA}$) and are much shorter than the third, C-N2, which is $1.450(4) \text{ \AA}$. The third nitro group is twisted exactly 90° from the plane of the first two.



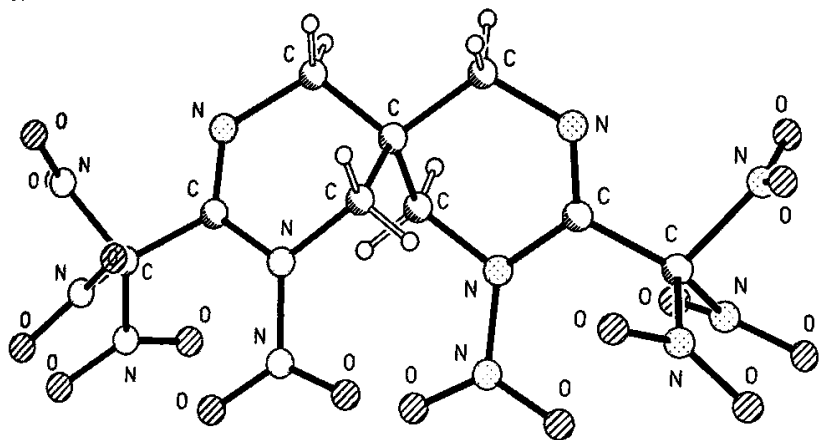
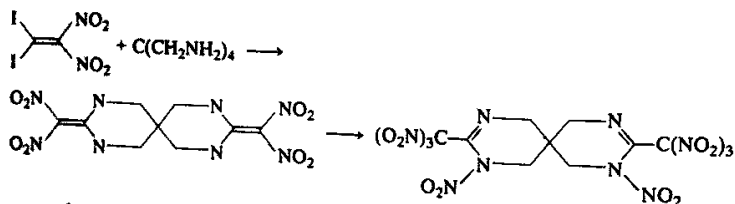


Fig. 20. The structure observed for a bicyclic octanitro compound formed by condensation of diiododinitroethylene with a polyamine and followed by further nitration.

amine as shown below.



The actual structure of the product is depicted in Fig. 20. It has a density of 1.81 g/cc.

VI. Cubane and Substituents

Cubane [29,30] is an appealing substance on which to base a synthesis of energetic compounds. It contains an inherent strain energy and, in addition, offers a number of regions in which energetic groups may be attached. We review here some investigations that have revealed characteristic structural features of the cubanes.

In an initial study [31] that was expected to reveal the structure of unsubstituted cubylcubane in the crystalline state, it was found that cubylcubane was cocrystallized with 2-*t*-butylcubylcubane (Fig. 21). It was nevertheless possible to obtain good insight into the structure of cubylcubane from the investigation of the mixed crystal. The cubes are virtually regular and are staggered with respect to each other (Fig. 22). The average

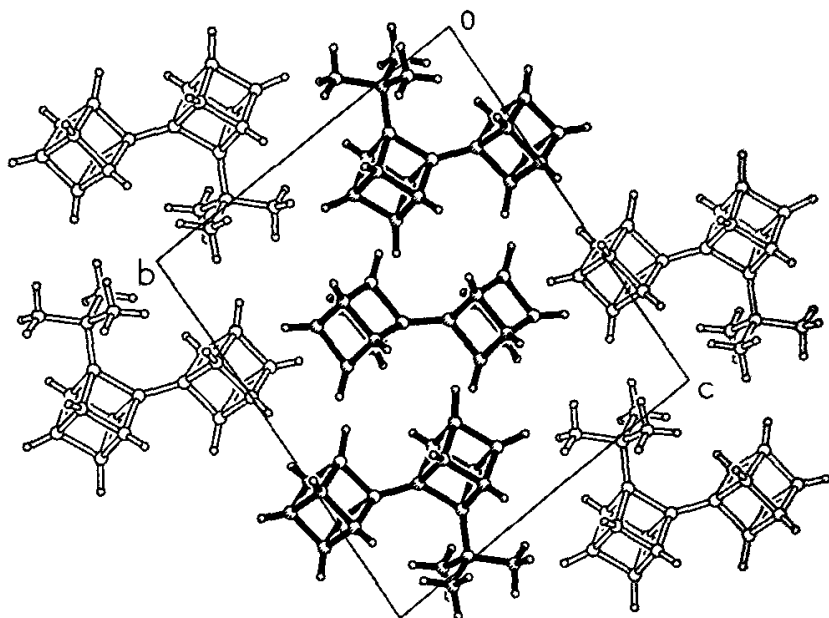
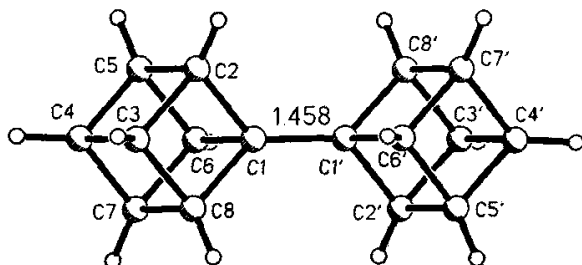


Fig. 21. The packing of molecules in the cocrystal of cubylcubane and 2-(*t*-butyl)-cubylcubane. The central molecule is cubylcubane; all of the surrounding molecules are 2-(*t*-butyl)-cubylcubanes. The three emphasized molecules comprise the contents of one unit cell (the centroids of only these three lie inside the cell).

Fig. 22. The molecular structure of cubylcubane, showing the distance measured for the short linkage bond by X-ray analysis of its cocrystal with 2-*t*-butylcubylcubane. A later investigation of pure cubylcubane crystals gave a result for this bond of 1.475(4)Å. The reason for this discrepancy is not entirely clear, but the standard deviations estimated for the bond lengths do not rule out its being a normal fluctuation caused by random experimental errors.



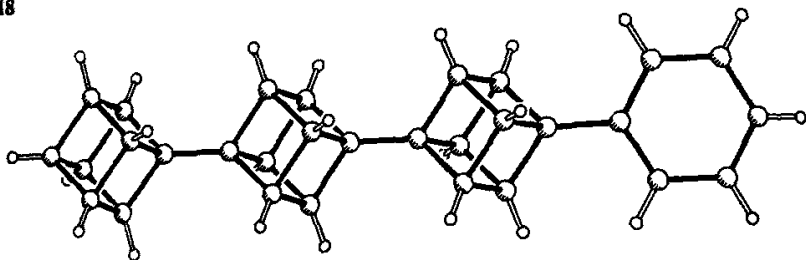


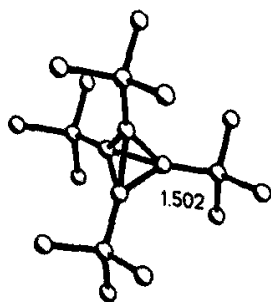
Fig. 23. The molecular structure of a phenyltercubyl compound. Still higher polymers of cubane exist but are exceedingly difficult to crystallize.

length of the cube edges adjacent to the linkage is $1.568(9)\text{\AA}$ and $1.553(8)\text{\AA}$ for all the others. The linkage distance, $1.458(8)\text{\AA}$, is much smaller than that for a normal single C-C bond ($\sim 1.54\text{\AA}$). A shortened linkage bond has now been observed in four structural investigations of cubylcubane or its derivatives [32] and also in a study [33] of a compound containing three cubes linked together (Fig. 23).

Other strained cage and ring systems appear to have reduced bond lengths. For example, the average cage bond length in tetra-*t*-butyl-tetrahydronaphthalene [34] is 1.485\AA and the adjacent bonds have a length of 1.502\AA (Fig. 24). The average ring bond length in bicyclopropyl [35] is 1.503\AA and the linkage bond length is 1.487\AA . Three-membered ring systems display a shortening of C-C single bond lengths both within the rings and

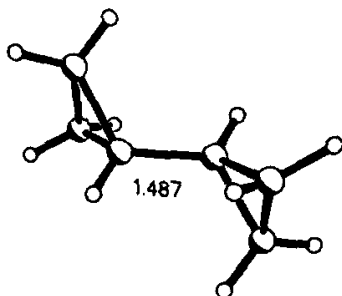
Fig. 24. Bond lengths in other strained hydrocarbons.

Tetra-*t*-Butyltetrahydronaphthalene



Average cage bond length 1.485\AA

Bicyclopropyl



Average ring bond length 1.503\AA

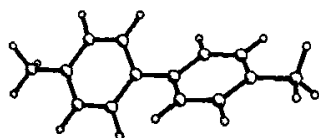
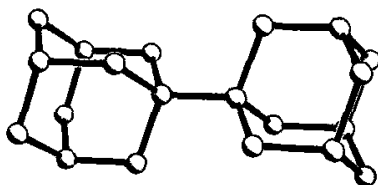
ADAMANTYLADAMANTANE - 1.578(2)Å (sp^3-sp^3)BITOLYL - (ave. of 2 det'ns) (sp^2-sp^2)

Fig. 25. Linkage bond lengths in hydrocarbons containing less strain.

exo to the rings. Molecular orbital calculations are consistent with these observations [36].

Linkage bond lengths in systems that do not have angular strain may be compared. In adamantyladamantane [37] there is no shrinkage. Rather, the bond stretches somewhat with a length of 1.578(2) Å (Fig. 25). In bitolyl [38] there are also no angular strains, although there is a twist about what may be considered a single bond linking the two aromatic rings (Fig. 25) of $\sim 38^\circ$. There is a definitive reduction of the linkage bond length from the normal single-bond range. The source of the shrinkage is most probably the influence of the aromatic rings rather than the out-of-plane twist.

Syntheses have been made of energetically substituted cubanes. For example, 1,3,5,7-tetranitrocubane [10] (shown in Fig. 26) has been synthesized. As noted previously, its density is 1.814 g/cc. Another is the fluorodinitroethyl ester of tetracarboxycubane [36] (Fig. 27). The density is 1.762 g/cc. An energetic ammonium perchlorate substitution of cubane has been made in the form of 1,4-bis-cubanediammonium perchlorate hydrate [40] (Fig. 28). The dashed lines in Fig. 28 represent some of the many hydrogen bonds that occur in the crystal whose density is 1.755 g/cc. An estimate of the dry density extrapolated from this work is 1.83 g/cc. It was obtained by subtracting the volume and mass of water from the unit cell contents. The volume of H_2O was taken to be the same as that in liquid water.

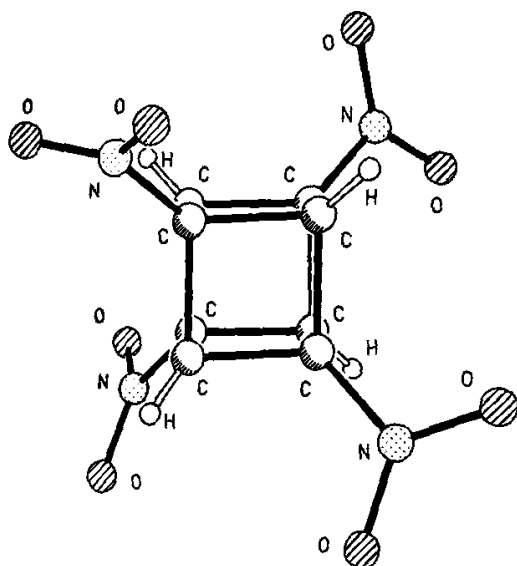
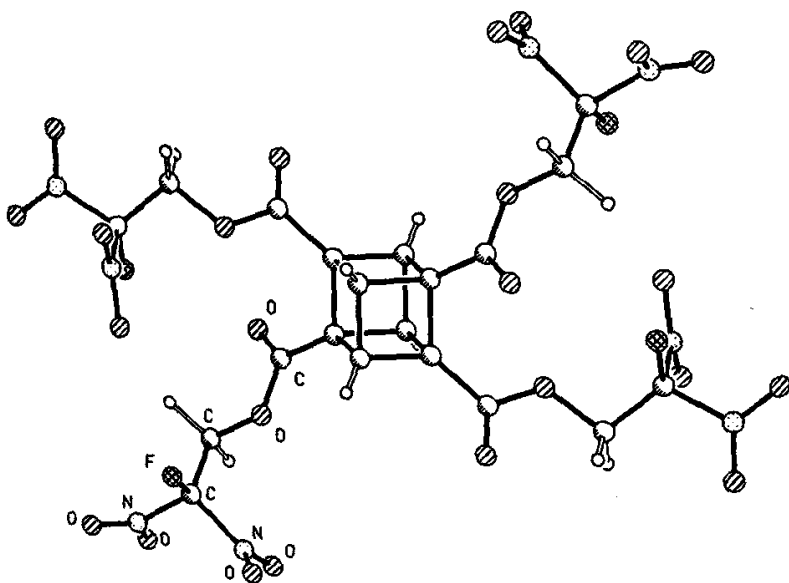
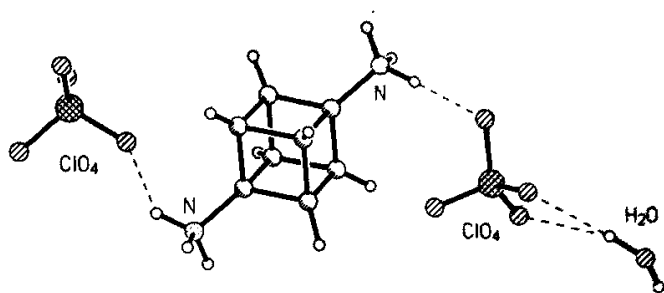


Fig. 26. The molecular structure of 1,3,5,7-tetranitrocubane; because of the packing in the crystal the nitro groups are not equivalent. The surroundings differ for each one, leading to slight (mainly torsional) differences in geometry.

Fig. 27. The structure of the tetrakis(2-fluoro-2,2-dinitroethyl)ester of the 1,2,4,7-tetracarboxylic acid of cubane.

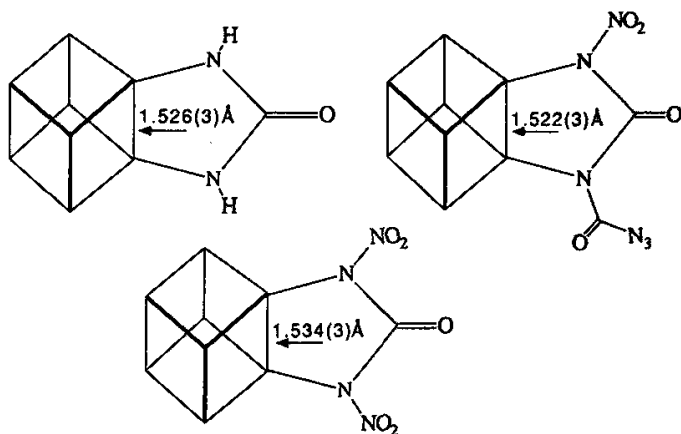




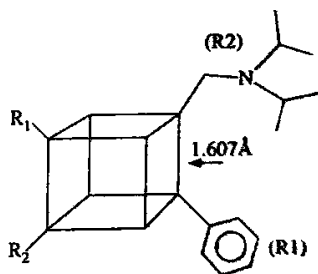
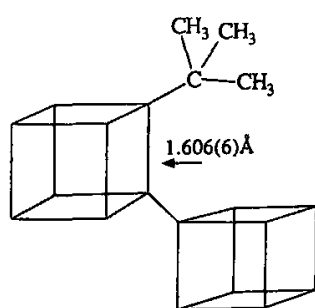
1,4-Bis-Cubanediammonium Perchlorate Hydrate

Fig. 28. The molecular structure of 1,4-bis-cubanediammonium perchlorate monohydrate.

Fig. 29. A comparison of some of the shortest and longest cubane cage distances, both of which occur at disubstituted cube edges.



Shortened 1,2-substituted Cubane Bonds



Elongated 1,2-substituted Cubane Bonds

Cubane has been fused to five-membered heterocyclic rings ([41]; Fig. 29, upper panel). A point of interest in these compounds is the shrinkage of the common C-C bond shared by the cubyl moiety and the ring. Its value ranges from 1.522–1.534 Å. On the other hand, bulky substitution on the cubane cage has led to observed lengthenings [31,42] of up to 1.607 Å (Fig. 29, lower panel). These results imply that cubane has a significant flexibility and thus can accommodate a larger variety of substitutions than may have been previously expected.

VII. Conclusions

In this article, a number of ways in which structure determination can serve the synthetic chemist have been illustrated. Questions concerning identification, conformation, configuration, bonding, and bond distances and angles have been answered with a high degree of accuracy. The area of study of energetic materials often presents unusual circumstances in which the use of structural analysis is virtually indispensable for characterizing the geometric nature of the substance of interest. Many of the examples in this chapter are illustrative of the difficulty in predicting structural features (e.g. the twisted olefins and the cyclic nitramines).

Modeling programs should be used with great caution and are safest when the questions asked are not too far from experimental experience. They work at their best when predicting parameters that are distributed about an equilibrium value with a small variance (i.e., when the energy increase for distortions is large). When a parameter is characterized as having a sharp, deep potential well about a well-defined equilibrium, accurate predictions for its value can be made with an incomplete knowledge of the shape of the potential well. The position of the minimum is needed, but effects of inaccuracy in force constants (numbers which define the shape of the curve) are minimal. When one approaches the problem of prediction of structural features bound by shallow potential wells, a highly accurate picture of the shape of the well (i.e., good values for harmonic and anharmonic force constants, as well as an accurate position for the minimum) is needed to produce even low-accuracy estimates.

Examples of shallow-well potentials are those governing the out-of-plane bends in peptides and nitramines, and potentials describing the local structure near bonds which do not fit well into formal single, double or aromatic categories, such as the twisted olefins discussed earlier and most unsaturated nitrogen heterocycles (pyrroles, triazoles, etc.). In these cases,

it has been shown that subtle influences such as dipole forces from remote substituents, solvent-association forces, and crystal-packing forces may produce large structural variations. Users of modeling programs should be aware of these considerations because if one is interested in predicting the features of unusual, currently unknown, molecules which lie at the frontiers of the art of chemical synthesis, there may be serious pitfalls.

Much greater information may be forthcoming from diffraction analysis when it is possible to apply it readily to the determination of accurate electron density distributions in complex materials. How soon that time will come is another unknown that is difficult to predict.

REFERENCES

1. The Cambridge Structural Database is available by annual lease from: Cambridge Crystallographic Data Centre (CCDC), University Chemical Laboratory, Lensfield Road, Cambridge CB2 1EW, England. A reference describing the database is: "The Cambridge Crystallographic Data Centre: Computer-Based Search, Retrieval, Analysis, and Display of Information." F. H. Allen, S. Bellard, M. D. Brice, B. A. Cartwright, A. Doubleday, H. Higgs, T. Hummelink, B. G. Hummelink-Peters, O. Kennard, W. D. S. Motherwell, J. R. Rodgers, and D. G. Watson (1979). *Acta Cryst.* **B35**, 2331-2339.
2. X-ray diffraction analyses have been performed at the Naval Research Laboratory for over 300 (310 as of September 1990) molecules synthesized in energetic materials research programs. The detailed results on these compounds are not available for "on-line" public access, but results for most of these compounds are available (if not already published) on request. An up-to-date index containing structural formulae and densities is available from the authors: Richard Gilardi, Clifford F. George, and Judith L. Flippen-Anderson; Laboratory for the Structure of Matter (Code 6030); Naval Research Laboratory; Washington, D.C. 20375.
3. "Chemistry of Detonations. I. A Simple Method for Calculating Detonation Properties of C-H-N-O Explosives." M. J. Kamlet and S. J. Jacobs. (1968). *J. Chem. Phys.* **48**, 23-35.
4. "On Underwater Detonations. I. A New Method for Predicting the CJ Detonation Pressure of Explosives." R. Gill, L. Asaoka, and E. Baroody. (1987). *J. Energ. Mater.* **5**, 287-307.
5. "Propellant Chemistry." S. F. Sarnar. Reinhold, New York. p. 112 (1967).
6. "A Study of the Crystal Structure of β -Cyclotetramethylene Tetranitramine by Neutron Diffraction." C. S. Choi and H. P. Boutin. (1970). *Acta Cryst.* **B26**, 1235-1240.
7. "The Crystal Structure of Cyclotrimethylene Trinitramine". C. S. Choi and E. Prince. (1972) *Acta Cryst.* **B28**, 2857-2862.

8. "Prediction of Crystal Densities of Organic Explosives by Group Additivity." J. R. Stine. (1981). Report No. LA-8920 (Los Alamos National Laboratory, Los Alamos, New Mexico 87545, U.S.A.). This report refers to many prior methods which differ only slightly in their theory and application.
9. "A Procedure for Estimating the Crystal Densities of Organic Explosives." D. T. Cromer, H. L. Ammon, and J. R. Holden. (1987). Report No. LA-11142-MS (Los Alamos National Laboratory, Los Alamos, New Mexico 87545, U.S.A.).
10. "X-ray Crystal Structures of 1,3,5-Trinitro and 1,3,5,7-Tetranitrocubane." R. Gilardi, Y. Xiong, and P. E. Eaton. *Acta Cryst.*, manuscript in preparation.
11. "Synthesis of 1,4-Dinitrocubane." P. E. Eaton, B. K. Ravi Shankar, G. D. Price, J. J. Pluth, E. E. Gilbert, J. Alster, and O. Sandus. (1984). *J. Org. Chem.* **49**, 185-186.
12. "Structure of 1,3,5,7-Tetranitroadamantane, $C_{10}H_{12}N_4O_8$." C. George and R. Gilardi. (1984). *Acta Cryst.* **C40**, 674-676.
13. "Structure of 6,6,10,10,-Tetranitropentacyclo[5.3.0.0^{2,5}.0^{3,9}.0^{4,8}]decane, $C_{10}H_8N_4O_8$." C. George, R. Gilardi, J. L. Flippen-Anderson, C. S. Choi, A. P. Marchand, and D. S. Reddy (1985). *Acta Cryst.* **C41**, 788-791.
14. "Synthesis of 4,4,8,8,11,11-Hexanitropentacyclo[5.4.0.0^{2,6}.0^{3,10}.0^{5,9}]undecane." A. P. Marchand, P. R. Dave, D. Rajapaksa, B. E. Arney, Jr., J. L. Flippen-Anderson, R. Gilardi, and C. George. (1989). *J. Org. Chem.* **54**, 1769-1771.
15. The MM2 molecular mechanics force field, the associated computer program, and its usage for many types of molecules are summarized in: "Molecular Mechanics" by U. Burkert and N. L. Allinger. (1982). American Chemical Society, Washington, D.C.
16. "Ab Initio MODPOT/VRDDO/MERGE Calculations on Energetic Compounds. II. Nitroexplosives: RDX and α -, β - and δ -HMX." P. C. Hariharan, W. S. Koski, J. J. Kaufman, R. S. Miller, and A. H. Lowrey. (1982). *Int. J. Quantum Chem., Quantum Chem. Symp.* **16**, 363-375.
17. "Analysis of Intra- and Intermolecular Interactions Relating to the Thermophysical Behavior of α -, β , and δ -Octahydro-1,3,5,7-Tetranitro-1,3,5,7-Tetraazocine." T. B. Brill and C. O. Reese. (1980). *J. Phys. Chem.* **84**, 1376-1380.
18. "Polynitropolyaza Caged Explosives, Part 3." A. P. Nielsen, D. W. Moore, and R. L. Willer (March, 1984). Report No. NWC-TP-6513 from the Naval Weapons Center, China Lake, California 93555, U.S.A.
19. "Structures of 1,3,5-Trinitro-2-oxo-1,3,5-triazacyclohexane (I) and 1,4-Dinitro-2,5-dioxo-1,4-diazacyclohexane (II)." R. Gilardi, J. L. Flippen-Anderson, and C. George. (1990). *Acta Cryst.* **C46**, 706-708.
20. "Ab Initio Study of Dimethylnitramine." F. R. Cordell (1987 Report, University of Texas, Austin, Texas). Gov. Rep. Announce. Index (U.S.) 87, Abstr. No. 750,665. NTIS Order No. AD-A183414, 112p.
21. "Structure of 1-Nitro-3-nitratoozetidine." R. Gilardi and C. George. *Acta Cryst.*, manuscript in preparation.

22. "N-Nitroaziridines: Structure Confirmed." M. J. Haire and R. L. Harlow. (1980). *J. Org. Chem.* **45**, 2264-2265.
23. "Synthesis and X-ray Crystal Structure of 1,3,3-Trinitroazetidene." T. G. Archibald, R. Gilardi, K. Baum, and C. George. (1990). *J. Org. Chem.* **55**, 2920-2924.
24. Gilardi, R. (1986). Unpublished MNDO calculations. Very similar results were obtained as in Ref. 20 with *ab initio* quantum calculations.
25. "A Survey of Strained Organic Molecules." J. F. Liebman and A. Greenberg. (1976). *Chem. Rev.* **76**, 311-365.
26. "Synthesis and Reactions of 1,1-Diododinitroethylene." K. Baum, T. Archibald, R. Gilardi, J. L. Flippen-Anderson, and C. George. *J. Org. Chem.*, manuscript in preparation.
27. "X-ray Analysis and the Structure of Organic Molecules." J. D. Dunitz. (1979). Cornell University Press, Ithaca (NY) and London.
28. "The Crystal Structure of *tert*-Butylammonium Trinitromethanide." C. George, J. L. Flippen-Anderson, and R. Gilardi. *Acta Cryst.*, manuscript in preparation.
29. "The Cubane System" and "Cubane." P. E. Eaton and T. W. Cole, Jr. (1964). *J. Amer. Chem. Soc.* **86**, 962-964 and 3157-3158.
30. "X-ray Structure Determination of Cubane." E. B. Fleischer. *J. Amer. Chem. Soc.* **86**, 3889-3890.
31. "X-ray Structures of Cubylcubane and 2-*tert*-Butylcubylcubane: Short Cage-Cage Bonds." R. Gilardi, M. Maggini, and Philip E. Eaton. (1988). *J. Am. Chem. Soc.* **110**, 7232-4.
32. The four distances referred to in the text are 1.458(8)Å for cubylcubane and 1.464(5)Å for 2-*tert*-butylcubylcubane in their cocrystal [31]; 1.475(4)Å for cubylcubane and 1.460(10)Å for 4,4'-dicarbomethoxycubylcubane. The latter two are reported in: "Crystal Structures of Cubylcubane and 4,4'-Dicarbomethoxycubylcubane." R. Gilardi, J. L. Flippen-Anderson, C. George and P. E. Eaton. *Acta Cryst.*, manuscript in preparation.
33. P. E. Eaton, K. Pramod, and R. Gilardi. Manuscript in preparation.
34. "Tetra-*tert*-butyltetrahedrane- Crystal and Molecular Structure." H. Irgartinger, A. Goldmann, R. Jahn, M. Nixdorf, H. Rodewald, G. Maier, K. Malsch and R. Emrich (1984). *Angew. Chem. Int. Ed. Engl.* **23**, 993-994.
35. "The X-ray Structure of Bicyclopropyl." J. Eraker and C. Romming. (1967). *Acta Chem. Scand.* **21**, 2721-2726.
36. "The Geometry of Small Rings. II. A Comparative Geometrical Study of Hybridization and Conjugation in Cyclopropane and the Vinyl Group." F. H. Allen. (1981). *Acta Cryst.* **B37**, 890-900.
37. "Concerning the Mechanism of Single-Bond Shortening. Evidence from the Crystal Structures of 1-Biapocamphane, 1-Binorbornane, and 1-Biadamantane." R. A. Alden, J. Kraut, and T. G. Traylor (1968). *J. Amer. Chem. Soc.* **90**, 74-82.
38. "The Crystal Structure of *p,p'*-Bitolyl." G. Casalone, C. Mariani, A. Mugnoli, and M. Simonetta. (1969). *Acta Cryst.* **B25**, 1741-1750.

39. "Synthesis of Nitro Substituted Cubanes." J. C. Bottaro, P. E. Penwell, R. J. Schmitt, C. D. Bedford, R. Gilardi, J. Flippen-Anderson, and C. George. (1991). *J. Org. Chem.*, in press.
40. R. Gilardi, C. George, and J. L. Flippen-Anderson, unpublished X-ray structure (1989); molecule synthesized by Dr. Glen Cunkle, Morton Thiokol Co., Elkton, Maryland.
41. "Cubanourea: A Cubane-propellane." P. E. Eaton, K. Pramod and R. Gilardi (1990). *J. Org. Chem.* 55, 5746-5750.
42. "Chemistry and Structure of Phenylcubanes." A. Bashir-Hashemi, H. L. Ammon, and C. S. Choi. (1990). *J. Org. Chem.* 55, 416-420.

2

Studies of Initial Dissociation Processes in 1,3,3-Trinitroazetidine by Photofragmentation Translational Spectroscopy

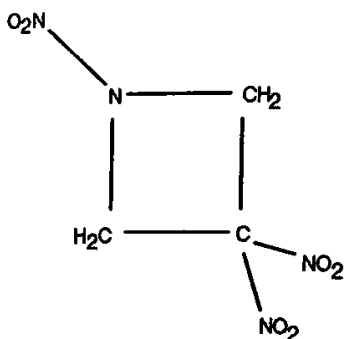
Deon S. Anex, John C. Allman, and Yuan T. Lee

I. Introduction and Overview

Interest in the chemistry of certain NO_2 -containing molecules stems from the use of these compounds as energetic materials. One class of these materials is the cyclic nitroalkyl nitramines, an example of which is 1,3,3-trinitroazetidine (TNAZ). These compounds are related to the energetic cyclic nitramines (HMX [1] and RDX [2], for example) through the replacement of one or two nitramine groups, NNO_2 , with *geminal*-dinitroalkyl groups, $\text{C}(\text{NO}_2)_2$. For example the nitroalkyl nitramine analog of the eight-membered ring HMX and the six-membered ring RDX are HNDZ [3] and DNNC [4], respectively. The four-membered ring in this series of cyclic nitroalkyl nitramines is TNAZ (Fig. 1), which contains one nitramine and one *geminal*-dinitroalkyl group. In these compounds, the inclusion of a *geminal*-dinitroalkyl group in the place of a nitramine group serves to increase their oxygen content.

Research in the field of energetic materials spans many disciplines. The spectrum of areas of interest extends from bulk, macroscopic fields such as engineering and material science to molecular dynamics, where the focus is on events of a truly microscopic scale. It is toward the molecular level of understanding that this article is focused. In order to fully understand the combustion of energetic materials, the details of the chemistry of the decomposition must certainly be understood. Issues of interest in this area include elucidation of the initial reaction steps, the dynamics of the dissociation, and the energy released during the reaction. Specifically, with respect to the current study, the effect of ring size and the substitution of

Fig. 1. TNAZ (1,3,3-trinitroazetidide), a cyclic nitroalkyl nitramine.



the *geminal*-dinitroalkyl groups for the nitramine groups are important issues to investigate.

A. Previous Work

This literature on the chemistry of the combustion of energetic materials is extensive, yet until recently the information available on the thermal decomposition of TNAZ was limited to studies from a single laboratory [5,6,7]. In one investigation from this group [5] solid TNAZ was placed on a nichrome ribbon that was resistively heated inside a variable pressure cell. Using rapid scan Fourier transform infrared interferometry, the gases evolved during pyrolysis were monitored by collecting a series of infrared spectra as the ribbon was heated. Through knowledge of the infrared absorption strengths of the gases present, concentration-versus-time profiles were obtained for various heating rates and cell pressures. In these studies, the first detected gases appeared 3 sec after the beginning of the heating (at a rate of 145 K/sec under 15 psi of N_2 to a final temperature of 905 K). The most abundant species was NO_2 , whose concentration declined after its initial appearance. The next most abundant species was NO which grew in after its initial appearance. Other detected species included HCN , H_2CO , CO , CO_2 , and a small amount of $HONO$ appearing after 6 sec. It was concluded that the loss of NO_2 was a major channel for decomposition and that there was no evidence for methylene nitramine (H_2CNNO_2) decomposition to H_2CO and N_2O . In a related study using the same techniques [6] it was found that the pressure-versus-time profiles for the gases evolved from TNAZ decomposition were sensitive to buffer gas pressure, pointing toward the importance of secondary bimolecular reactions and condensed phase chemistry.

B. Photofragmentation Translational Spectroscopy

More recently, emphasis has been placed on understanding the initial decomposition steps in several NO_2 -containing molecules using molecular beam methods [8,9]. These techniques have the advantage of addressing the identification of the reaction pathways and the determination of energy released into translation for isolated gas phase molecules. Although a significant portion of the combustion of energetic materials is related to condensed phase reactions, the understanding of the chemistry of the isolated species is certainly pertinent. First, the understanding of the initiation of reactions in these materials can be increased by understanding the primary decomposition steps. Second, there are both gas phase- and condensed phase components to the combustion of these materials. Third, theoretical understanding of the dynamics of the decomposition begins with the modeling of isolated molecules. The results of the theoretical efforts and the molecular beam studies may be directly compared.

The method discussed here is photofragmentation translational spectroscopy. In this method, the molecule of interest is expanded from a nozzle into a vacuum, and then the expansion is collimated to form a molecular beam. The molecular beam is then crossed with the output of a pulsed CO_2 laser which excites the molecule of interest above the dissociation threshold, relying on infrared multiphoton excitation to induce decomposition. In order to dissociate, a molecule must absorb approximately 20 infrared photons.

The products of the decomposition then recoil from the molecular beam, and those traveling in the correct direction enter the detector, which is placed off the axis of the molecular beam at a particular angle. In the detector, they are ionized, separated according to mass-to-charge ratio by a quadrupole mass spectrometer, and registered using ion counting techniques. A record of ion counts versus time from the laser excitation, known as the time-of-flight spectrum, reflects the time it takes for a particular neutral fragment of the reaction to reach the ionizer from the interaction region. This flight time is related to the velocity of the fragment, which in turn is related to the translational energy released in the reaction.

The techniques used in these experiments have several features important for the study of the decomposition of energetic materials. First, the excitation step using the CO_2 laser infrared multiphoton absorption provides a way of heating the molecule under isolated conditions. After an initial coherent multiphoton absorption step, the infrared photons are sequentially absorbed, proceeding through the high density of states region

known as the quasicontinuum as the molecule is excited higher and higher in the vibrational manifold. At these high levels, the vibrational motions are no longer isolated to a particular part of the molecule, but are spread over its entirety. Furthermore, successive absorption and stimulated emission induced by the high power laser is also similar to collisional excitations and deexcitations in the thermal excitation in the bulk phase. As a result, the vibrational excitation is very similar to that obtained by conventional heating, and the results may be directly related to decomposition studies conducted in bulk phases.

Second, the molecules dissociate under collision-free conditions. This precludes the possibility of secondary bimolecular reactions. Additionally, the fragments travel undisturbed to the detector so their velocities reflect the energy released into translation during the reaction.

Third, the fragments are detected using mass spectroscopic techniques which allow the identification of the chemical makeup of the reaction products. This identification is aided by the fact that the products from different reaction channels tend to have different velocity distributions and shapes in the time-of-flight spectrum, which allows the determination of the identity of all the daughter ions corresponding to a particular parent. The mass spectrometer is also a universal detector, not requiring any prior knowledge of the composition, spectroscopy, or internal energy of a fragment.

The interpretation of the data obtained from photofragmentation translational spectroscopy, the time-of-flight spectrum, is aided by considering a Newton diagram (Fig. 2). In the experiment, the measured velocities are in the laboratory reference frame, rather than in the molecular (center-of-mass) frame. It is the velocity in the center-of-mass frame (from which the translational energy of the fragment is derived) that is of interest. The measured laboratory velocity is the vectorial sum of the initial molecular beam velocity (which defines the velocity of the center of mass) and the velocity of the recoiling fragments in the center-of-mass frame. The Newton diagram is a pictorial presentation of this summing of velocities.

The Newton diagram shown in Fig. 2 has velocities pertinent to the present investigation and will be referred to later in the discussion of the experimental results. At the bottom of the diagram extending upward is a vector, labeled V_{beam} , representing the average molecular beam velocity (the spread in velocities, amounting to roughly 20% is omitted for simplicity). Extending from the tip of this vector is a second one that represents the velocity of a fragment recoiling in the center-of-mass frame. It should be noted that a second vector exists (not shown) that points in the opposite direction and corresponds to the partner fragment in the reaction. The velocity of the second fragment is related to the velocity of the first through

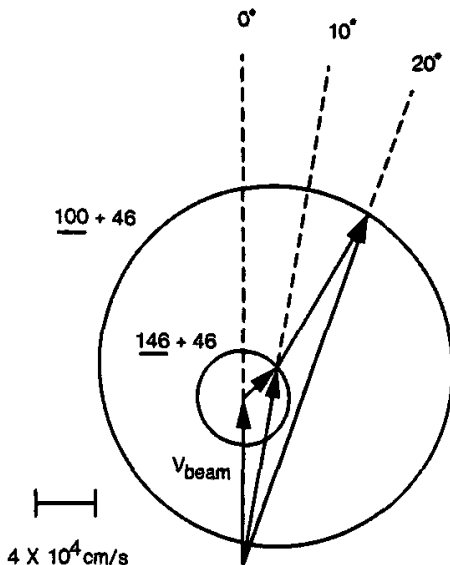


Fig. 2. Newton (velocity vector) diagram for the decomposition of TNAZ. The vector labeled V_{beam} represents the molecular beam velocity. The smaller circle represents the primary NO_2 loss channel with the illustrated center of mass velocity corresponding to the maximum energy released into translation, 7.2 kcal/mol, in the high fluence experiment. The larger circle represents the secondary loss of NO_2 . Again, the velocity shown is for the maximum energy released into translation in the high fluence experiment, 55.2 kcal/mol. The dashed lines indicate the molecular beam-to-detector angles and are appropriately labeled. The numbers are the masses of the recoiling fragments, with the underscore indicating the detected one.

the conservation of linear momentum in the center-of-mass frame. The pair of products related by conservation of momentum is often referred to as being "momentum matched."

The masses used in calculating the velocity of the indicated fragment in Fig. 2 were 146 and 46 amu, which correspond to the pair of fragments produced in the primary dissociation of TNAZ. The velocity shown is for the heavier fragment and was calculated for the maximum translational energy released in the reaction. This information was obtained from the analysis of time-of-flight data collected, which will be discussed later.

The velocity vector in the laboratory frame is shown in Fig. 2 as the resultant vector obtained from summing the molecular beam velocity vector and the velocity vector in the center-of-mass frame. The direction of the laboratory frame vector in this example is at 10° relative to the molecular beam angle. This is the molecular beam-to-detector angle that is determined by the placement of the detector relative to the molecular beam axis.

Infrared multiphoton infrared excitation produces molecules that dissociate in all directions in the center-of-mass frame. Therefore, the vector in Fig. 2 representing the velocity of recoil in the center-of-mass frame is actually one of a family of vectors originating at the tip of the molecular beam velocity vector and pointing in all directions. The resultant vectors from the summation of these with the beam velocity vector all fall on the smaller circle shown in Fig. 2. The point where this circle intersects the line pointing toward the 10° molecular beam-to-detector angle represents the laboratory velocities at which this center-of-mass velocity is observed at this angle. Notice that one such laboratory vector has been discussed already, the one moving faster than the beam velocity. A second intersection of the circle with the 10° line occurs at a slower laboratory velocity, showing that the center-of-mass velocity being considered appears at two laboratory velocities.

The complete Newton diagram for the reaction is more complicated. First, there are a range of center-of-mass recoil velocities, not simply the one considered here. In the complete picture there are many circles centered on the tip of the molecular-beam-velocity vector, each one corresponding to a different velocity of recoil. The contribution of each velocity to the observed time-of-flight spectrum is reflected (in units of energy, rather than velocity) in the center-of-mass translational distribution discussed below. Second, there may be secondary products resulting from the subsequent decomposition of the primary fragments. A part of the Newton diagram illustrating secondary dissociation is shown in Fig. 2 but will be discussed later.

The power of photofragmentation translational spectroscopy was demonstrated in the elucidation of the initial steps in RDX decomposition following infrared multiphoton excitation [9]. In this study it was shown that two competing primary steps were elimination of NO_2 and the triple concerted reaction yielding three methylene nitramine (H_2CNNO_2) fragments. After the primary NO_2 loss channel, the remaining fragment continues to decompose in competing secondary steps—loss of HONO, and loss of a second NO_2 . The methylene nitramine produced in the concerted primary step then decomposes in another two secondary steps to yield HCN and HONO in one and N_2O and H_2CO in the other.

Later studies investigated the thermal decomposition of TNAZ using photofragmentation translational spectroscopy. The details are presented in the following section by first describing the experimental technique used in some detail. This is followed by a presentation of the experimental results that include the time-of-flight spectra collected under conditions of high- and low-laser fluence. Then the forward convolution method of

analyzing the data is explained, followed by the analysis of the TNAZ time-of-flight spectra. Finally, the results are interpreted and discussed with respect to other studies.

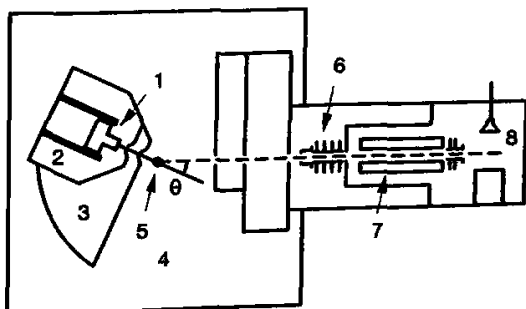
II. The Thermal Decomposition of TNAZ

A. Apparatus

A detailed description of the molecular beam apparatus used, the rotating source machine, is available elsewhere [10]. For the present discussion a general outline of the salient features will be given, referring to the schematic diagram in Fig. 3. The important parts of the rotating source machine are labeled with numbers in this diagram.

The molecular beam is formed by supersonic expansion from a heated oven source (1), shown in Fig. 3. The expansion is then collimated by a skimmer to form the molecular beam (*solid line*) as it passes from the source chamber (2) into the source differential region (3). From there the molecular beam passes through a second skimmer into the main chamber (4). The laser light travels in a direction perpendicular to the plane of the drawing in Fig. 3 and crosses the molecular beam at (5). This point is also on the axis of the detector, which is denoted by the dashed line. The oven source and separately pumped source and source-differential chambers are rotatable as a unit about the axis down which the laser beam travels. This rotation allows the molecular beam to detector angle (θ) to be varied.

Fig. 3. Schematic drawing of the molecular beam apparatus. The labeled parts are: (1) heated oven source, (2) source vacuum chamber, (3) source differential vacuum chamber, (4) main vacuum chamber, (5) crossing point of the laser beam with the molecular beam, (6) electron bombardment ionizer, (7) quadrupole mass spectrometer and (8) Daly ion detector.



From the interaction region (5), those fragments recoiling toward the detector travel to the ionizer (6) of the mass spectrometer. In the flight from the interaction region to the ionizer, the reaction products separate according to their velocities. After ionization, the particles pass through a quadrupole mass spectrometer (7) where they are filtered according to mass-to-charge ratio before their arrival time is registered by a Daly type detector (8) and a multichannel scaler.

B. Methods

The molecular-beam source had been used previously in the study of the unimolecular decomposition of RDX [9]. It consists of a heated reservoir for subliming the solid sample material followed by a chamber near the molecular beam nozzle in which gas is further heated before expansion. The reservoir temperature and nozzle temperature may be varied independently. The carrier gas enters the heated reservoir where the sample material is entrained, then passes through to the nozzle to form the molecular beam. Helium at 34 torr was used as the carrier gas. Solid TNAZ (Fluorochem; Azusa, CA) is recrystallized from CH_2Cl_2 and maintained at 95°C in the source reservoir during the experiment while the nozzle is held at 105°C . The opening of the nozzle is modified to allow formation of the molecular beam by expansion through a 0.5-mm diameter orifice. The expansion is collimated by a skimmer located 2.5 cm downstream from the nozzle. This skimmer is heated to prevent the condensation of TNAZ that would clog the opening if allowed to accumulate. From this skimmer, the molecular beam passes through a differentially pumped region and through a second (unheated) skimmer into the main chamber. The arrangement of the skimmers defines the molecular beam to a divergence of 1° (half angle).

In the main chamber the molecular beam is crossed with the output of a Lumonics TEA-820 pulsed CO_2 laser. Data are collected under two excitation conditions, high and low fluence. For the high fluence experiments the laser light is focused at the crossing of the molecular beam with a 23-cm focal length lens. From the examination of the burn marks in cellophane tape, the laser spot size at the crossing is determined to be 2.4 by 4.4 mm. With a pulse energy of 1.1 J, this results in a fluence of $10.4 \text{ J/cm}^2/\text{pulse}$. For the low fluence experiments, the lens is moved until the laser spot is 5.2 by 5.2 mm at the molecular beam crossing. By reducing the laser discharge voltage and by placing an attenuating screen in the beam near the laser, the pulse energy can be reduced to 382 mJ/pulse , producing a fluence of $1.4 \text{ J/cm}^2/\text{pulse}$.

After excitation from the laser light, molecules may decompose and their fragments recoil from the molecular beam. Those fragments traveling down the detector axis fly 36.7 cm and then are ionized by electron bombardment (after passing through several stages of differential pumping in the detector chamber), are mass selected in a quadrupole mass spectrometer, and their arrival time at the detector is registered using ion-counting techniques. The time-of-flight spectrum is generated by measuring ion counts versus time from the laser excitation using a multichannel scaler. The accumulated signal is then transferred to a computer for storage and analysis.

The molecular beam apparatus is constructed such that the molecular beam source and source differential region may be rotated about the line upon which the laser approaches the molecular beam crossing. This is done so that the molecular beam-to-detector axis angle may be varied.

To measure the velocity distribution of the TNAZ in the beam before dissociation, the source is rotated to send the molecular beam into the detector and the beam is chopped with a single shot time-of-flight wheel. The pulses of gas allowed through the slit in the chopper wheel travel 22.6 cm to the ionizer in the detector. The time-of-flight spectrum is then measured in the usual way (as described above) and the velocity distribution obtained is used in the analysis of the time-of-flight data from the laser-induced decomposition. The molecular beam time-of-flight measurements are made at several mass-to-charge ratios (daughter ions of TNAZ) at the beginning and at the end of each day of data collection in order to confirm that the beam conditions remain stable for that day. These beam time-of-flight measurements are also useful for collecting the mass spectrum of TNAZ, determining the ion flight time through the detector, and for insuring that no decomposition of the compound in the molecular beam source occurs.

C. Experimental Results

From measuring the time-of-flight spectrum of a chopped molecular beam sent directly into the detector, it is found that the molecular beam has an average velocity of 1.1×10^5 cm/sec with a velocity spread of 23% (full width). This information is used later in the analysis of the data.

From the TNAZ mass spectrum obtained from the molecular beam time-of-flight measurements, it is found that the compound easily fragments upon ionization. In fact the signal at the parent mass-to-charge ratio ($m/e = 192$) was only 1% of that obtained at the most abundant peak, of NO_2^+ ($m/e = 46$). That the decomposition of the parent molecule was

occurring during ionization rather than in the molecular beam source was demonstrated by comparing the molecular beam time-of-flight spectrum of the parent mass of TNAZ to that of NO_2 . If the compound were decomposing in the molecular beam source, one would expect the formation of NO_2 . This NO_2 would then be accelerated to a higher velocity in the supersonic expansion than would the undecomposed TNAZ (due to a difference in the velocity slip of the two species) and would result in a difference in time-of-flight spectra measured from signal at $m/e = 192$ when compared to that from $m/e = 46$. No such difference is seen, indicating that the TNAZ emerges from the molecular beam source intact.

The propensity of TNAZ to fragment upon ionization would also make one expect that the products of its decomposition would also tend to fragment when ionized. This expectation is borne out by the experiments discussed here, where care was taken to distinguish the products of the decomposition from the daughter ions formed by dissociation during the ionization of the reaction products. The first strategy is to reduce the laser fluence until only the first decomposition channel is observed. As will be shown below, at high-laser fluence the products of the reaction continue to absorb photons and undergo further decomposition. Second, representative daughter ions of the reaction products are measured to identify the parent. Third, by applying the constraint of conservation of linear momentum of the two recoiling fragments, the matching of pairs of products to a common reaction channel can be confirmed during analysis.

1. Low-Laser Fluence Excitation. By reducing the laser fluence to $1.4 \text{ J/cm}^2/\text{pulse}$ a single reaction channel is observed. Representative time-of-flight spectra under low fluence conditions are shown in Figs. 4 and 5. The highest mass-to-charge ratio (m/e) observed for fragments recoiling from the molecular beam axis due to laser induced dissociation is $m/e = 100$ (the parent ion of TNAZ has a mass-to-charge ratio of 192). The time-of-flight spectrum for this species measured at a detector angle 7° from the molecular beam axis is shown in Fig. 4 as scattered points. As will be discussed below, this spectrum is interpreted as arising from loss of NO_2 due to the laser induced decomposition followed by loss of a second NO_2 upon ionization. The solid line in the data is a fit assuming this scheme.

In a search for other reaction channels, a number of time-of-flight spectra were also collected with the mass spectrometer tuned to other mass-to-charge ratios. Time-of-flight data collected at $m/e = 99, 72, 54, 53, 52, 50, 47, 44, 40, 39, 38, 36, 27, 26$, and 17 all had the same shape as the $m/e = 100$ time-of-flight spectrum and are interpreted as being daughter ions from the same channel as that observed at $m/e = 100$. At $m/e = 46$ (NO_2^+) a new feature is seen in the time-of-flight data. The

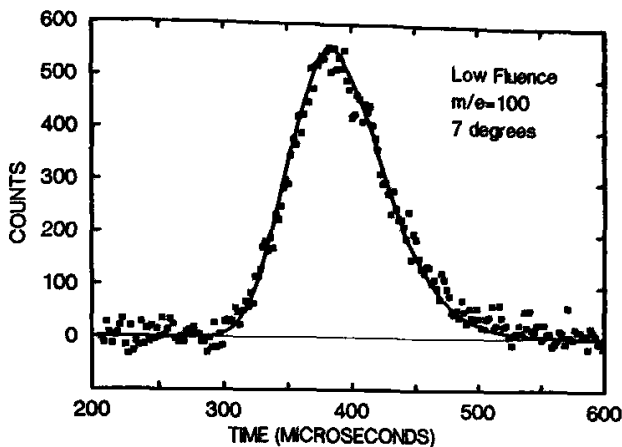
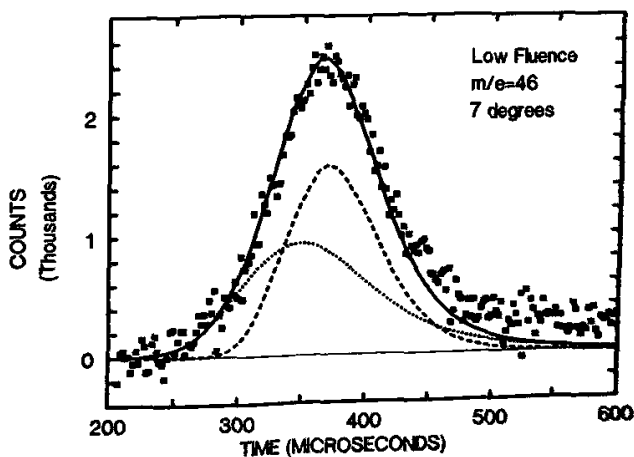


Fig. 4. Time-of-flight spectrum detected at $m/e = 100$ and 7° after low-laser fluence excitation. The scattered points are the experimental data, and the solid line is a fit to the data in which the heavier product of Reaction 1 (primary NO_2 loss) fragments during ionization to yield an ion at $m/e = 100$. The translational energy distribution used in the fit is shown in Fig. 12. As in all the time-of-flight spectra shown, the average level of the background has been subtracted.

Fig. 5. Time-of-flight spectrum detected at $m/e = 46$ (NO_2^+) and 7° after low-laser fluence excitation. The scattered points are the experimental data, and the solid line is a fit using Reaction 1 (primary NO_2 loss) and the translational energy distribution shown in Fig. 12. The dashed line is the component of the fit due to the heavier product of the reaction, and the dotted line is the component of the fit due to the NO_2 reaction product.



$m/e = 46$ data are shown in Fig. 5 as scattered points. The $m/e = 46$ daughter ion of the feature shown in Fig. 4 appears in Fig. 5 peaking near $375 \mu\text{sec}$. Additional signal is seen at faster times. These data are interpreted as arising from the NO_2 that is the partner of the fragment giving rise to the $m/e = 100$ signal shown in Fig. 4. The dashed line in Fig. 5 is the fit to the data obtained from the $m/e = 100$ fit. The dotted line is calculated from this fit using conservation of linear momentum between the recoiling fragments. The solid line represents the sum of the two components, yielding the total fit. Time-of-flight data collected at $m/e = 30$ (NO^+) have the same shape as the $m/e = 46$ data and are interpreted as arising from daughter ions of the two fragments of the single observed channel. No additional channels are seen in the $m/e = 30$ data. Time-of-flight data collected at $m/e = 192$ show no signal, indicating that there is no interference in the data from TNAZ clusters.

Additional data can be collected using the low-laser fluence at other angles. No additional signal is seen under these conditions. At 10° no signal is observed at $m/e = 146$ or $m/e = 145$. The highest mass-to-charge ratio with signal due to laser induced decomposition is the single channel detected at $m/e = 100$ with similarly shaped at $m/e = 99, 52, 40$, and 17 . Again, a faster signal is detected at $m/e = 46$ and 30 . (The $m/e = 30$ was also collected at 20° , and data from these wider angles was used in the analysis to refine the fits but are not shown here.)

2. High-Laser Fluence Excitation. At the higher laser fluence ($10.4 \text{ J/cm}^2/\text{pulse}$) the products of the primary reaction apparently continue to absorb photons and decompose. As in the low-fluence results, the highest mass-to-charge ratio showing laser induced signal is $m/e = 100$. The data collected at this mass-to-charge ratio at 7° are shown as the scattered points in Fig. 6. Although the signal level is lower than that observed at lower laser fluence, the shape of this feature in the time-of-flight spectrum is similar to the one shown in Fig. 4 and is interpreted as arising from the same single primary channel observed in the low-fluence experiment (i.e., loss of NO_2 .) As before, the solid line is a fit to the data from the analysis which will be discussed later.

Signal at other mass-to-charge ratios was collected in a search for evidence of other reaction channels. Proceeding to lower mass-to-charge ratios, all observed time-of-flight spectra resemble the $m/e = 100$ data until $m/e = 54$ is reached. The new aspects of this signal are best seen in the $m/e = 54$ data collected at a detector angle 10° from the molecular beam as shown as the scattered points in Fig. 7. The data peaking at approximately $375 \mu\text{sec}$ are a daughter ion corresponding to the channel shown at $m/e = 100$ (Fig. 6). The faster signal in Fig. 7 is interpreted as arising from

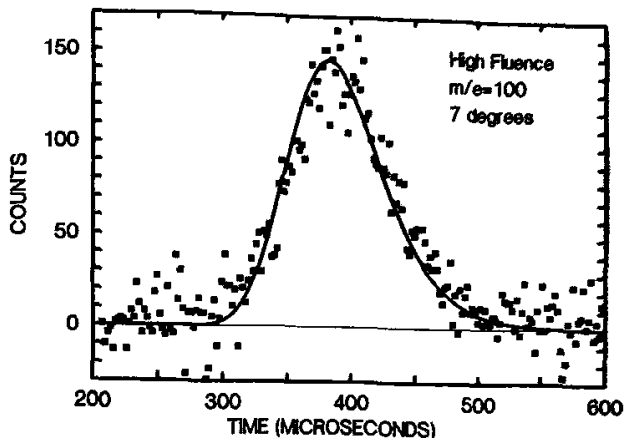
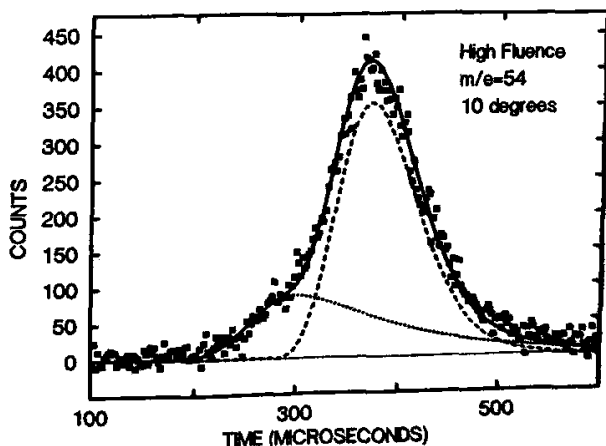


Fig. 6. Time-of-flight spectrum detected at $m/e = 100$ and 7° after high-laser fluence excitation. The scattered points are the experimental data, and the solid line is a fit to the data in which the heavier product of Reaction 1 (primary NO_2 loss) fragments during ionization to yield an ion at $m/e = 100$. The translational energy distribution used in the fit is shown in Fig. 13.

Fig. 7. Time-of-flight spectrum detected at $m/e = 54$ and 10° after high-laser fluence excitation. The scattered points are the experimental data and the solid line is a fit to them. The component of the fit indicated by the dashed line is the heavier product of Reaction 1 (primary NO_2 loss) which fragments upon ionization to yield an ion at $m/e = 54$. The dotted line is the fit for the $m/e = 54$ ion of the heavier product of Reaction 2 (secondary NO_2 loss) using the translational energy distribution shown in Fig. 14.



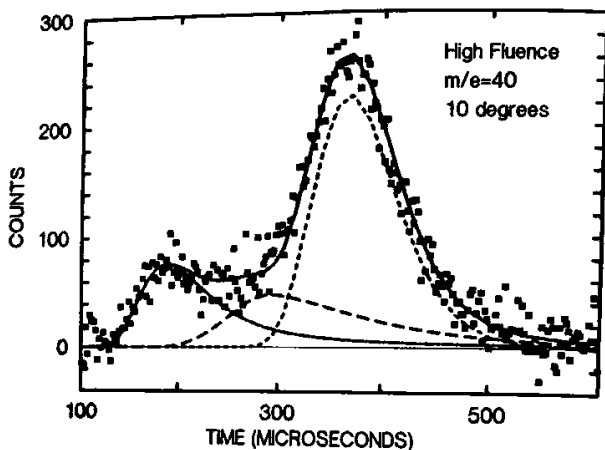


Fig. 8. Time-of-flight spectrum detected at $m/e = 40$ and 10° after high-laser fluence excitation. The scattered points are the experimental data and the solid line is a fit to them. The component of the fit indicated by the shorter dashed line is the heavier product of Reaction 1 (primary NO_2 loss) which fragments upon ionization to yield an ion at $m/e = 40$. The longer dashed line represents the $m/e = 40$ ion of the heavier product of Reaction 2 (secondary NO_2 loss). The dot-dashed line represents the C_3H_4 formed in Reaction 3.

secondary loss of NO_2 as the product of the primary NO_2 loss continues to absorb photons and decomposes. In this interpretation, the reaction product then loses a third NO_2 during ionization to produce $m/e = 54$. The data analysis produces the dashed line that represents a fit to the primary NO_2 loss channel and the dotted line which gives the fit to the secondary NO_2 loss channel. The solid line is a sum of these two which is the total fit to the data.

In continuing to lower mass-to-charge ratios, the time-of-flight spectra resemble the $m/e = 54$ signal (skipping temporarily NO_2^+ at $m/e = 46$) until $m/e = 40$. The $m/e = 40$ data collected at 10° are shown as the scattered points in Fig. 8. A third channel is clearly seen peaking a quite short time near $200 \mu\text{sec}$. This signal is attributed to a tertiary channel in which the secondary reaction product decomposes to give C_3H_4 (detected at $m/e = 40$) by ejecting N-NO_2 . The fit to the primary and secondary reactions is given by the short- and long-dashed lines, respectively. The tertiary channel is shown by the long-dashed line which arises from analysis that only attempts to match the fastest edge of the signal. Again, the solid line is the sum of the fits of the individual channels.

The signal due to NO_2^+ detected $m/e = 46$ at 10° is shown as the scattered points in Fig. 9. This signal contains many contributing components because this mass-to-charge ratio represents not only the NO_2 lost in the

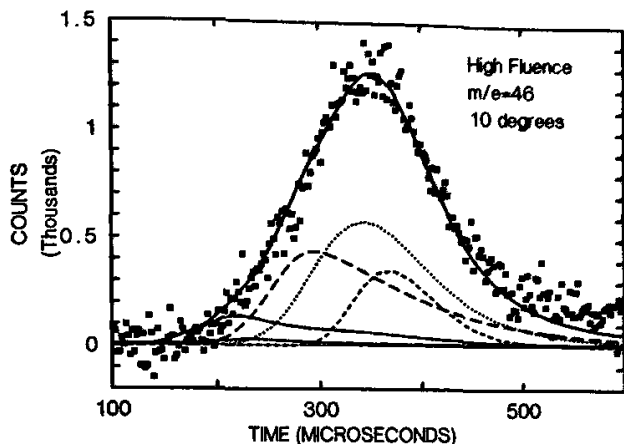


Fig. 9. Time-of-flight spectrum detected at $m/e = 46$ (NO_2^+) and 10° after high-laser fluence excitation. The scattered points are the experimental data and the solid line is a fit. The shorter dashed line and the dotted line are the products of Reaction 1. The longer dashed line and the dash-dot-dot line are the products of Reaction 2. The product of Reaction 3 corresponding to the ejected $\text{N}-\text{NO}_2$ is indicated by the dash-dot line.

primary and secondary steps, but also a significant daughter ion of the heavier counterpart also produced in these reaction channels. All components of the fit fall inside the envelope of the $m/e = 46$ data. The time-of-flight spectrum for $m/e = 30$ at 10° shown in Fig. 10.

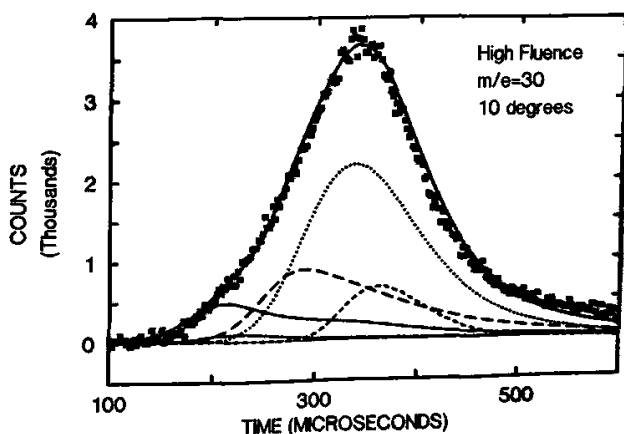


Fig. 10. Time-of-flight spectrum detected at $m/e = 30$ and 10° after high-laser fluence excitation. The scattered points are the experimental data and the solid line is a fit to them. The components of the fit are the same as in Fig. 9.

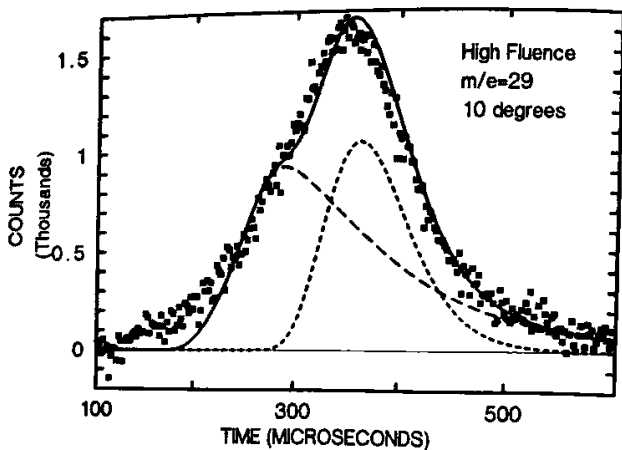


Fig. 11. Time-of-flight spectrum detected at $m/e = 29$ and 10° after high-laser fluence excitation. The scattered points are the experimental data and the solid line is a fit to them. The components of the fit are the heavier product of Reaction 1 (shorter dashed line) and the heavier product of Reaction 2 (longer dashed line). Note the unexplained signal near $175 \mu\text{sec}$.

The sole observation of signal inconsistent with the other channels is found in the $m/e = 29$ data (Fig. 11). In this time-of-flight spectrum, a small amount of additional signal amounting to several hundred ion counts appears in a broad feature. This signal was not assigned to a particular channel, but speculation as to its origin is discussed later.

III. Analysis and Discussion

A. The Forward Convolution Method

As noted earlier, the velocities measured in the time-of-flight spectra are in the laboratory reference frame. The quantities of interest for molecular dissociation are those in the center-of-mass (molecular) frame. The analysis is done to obtain the translational energy released in the center-of-mass reference frame from the measured time-of-flight spectra. In order to do this, the measured time-of-flight data are analyzed using the forward convolution method. In this procedure, the center-of-mass translational energy distribution, the $P(E_T)$, is estimated from the gross features of the measured time-of-flight spectrum. This trial translational energy distribution is then used to calculate the time-of-flight spectrum that it would produce. During this calculation, averaging is performed over the mea-

sured initial molecular beam velocity distribution, molecular beam angular divergence, angular acceptance of the detector, and the finite length of the ionizer. The calculated time-of-flight spectrum is shifted to account for the transit time of the ions from the ionizer to the ion counter and is then compared with the observed spectrum. The trial translational energy distribution is then adjusted to refine the fit to the data and the procedure is repeated until the calculated time-of-flight spectrum matches the data.

For the analysis of the secondary reaction channels, the forward convolution technique is also used, but with additional averaging over the velocities of the fragmenting products of the primary reaction channel [11]. Here, the decomposing species are no longer traveling in a well-collimated molecular beam with a narrow velocity distribution. On the contrary, these species have recoiled from the molecular beam in all directions with velocity distributions defined by the primary decomposition.

The problem is illustrated in the Newton diagram in Fig. 2. The long arrow extending from the tip of the vector for the primary channel center-of-mass velocity (discussed earlier) represents the velocity of a fragment produced in a secondary dissociation step. Specifically, it corresponds to the heavier fragment in the primary step losing a second NO_2 group. The velocity vector is for the heavier of the secondary fragments (with a molecular weight of 100 amu) recoiling with the maximum translational energy released, which was obtained from the analysis of the TNAZ data. The measured laboratory velocity is the vectorial sum of the molecular beam velocity, the primary velocity, and the secondary velocity. This resultant vector is shown by the long arrow extending from the base of the molecular beam velocity vector to the tip of the secondary velocity vector.

As is true for the primary dissociation step, the secondary fragments recoil in all directions, so there is not a single secondary vector, but a family of them. The tips of the resultant vectors obtained from summing each of these secondary velocities with the molecular beam velocity and with the primary velocity all fall on the large circle in Fig. 2. As is true for the primary steps, the laboratory velocities corresponding to these center-of-mass velocities may be obtained from the intersection of these circles with the lines indicating the molecular beam-to-detector angles.

The full Newton diagram is much more complicated than what is shown in Fig. 2. First, there is a set of secondary velocity vectors originating at the tip of every primary velocity vector. The circle corresponding to only one such set is shown. Second, although the detected laboratory velocity must be in the plane containing the molecular beam and detector axes (the plane of Fig. 2), the primary and secondary vectors may be out of this plane. For example, the primary step may be such that the fragment velocity is out of the plane, but the secondary velocity may be such that the resultant

(laboratory) velocity is again in the plane. As a result, the full Newton diagram is composed of spheres, rather than the circles shown in Fig. 2.

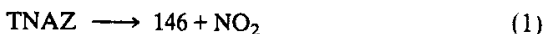
To obtain the calculated time-of-flight spectrum for the secondary channel from its trial translational energy distribution, an average must be performed over all primary velocities and angles of recoil from the beam as well as the same instrumental parameter functions considered in the primary step.

In analyzing data from an experiment on a molecule that decomposes via several reaction channels (including primary and secondary steps), the strategy is to begin with the highest mass-to-charge ratio that is observed. Often this is due to a single reaction channel and the translation energy distribution may be uniquely defined by these data. In proceeding to lower mass-to-charge ratios, additional reaction channels are observed as well as daughter ions of the previously analyzed channel. The signal from these channels may overlap, but since the translational distribution for one of the channels has already been obtained, its contribution to the signal may be established and the translational energy distribution for the second channel may be determined. This division of the signal into its components is further aided by the fact that different channels often appear at different velocities due to different amounts of energy released and to different masses of the fragments. As one proceeds to lower mass-to-charge ratios, the time-of-flight spectra become more complicated as more reaction channels appear. By continuing the strategy of using information from the data obtained at higher mass-to-charge ratios to identify the signal from daughter ions, these time-of-flight spectra may be interpreted and the new channels analyzed. As a check, the center of mass velocities of two fragments arising from a single reaction channel must be related through the conservation of linear momentum. As a result, the time-of-flight spectrum of the second fragment of a pair may be calculated from the analysis of the first. This may be used to confirm that the correct reaction channel is being used in the analysis and to rule out other possibilities. Finally, all daughter ions must be consistent with the makeup of the parent, allowing identification of a particular parent when all daughter ions have been collected, and the shapes of their features in the time-of-flight spectrum indicate they are from a common reaction product.

B. Low-Laser Fluence

The extensive fragmentation of TNAZ and its reaction products upon electron impact ionization necessitates caution in the assignment of features in the time-of-flight data to specific reaction channels. To identify the primary decomposition step, the laser fluence is reduced until a single

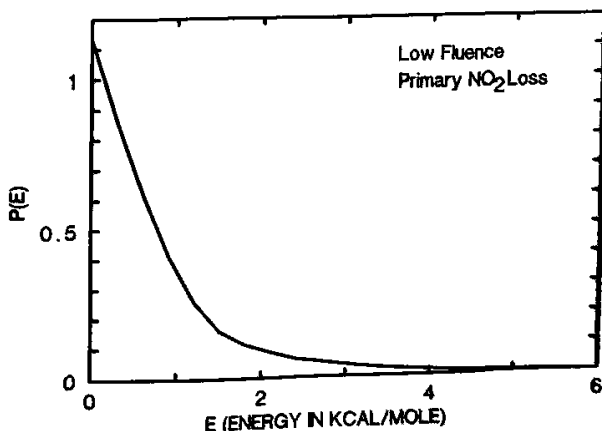
feature appears in the time-of-flight spectrum. The highest mass-to-charge ratio at which this feature appears is $m/e = 100$ (Fig. 4). The parent mass of TNAZ is at $m/e = 192$, so the $m/e = 100$ signal has arisen from loss of two NO_2 groups. That one NO_2 is lost in a laser-induced decomposition step and the other is lost during ionization can be proven by considering the momentum-matched reaction products. To do this, the $m/e = 100$ data are analyzed assuming they came from primary loss of NO_2 . The derived center-of-mass translational energy distribution is shown in Fig. 12. This distribution is then used to predict the $m/e = 46$ time-of-flight spectrum which arises from the NO_2^+ coming from ionization of NO_2 formed in the reaction and appearing as a daughter ion of the heavier fragment. As is seen in Fig. 5, all of the signal is accounted for by the single proposed channel



where the heavier fragment in the reaction is identified by its molecular weight in amu. If there were additional NO_2 loss channels, there would be additional signal at $m/e = 46$ arising from the NO_2 produced as well as from fragmentation of the heavier partner. Therefore, TNAZ decomposes by a single reaction pathway (Reaction 1) after low-fluence excitation. This is contrast to the high-fluence excitation, which results in sequential NO_2 loss.

The shape of the translational energy distribution reveals information on the dynamics of the dissociation. The translational energy distribution shown in Fig. 12 for Reaction 1 peaks at zero kinetic energy and extends to

Fig. 12. The translation energy distribution for primary NO_2 loss (Reaction 1) after low-fluence laser excitation. The distribution extends to 5.7 kcal/mol.



5.7 kcal/mol and corresponds to an average energy of 0.85 kcal/mol released into translation. It should be noted that the heavier fragment requires a minimum of 1.3 kcal/mol released into translation to reach 7° . As a result, the shape of the translational energy distribution below 1.3 kcal/mol is simply an extrapolation of the rest of the curve. The NO_2 fragment provides information down to 0.4 kcal/mol, but some of this signal is overlapped by signal due to the other fragment.

The low translational energy released indicates that the reaction proceeds via simple bond rupture. In this interpretation, there is no additional exit barrier to the breaking of the bond and the available energy above the threshold for dissociation is statistically distributed among the vibrational degrees of freedom in the excited molecule. The coordinate corresponding to the dissociation path reflects this statistical distribution of energy. It is exceedingly unlikely that all of the available energy will appear in translation, thus the distribution peaks at low energy and then monotonically decreases to zero. As there is no barrier to the reaction, the fragments are not accelerated as they recoil from each other so the statistical distribution of energy in the dissociation coordinate is preserved in the derived translational energy distribution.

The derived translational energy distribution can be compared to other related molecules studied by photofragmentation translational spectroscopy. In the infrared multiphoton decomposition of RDX [9] a primary NO_2 loss channel is observed. The derived translation energy distribution for this channel in RDX is very similar to the one derived for TNAZ, peaking at zero and extending to about 9 kcal/mol. Similar NO_2 loss channels in the decomposition of nitroalkanes [8] also have translational energy distributions peaking at zero and extending to approximately 10 kcal/mol.

C. High-Laser Fluence

High fluence excitation results in primary NO_2 loss followed by additional decomposition as the fragments absorb more photons. First, the primary NO_2 loss channel will be considered. As in the low fluence excitation experiments, the highest mass-to-charge ratio exhibiting laser induced signal is $m/e = 100$. This is assigned to loss of NO_2 (Reaction 1) due to infrared multiphoton dissociation followed by NO_2 loss during ionization. The translational energy distribution derived for this channel is shown in Fig. 13. The shape of the distribution is quite similar to the one derived for the low fluence case, but has an average energy of 1.1 kcal/mol and extends to 7.2 kcal/mol. The signal-to-noise ratio in the high fluence experiment is a bit worse than in the low fluence experiment (compare

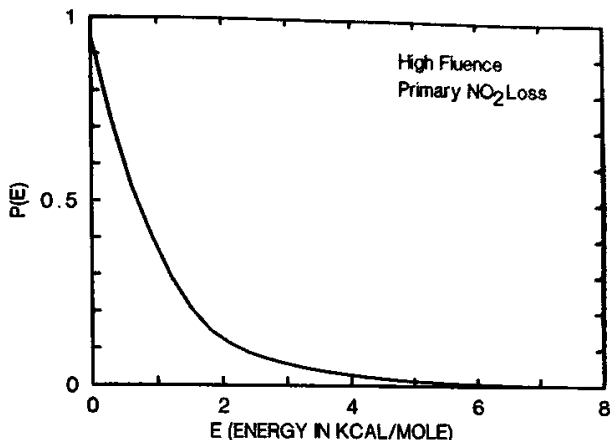


Fig. 13. The translation energy distribution for primary NO_2 loss (Reaction 1) after high-fluence laser excitation. The distribution extends to 7.2 kcal/mol.

Fig. 4 to Fig. 6). This is due to the depletion of the heavier primary product due to further infrared multiphoton dissociation. As a result, the fit to the primary fragment is refined using another daughter ion which has a better signal-to-noise ratio, $m/e = 54$, shown in Fig. 7.

The first evidence of secondary dissociation appears in the time-of-flight spectrum of $m/e = 54$. This ion corresponds to a loss of a total of three NO_2 groups from TNAZ. Since the ion giving the $m/e = 100$ differs from the $m/e = 54$ ion by one NO_2 group, it is reasonable to expect that the faster $m/e = 54$ signal is due to secondary decomposition of the heavier fragment (produced by Reaction 1) via loss of NO_2



where the fragments are again denoted by their molecular weight. The heavier fragment of this reaction then loses another NO_2 group upon ionization.

The translational energy distribution derived from the secondary NO_2 loss channel is shown in Fig. 14. It extends to 55.2 kcal/mol and releases an average of 11.7 kcal/mol into translation. The shape of this curve is defined by the data collected at molecular beam-to-detector angles of 7, 10, and 20°. The importance of fitting the 20° data can be appreciated by considering the Newton diagram in Fig. 2. At 7 and 10° both primary and secondary channels are observed, but at 20° the secondary channel is all that is seen since the primary channel does not release enough energy into translation for the fragments to recoil to 20°. The 20° data allow the

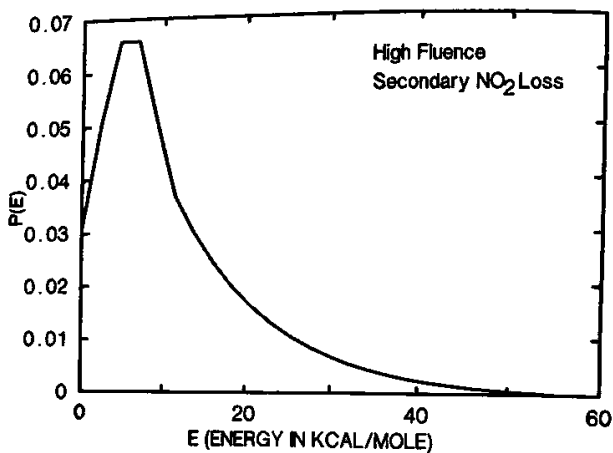


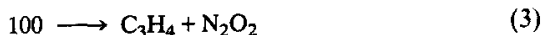
Fig. 14. The translation energy distribution for secondary NO_2 loss (Reaction 2) after high-fluence laser excitation. The distribution extends to 55.2 kcal/mol.

elucidation of the low energy part of the translational energy distribution which is obscured by the primary channel at smaller angles. In contrast to the primary reaction steps, the secondary translational energy distribution can be measured all the way down to zero translational energy, since the primary step has already released enough energy to carry some of its fragments clear of the molecular beam. It is the fit of the 20° data that requires the translational energy distribution to peak away from zero. The 7° and 10° data are insensitive to this part of the distribution. The high energy portion of the translational energy distribution, on the other hand, is determined by the fastest signal at all angles.

The shape of the translational energy distribution for the secondary NO_2 loss and the energy released are significantly different from the primary NO_2 loss. This would imply a small barrier to the loss of the second NO_2 and would account for the higher translational energy release and the peak away from zero as the fragments are accelerated away from each other during dissociation. It is interesting to compare these results to the sequential NO_2 loss channel observed for RDX [9]. As mentioned above, the primary NO_2 loss steps are very similar in RDX and TNAZ. Additionally, substantially more translational energy is released in the second NO_2 loss step than the first in each molecule. For TNAZ, the maximum translational energy is 55.2 kcal/mol and for RDX it is near 30 kcal/mol. The shape of the two translational energy distributions differs, however, at low energy.

For RDX the distribution peaks at zero, but for TNAZ the peak is near 5 kcal/mol. The RDX data may have been obscured in the low energy part of the secondary NO_2 loss due to the many other channels participating in the decomposition of this molecule. One may speculate that the secondary loss of NO_2 in RDX also proceeds over a small barrier, which would explain the noticeably higher translational energy released in the second NO_2 loss step compared to the first.

All time-of-flight spectra are consistent with the sequential loss of two NO_2 groups as one proceeds to lower mass-to-charge ratio until $m/e = 40$. At this mass-to-charge ratio a new feature is seen in the time-of-flight spectrum. This feature is the fastest in any of the TNAZ time-of-flight measurements. A corresponding peak does not appear at $m/e = 41$, but it does appear at $m/e = 39, 38, 37,$ and 36 . This feature must therefore be due to C_3H_4 . Note that this fragment can be found in the hydrocarbon portion of the ring in TNAZ. That the $m/e = 40$ data are due to the parent mass of this reaction product can be demonstrated by inspecting other time-of-flight spectra. The $m/e = 46$ data (Fig. 9) show no signal as fast as the $m/e = 40$ data, showing that the fragment does not have a NO_2 group attached. As was already seen at $m/e = 54$, there is no fast signal due to $\text{C}_3\text{H}_4\text{N}$ which could have been the parent mass of the $m/e = 40$ signal. By elimination, the $m/e = 40$ signal is indeed from the parent ion of the reaction fragment. Also noting from the other time-of-flight data that the fast $m/e = 40$ data are the fastest signal measured indicates that the C_3H_4 must have recoiled from something heavier than itself (as a consequence of the conservation of linear momentum). This suggests that the reaction channel is



The 100 amu fragment in this scheme is generated by the sequential loss of NO_2 as discussed above.

The reaction channel that produces the C_3H_4 is a tertiary process, the analysis of the detailed translational energy distributions is beyond the scope of the software used in the forward convolution treatment of the data. In addition, the information derivable from such an analysis is limited since the velocity of the tertiary products must be averaged over the secondary product velocity and angular distributions (which have already been averaged over those of the primary). Although the exact shape of the translational energy distribution cannot be derived for Reaction 3, the maximum energy released and the qualitative shape may be obtained.

First, for the derivation of the maximum energy released in the tertiary channel it should be noted how the fastest signal due to sequential decompositions at a given angle arises. When the velocity vectors corresponding to the maximum translational energy released in each step are in the same direction and the resultant vector lies along the detector angle, then the maximum velocity signal is obtained. If one is interested in the maximum energy release for the final step (as is the case discussed here) one may simply combine the first steps into a "pseudo-primary" step and consider the final step as a secondary step. If the maximum energy for the pseudo-primary step is taken to be the sum of the primary and secondary steps and the masses of the two recoiling NO_2 fragments are combined and scaled to give the same maximum velocity observed in the primary and secondary decomposition, then the fastest edge of the data may be fit with a "secondary" process corresponding to Reaction 3. This is what was done to fit the fastest signal in the $m/e = 40$ data shown in Fig. 8. The maximum energy released in this step is 29 kcal/mol according to this analysis.

Also, a rough idea of the shape of the translational energy distribution may be obtained from the fit. If a monotonically decreasing function is used, there is too much slower signal. A distribution peaked away from zero fits much better. This implies that there is a strong repulsion between the recoiling fragments that accelerates them apart.

The NO_2^+ signal appearing at $m/e = 46$ is quite useful since it must be consistent with the proposed reaction mechanism. Since TNAZ contains three NO_2 groups, almost every possible reaction channel will give rise to a signal at $m/e = 46$ for one or both fragments. An exception is the tertiary channel, since N_2O_2 may not necessarily produce a signal at $m/e = 46$. If all the $m/e = 46$ signal is accounted for by predicting the time-of-flight spectrum using information derived from signal collected at other mass-to-charge ratios, one can be confident that no spurious channels have been included. In addition any obvious parts of the observed signal not accounted for by the fits will indicate that another channel must be included. The second test is not as stringent as the first, since the weight of each component in the fit may compensate for a missing channel.

Figure 9 shows the data collected for $m/e = 46$ at 10° . The fit is obtained by including all the signal calculated for the momentum-matched NO_2 and from the NO_2^+ daughter ion from the primary and secondary channels. As can be seen, the calculated components are consistent with the observed data.

Figure 10 shows the $m/e = 30$ (NO^+) signal. This signal is important for the same reasons cited for the $m/e = 46$ data, that is to check the consistency of the proposed mechanism. The $m/e = 30$ is especially important

because any HONO elimination will appear as fast signal at this mass-to-charge ratio [8,9]. Also, evidence of nitro-nitrite rearrangement [5,8] followed by NO elimination would appear here. Again, the proposed mechanism is consistent with the observed data when the analysis of the other signals is used to predict this one.

D. Comparison with Other Studies

So far the discussion has focused on channels that have been observed and have been shown to be important in the initial decomposition of TNAZ. Equally important is the demonstration of what channels are not important and do not play a role in the initial unimolecular steps. Evidence of concerted dissociation of the TNAZ ring analogous to the triple concerted reaction in RDX would appear as the parent ion of methylene nitramine at $m/e = 74$, as well as at its fragments at $m/e = 47, 44, 27$, or 30. No evidence of additional fragments were found at any of these masses or at any of the likely daughter ions. There was no evidence for the molecular elimination of HONO. This was searched for by looking for a fast component in the $m/e = 30$ (NO^+) and $m/e = 17$ (OH^+) time-of-flight spectra. Inspection of the $m/e = 162$ and $m/e = 116$ data, which represent the heavier fragment of the reaction channel eliminating NO and this fragment after losing NO_2 in the ionization step, respectively, show no evidence of this process. In addition, no additional channels appear at the N_2O or CO_2 masses.

The conclusion drawn that the first two steps in the decomposition of TNAZ involve NO_2 loss agrees with the observation by Brill and co-workers [5] that gaseous NO_2 was the most abundant species in the initial phases of the thermal decomposition of bulk TNAZ. That the NO_2 concentration decreases from its initially observed level in the bulk study is evidence that this species is already undergoing significant secondary reactions at the time of its initial appearance; yet the surmise that the NO_2 is a primary product is correct. Additionally, the observation that no methylene nitramine formation occurs agrees with the same conclusion drawn from the bulk study where the $\text{N}_2\text{O}/\text{H}_2\text{CO}$ pair was not present. However, the absence of NO as an initial product in the molecular beam experiment, shows that the NO observed in the bulk decomposition study is not due to gas phase unimolecular nitro-nitrite isomerization followed by NO loss.

With respect to the RDX decomposition observed in the previous molecular beam study [9], the TNAZ decomposition is much simpler. In the TNAZ study, no concerted ring decomposition was observed analogous to what was observed in the triple-concerted reaction of RDX. The

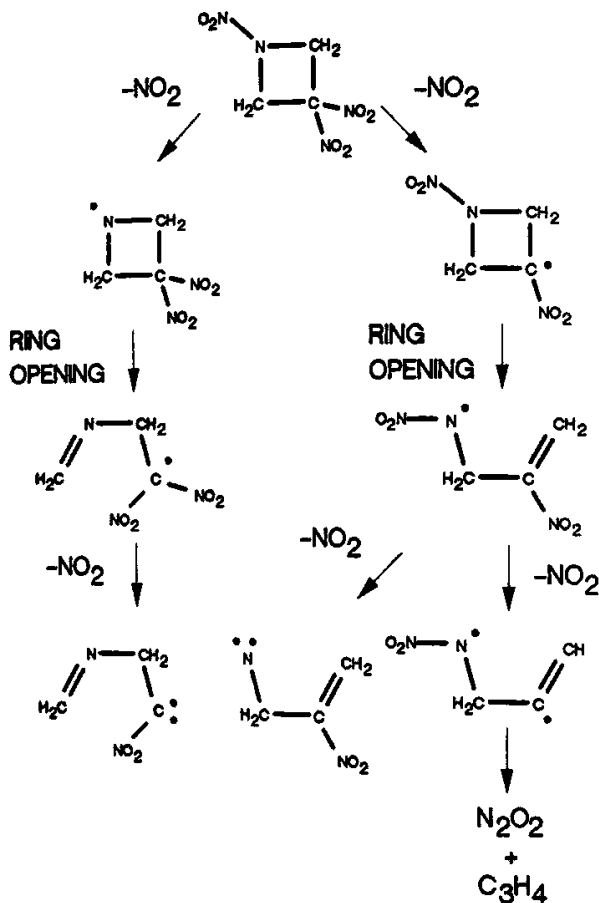


Fig. 15. Reaction summary. The series of reactions that yield the observed products in the decomposition of TNAZ are shown. Since the present method cannot distinguish the position of the NO_2 lost in each step, all possible branches are included.

RDX did contain a reaction pathway involving sequential NO_2 loss, however, analogous to that in the decomposition of TNAZ. The energy released into translation in the primary NO_2 steps in the two molecules is similar, but in the second NO_2 loss step, TNAZ released more energy into translation. In contrast to RDX, no secondary HONO loss was observed in TNAZ after the initial NO_2 loss.

The reaction scheme consistent with the observed time-of-flight spectra is shown in Fig. 15. These data are sensitive to the sequential loss of

NO_2 fragments but cannot determine the order of their removal directly. As a result, the reaction scheme is presented with all the possible branches. The branch leading to the production of C_3H_4 occurs as drawn, but other branches may compete.

By examining the intermediates in the reaction scheme, one may speculate on the origin of the unexplained signal in the $m/e = 29$ (HCO^+) time-of-flight spectrum. For example, the intermediates produced in the ring opening step may reform a cyclic structure. One possibility is the attack of an O atom on the NO_2 group attacking the double bond. This would produce a six-membered ring. It is possible that such a structure could be the fragment, producing a species that contains the HCO species needed to form the $m/e = 29$ fragment.

IV. Summary

After infrared multiphoton excitation of TNAZ in a molecular beam, the molecule decays by a series of reaction steps. As is shown by the lower-laser fluence results, the sole primary reaction channel is the loss of NO_2 . Under higher fluence reaction conditions, the remaining fragment dissociates by losing a second NO_2 fragment. After the loss of two NO_2 groups, the remaining fragment decomposes into C_3H_4 and N_2O_2 . This tertiary step suggests that in some of the molecules the initial NO_2 groups lost are from the *geminal*-dinitroalkyl group. There is no evidence of HONO elimination, nitro-nitrite rearrangement followed by NO loss, or a concerted-ring scission as seen in RDX. The reaction scheme consistent with this experiment is summarized in Fig. 15.

Molecular beam studies provide a useful compliment to bulk phase decomposition studies. The knowledge of which steps are the initial ones in the decomposition will allow the results of bulk phase studies to be analyzed with an eye toward understanding the secondary bimolecular reactions and the role of condensed phase chemistry. The molecular beam studies are also useful in conjunction with theoretical efforts. The dynamics of TNAZ decomposition should be theoretically tractable and when available they will be easily tested against molecular beam results.

ACKNOWLEDGMENT

This work was supported by the Office of Naval Research under Contract No. N00014-89-J-1297.

REFERENCES/ENDNOTES

1. HMX is octahydro-1,3,5,7-tetranitro-1,3,5,7-tetrazocine.
2. RDX is hexahydro-1,3,5-trinitro-1,3,5-triazine.
3. HNDZ is 1,3,3,5,7,7-hexanitro-1,5-diazacyclooctane.
4. DNNC is 1,3,5,5-tetranitrohexahydropyrimidine.
5. Y. Oyumi and T. B. Brill, *Combust. Flame*, **62**, 225 (1985).
6. Y. Oyumi and T. B. Brill, *Combust. Flame*, **68**, 209 (1987).
7. Y. Oyumi, T. B. Brill, A. L. Rheingold and T. M. Haller, *J. Phys. Chem.*, **89**, 4317 (1985).
8. A. M. Wodtke, E. J. Hints and Y. T. Lee, *J. Phys. Chem.*, **90**, 3549 (1986).
9. X. Zhao, E. J. Hints and Y. T. Lee, *J. Chem. Phys.*, **88**, 801 (1988).
10. A. M. Wodtke and Y. T. Lee, *J. Phys. Chem.*, **89**, 4744 (1985).
11. X. Zhao, PhD Thesis, University of California, Berkeley, 1988.

3

Studies of Molecular Dissociation by Means of Ultrafast Absorption and Emission Spectroscopy and Picosecond X-Ray Diffraction

P. M. Rentzepis and B. Van Wonterghem

I. Introduction

Molecular dissociation is a large field that encompasses gas phase reactions such as the dissociation of large hydrocarbons, combustion of fuels, liquid phase organic and inorganic reactions, surface catalyzed reactions; practically every molecule dissociates under the appropriate conditions. In addition, another important process involves the rapid dissociation of energetic materials such as propellants and explosives.

Even though a vast amount of research has been devoted to the understanding of mechanisms of dissociation, with few exceptions (e.g., small molecules in the gas phase,) the dissociation mechanism of molecules and the structure of intermediate states and species, especially of large energetic molecules in the condensed phase, remains unknown.

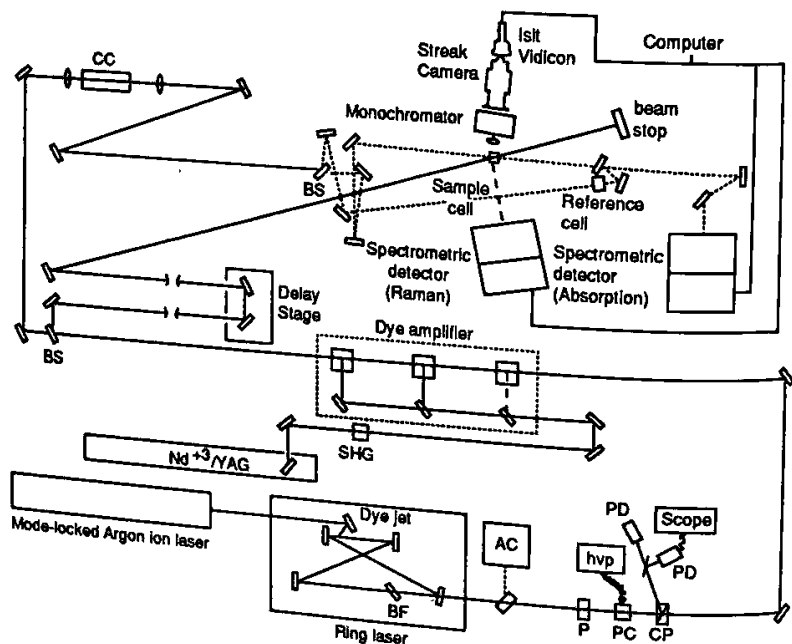
Here, experimental results are presented that suggest that the decomposition of haloaromatics in the condensed phase, proceeds via the triplet manifold. We also present data that help to identify the intermediate states, their kinetics, and the radicals formed as a result of the photodissociation process. Additionally, a new method, picosecond x-ray diffraction (PXR) is described. This method is capable of time-resolved x-ray diffraction in the picosecond scale and has the potential of generating a set of diffraction histograms which depict, in real time, the evolution of the structure of excited states and intermediates during decomposition or in the course of a chemical or biological reaction. Processes such as dissociation, isomerization, melting, and nucleation are but a few examples that

can be investigated by means of PXR with picosecond and subpicosecond time resolution and structural definition equal to normal, cw, x-ray diffraction.

II. Photodissociation of Haloaromatics

In a most interesting research paper, Bersohn [1] observed by means of the angular distribution of fragments, that the iodonaphthalene dissociation rate was about 10 times slower than the dissociation of methyl iodide (0.5 ps vs. 0.07 ps, respectively). Similar experiments with a homologous series of bromine substituted aryl compounds exhibited smaller anisotropy values and corresponding longer excited state lifetimes. The comparable rates of the iodo compounds were two orders of magnitude larger than the analogous bromo compounds. This suggested that intersystem crossing plays a dominant role in the dissociation mechanisms of these compounds. By means of ultrafast spectroscopy, we have been able to observe the

Fig. 1. Experimental system for absorption and emission ultrafast spectroscopy.

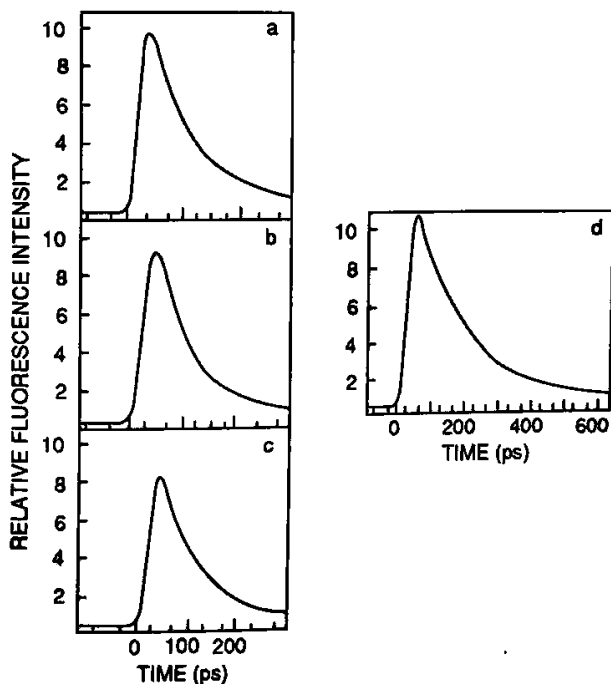


intermediate states and measure the lifetimes of all the steps involved during the course of this photodissociation process [2].

The data presented are in the form of time-resolved absorption and emission spectra obtained by the use of the experimental system shown in Fig. 1. This optical system is based upon a cw-mode-locked Nd/YAG and dye laser. The pulse duration can be tuned from 100 to 0.1 ps by means of etelons and compression techniques.

The materials used are spectra grade and further purified by recrystallization or passing through a column of activated alumina to eliminate impurities to the level necessary to avoid solvent or spurious fluorescence. The picosecond data are recorded either via a streak camera, emission, or by means of imaging devices for absorption. The data are analyzed and plotted by a microvax computer [3]. Typical time-resolved emission data are shown in Fig. 2 for bromonaphyls which have been excited by a 266-nm,

Fig. 2. Time-resolved emission of bromonaphthalenes in hexane at room temperature resulting from excitation by a 266-nm, 10-ps pulse. The emission is within the range of 310–550 nm. Plots of emission intensity vs. time (ps) for: (a) 1-bromonaphthalene, (b) 1-bromo-2-methylnaphthalene, (c) 1-bromo-4-methylnaphthalene, and (d) 2-bromonaphthalene.



10-ps pulse. For chloronaphthalenes, the fluorescence lifetimes of the lowest electronically excited state of 1-chloronaphthalene and 2-chloronaphthalene in hexane at 20°C are 2.4 and 3.3 ns, respectively. The time-resolved emission of hexane solutions of 1-bromonaphthalene, 1-bromo-2-methylnaphthalene, and 1-bromo-4-methylnaphthalene are shown in Figs. 2a-c, respectively. From these curves, the fluorescence lifetime of bromonaphthalene is calculated to be approximately 75 ± 10 ps. The 2-bromonaphthalene fluorescence lifetime (Fig. 2d) is measured to be twice as long as the 1-bromo analogs (i.e., 150 ± 10 ps). Note that the lifetime of 1-(chloromethyl)naphthalene is 450 ps, which is shorter by a factor of 4 than 1-chloronaphthalene. Similar experiments to the chloronaphthalenes were also performed with bromoanthracenes. These results are discussed and listed in Table I.

A. Haloanthracenes

Hexane solutions of 9-bromoanthracene and 9,10-dibromoanthracene were excited with a single 355-nm, 1-ps pulse. The fluorescence of 9-bromoanthracene displayed a biphasic decay which was resolved by using biexponential computer fittings. The short- and long-lifetime components

Table I. Room Temperature ($\sim 20^\circ\text{C}$) Fluorescence Lifetimes of Halonaphthalenes and Haloanthracenes in Hexane

Sample	λ (nm)	τ_f (ps)	τ_f (ns)
4, 4-dibromobiphenyl	265	30	
4-bromobiphenyl	265	35	
1-bromonaphthalene	265	75	
1-bromo-4-methylnaphthalene	265	80	
1-bromo-2-methylnaphthalene	265	72	
2-bromonaphthalene	265	150	
1-(chloromethyl)naphthalene	265	490	
2-(bromomethyl)naphthalene	265	n.d. ^a	
1-chloronaphthalene	265	2400	
2-chloronaphthalene (zone refined > 99%)	265	3300	
2-chloronaphthalene	265	3500	
9-bromoanthracene	355	100	
9, 10-dibromoanthracene	355	1300	
2-iodoanthracene	265	14	
9-iodoanthracene	265	35	
2-iodoanthracene	355	17	
9-iodoanthracene	355	55	

^an.d., not detected.

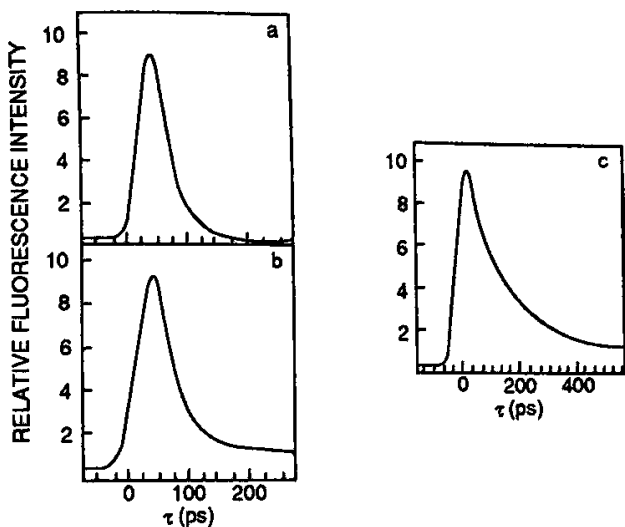


Fig. 3. Emission decay kinetics of 9-bromoanthracene dissolved in hexanes. The sample was excited with a 355 nm pulse. $310 < \lambda_n < 550$ nm, temperature, 20°C. (a) 1-bromonaphthalene, (b) 1-bromo-2-methylnaphthalene, (c) 2-bromonaphthalene in hexane.

were determined to be 100 ps and ~ 3 ns, respectively. The amplitude of the short-lifetime component is about five times larger than that of the long component. A single exponential decay with a time constant of 1.3 ns was found to fit the decay of 9, 10-dibromoanthracene. The data recorded by the streak camera and the computer fit for 9-bromoanthracene are shown in Fig. 3.

2-Iodoanthracene and 9-iodoanthracene in hexane were also excited with a single 355-nm pulse. The emission kinetic data recorded by the picosecond fluorimeter are shown in Fig. 4a and b. When 2-iodoanthracene is excited with a 266-nm pulse, the fluorescence decays exponentially with a lifetime of 14 ± 3 ps. However, when the sample is excited with a 355-nm pulse, the fluorescence decay becomes biexponential, with a short-lifetime component of 17 ± 4 ps and a long component of 3.4 ns. These results are shown in Fig. 4. The long-life component is essentially the same as the lifetime of anthracene in the same solvent. hexane. The amplitude ratio of the short- to the long-lifetime component was calculated to be 15:1. The 9-iodoanthracene fluorescence decay lifetime was also biphasic. The short component of the 9-iodoanthracene was 40 ± 10 ps when excited with a 265-nm pulse and 60 ± 10 ps after 355-nm excitation. A summary of the fluorescence kinetic data is presented in Table I.

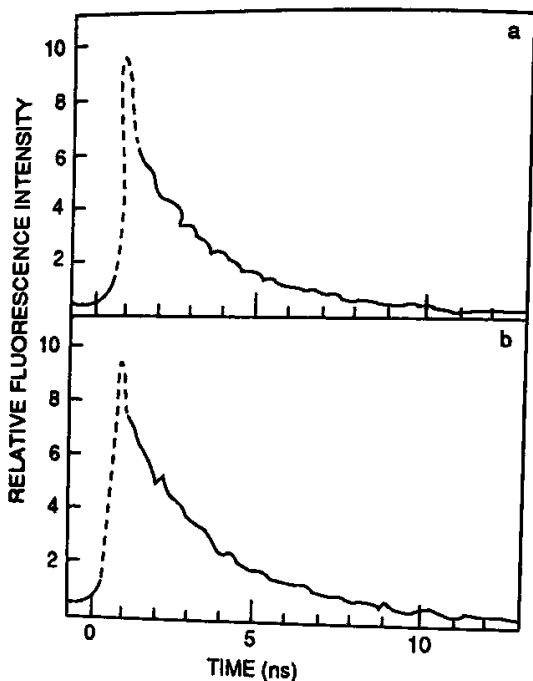


Fig. 4. Time-resolved fluorescence at low streak speeds of (a) 2-iodo and (b) 9-iodoanthracene in hexane solutions excited by a 355-nm pulse. The lifetime of the long-lifetime component is 3.4 ± 0.4 ns for both compounds, and is the same as that of anthracene.

B. Transient Absorption Spectra of Halonaphthalenes

Transient absorption spectra of bromonaphthalenes were measured at 25, 100, and 500 ps after excitation with a single picosecond pulse. The data for 1-bromonaphthalene in hexane are shown in Fig. 5a, b, and c for 25, 100, and 500 ps, respectively. The transient spectrum of 1-bromonaphthalene in the range of 400–480 nm, recorded 25 ps after excitation, is shown in Fig. 5a. This spectrum displays the expected diffused band structure of excited singlet–singlet transitions of large fused aromatics but still maintains some characteristics of the ground state singlet–singlet S_0 – S_1 absorption (Fig. 5b) spectrum. In fact, the 100-ps (Fig. 5b) spectrum is a superposition of the 25- and 500-ps (Fig. 5c) spectra. The 500-ps (Fig. 5c) spectrum displays a 425-nm peak and practically no intensity at long wavelengths. We believe that Fig. 5c displays the spectrum of the $T_n \leftarrow T_1$ absorption.

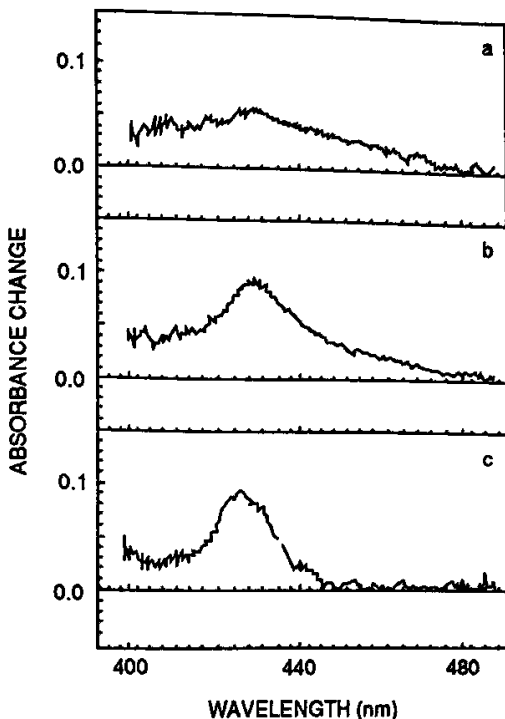


Fig. 5. Transient absorption spectra of 1-bromonaphthalene in hexane at room temperature excited with a 266-nm, 1-ps pulse, recorded at (a) 25 ps after excitation, (b) 100 ps after excitation, (c) 500 ps after excitation.

C. Temperature Dependence of Fluorescence Decay

Gaseous 1- and 2-bromonaphthalene at 80°C, 1-mm Hg vapor pressure, was contained in an evacuated 5-mm cell attached to a glass side arm which housed the solid bromonaphthalene. The gaseous samples were excited with a 266-nm, 1-ps pulse and monitored at 330 nm to eliminate the excitation light and nonrelaxed fluorescence. The fluorescence lifetimes of both compounds in the gas phase at this temperature were found to be shorter than in hexane solutions at about the same temperatures.

The gas-phase fluorescence lifetime could not be measured with the same time resolution as that of liquid solutions because the gas-phase sample contained a much smaller number of molecules in the optical path of the beam than the liquid samples. Streak camera records of the gas-phase fluorescence decay lifetimes are shown in Fig. 6.

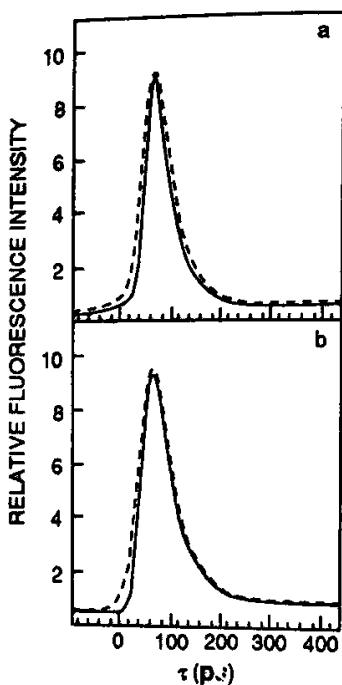


Fig. 6. Kinetics of gas-phase fluorescence of (a) 1-bromo and (b) 2-bromonaphthalene at 80°C.

D. Discussion

It has been proposed that predissociation of haloaromatics proceeds via intersystem crossing to the triplet state [4, 5, 6, 7]. Under this mechanism, it is expected that spin-orbit coupling would be a predominant operating parameter and, therefore, that rate of intersystem crossing and predissociation should increase from chloro to bromo to iodo substituents. The results presented here support this proposal, however, the magnitude of the values of rate increase from chloro to bromo to iodo substituents is not in strict agreement with calculations based on the spin-orbit matrix elements and the atomic number of the substituents. Our data also show that the position of the substituent on the ring plays a very important role on the rate of intersystem crossing. This is shown clearly in Table I for the case of 1-bromonaphthalene ($\tau_f = 75$ ps) and 2-bromonaphthalene ($\tau_f = 150$ ps).

The advantage of having both absorption and emission spectra under the same experimental conditions is that it allows for the complete identifi-

cation of the process investigated not possible by either method alone. The prompt risetime of the fluorescence provides evidence that relaxation within the excited singlet-state manifold is completed within the resolution of the streak camera. The fluorescence decay lifetime determines the relaxation rate of the single state, however, it does not provide evidence for the state to which the energy is dissipated. This information is given by the transient absorption spectra. In fact, the decay lifetime of the fluorescence, coupled with the rate of the disappearance of the $S_n \leftarrow S_1$ transient absorption and risetime of the $T_n \leftarrow T_1$ spectrum provides unequivocal proof for the pathway leading to the dissociation process.

The transient absorption spectra monitored at selected intervals of time after excitation with a picosecond displays the excited state population and changes as a function of time. This provides an accurate means for identifying the state to which the molecule relaxed from the initially prepared excited state. In the case of haloaryl compounds in solution, we believe that within 5 ps, the excited molecule relaxes to the lowest vibronic level of the lowest excited singlet S_1 ($\nu = 0$) because no hot fluorescence was observed after 5 ps, (i.e., at the resolution of our streak camera). The haloaryl compounds are known to phosphoresce in low-temperature glasses with high quantum efficiency (~ 0.3 for bromo- and iodonaphthalene at 77 K). In the gas phase, however the work of Bersohn *et al.* [8] has shown that predissociation is the primary channel for the energy dissipation and molecular relaxation. The key question to be answered in this study was the relaxation rate from S_1 ($\nu = 0$) and whether in nonviscous solutions ($\eta = 0.5$ cp) at room temperature, predissociation is the predominant mechanism for the energy dissipation of these aryl compounds. The combination of the time-resolved emission and the transient absorption spectra provided the means necessary for elucidating these processes and allow the proposal of a mechanism for the dissociation with a large degree of certainty.

1. *Halonaphthalenes.* The emission decay time constant of 1-bromonaphthalene was measured as 75 ± 10 ps (see Table I). From the transient absorption spectra at 25-, 100-, and 500-ps after excitation, as shown in Fig. 5(a-c), it is evident that a new state develops as the original excited state decays. We attribute the spectrum observed immediately after the population of S_1 , to $S_1 \rightleftharpoons S_n$ transition. This is based on two mutually supporting experimental observations: first, the emission decay lifetime is, by a factor of 3, larger than the time after excitation when the absorption spectrum was recorded, (i.e., 75 ps vs. 25 ps). Second, the transient absorption spectrum of bromo- is very similar to the transient

absorption spectra of chloronaphthalene, which must be the $S_1 \rightleftharpoons S_n$ spectrum since 1-chloronaphthalene has an emission decay lifetime of 2400 ps.

The absorption spectrum of 1-bromonaphthalene, recorded 500 ps after excitation, corresponding to several lifetimes longer than the decay lifetime of fluorescence, is assigned to either $T_n \rightleftharpoons T_1$ transitions, or possibly to the naphthyl radical. Experiments in the gas phase by Bersohn *et al.* [1,7,8] provided strong evidence for the predissociation of bromoaryls on time scales much longer than the 1-ps, rotational correlation time of these molecules. Our solution, transient absorption spectra, at 500 ps after excitation, Fig. 5(c), show a band with a maximum at ~ 425 nm, in good agreement with the reported triplet-triplet spectra. These bear no similarity to the radical at low temperatures. We cannot, however, completely exclude the possibility of a radical especially in the gas phase, in view of the strong gas-phase evidence presented by Bersohn *et al.* [7]. Neither can we assume that the gas phase and solution energy dissipation mechanisms and rates are the same.

2. *Haloanthracenes.* The iodoanthracenes excited by either 265 or 355 nm were found to fluoresce with a lifetime slightly depending on the excitation wavelength (see Table I). The position of the iodo substituent increases the emission lifetime by a factor of about 2 between 2- and 9-iodoanthracene. Absorption spectra for the 2 and 9 position of iodo substitution show little intensity from 25 to 500 ps after excitation. In lieu of the very short lifetime of the 2-iodoanthracene fluorescence, it is not expected that the $S_n \rightleftharpoons S_1$ spectrum will have sufficient intensity to be observed. However, if the molecule relaxes to a triplet state and remains there for several picoseconds before it dissociates, a strong $T_n \rightleftharpoons T_1$ spectrum would have been recorded as in the cases of the bromo and chloro derivatives. In the case of a 9-iodoanthracene/hexane solution, where the emission lifetime was found to be 35 ps, absorption spectra recorded 25 ps after excitation show a low intensity absorption which changes shape and increases in intensity after 100 ps and further changes in shape after 500 ps. Even though the intensities of these spectra are not sufficiently high to allow an accurate assignment, the absorption at 25 ps after excitation would most probably correspond to a $S_n \rightleftharpoons S_1$ transition, the 100-ps spectrum to a triplet-triplet contribution, and the 500-ps spectrum to the depletion of the triplet state. These assignments are not definitive because of the low intensities of the transient spectrum, however, they are consistent with the emission lifetime measurements.

Struve *et al.* [9] have shown that the emission of 9-iodoanthracene becomes shorter as the temperature of the sample increases. In the case of a liquid solution, vibronic relaxation within the excited-state manifold is

extremely fast and, therefore, dominates intersystem crossing (ISC) from upper vibronic levels. In the gas phase, this is valid for 1-bromonaphthalene and 2-bromonaphthalene, where the fluorescence lifetime in the gas phase at 80°C is less than 25 ps compared to 70 ps at 60°C, and 130 ps at 70°C for 1-bromo and 2-bromonaphthalene, respectively. The possibility of the hot fluorescence being caused by $S_2 \rightarrow S_0$ fluorescence was eliminated by the use of optical cutoff filters which removed the wavelength range of emission from the second excited electronic state. The vapor pressure of 1- and 2-bromonaphthalenes at 80°C is ~ 1 mm. Therefore, we can safely assume a collision-free condition during the lifetime of fluorescence.

The mechanism proposed, based on the emission and absorption data presented in Fig. 2-6 and Table I, suggests that the excited singlet state population decays predominantly via intersystem crossing to the triplet state with the rates decreasing from iodo to bromo to chloro substituents. The triplet state does not disappear within the first 500 ps after excitation for the bromo and chloro substituents; the predissociation of iodoanthracene also proceeds via the triplet, however, at a much higher rate. Halo substitution of the methyl group of the aromatics is found to increase the rates of intersystem crossing and predissociation.

3. Naphthyl Radicals. The proposed mechanism for the photodissociation of haloaryls via the triplet state was unequivocally proven by the observation of the emission spectrum of the naphthyl radical [10]. The detection of the naphthyl radical was achieved by the use of a two-color laser experiment. A sample of 1-(chloromethyl)naphthalene in solution was irradiated with a 266-nm, 1-ps pulse followed by another picosecond pulse at 355 nm. We should note that the 355-nm wavelength laser light is not absorbed by the parent molecule (Fig. 7,b). However, the 355-nm light was absorbed by a new species formed as a consequence of irradiation and subsequent dissociation of the chloromethylnaphthalene with the 266-nm, 1-ps pulse. The dissociation species was formed at the same rate as the disappearance of the triplet state of the parent species upon absorption of 355-nm light. The emission spectrum is reproduced in Fig. 7,a. This emission spectrum exhibits the typical aromatic bands in the region of 550-700 nm. All 1-X-methylnaphthyls (X = Cl, Br, or I,) showed the same emission spectrum after 266 and 355-nm laser irradiation. The 1-X-methylnaphthyl spectrum emission of dissociation product was found to be different than the 2-X-methylnaphthyl emission spectrum (Fig. 8). However, all the 1-X emission spectra (Fig. 9), and all three 2-X-methylnaphthyl emission spectra (Fig. 10) were identical regardless of whether they originated from chloro, bromo, or iodo methylnaphthalenes [11]. This is expected assuming the

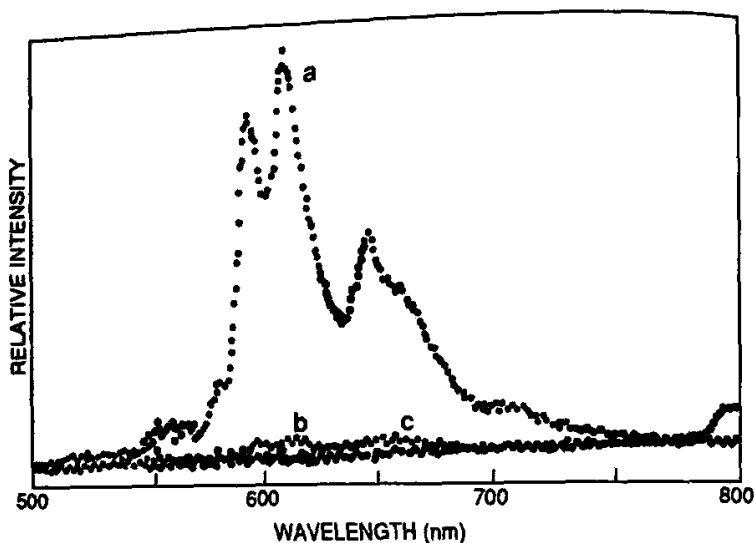
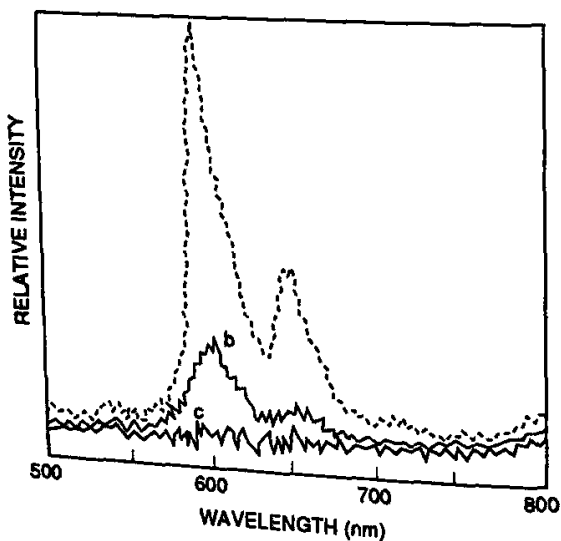


Fig. 7. Emission spectra of the 1-naphthyl radical generated by photolysis of 1-(chloromethyl)naphthalene (a) excited by a 266-nm pulse followed by a 355-nm pulse 320 ps later; (b) using only the 266-nm pulse; (c) using only the 355-nm beam.

Fig. 8. The same as Fig. 7 except that 2-(bromomethyl)naphthalene was used. See Fig. 7 for b, c; x, Br (see text).



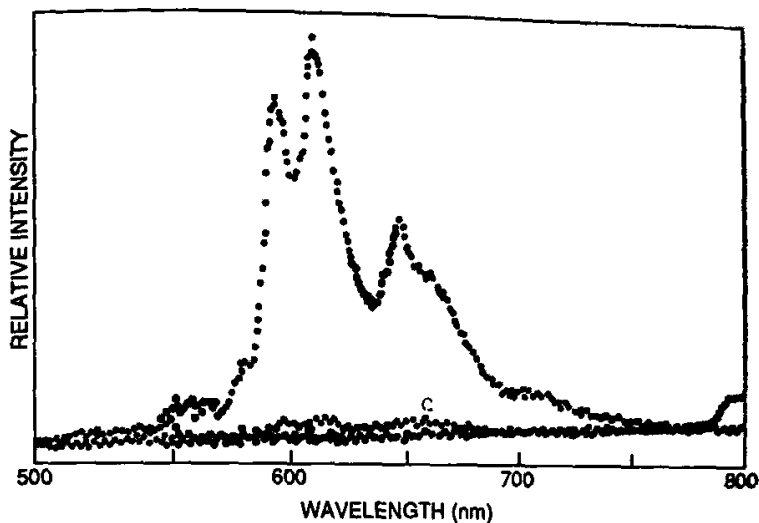
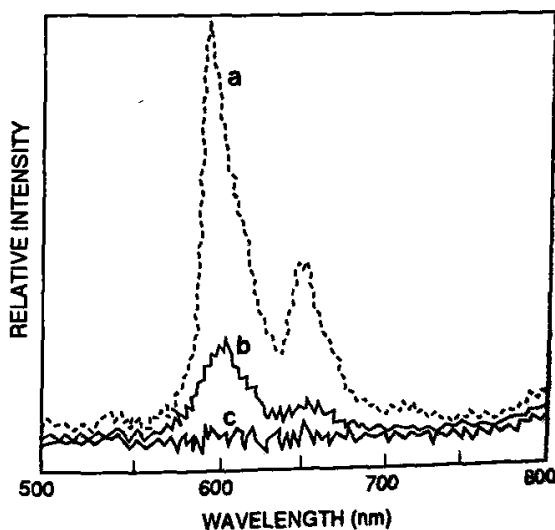


Fig. 9. The same as Fig. 7 except that 1-(bromomethyl)naphthalene was used. See Fig. 7 for a, b, c; x, Br (see text).

Fig. 10. The same experiment as Fig. 7 except that 2-(chloromethyl)naphthalene was used and the delay between the 266-nm photolysis pulse and the 355-nm radical pulse was 500 ps. Spectra for all 2-X-(x, Cl, Br, or I) species were identical.



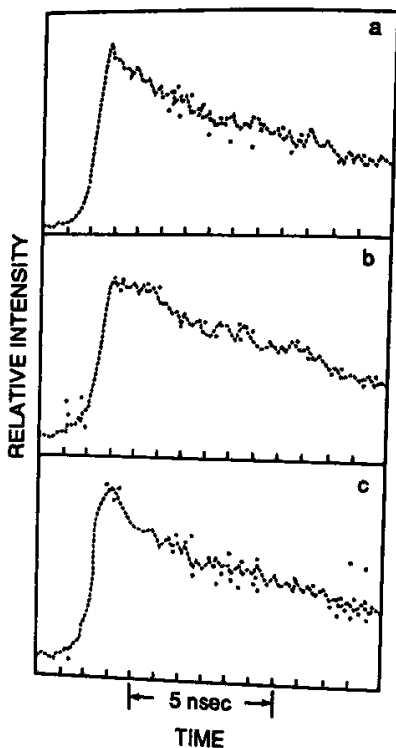


Fig. 11. Time-resolved emission of the 1- and 2-naphthylmethyl radicals observed at wavelengths longer than 570 nm. 1-Naphthylmethyl radical emission induced by a 355-nm pulse (a) 60 ps after 266 excitation, (b) 320 ps after excitation, and (c) 2-naphthylmethyl radical observed 60-ps after 266-nm excitation.

spectra are due to the 1-methylnaphthyl or 2-methylnaphthyl radicals. Even though the spectra of the resulting radicals were the same for each position of substituted halogens, the kinetics and the rates of radical formation strongly depended on the halogen species, with the rates decreasing from iodo > bromo > chloro. The risetime and kinetics of radical formation and decay are shown in Fig. 11. This figure shows that the formation of the radical is prompt, suggesting that fast intersystem crossing, as shown in Figs. 2-6, leads to radical formation. The lifetime of the radical in solution was found to be ~ 40 ns.

This sequence of experiment—excitation, absorption, and emission spectra of parent species and its transient states followed by emission spectra, risetime, and kinetics of the radical—have provided a successful means for determining the exact sequence of all events and intermediates during the course of the photodissociation process.

III. Picosecond X-Ray Diffraction

A. Introduction

Although picosecond electronic, Raman, and vibrational spectroscopy have been advanced in the past twenty-five years to a superb spectroscopic tool, the ultimate experiment would be the direct recording, in real time, of the evolution in structure during the course of a chemical reaction. Probably the best, if not the only, means to achieve this goal is by time-resolved x-ray diffraction. We have designed and built a laboratory size picosecond x-ray, PXR system that is capable of generating picosecond x-ray pulses [11]. We have also designed and built the necessary real time, picosecond detection equipment that allows us to achieve this goal and record time-resolved x-ray diffraction of ultrafast intermediates.

Developments in lasers and x-ray optics [12] have enabled the design and construction of x-ray lasers [13] and the generation of short-duration x-ray pulses [14]. In addition to the large systems available at the National Laboratories and other centers; two means for tabletop picosecond x-ray pulse generating devices are becoming available: (1) soft x-ray emission from excited plasmas generated by focusing high-intensity short duration laser pulses onto a solid target and (2) the utilization of electron bunches generated by means of picosecond laser pulses to induce hard x-rays by striking metal anodes. A brief description of source, diagnostics, and means for obtaining time-resolved, picosecond, x-ray (PXR) diffraction of transient structures follows.

X-rays are usually generated using thermionic electron sources. Even when driven by ultrashort laser pulses [15] the emitted electrons have long pulse widths (> 10 ns) and are therefore not suitable for picosecond pulse x-ray generation. We have successfully utilized photoemission as a means of generating ultrashort electron bunches and subsequently picosecond duration x-ray pulses. Photoemission is known to have an extremely short response time in most materials, consequently the electron current practically follows the laser pulse intensity envelope under the appropriate conditions.

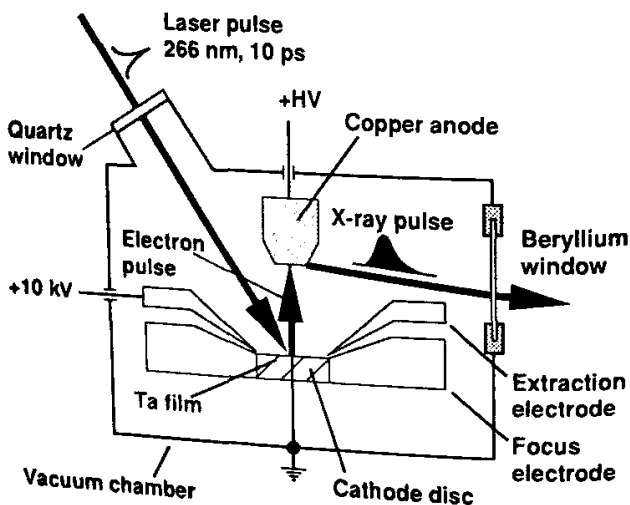
Even though the quantum efficiency for photoelectron ejection at the visible and ultraviolet region of the spectrum [16] from semiconductor cathodes such as Cs_3Sb is 3 to 4 orders of magnitude higher than that of metals, we find that the damage threshold for Cs_3Sb is too low for the generation of high intensity electron bunches at relatively high repetition rates and acceleration potentials. When one also considers the ultra-high vacuum requirements (10^{-10}) and the depletion of cesium under the 10^{-10} Torr vacuum, the disadvantages become sufficient to warrant the use of

other photocathode materials. Several of the metallic surfaces that we have used, such as Ta and Ti, are relatively resistant to atmospheric gases. Therefore, they can be used at relatively low vacuum conditions. These metal photocathodes also have a much longer useful lifetime and are easier to prepare. Using a tantalum film as the photocathode material and 266-nm picosecond pulses from a pulsed-mode locked Nd:YAG laser, we generate electron bunches with a charge of 3 nC per pulse. These electron pulses are accelerated and focused onto a copper anode, inducing x-ray pulses with a brightness of $6.2 \times 10^6 \text{ cm}^{-2}\text{sr}^{-1}$ at the Ka wavelength (1.54 Å). The pulse widths are measured using an x-ray streak camera and are $\sim 50 \text{ ps}$.

B. The PXR Experimental System

The photocathode consists of a cylindrical, polished 15-mm diameter, nickel substrate. It is mounted on a high-voltage feedthrough, which is maintained at a pressure below 2×10^{-9} Torr. A schematic representation of the chamber that houses the electron and x-ray source is presented in Fig. 12. The photocathode substrate fits into Pierce focusing electrode with an additional field-shaping electrode added to increase the extraction field

Fig. 12. Schematic diagram of the x-ray diode. Photoelectrons generated by 266-nm, 10-ps pulses on a tantalum photocathode are accelerated and strike the anode emitting x-ray photons.



near the photocathode surface. This electrode is very important since most of the pulse-broadening effects occur near the photocathode surface. Because of the high work function of tantalum ($f_0 = 4.16$ eV), 266-nm, 10-ps pulses with a maximum energy of 2 mJ per pulse and a repetition rate of 1 kHz are used.

A maximum quantum efficiency for this cathode of 4×10^{-5} is observed. At higher incident laser energies, plasma formation occurs resulting in very long current and x-ray pulses. A 3 nC-per-electron pulse was the maximum charge measured for this diode configuration at an accelerating voltage of 50 kV.

The electrons emitted by the photocathode are subsequently accelerated to 50 kV and focused on to a toroid-shaped anode. The anode is made of oxygen-free, high conductivity copper and is maintained at a high positive potential. The electron pulses interact with the copper anode forcing the emission of Cu-K α x-ray photon pulses, which exit the vacuum chamber through a thin beryllium-foil window. A bend germanium crystal monochromator disperses and focuses the x-rays onto the sample. The duration of the x-ray pulses is measured by a Kentech x-ray streak camera fitted with a low density CsI photocathode. The pulse width of the x-rays at 50 kV anode-cathode potential difference is about 50 ps. This value is an upper limit for the width of the x-ray pulses because the transit time-spread of the streak camera has to be taken into consideration. A gold photocathode (100 Å Au on 1000 Å perylene) is used to record the 266-nm excitation laser pulses. The intensity of the x-rays is 6.2×10^6 photons $\text{cm}^{-2}\text{sr}^{-1}$ (per pulse), and is measured by means of a silicon diode array x-ray detector which has a known quantum efficiency of 0.79 for 8 kV photons.

The experimental system built for PXR time-resolved diffraction experiments is shown in Fig. 13. To increase the average x-ray power emitted, a high repetition rate laser source is necessary to drive the photocathode. This system consists of a high power Nd:YLF CW-mode locked laser and regenerative amplifier, based upon two Coherent Antares Nd:YLF laser heads, and is operated at a repetition rate of up to 3 kHz (Fig. 13). By means of a beam splitter, the pulses are separated into two parts. One part is converted to the 4th harmonic (266 nm), which is focused on the photocathode generating the picosecond electron bunches, which in turn are accelerated and focused on the anode producing x-ray photons with a time width of less than 70 ps. The x-rays are subsequently focused onto a position sensitive x-ray detector by means of a Ge monochromator. Alternatively, Laue diffraction patterns can be obtained using a collimated undispersed x-ray beam. The other fraction of the laser beam (Fig. 13) follows the path of the 532-nm beam and is used for excitation of the

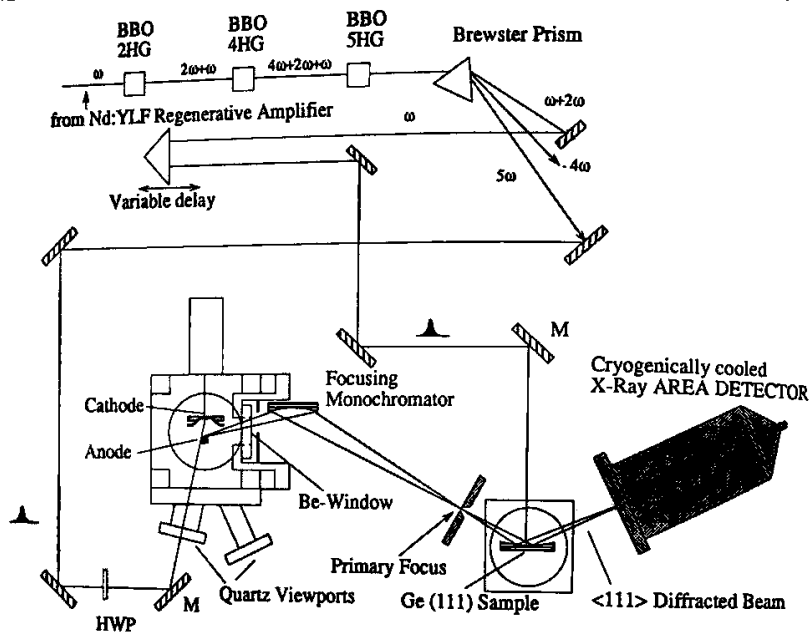
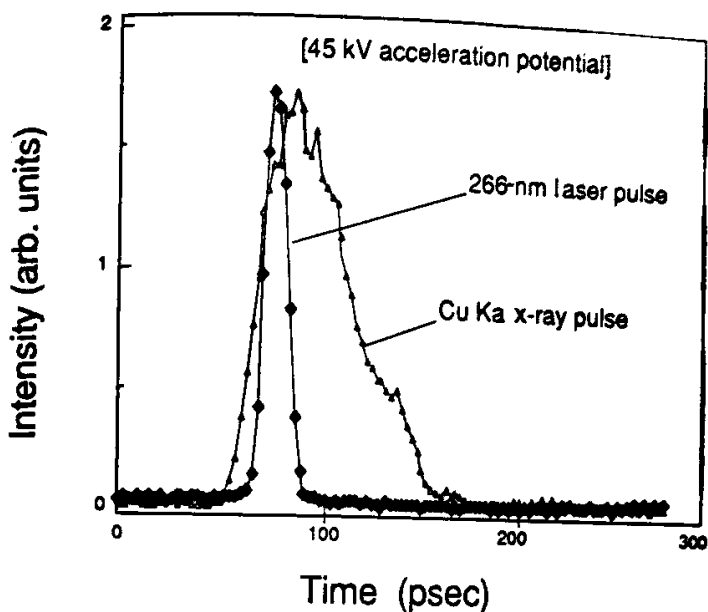


Fig. 13. Schematic representation of the picosecond x-ray (PXR) system showing experimental setup for time-resolved x-ray diffraction.

sample. It should be noted that although we discuss only the use of 532-nm excitation wavelength, other wavelengths are easily generated by means of well-known conversion techniques, stimulated Raman, or tunable dye lasers pumped by the picosecond laser.

The two pulsed beams (laser excitation and PXR probe) are synchronized to arrive at the sample either at the same time or at a preselected delay by translating either of the two delay stages by increasing or decreasing the optical path length and consequently the transit time of either beam. This represents an essential advantage of this technique over previous time-resolved x-ray diffraction experiments using synchrotron radiation sources, where the lack of sufficient synchronization between the excitation laser pulse and the x-ray probing source is one of the limiting factors for the experimental time resolution.

This experimental system has enabled us to perform picosecond time-resolved x-ray diffraction experiments. One of the earliest experiments consists of a Ge (111) crystal bent for maximum reflection of 8 keV x-ray photons, similar to a sensitive double-crystal monochromator. The x-ray diffraction spectra are recorded before excitation. This diffraction exhibits the normal diffraction pattern characteristic of this surface. In



266-nm laser pulse: Au photocathode
 Cu Ka 1.54 Å pulse: low density CsI photocathode

Fig. 14. Streak camera traces of the laser and x-ray pulses.

subsequent experiments, a laser pulse impinges upon the Ge (111) crystal causing lattice distortion. A picosecond x-ray pulse is synchronized to arrive at the sample at the same time as the laser light pulse strikes the surface. The spectrum recorded by the Ge (111) diffracted x-ray pulses reflects the changes in the structure caused by the laser interaction with the crystal surface as a function of time. The time resolution of the experiment is essentially equal to the time width of the x-ray pulses utilized which is approximately 50 ps as measured by the x-ray streak camera. The temporal width of the laser and x-ray pulses are shown in Fig. 14. By deconvolution of the pulses, it is possible to achieve better time resolution. It must be noted, however, that this is an upper limit because the transit time spread within the streak camera and photocathode must be taken into account.

This somewhat brief description of the PXR system has made evident the general aspects of this unique experimental ultrafast x-ray system. The experimental procedure for time-resolved x-ray diffraction presented is based upon the pump-probe scheme first introduced several years ago in picosecond spectroscopy [17]. The laser in these experiments is used to create x-ray pulses and also functions as an excitation source for the sample. To detect the very weak signals of diffracted x-rays, a unique

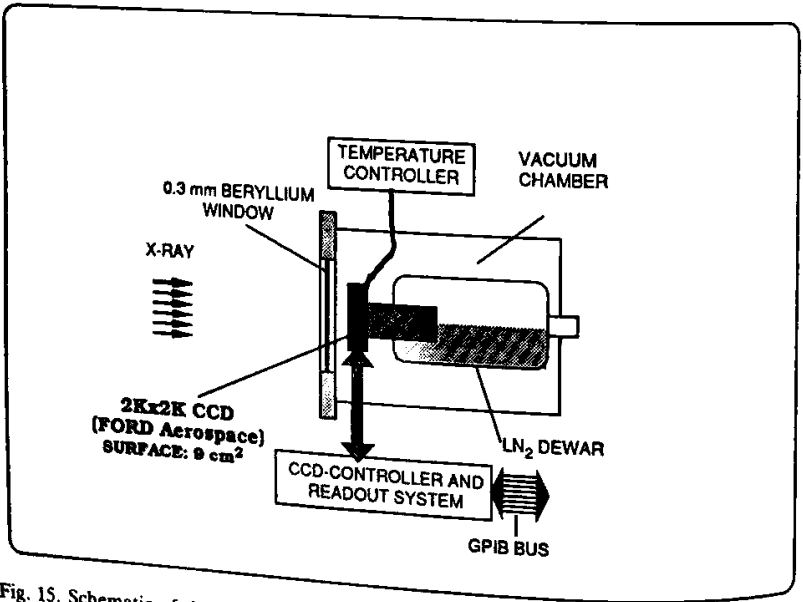
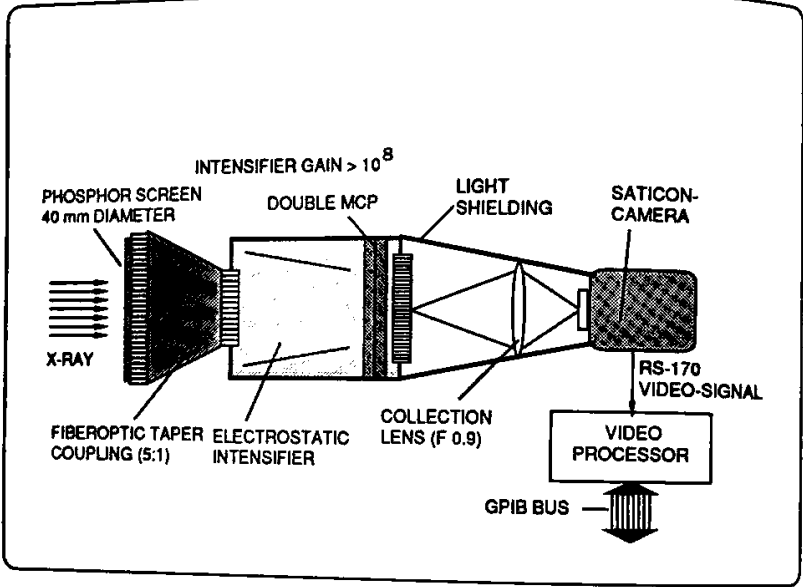


Fig. 15. Schematic of the two detectors used for the time-resolved x-ray experiments. The upper figure displays an image intensifier and camera. The lower is a direct detection liquid-nitrogen cooled CCD.

detector that employs a liquid nitrogen cooled $2K \times 2K$ CCD array is used. This detector practically eliminates all dark noise, thus making it possible to detect the equivalent of one diffracted x-ray photon per second [18]. This detector is shown in Fig. 15.

Several other types of time-resolved PXR experiments are ongoing, including melting, crystallization, and dissociation of simple molecular species that will allow calibration of the PXR system and provide a data base necessary for subsequent large molecule diffraction experiments. Other applications including time-resolved molecular holography, plasma diagnostics, and x-ray diffraction of metastable species are also feasible.

ACKNOWLEDGMENTS

This work was supported by the W. M. Keck Foundation and by the Advanced Research Projects Agency of the Department of Defense, and was monitored by the U.S. AFOSR under Contract No. F49620-89-C-0104. We also thank Drs. R. Bredthauer and R. Nelson of Ford Aerospace for their invaluable help with the CCD camera.

REFERENCES

1. A. Fredman, S. C. Yang, M. Kawasaki; and R. Bersohn. *J. Chem. Phys.* **73**, 1028 (1980).
2. E. D. Hillinski, D. Huppert, D. F. Kelley, S. V. Milton, and P. M. Rentzepis. *J. Am. Chem. Soc.* **77**, 1214 (1982).
3. D. Huppert, S. D. Rand, A. H. Reynolds, and P. M. Rentzepis. *J. Chem. Phys. Chem. Soc.* **106**, 1951 (1984).
4. G. Porter and E. Strachan. *Faraday Soc.* **54**, 1595 (1958).
5. F. J. Wilkenson. *J. Phys. Chem.* **66**, 2564 (1962).
6. A. Levy, D. Meyerstein, and M. Ottolenghi, *J. Phys. Chem.* **77**, 3044 (1973).
7. S. J. Kawasaki and R. Bersohn. *J. Chem. Phys.* **66**, 2647 (1977).
8. M. Dzvonik, S. Yang, and R. Bersohn. *J. Chem. Phys.* **61**, 4408 (1974).
9. C. G. Morgante and W. S. Struve. *Chem. Phys. Lett.* **68**, 272 (1972).
10. D. F. Kelley, S. V. Milton, D. Huppert, and P. M. Rentzepis. *J. Chem. Phys.* **87**, 1842 (1983).
11. B. Van Wonerghem and P. M. Rentzepis. *Appl. Phys. Lett.* **56**, 1005 (1990).
12. N. M. Ceglio. *J. X-Ray Sci. and Tech.*, **1**(1), pp. 7-78, (1989).
13. D. L. Mathews, P. L. Hagelstein, M. D. Rosen et al. *Phys. Rev. Lett.*, **54**(2), 110, (1985).
14. B. Van Wonerghem and P. M. Rentzepis. *Bull. Am. Phys. Soc.*, **34**, 892. (1989).
15. C. Lee and P. E. Oettinger. *J. Appl. Phys.* **58**(5), pp. 1996-2000. (1985).
16. A. H. Sommer. *Photoemissive Materials*, Wiley, New York (1968).
17. P. M. Rentzepis. *Chem. Phys. Lett.* **2**, 117 (1958).
18. The CCD chip was made by Ford Aerospace Corp. and the camera by Photometrics.



4

Computer-Aided Design of Monopropellants

Peter Politzer, Jane S. Murray, M. Edward Grice,
and Per Sjoberg

I. Introduction

The specific impulse is widely used as a means of characterizing and evaluating propellants and is viewed as a key measure of propellant performance [1]. An energetic molecule develops thrust (or recoil force) due to the discharge of gaseous products when it undergoes combustion. The specific impulse, I_S , is the integral of the thrust, per unit weight of material, over the time of combustion.

Propellants are explosive materials with low rates of combustion that will ideally burn at uniform rates after ignition without requiring interaction with the atmosphere [1,2]. They frequently involve several components, including an energetic oxidizer, a plasticizer to facilitate processing, and a polymeric binder. The specific impulse of such propellants is necessarily that of the composite mixture. Our focus here is on chemical and structural factors affecting the specific impulse of the oxidizer, which will be designated as a monopropellant.

To provide some theoretical basis for this discussion, we begin with a simplified treatment of specific impulse based on kinetic theory, followed by a brief review of our methods used for computing I_S . Specific impulse results for a large variety of compounds are presented, and characteristics that have been identified as favoring a high specific impulse are discussed in detail. Some perspective on the importance of certain factors involved in computing I_S is also given. Finally, we shall demonstrate how computational specific impulse analyses provide a starting point for the successful design of high-performance propellants.

II. Theoretical Background

The specific impulse, I_S , is often expressed in terms of the absolute temperature in the combustion chamber T_c , and the number of moles of gaseous products produced per unit weight of propellant N by the simplified relationship given as Eq. (1) [1].

$$I_S \sim T_c^{1/2} N^{1/2} \quad (1)$$

This proportionality can be rationalized in the following manner based on kinetic theory.

I_S is directly related to the thrust that is developed by a propellant when it undergoes combustion; thrust is the recoil force that is produced by the formation and discharge of the gaseous products.

$$\begin{array}{ccc} \xleftarrow{\text{thrust}} & x < 0 & \xrightarrow{\text{gas discharge}} \\ & x = 0 & \end{array}$$

By Newton's second law

$$\text{thrust} = \text{recoil force} = \sum_i \frac{d}{dt} (m_i v_{x_i}) \quad (2)$$

where m_i is the total mass of the molecules of type i that are formed in the combustion, and v_{x_i} is their velocity component in the x direction.

From kinetic theory, the kinetic energy of one mole of a gas having molecular weight M and at an absolute temperature T is

$$\text{kinetic energy} = \frac{Mv^2}{2} = \frac{3}{2} RT \quad (3)$$

Considering only the contribution to the kinetic energy coming from the velocity component in the x direction

$$\frac{Mv_x^2}{2} = \frac{1}{2} RT$$

or

$$v_x = \left(\frac{RT}{M} \right)^{1/2} \quad (4)$$

If all of the gases in the propellant combustion reaction are assumed to be at the same temperature T_c then

$$v_{x_i} = \left(\frac{RT_c}{M_i} \right)^{1/2} \quad (5)$$

4. Computer-Aided Design of Monopropellants

Combining Eqs. (2) and (5)

$$\text{thrust} = \sum_i \frac{d}{dt} \left(m_i \sqrt{\frac{RT_c}{M_i}} \right) = \sum_i \frac{d}{dt} \left(\frac{m_i^2 RT_c}{M_i} \right)^{1/2} \quad (6)$$

I_S is defined as the integral of the thrust per unit weight of propellant over the time of combustion t_c ,

$$I_S = \int_{t=0}^{t_c} \frac{\text{thrust}}{w} dt = \frac{(RT_c)^{1/2}}{w} \int_{t=0}^{t_c} \sum_i \frac{d}{dt} \left[\frac{m_i^2}{M_i} \right]^{1/2} dt \quad (7)$$

where w is the weight of the propellant. After integrating

$$I_S = \frac{(RT_c)^{1/2}}{w} \sum_i \left(\frac{m_i^2}{M_i} \right)^{1/2} \quad (8)$$

The derivation of Eq. (8) involved a number of approximations and assumptions (e.g., ideal behavior, uniform temperature). Its value, therefore, is in roughly indicating how the specific impulse depends upon the combustion temperature and the quantities of product gases. It will accordingly be written simply as a proportionality

$$I_S \sim \frac{T_c^{1/2}}{w} \sum_i [m_i^{1/2} N_i^{1/2}] \quad (9)$$

in which $N_i = (m_i)/M_i$ is the number of moles of gas i formed during the combustion.

Equation (9) can be converted to the simplified form of Eq. (1) by means of two rather drastic approximations:

$$\sum_i m_i^{1/2} N_i^{1/2} \approx \sum_i m_i^{1/2} \sum_i N_i^{1/2} \quad (10)$$

$$\sum_i m_i^{1/2} \approx \left(\sum_i m_i \right)^{1/2} \quad \sum_i N_i^{1/2} \approx \left(\sum_i N_i \right)^{1/2} \quad (11)$$

Since $\sum_i m_i = w$, and defining N as the total number of moles of gaseous products per unit weight of propellant, $N = (\sum N_i)/w$, then introducing Eqs. (10) and (11) into Eq. (9) yields Eq. (1).

$$I_S \sim T_c^{1/2} N^{1/2} \quad (1)$$

While the approximations represented by Eqs. (10) and (11) are certainly not generally valid, we have found that the results obtained with Eqs. (1) and (9) usually differ by no more than 3%. It may be that fortunate cancellations of errors are occurring.

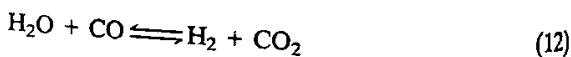
Our specific-impulse calculations have involved the use of the relationship given in Eq. (1). In the following section we discuss methods for determining the amounts of gaseous products m_i and the combustion temperature, T ; these are quantities needed to apply this formula. It is our aim to provide some perspective on the importance of various factors involved in obtaining I_S values.

III. Application of Specific Impulse Formula

In order to apply Eq. (1), it is necessary to establish the identities and amounts of the various gaseous products and to determine the combustion temperature.

A. Gaseous Products

Depending upon the composition of the propellant, the major components of the gaseous products may include CO , CO_2 , N_2 , H_2O , or HF , with lesser quantities of other molecules and radicals such as H_2 , NO , H , O , CHO , and N_2O . The proportions and consequently amounts of these various possible products depend upon the stoichiometry of the combustion process plus the effects of whatever other equilibria and/or dissociations may be occurring such as the water-gas reaction



We use a program obtained from the Naval Weapons Center [3] to predict which products will be formed and in what quantities; these predictions are based upon quantitative estimates of the extents of these various reactions, using data such as equilibrium constants.

B. Combustion Temperature

A simple approach to obtaining a rough approximation of the combustion temperature involves assuming that the heat of combustion of the propellant is used entirely to heat the product gases to the combustion temperature, so that

$$-\Delta H_{\text{comb}} = C_{P, \text{gases}} (T_c - T_0) \quad (13)$$

and

$$T_c = T_0 - \frac{\Delta H_{\text{comb}}}{C_{P, \text{gases}}} \quad (14)$$

ΔH_{comb} is the enthalpy of combustion, $C_{p, \text{gases}}$ represents the total heat capacity of the gaseous products, and T_0 and T_c are the initial and the combustion temperatures. In Eqs. (13) and (14) it is assumed that ΔH_{comb} is constant over the temperature range between T_0 and T_c , and that the pressure in the combustion chamber remains constant due to a steady-state situation; the rates of formation and discharge of product gases are taken to be equal. The Naval Weapons Center program uses a less idealized approach to obtain the combustion temperature; for example, the temperature dependence of gaseous heat capacities is taken into account.

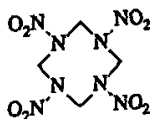
ΔH_{comb} can be calculated from a knowledge of the molar heats of formation of the propellant and the gaseous products [Eq. (15)]. The latter are known [1, 3], while the former can be determined in a number of ways; for example, a reasonable estimate can often be obtained from

$$\Delta H_{\text{comb}} = \sum_i^{\text{products}} N_i \Delta \bar{H}_{f,i} - N_{\text{prop}} \Delta \bar{H}_{f,\text{prop}} \quad (15)$$

standard bond enthalpies plus any strain contributions. In our work, we compute gas phase heats of formation with the semi-empirical AM1 procedure [4], and correct these for crystal effects according to a procedure outlined by Ritchie [5]. Equations (14) and (15) show that a high combustion temperature (and hence specific impulse) is favored by a large positive propellant heat of formation.

IV. Calculated Specific Impulse Values

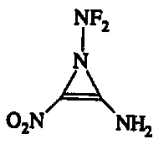
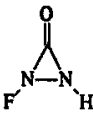
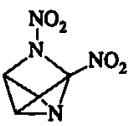
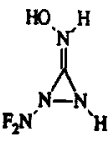
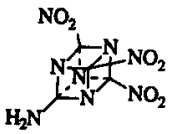
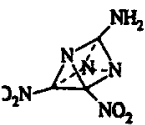
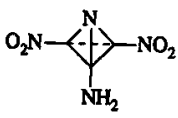
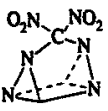
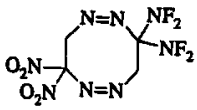
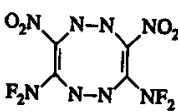
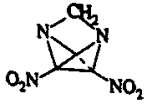
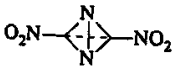
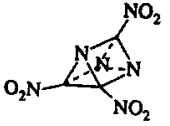
We have calculated the specific impulses of a large number of molecules using Eq. (1) in the manner described in the previous section. To facilitate comparisons, our values are given relative to that of HMX (1; 1,3,5,7-tetranitro-1,3,5,7-tetraazacyclooctane). The results of some of these calculations are given in Tables I–III. Table I lists compounds with calculated



1

specific impulses at least 12% better than HMX; Tables II and III contain molecules that are 1–10% better, and the same or worse than HMX, respectively. The molecules in these tables encompass a wide variety of structural types, including both neutral and ionic, strained and unstrained.

Table I. Molecules with Estimated Specific Impulse at Least 12% Better than HMX

	Molecule	Relative I_s		Molecule	Relative I_s
1	HMX	1.00	9		1.16
2		1.25	10		1.15
3		1.22	11		1.15
4		1.20	12		1.14
5		1.18	13		1.14
6		1.18	14		1.14
7		1.17	15		1.14
8		1.17	16		1.13

(table continues)

Table I (Continued)

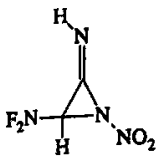
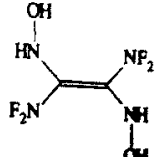
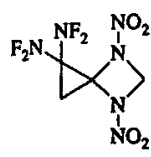
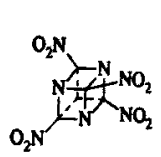
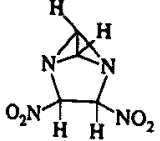
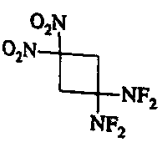
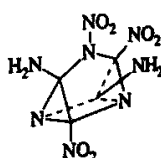
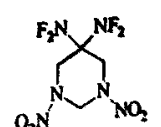
	Molecule	Relative I_s		Molecule	Relative I_s
17		1.13	19		1.12
18		1.12	20		1.12

Table II. Molecules with Estimated Specific Impulse 1-10% Better Than HMX

	Molecule	Relative I_s		Molecule	Relative I_s
1	HMX	1.00	24		1.09
21		1.10	25	$(\text{H}_2\text{N})_3\text{C}^{(+)} \text{ } ^{-}\text{C}(\text{NF}_2)_2\text{NO}_2$	1.09
22		1.10	26		1.08
23	$(\text{HONH})_3\text{C}^{(+)} \text{ } ^{-}\text{C}(\text{NF}_2)_3$	1.09	27		1.08

(table continues)

Table II (Continued)

Molecule	Relative I_s	Molecule	Relative I_s
	1.07		1.03
	1.06		1.03
	1.06		1.03
	1.05		1.03
	1.05		1.02
	1.04		1.02
	1.04		1.02

(table continues)

Table II (Continued)

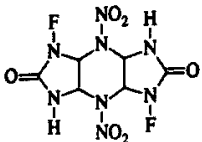
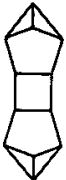
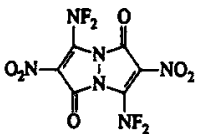
Molecule	Relative I_s	Molecule	Relative I_s
42	1.02	44 $(H_2N)_3C^{(+)}(-)C(NO_2)_2$ NF ₂	1.01
43	1.01	45	1.01

Table III. Molecules with Estimated Specific Impulse Same as HMX or Worse.

Molecule	Relative I_s	Molecule	Relative I_s
1 HMX	1.00	49	0.98
46	0.99	50	0.97
47	0.98	51 $(H_2N)_2C^{(+)}(-)C(NO_2)_3$ NF ₂	0.96
48	0.98	52	0.96

(table continues)

Table III (Continued)

	Molecule	Relative I_s		Molecule	Relative I_s
53		0.96	56		0.84
54		0.93	57		0.82
55		0.88			

cyclic and caged compounds. They are substituted primarily with NO_2 , NF_2 , and NH_2 groups.

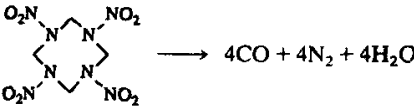
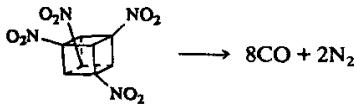
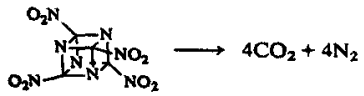
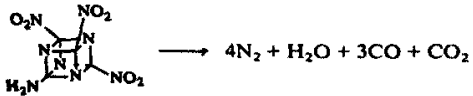
From an examination of the specific impulse formula [Eq. (1)] it can be inferred that a high I_s value is promoted by

1. the formation of light gaseous combustion products, since then a greater number of moles is produced per unit weight of propellant, and
2. a high positive heat of formation (per unit weight), since this leads to a greater release of energy upon combustion and a higher combustion temperature T_c .

Thus, from the standpoint of specific impulse, it is preferable that a pair of available oxygens be used to form $\text{CO} + \text{H}_2\text{O}$ rather than CO_2 , since the former corresponds to two moles of gas from 46 g of propellant and the latter to just one mole from 44 grams. [This conclusion is not altered by the effects of the water-gas equilibrium, Eq. (12), because the latter does not change the total number of moles of gases.] The heat of formation is frequently taken to be indicative of the "energy content" of a propellant, and in some circumstances it is quite appropriate to do so. However there are some limitations upon this interpretation, as will be pointed out later.

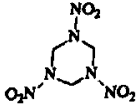
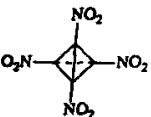
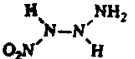
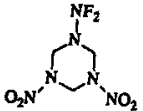
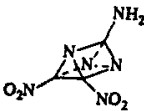
In Table IV are given idealized stoichiometric decomposition reactions for HMX and ten other molecules taken from Tables I-III. All nitrogens are assumed to go to N_2 , and fluorines to HF, while oxygens preferentially

Table IV. Stoichiometric Oxidation Reactions and Some Properties of Cubane Derivatives

Molecule	Reaction	Molecular weight, M	$\frac{n}{M}$	Relative $\Delta H_f^{a,b}$	Relative I_s^a
HMX					
1		296	.041	1.00	1.00
Cubanes and Azacubanes					
55		464	.026	3.74	0.97
32		284	.035	4.14	1.05
20		288	.028	12.28	1.12
11		258	.035	10.98	1.15

(table continues)

Table IV (Continued)

Molecule	Reaction	Molecular weight, M	$\frac{n}{M}$	Relative $\Delta H_f^{a,b}$	Relative I_s^a
Others					
46	 $\longrightarrow 3N_2 + 3H_2O + 3CO$	222	.032	2.84	1.00
36	 $\longrightarrow 4CO_2 + 2N_2$	232	.026	6.92	1.03
37	 $\longrightarrow 2H_2O + 2N_2$	92	.043	2.08	1.03
28	 $\longrightarrow 3N_2 + 2HF + H_2O + 3CO + H_2$	228	.044	1.41	1.07
4	 $\longrightarrow 3N_2 + 3CO + H_2O$	186	.038	12.07	1.20
2	 $\longrightarrow N_2 + CO + HF$	76	.039	12.04	1.25

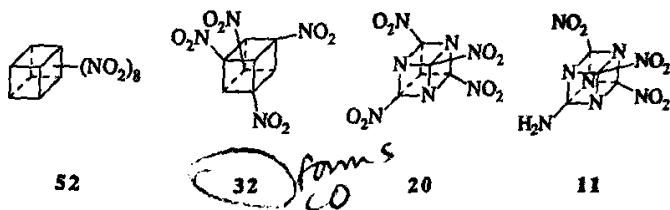
^aThese values are given relative to HMX (1).

^bThe calculated heats of formation used to obtain the relative values in this table are available in Ref. 1.

4. Computer-Aided Design of Monopropellants

form H_2O (if hydrogens are available) and otherwise CO and CO_2 in that order. We use such reactions to calculate the quantity n/M in which n is the number of moles of gaseous products and M is the molecular weight of the monopropellant. n/M provides a rough (and quickly determined) estimate of the number of moles of gaseous products available per unit weight of propellant. Also included in Table IV are relative heats of formation obtained from calculated values in units of calories/gram. It is seen in Table IV that neither the n/M nor the relative ΔH_f values follow the same trend as does the relative I_S .

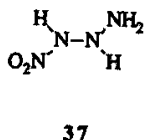
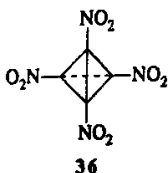
The cubane derivatives in Table IV, 52, 32, 20 and 11 provide an interesting illustration of how a combination of factors determines I_S . Octanitrocubane 52 has a somewhat smaller ΔH_f and a significantly smaller n/M



value than does the tetranitro analogue 32; thus both of these factors are in favor of the latter having the higher specific impulse, as is calculated to be the case (see Table IV). Structure 20 has a higher ΔH_f than does 11, but the n/M values of this pair vary in the reverse order, as do their relative I_S values.

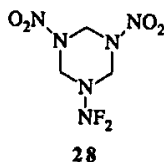
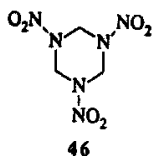
Several key points are brought out by the results for these cubane derivatives. First, complete nitration of all available sites is not necessarily to be sought; the presence of some hydrogens is generally very beneficial. These can take up a portion of the oxygens to form water (which is one of the lighter potential gaseous products) and thus more of the carbon will be oxidized only to CO rather than CO_2 . The desirability of using oxygens to form H_2O and CO , as opposed to CO_2 , has already been pointed out. A judicious combination of NO_2 groups with NH_2 substituents or unsubstituted (hydrogen-bearing) carbons can significantly improve the specific impulse, as can be seen for example by comparing 55 and 32 or 20 and 11 in Table IV, or 4 and 16 in Table I. (In dealing with strained systems. however, it must be kept in mind that the simultaneous presence of NO_2 and NH_2 on adjacent tertiary carbons can sometimes introduce significant instability. We have analyzed this problem in detail elsewhere [6-9].) Another important observation is that the introduction of aza nitrogens increases I_S [compare 32 and 20].) This can be attributed to the greater heats of formation of the aza analogues.

Tetranitrotetrahydrene **36** and 1-amino-2-nitrohydrazine **37** are structurally dissimilar but have identical relative I_S values of 1.03. Table IV shows that the former has a fairly low n/M value but a reasonably high heat



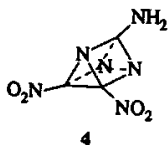
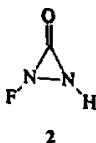
of formation; the reverse is true for **37**. Yet, their I_S values are the same. This example emphasizes again how the interplay between two key factors helps to determine the specific impulse.

It is interesting to compare RDX (**46**; 1,3,5-trinitro-1,3,5-triazacyclohexane) and 1-difluoroamino-3,5-dinitro-1,3,5-triazacyclohexane (**28**) (Table IV). The latter has a calculated specific impulse approximately 7% better than RDX. This is evidently largely due to the increase in the



number of moles of gaseous products per unit weight of propellant that can be achieved by replacing an NO_2 by an NF_2 . Thus, from the standpoint of specific impulse, the presence of fluorine (e.g., in the form of the NF_2 group) is indeed desirable. This will be discussed further in the next section.

Molecules **2** and **4** have high specific impulse values, calculated to be 25 and 20% better than HMX, respectively. Both of these compounds have relatively high heats of formation and produce fairly large amounts of



gaseous products per unit weight, as estimated by stoichiometry (Table IV). Our calculated results point out quite clearly that to greatly improve over HMX in terms of specific impulse (e.g., as in the cases of **2** and **4**) it is necessary to combine molecular features that lead to each of these desired consequences.

V. Perspectives

In calculating the specific impulses reported in Tables I-IV, we have used the Naval Weapons Center program [3] to predict the types and quantities of gaseous products formed from each particular monopropellant. However, it is possible to use simpler approaches to estimate these quantities. We have explored the use of one such technique, which assumes that the products are limited to CO, CO₂, H₂O, N₂, H₂ and HF [10]. Except for fluorine-containing systems, the relative I_S values calculated in this manner [via Eq. (1)] follow in general the same pattern as those obtained using the more rigorous Naval Weapons Center method for determining the profiles of the gaseous products. This is a useful finding, which supports our use of the stoichiometric n/M ratio as a rough measure of the number of moles of gaseous products per unit weight propellant.

The relative specific impulse is also not highly sensitive to the method used for obtaining the heat of formation. For example, the trends in I_S observed in Tables I-III are in general well reproduced using heats of formation computed with the AM1 procedure alone without the correction for crystal effects.

As mentioned earlier, the heat of formation of a molecule is often viewed as a measure of its energy content. It is important to recognize, however, that ΔH_f is actually a *change* in enthalpy, and thus depends upon the initial (i.e., reference) systems as well as the molecule of interest. Thus a fluorine-containing compound may have a rather low ΔH_f because it is relative to very weakly bonded F₂, and yet may release considerable energy upon decomposition if this produces the strongly bonded HF. In such a case, it can be misleading to take ΔH_f as an indicator of available energy. For example, Table IV shows that ΔH_f of RDX (46) is twice as great as that of 1-difluoroamino-3,5-dinitro-1,3,5-triazacyclohexane (28). While the latter does have a better n/M ratio, by a factor of 1.4, it may nevertheless seem surprising that 28 has the higher specific impulse. This can be understood, however, in terms of the F₂/HF effect.

Our earlier observation that the presence of aza nitrogens is accompanied by a larger heat of formation can similarly be explained by noting that the reference state for these is the very stable N₂ molecule. Since this is also their ultimate decomposition product, the increase in ΔH_f does reflect a greater energy content. This conclusion may seem to be inconsistent with recent work in which we have shown that aza nitrogens have a stabilizing effect upon many molecules, both strained and unstrained [11,12], which we attribute to delocalization of their lone pairs [13]. This apparent contradiction can be resolved, however, by recognizing that different reference states are involved in the two situations. The observed aza stabilization, as

detected by isodesmic reaction analyses, is relative to certain "standard" C-N, C-C, C-H and N-H bonds, as found in $\text{H}_3\text{C-NH}_2$ and $\text{H}_3\text{C-CH}_3$, whereas heats of formation are relative to N_2 (g), H_2 (g), C(s), etc. Thus aza nitrogens have the attractive feature that their stabilizing influence may be beneficial from the standpoint of synthesis, especially in the case of strained systems, but yet should not impair (may indeed improve) detonation or propellant performance.

VI. Summary

In designing molecules to have high specific impulse values and thus to merit consideration as monopropellants, it is generally desirable to try to satisfy two key criteria: (a) combustion should lead to light gaseous products, so as to maximize the number of moles of gases produced per unit weight of propellant; and (b) the compound should have a large positive heat of formation (on a weight basis), since this results in a high combustion temperature. We have presented a rationalization based on simplified kinetic theory arguments to justify the importance of these two factors, and we have further demonstrated it through a comparative analysis of our calculated relative I_S values for a large number of molecules. To achieve significant improvement over HMX in specific impulse, it seems necessary to combine molecular features that will lead to both of the consequences (a) and (b). The presence of strain and aza nitrogens favors a high heat of formation, while the inclusion of some hydrogens and fluorines, results in light gases (H_2O and HF) being formed as combustion products.

ACKNOWLEDGMENT

We greatly appreciate the support of this work by the Office of Naval Research through contract #N00014-85-K-0217.

REFERENCES

1. R. Meyer, *Explosives*, VCH, Weinheim, W. Germany, 1987.
2. M. Grayson and D. Eckroth, eds., *Kirk-Othmer Encyclopedia of Chemical Technology*, third edition, John Wiley & Sons, New York, 1980, Vol. 9, p. 620.
3. Newpep program obtained from the Naval Weapons Center, China Lake, CA.
4. D. A. Liotard, E. F. Healy, J. M. Ruiz, and M. J. S. Dewar, Quantum Chemistry Program Exchange, Program No. 506, 1989.
5. J. P. Ritchie and S. M. Bachrach, in "Report on Working Group Meeting on Sensitivity of Explosives," New Mexico Institute of Mining and Technology,

- Socorro, NM, March 1987. (G. R. Husk, ed., Army Research Office, Research Triangle Park, NC 27709).
6. P. Politzer, G. P. Kirschenheuter, and J. Alster, *J. Amer. Chem. Soc.* **109**, 1033 (1987).
 7. M. Grodzicki, J. M. Seminario, and P. Politzer, *J. Phys. Chem.* **94**, 624 (1990).
 8. J. S. Murray, J. M. Seminario, and P. Politzer, *Structural Chem.*, **2**, 153 (1991).
 9. J. S. Murray, M. Concha, J. M. Seminario, and P. Politzer, *J. Phys. Chem.* **95**, 1601 (1991).
 10. Per Sjoberg, Ph. D dissertation, University of New Orleans, 1989.
 11. J. S. Murray, P. C. Redfern, J. M. Seminario, and P. Politzer, *J. Phys. Chem.*, **94**, 2320 (1990).
 12. J. S. Murray, J. M. Seminario, P. Lane, and P. Politzer, *J. Mol. Struct. (THEOCHEM)*, **207**, 193 (1990).
 13. M. J. S. Dewar, *J. Amer. Chem. Soc.* **106**, 669 (1984).



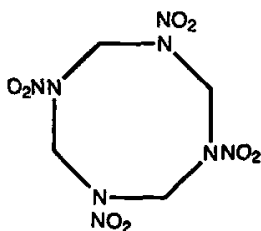
5

Polycyclic Amine Chemistry

Arnold T. Nielsen

I. Introduction

The need exists for new high-energy, high-density materials with densities greater than 2.0 g/cm^3 and with detonation velocities (D) approaching $10 \text{ mm}/\mu\text{sec}$. Such powerful explosives would have detonation pressures (P_{CJ}) greater than 400 kilobars (kbar). Known explosives 1,3,5,7-tetranitro-1,3,5,7-tetraazacyclooctane (HMX, 1) and hexanitrobenzene (HNB, 2) have densities near 2.0 g/cm^3 , detonation pressures near 400 kbar, and detonation velocities around 9.1 to $9.5 \text{ mm}/\mu\text{sec}$. To achieve greater detonation velocities and pressures explosives of higher density are required.

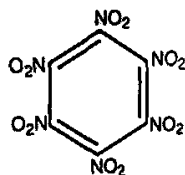


1

d 1.90 g/cm^3

D $9.1 \text{ mm}/\mu\text{sec}$

P_{CJ} 390 Kbar



2

2.0

9.4

406

The densities and detonation velocities of unknown explosives may be calculated with reasonable accuracy (± 2 to 5% depending on structure) (Refs. 1-5). If the molecule is known, its energy parameters may be calculated more accurately from its heat of formation (Refs. 4,5). The equations shown below demonstrate the importance of the density of the explosive

itself relative to its energy. They show that the detonation pressure at the shockwave front is proportional to the square of the density. Thus, a slight increase in density can significantly increase the energy of an explosive.

$$D = A\phi^{1/2}(1 + B\rho_0) \quad P = K\rho_0^2\phi \quad \phi = NM^{1/2}Q^{1/2}$$

D = detonation velocity (Km/s)

P = detonation pressure (Kbar)

ρ_0 = initial density of explosive (g/cm^3)

N = moles of gaseous detonation products/g

M = average molecular weight of detonation product gases

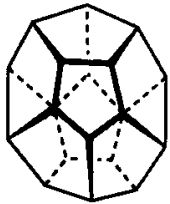
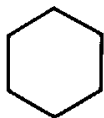
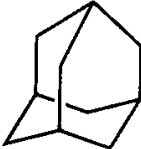
Q = chemical energy of the detonation reaction (cal/g)

A, B, K = constants

Certain structural parameters are known to maximize density. In addition to high symmetry, these include an optimum number of quaternary and/or tertiary carbons, tertiary nitrogens, and condensed rings. Thus, density should generally increase as one proceeds in the structural alteration from acyclic \longrightarrow monocyclic \longrightarrow bicyclic \longrightarrow polycyclic \longrightarrow condensed polycyclic (caged). The most dense molecular arrangement is found in polycyclic caged molecules. Examples of some caged molecules are shown in Table I.

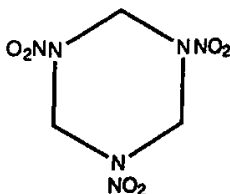
The densities of the monocyclic compound, with the corresponding caged molecule composed on the same ring-sized units, are compared. It can be seen that the caged densities are higher than those of the monocycles. For example, the density of cubane ($1.28 \text{ g}/\text{cm}^3$) (Refs. 6,7) is nearly double that of cyclobutane (0.70). Dodecahedrane is one of the most dense caged hydrocarbons known (1.45) (Refs. 8,9); again, its density is nearly double that of the monocycle cyclopentane (0.74). Adamantane, when compared to the monocycle cyclohexane, does not show as much of an increase in density; however, the number of hydrogens removed is not large. On the other hand, if one removes all of the hydrogens leading to the completely condensed adamantane-derived material diamond ($d = 3.51$), a very significant increase in density is observed. It must be noted that it is not sufficient to simply remove hydrogens to achieve a large density increase. Removing six hydrogens from the monocyclic cyclohexane to produce the monocycle benzene ($d = 0.88$) does not alter the density significantly. To achieve very high density a condensed polycyclic cage is required.

Table I. Densities of Caged Hydrocarbons

Monocycle	Density (g/cm ³)	Caged	Density (g/cm ³)
	0.70		1.28
	0.74		1.45
	0.78		1.07

II. Approaches to Synthesis of Caged Nitramine Explosives

Two of the most important military explosives are RDX (1,3,5-trinitro-1,3,5-hexahydrotriazine (3) and HMX (1) (Refs. 10-17).



3 (RDX)

$$d = 1.81 \text{ g/cm}^3$$

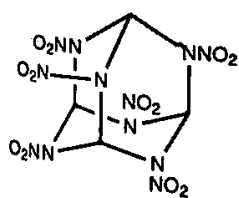
$$D = 8.85 \text{ mm}/\mu\text{sec}$$

$$P_{CJ} = 338 \text{ kbar}$$

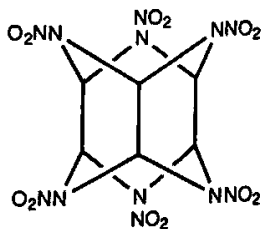
Thus, the preferred approach to caged nitramines is usually the first method, which departs from a caged polyamine containing the required number of amino groups in the desired positions.

The problem of polyaza caged nitramine synthesis may be reduced to two subproblems. First, the polyaza caged ring system must be synthesized. Second, a suitable methodology must be applied that ultimately introduces nitro groups on all of the endocyclic nitrogens of the cage to yield the caged nitramine. The problem presents several difficulties. The most serious one is the synthesis of the required polyamine cage: none of the desired polyaza structures were known for proposed target explosives at the time this research was initiated. A second problem is the vulnerability of aminal and orthoamide nitrogen structures within the cages to ring-opening reactions when subjected to nitration reaction conditions. The acidic and oxidizing medium of a nitration mixture could easily destroy such structures. New nitration procedures may be required.

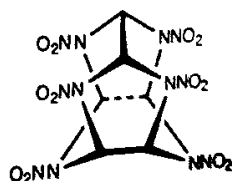
Target polycyclic nitramine explosives have been selected having the desired structural features leading to high density and energy. In the present discussion synthetic methodology that might lead to three target molecules is discussed. These are hexanitrohexaazaadamantane (7), -wurtzitane (8) and -isowurtzitane (9). Calculated values (Refs. 1-5) shown reveal that these substances have explosive properties potentially superior to those of HMX (1). The name isowurtzitane is ascribed to the cage system 9 due to its close relationship to wurtzitane. The isomeric hydrocarbons wurtzitane and isowurtzitane have the same adjacent groupings of atoms (six methylene bridges, six methines at bridgeheads, and three CHCH groups bonded through methylenes).



7



8



9

$d(\text{calcd})$	2.1 g/cm ³
$D(\text{calcd})$	9.5 mm/ μsec
$P_{\text{Cl}}(\text{calcd})$	434 kbar

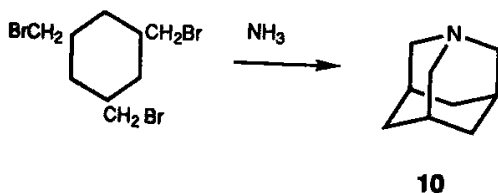
2.1
9.4
420

2.1
9.4
420

III. Polyazaadamantanes

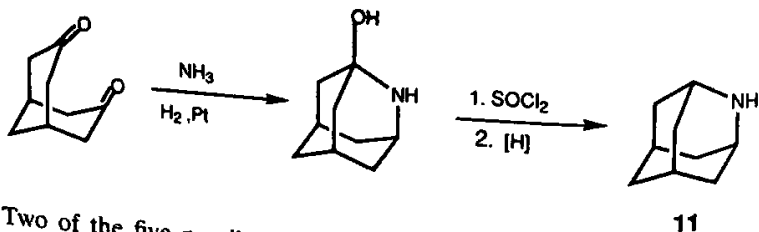
More examples of azaadamantanes are known than those of any of the other caged azapolycyclics under discussion. Although the hexaaza system (7) is unknown, azaadamantane examples have been reported containing one, two, three, and four endocyclic nitrogens. It should be reemphasized that for the purpose of synthesizing caged nitramine explosives, only those cages having nitrogen at a bridge (rather than a bridgehead) are desired precursors. The synthesis of heteroadamantanes has been reviewed (Refs. 21,22).

Both of the possible monoazaadamantanes are known. Three independent investigators prepared 1-azaadamantane (10) (1954, 1956) (Refs. 23-25).

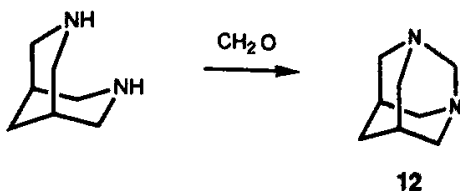


Alternate syntheses were reported later (Refs. 26,27). Synthetic routes leading to ring-substituted derivatives of 1-azaadamantane have been reported (Refs. 28-33), including the C-nitro energetic material 3,5,7-trinitro-1-azaadamantane (Ref. 28). We have also prepared this latter compound in our laboratory and confirmed its structure by x-ray crystallography.

The other isomer, 2-azaadamantane (11), was first prepared by Stetter in 1964 (Refs. 34,35); it is the first example of an azaadamantane to be prepared that contains a nitrogen at a bridge. Several ring-substituted derivatives of 2-azaadamantane have been obtained by various synthetic routes (Refs. 36-42).

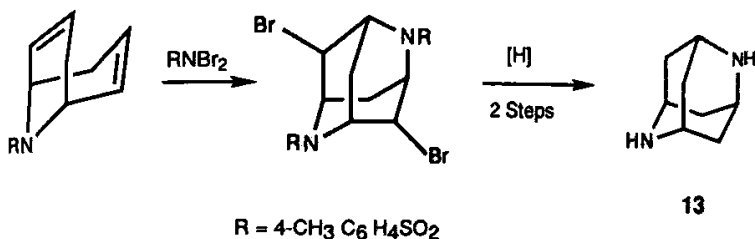


Two of the five possible diazaadamantanes are known (1,3- and 2,6-isomers). 1,3-Diazaadamantane (12) was first reported by two independent groups in 1955 (Refs. 43,44); another synthesis was described later

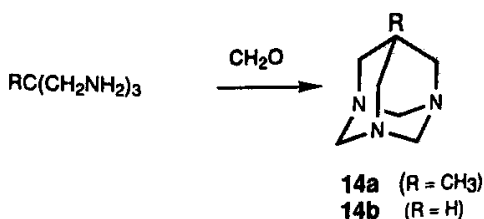


(Ref. 45). Many derivatives of 1,3-diazaadamantane have subsequently been reported (Refs. 46–60).

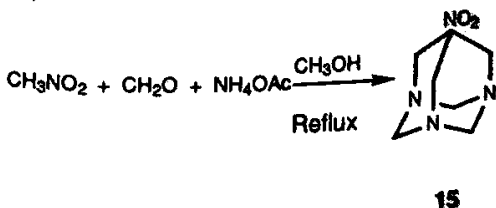
2,6-Diazaadamantane (**13**) was first reported by Stetter and Heckel in 1972 (Refs. 61,62). Two other syntheses were reported in 1973 (Refs. 63,64).



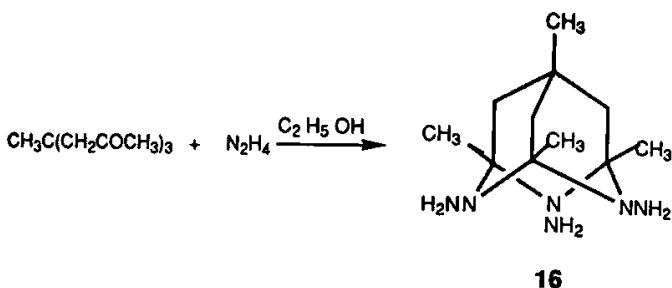
Only three of eleven possible triazaadamantanes are known (1,3,5-, 2,4,9- and 2,4,10-isomers). Stetter was first to prepare one of these, 7-methyl-1,3,5-triazaadamantane (**14a**) in 1951 (Ref. 65). The parent unsubstituted compound **14b** was obtained by Meurling in 1975 (Ref. 66).



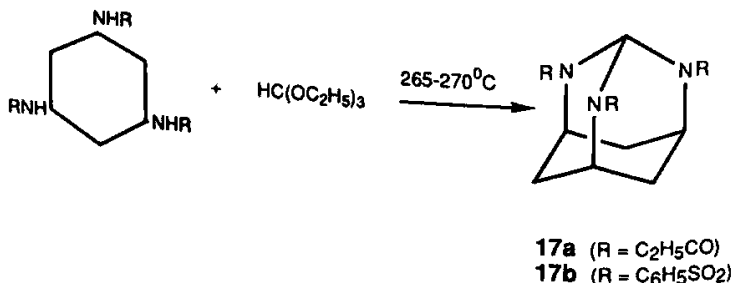
These syntheses depend on the reaction of a trimethylaminomethane with formaldehyde. Reaction of formaldehyde with nitromethane and ammonium acetate in refluxing methanol leads to 7-nitro-1,3,5-triazaadamantane (**15**) (Refs. 67–76).



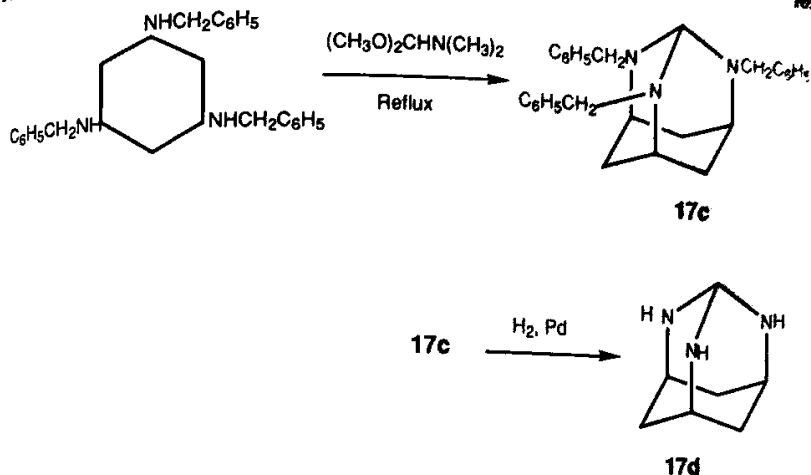
One 2,4,9-triazaadamantane derivative has been prepared. By reaction of hydrazine with 1,1,1-trisacetonylethane in ethanol solvent, Quast and Berneth obtained a 65% yield of 1,3,5,7-tetramethyl-2,4,9-triamino-2,4,9-triazaadamantane (**16**) (Refs. 77,78). Reaction of the triketone with ammonia gave a dioxaminoazaadamantane derivative. Attempts to prepare an *N,N',N''*-unsubstituted- 2,4,9-triazaadamantane were unsuccessful.



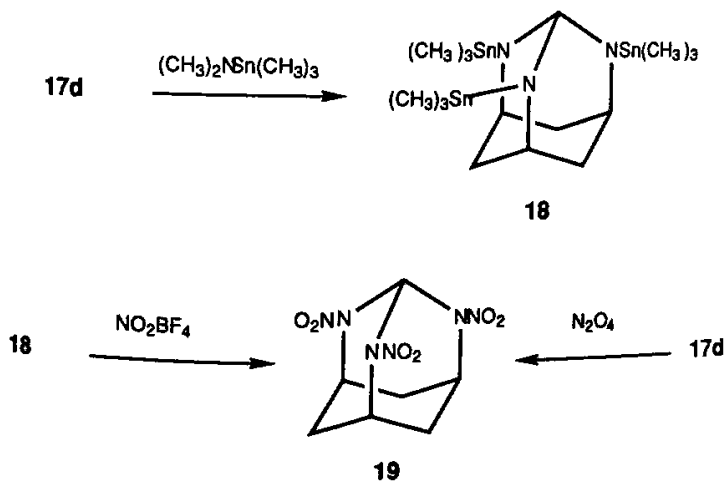
Several 2,4,10-triazaadamantane derivatives have been prepared; they are caged orthoamide structures. The first of these reported were the tris-*N*-propionyl and *N*-benzenesulfonyl derivatives **17a,b** prepared by Stetter (1970) (Ref. 79). These were obtained by heating the *cis*- or *trans*-1,3,5-trisamidocyclohexanes with ethyl orthoformate at 265–270°C. Stetter also obtained the tris-*N*-methyl and *N*-benzyl derivatives in a similar manner at 30% yield (Ref. 80). We found that the *N*-benzyl derivative **17c** could be obtained in higher yield (75%) by refluxing the tris-*N*-benzylaminocyclohexane with dimethylformamide dimethyl acetal (Ref. 81); the structure of **17c** was confirmed by x-ray crystallography.



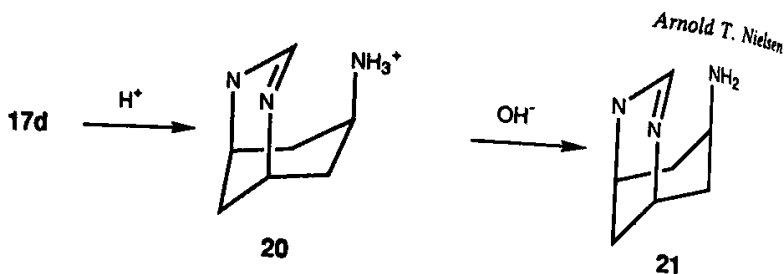
Hydrogenolysis of the benzyl groups in **17c** with hydrogen and palladium on charcoal catalyst (in ethanol solvent) led to the parent orthoamide 2,4,10-triazaadamantane **17d**. Reaction of **17d** with dimethylaminotrimethyl tin gave the *N,N',N''*-tristrimethylaminotin derivative **18**. Reaction



of **18** with nitronium tetrafluoroborate in acetonitrile solvent produced 2,4,10-trinitro-2,4,10-triazaadamantane **19**, the first example of a caged nitramine. It is also the first example of a trinitro orthoamide (Ref. 81). Reaction of **17d** in strongly alkaline medium (added aqueous sodium hydroxide) with nitric oxide in air also gave **19** (low yield).



The orthoamide **17d** is a crystalline hygroscopic solid, stable on dry storage at 0°C. It is a strong base. In solution in D₂O it exhibits a sharp characteristic singlet at $\delta 7.6$, which is unchanged on standing for several hours. The molecule is very sensitive to acids. Acidification of the solution produces immediate disappearance of the $\delta 7.6$ singlet and the appearance



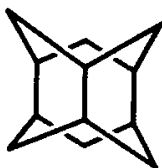
of a new singlet of equal intensity at $\delta 8.3$, assigned to the amidinium cation-CH proton in **20**. On again making the solution basic by addition of potassium carbonate (pH9) the spectrum remains virtually unchanged and is presumably that of the free amidine base **21**.

The only known adamantane containing more than three endocyclic ring nitrogens is hexamethylenetetramine (hexamine, 1,3,5,7-tetraazaadamantane, **4**). It is readily prepared by reaction of formaldehyde and ammonia and was first described by Butlerov in 1859 (Ref. 82). Its preparation and properties have been reviewed (Ref. 83). The mechanism of formation from formaldehyde and ammonia has been studied (Refs. 84,85). Hexamine is employed as a reactant in the synthesis of RDX (**3**) and HMX (**1**).

In summary, most of the known synthetic routes to azaadamantanes depend on condensation of an amine or ammonia with a carbonyl compound or equivalent (aldehyde, ketone, ortho ester, acetal) or other active methylene compound, such as nitromethane. The syntheses of **10** and **13** employed bromo intermediates in displacement or addition reactions.

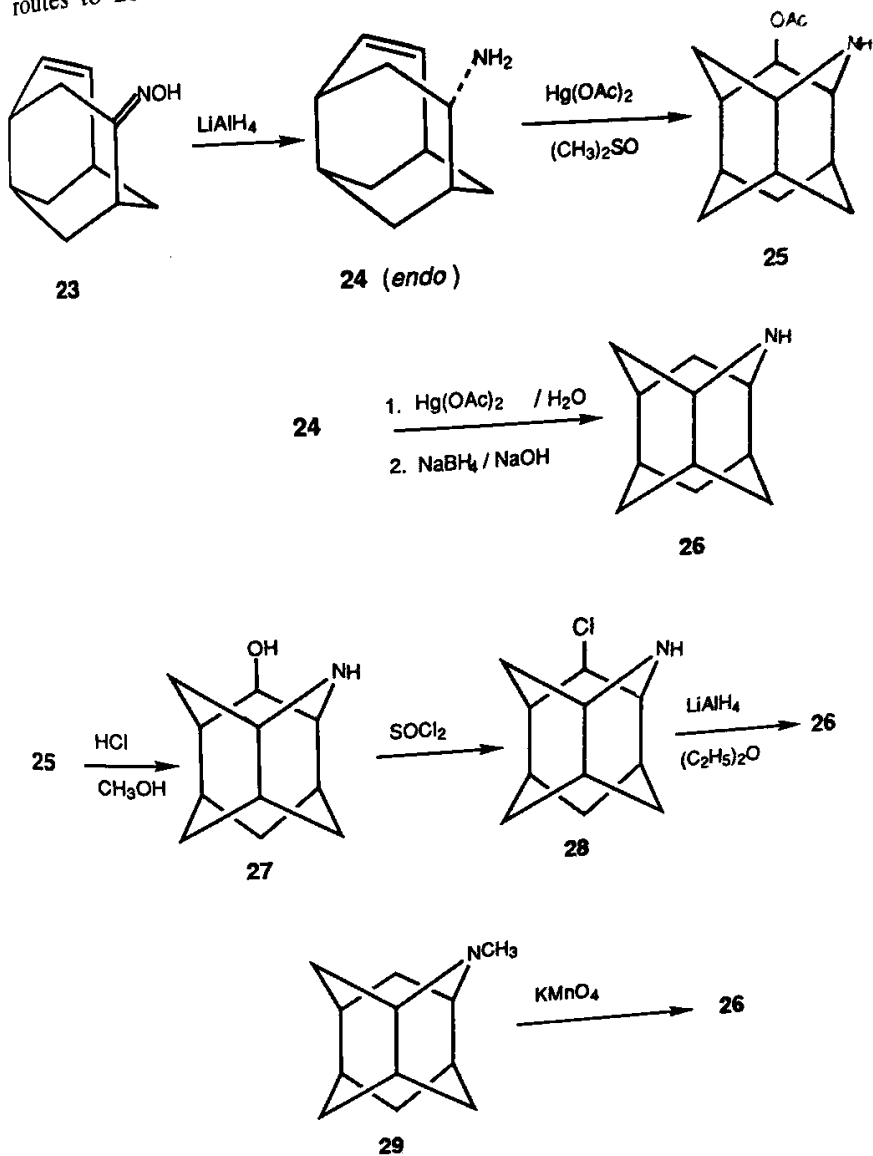
IV. Polyazawurtzitanes

Only two types of azawurtzitanes are known, 3-aza- and 3,5,12-triaza compounds. The parent hydrocarbon wurtzitane (**22**, also called iceane) was first synthesized by Cupas and Hodakowski in 1974 (Ref. 86a); its



density, determined by x-ray crystallography is 1.04 g/cm^3 , similar to that of adamantane (Table I) (Ref. 86b).

Only one monoazawurtzitane is known. 3-Azawurtzitane (**26**, Scheme 1) was reported by Klaus and Ganter in 1980 (Ref. 87). Several synthetic routes to **26** were described. The oxime **23** on reduction with lithium

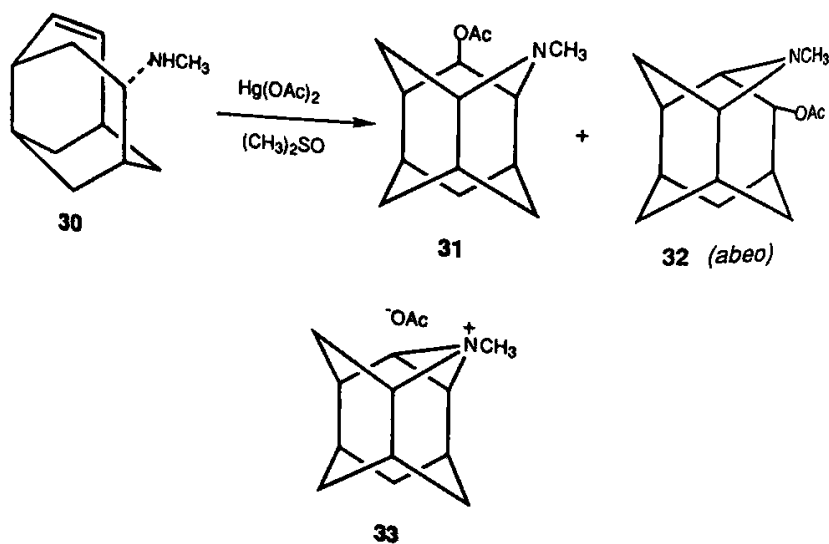


Scheme 1

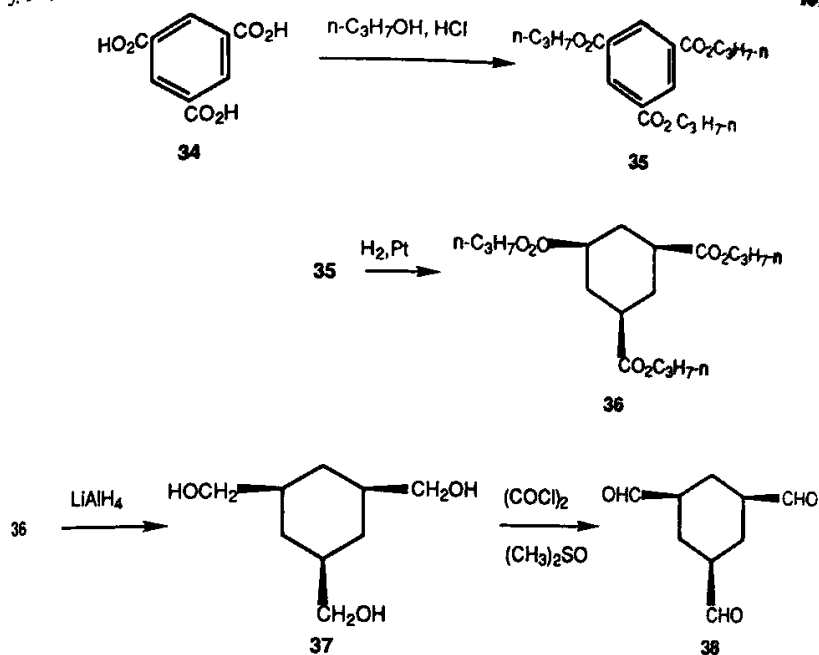
aluminum hydride gave the desired *endo* amino derivative **24** in 66% yield. Treatment of **24** with mercuric acetate in dimethyl sulfoxide produced 5-acetoxy-3-azawurtzitane **25** in 49% yield. By reaction of **24** with mercuric acetate in aqueous medium, the intermediate acetate **25** was reduced *in situ* by sodium borohydride in basic medium to yield 3-azawurtzitane **26** directly. The acetate **25** could be hydrolyzed to 3-aza-5-wurtzitanol (**27**), which with thionyl chloride produced the 5-chloro derivative **28**. Lithium aluminum hydride reduction of **28** also produced **26**. The *N*-methyl derivative of **26** was also prepared (**29**), which could be oxidized to **26** with potassium permanganate.

If certain *endo* substituents are present in the 5-position, mixtures of 3-azawurtzitanes (such as **31** and 3(4 \rightarrow 5)*abeo*-3-azawurtzitanes, such as **32**) are sometimes obtained (Scheme 2). For example, mercuric acetate in dimethyl sulfoxide treatment of *N*-methyl olefin **30** produced a mixture of 5-acetoxy-3-methyl-3-azawurtzitane (**31**, 62% yield) and 4-acetoxy-3-methyl-3(4 \rightarrow 5)*abeo*-3-azawurtzitane (**32**, 17% yield). These reactions are believed to proceed through an intermediate aziridinium ion **33**.

The other known azawurtzitane ring system, 3,5,12-triazawurtzitane was first reported from our laboratory in 1987 (Ref. 88). Several 3,5,12-trisubstituted-3,5,12-triazawurtzitanes (3,5,12-tetraazatetracyclo[5.3.1.1^{2,6}.0^{4,9}]*dodecanes*, **40a-e**) have been obtained by condensation of 1,3,5-triformylcyclohexane (**38**) with selected amines.



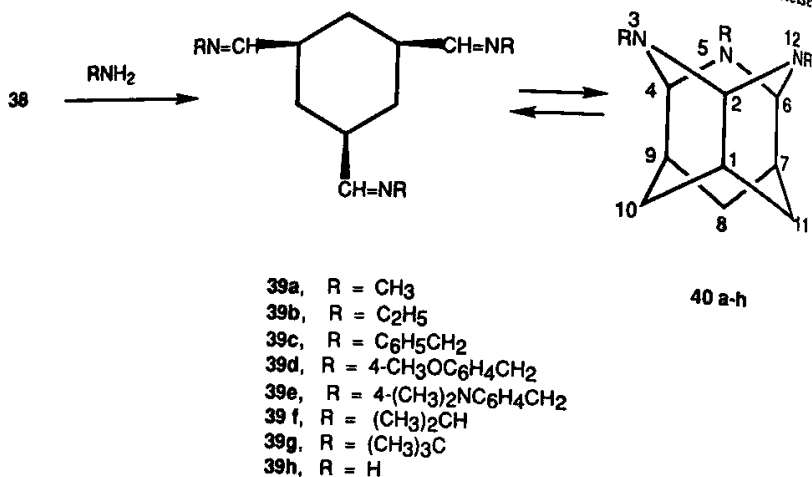
Scheme 2



Scheme 3

The trialdehyde **38** was obtained in four steps in 60–65% overall yield from trimesic acid (**34**, Scheme 3). Esterification of **34** with 1-propanol in excess, by refluxing with hydrogen chloride catalyst, leads to triester **35** in quantitative yield. Hydrogenation of **35** in acetic acid solvent (Pt catalyst) yields pure *cis,cis*-cyclohexane-1,3,5-tricarboxylate ester **36**, also in quantitative yield. Reduction of ester **36** with lithium aluminum hydride in tetrahydrofuran solvent produces *cis,cis*-1,3,5-tris(hydroxymethyl)cyclohexane (*cis,cis*-**37**) in 90–95% yields. Swern oxidation of triol **37** led to *cis,cis*-1,3,5-triformylcyclohexane **38** in 70% yield. The stereochemistry of **38**, as well as that of precursors **36** and **37**, was established as *cis,cis* in each case by high resolution ^1H NMR.

The reaction of *cis,cis*-1,3,5-triformylcyclohexane (**38**) with primary amines in ether solvent at 25°C leads to triimines (**39**), and in some cases to 3,5,12-trisubstituted-3,5,12-triazawurtzitanes **40** (Scheme 4). Crystalline triazawurtzitanes **40a–e** were obtained with methylamine, ethylamine, benzylamine, 4-methoxybenzylamine and 4-(dimethylamino)benzylamine in high yields (Table II). The reaction is analogous to the trimerization of acyclic aldimines ($\text{CH}_2=\text{NR}$ or $\text{RCH}=\text{NH}$) leading to 1,3,5- or 2,4,6-trisubstituted-1,3,5-hexahydrotriazines (Refs. 89–92). Structures **40a–e** are supported by the NMR and mass spectra and infrared spectra. The



Scheme 4

wurtzitane stability decreases in the order of N-substitution: benzyl > 4-methoxybenzyl > 4-(dimethylamino)benzyl > methyl > ethyl. With isopropylamine and *tert*-butylamine, no evidence of the wurtzitane structure is seen in the infrared or ¹H NMR spectra (a 10-Hz doublet near δ3.9 in CDCl₃ solvent) and the products isolated are crystalline triimines (**39f,g**). Reaction of **38** with a large excess of methylamine over potassium hydroxide gave triimine **39a**. The structure of the benzyl derivative **40c** was established by x-ray crystallography.

In solution in various solvents, all of the wurtzitanes are observed to be in equilibrium with the corresponding triimines. With the benzylamines

Table II. Synthesis of
3,5,12-Trisubstituted-3,5,12-triazawurtzitanes

Compound	R	Yield, % ^a	Mp, °C ^b
40a	CH ₃		
40b	C ₂ H ₅	99	64–65 ^c
40c	C ₆ H ₅ CH ₂	88	50–60 ^c
40d	4-CH ₃ OC ₆ H ₄ CH ₂	83	92–97 ^d
40e	4-(CH ₃) ₂ NC ₆ H ₄ CH ₂	71	91–100 ^d
		100	115–129 ^d

^a Crude product.

^b The wide melting point range is attributed to triimine formation on heating.

^c Melting point of crude product; attempted recrystallization caused decomposition.

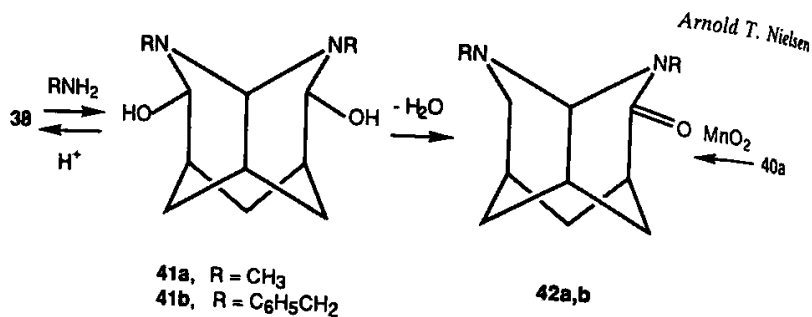
^d Melting point after recrystallization from pentane or hexane (ca. 50% recovery).

40c-e in CDCl_3 , the equilibrium concentration of the favored wurtzitane forms (reached in about four hours at 25°C) is approximately 80, 80, and 70%, respectively. With the methyl and ethyl wurtzitane derivatives **40a,b**, conversion to the triimine forms **39a,b** is much more rapid and complete. With the ethyl compound **40b** in CDCl_3 , the half-life is approximately ten minutes; within one hour, conversion to the triimine **39b** is virtually complete; in pyridine- d_6 the conversion to the triimine is slower, but practically complete within 18 hours. The methyl derivative **40a** behaves like **40b**, also completely converting to its triimine **39a** in CDCl_3 within 18 hours. Removal of the CDCl_3 solvent from solutions of **40a,b** after 18 hours produces an oily mixture of triimine and wurtzitane (approximately 1:1) as seen in the rapidly determined ^1H NMR spectra. The solvent effect on the equilibrium between **39** and **40** was examined for the 4-dimethylamino derivative **40e** in three solvents. The equilibrium concentration of **40e** was found to be approximately 85% in CD_2Cl_2 , 70% in CDCl_3 , and 55% in CD_3CN .

The reaction of ammonia with *cis,cis*-1,3,5-triformylcyclohexane **38** under various conditions leads to a polymeric substance, believed to be a polymer of the triimine **39h** ($\text{R} = \text{H}$). At very high pH (>12), the rate of polymerization is slower and some of the parent 3,5,12-triazawurtzitane **40h** is believed to be present [higher pH also favors stabilization of the related 1,3,5-hexahydrotriazine (Ref. 85)]. Evidence for the formation of **40h** in solution is seen in the ^1H NMR spectrum of the reaction mixture obtained from trial **38** and ND_4OD in D_2O . A singlet at $\delta 5.0$ is assigned to the 2,4,6-hydrogens since the 1,7,9-hydrogens presumably were exchanged by deuterium to produce **40h-1,3,5,7,9,12- d_6** . In solutions containing NH_4OH as well as ND_4OD , this signal is seen as a doublet at $\delta 4.7$ ($J = 10$ Hz) in **40h** due to coupling between the 2,4,6- and 1,7,9-hydrogens. Attempts to trap **40h** as its 3,5,12-triacetyl derivative (**40**, $\text{R} = \text{COCH}_3$) by reaction with acetic anhydride or ketene in strongly basic solution met with only partial success because of the low equilibrium concentration of **49h** under the reaction conditions.

Reaction of trial **38** with phenylhydrazine or hydrazine leads to its trishydrazone derivatives. These products polymerize with great ease and are not cyclized to 3,5,12-triamino-3,5,12-triazawurtzitane derivatives (**40**, $\text{R} = \text{C}_6\text{H}_5\text{NH}$ or NH_2).

The reaction of 1,3,5-triformylcyclohexane (**38**) with primary amines in refluxing ethanolic acetic acid takes a different course. The equilibrium mixture in this reaction includes significant amounts of carbinolamine intermediates, including partially cyclized tricyclics such as **41** (Scheme 5). From methylamine, the final product is a crystalline amide (3,5-dimethyl-2-oxo-3,5-diazatricyclo[5.3.1.0^{4,9}]decane (**42a**, 41% yield). The same type of reaction occurred between trial **38** and excess benzylamine in the presence of an acidic ion exchange resin catalyst in refluxing toluene, leading to the



Scheme 5

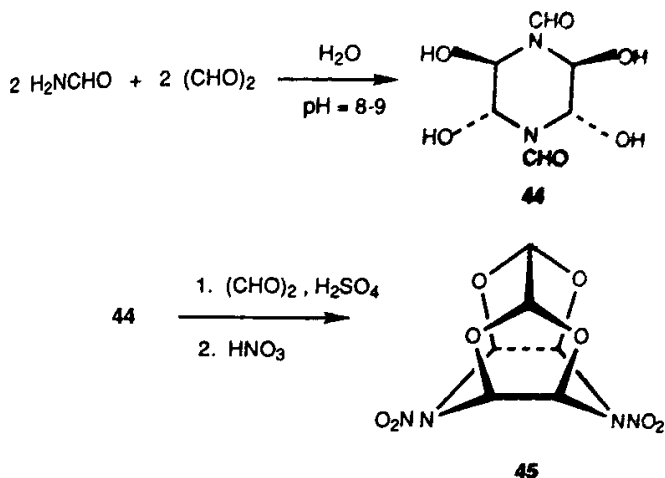
dibenzyl derivative **42b** in 36% yield. The more vigorous acid-catalyzed reaction conditions employed in these reactions, compared to those leading to the triazawurtzitanes **40**, may favor a hydride transfer in **41**, possibly with an iminium ion intermediate. The product **42a** was also obtained (42% yield), with loss of methylamine, by oxidation of triazawurtzitane **40a** (R=CH₃) with manganese dioxide at 25°C in chloroform solvent. Oxidation occurs at the bridgehead methine, ultimately leading to **42a**.

Both of the known azawurtzitanes have nitrogens at bridges, not bridgeheads. These substances appear to be somewhat less stable than azadamantanes containing bridged nitrogens. Under certain conditions the azawurtzitanes readily undergo reactions leading to destruction of the cage. Their syntheses include the carbonyl-amine condensation and olefin addition reactions of the type employed in the preparation of azaadamantanes.

V. Polyazaisowurtzitanes

Three polyazaisowurtzitane ring systems are known. These include diaza, tetraaza, and hexaaza examples; all, directly or indirectly, are obtained by condensations of glyoxal with amines. Unlike adamantane and wurtzitane, the parent hydrocarbon isowurtzitane **43** is unknown.

**43**

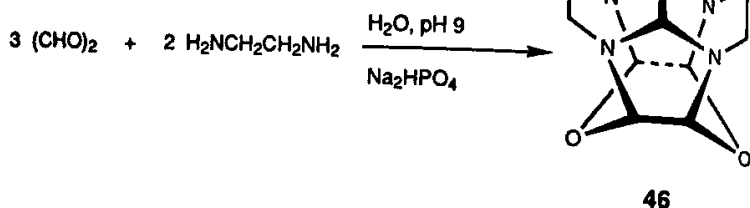


Scheme 6

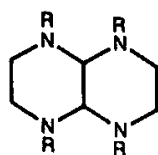
4,10-Dinitro-4,10-diaza-2,6,8,12-tetraoxatetracyclo[5.5.0.0^{5,9}.0^{3,11}]dodecane (4,10-dinitro-4,10-diaza-2,6,8,12-tetraoxaisowurtzitane, **45**) has been prepared by Boyer and co-workers (Ref. 93). The synthesis involves two laboratory steps, starting with the condensation of formamide with glyoxal at pH 8–9 (sodium bicarbonate buffer) to yield *trans,trans*-1,4-diformyl-2,3,5,6-tetrahydropiperazine (**44**, 60% yield, Scheme 6) (Refs. 94,95). Conversion of **44** to **45** occurs by addition of a mixture of **44** and glyoxal trimer to sulfuric acid at 0°C, followed by addition of nitric acid to produce **45** in 92% yield. The mechanism of formation of **45** is unknown, but may involve a diformyl isowurtzitane intermediate (**45**, NO₂ = CHO). However, when the reaction was conducted in sulfuric acid alone, no intermediates could be isolated. The structure of **45** was established by x-ray crystallography. At 100 K its density was found to be 2.03 g/cm³ (1.99 at 25°C by flotation), a value unusually high for a dinitramine.

The second known azaisowurtzitane, the tetraazaisowurtzitane 2,6,-ethylene-8,12-ethylene-4,10-dioxa-2,6,8,12-tetraazatetracyclo[5.5.0.0^{5,9}.0^{3,11}]dodecane (2,6-ethylene-8,12-ethylene-4,10-dioxa-2,6,8,12-tetraazaisowurtzitane, **46**) was reported by Edwards and Weiss in 1968 (Ref. 96). It was obtained in 20% yield by condensation of glyoxal with ethylenediamine in dilute aqueous solution buffered to pH 9 with Na₂HPO₄. Its structure was established by x-ray crystallography (Ref. 97).

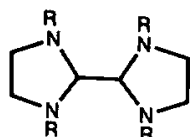
In aqueous ethanol solution glyoxal also reacts readily with ethylenediamine and *N,N'*-disubstituted ethylenediamines to yield other products, including *cis*- and *trans*-1,4,5,8-tetraazadecalins (**47**), 2,2'-biimidazolidines (**48**) and 9,10-dioxa-1,4,5,8-tetraazaperhydroanthracenes (**49**), among



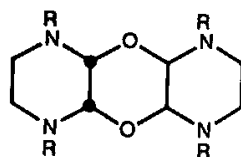
others (Refs. 98–106). The products obtained depend on the amine substituent and the reaction conditions. When R is benzyl, the principal products can be *trans*-**47**, **48** or **49**. When R is phenyl one obtains only **48**. When R is hydrogen or methyl the product is principally **47**. Substituted dioxatetraazaperhydroanthracenes have been isolated in 5–11% yields when R = methyl, isopropyl, and benzyl; the stereochemistry has been established as *cis-transoid-cis*- in each case by NMR spectroscopy (Ref. 106). The x-ray crystal structure of **49** (R = isopropyl) has been established. The *cis* and *trans*- forms of **47** may be equilibrated in hot deuteriochloroform solvent.



47

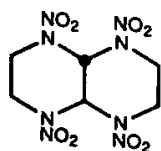


48



49

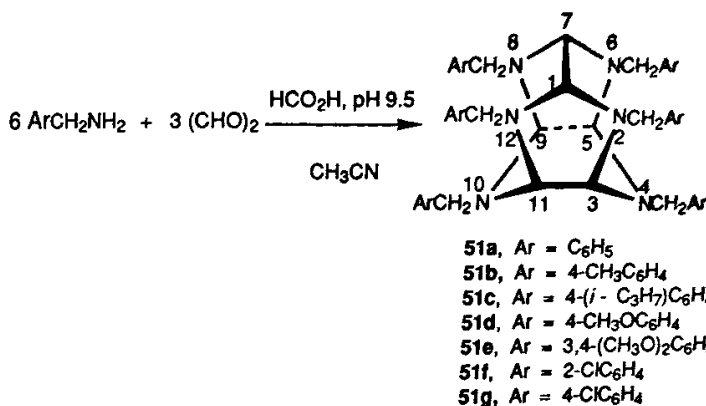
trans-1,4,5,8-Tetraazadecalin (**47**, R = H) was nitrosated to produce *trans*-1,4,5,8-tetranitroso-1,4,5,8-tetraazadecalin (**47**, R = NO). Stepwise reaction of the tetranitroso compound with 100% nitric acid produced *trans*-1,4,5,8-tetranitro-1,4,5,8-tetraazadecalin (**50**) in 47% overall yield from glyoxal and ethylenediamine. Its crystal structure was established by x-ray crystallography ($d = 1.84 \text{ g/cm}^3$) (Ref. 104).



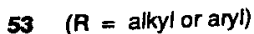
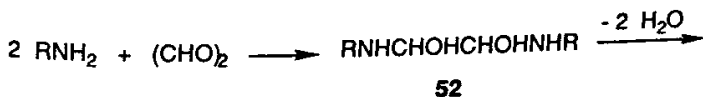
50

The third known polyazaisowurtzitanes was first prepared in our laboratory by a facile condensation of glyoxal with benzylamine to produce a new polyazapolycyclic ring system, 2,4,6,8,10,12-hexabenzyl-2,4,6,8,10,12-

hexaazatetracyclo[5.5.0.0^{5,9}.0^{3,11}]dodecane (hexabenzylhexaazaisowurtzitane, **51a**). (Ref. 107) The reaction is also successful with phenyl-substituted benzylamines leading to derivatives **51b-g**. The caged product is unusual in that all of the endocyclic nitrogens are at bridges, with none at bridgeheads as in hexamine **4**.



The new condensation reactions of amines with glyoxal to yield hexaazaisowurtzitane derivatives **51** appear to be limited to benzylamine and certain phenyl-substituted benzylamines. Primary aliphatic amines and anilines usually form dicarbinolamines **52** or diimines **53** (Refs. 108-112). With certain arylamines, such as 2-chloroaniline or aniline itself, one may obtain **52** or 1,1',2,2'-tetrakis(arylamino)ethanes (Ref. 109). The condensation of benzylamine with glyoxal was apparently not described in the literature prior to our report (Ref. 107). However, condensations of α -methylbenzylamine and α,α -dimethylbenzylamine with glyoxal have been reported to produce diimines (**53**, R = C₆H₅CHCH₃ and C₆H₅C(CH₃)₂, respectively) (Refs. 111,112).



Hexabenzylhexaazaisowurtzitane (**51a**) is prepared in a very facile manner by condensation of nearly stoichiometric quantities of benzylamine with 40% aqueous glyoxal in aqueous acetonitrile solvent at 25°C. An acid catalyst (formic acid, 0.1 molar % of the amine) is required. The solution

Table III. Synthesis of Hexabenzylhexaazaisowurtzitanes

Compounds	Phenyl substituent	Mp, °C ^a	Yield, % ^b	
			Procedure A	Procedure B
51a	H	154–155	80	64
51b	4-CH ₃	172–174	68	49
51c	4- <i>i</i> -C ₃ H ₇	144–145	24	52
51d	4-CH ₃ O	148–150	60	35
51e	3,4-(CH ₃ O) ₂	160–161	50	11
51f	2-Cl	208–211	68	15
51g	4-Cl	212–214	46	15

^a Melting point of analytical samples recrystallized from acetonitrile.

^b A modified procedure B was employed (except for 51a) in which all of the reactants are mixed at once and methanol is used as the solvent.

reaches a pH of about 9.5 at this point. The yield appears to be independent of the carboxylic acid catalyst employed if the pH is optimum. The reaction is rapid and nearly complete within a few hours. Crystalline 51a separates from the reaction mixture (75–80% yield). Six phenyl-substituted derivatives of 51a were prepared by this same procedure (procedure A in Table III). Substituents included 4-methyl, 4-isopropyl, 4-methoxy, 3,4-dimethoxy, 2-chloro, and 4-chloro to produce good yields of phenyl-substituted derivatives 51b–g (Table 3). Aqueous methanol may also be employed as a solvent in the reaction (procedure B), but yields of 51a–g are usually lower. The yields by procedure B listed in Table 3 are for an unoptimized modification in which all the reactants are mixed at once rather than adding the glyoxal slowly. The reaction is much slower in methanol than in acetonitrile, requiring several days instead of a few hours to reach completion.

The hexaazaisowurtzitane ring system 51 is considerably more stable toward acids than is the related triazawurtzitane 40c, which undergoes very facile ring opening in the presence of acid catalysts, even weak ones. Also, in aprotic solvents such as chloroform-*d* and acetonitrile-*d*₃, 40c is in equilibrium with its monocyclic form 39. On the other hand, hexabenzylhexaazaisowurtzitanes 51a–g show no evidence of equilibration nor of decomposition in aprotic solvents by NMR assay. Furthermore, they are rather stable toward acids in aprotic solvents. The hexabenzyl compound 51a, for example, forms stable hydrochloride and hydrobromide salts in benzene, from which 51a may be regenerated by treatment with sodium hydroxide. However, 51a is completely decomposed by heating in acetic acid at 50°C for an hour or by treatment with 10% acetic acid in methylene chloride for several hours at 25°C. The decomposition products are unidentified oils.

glyoxal in 50% aqueous ethanol or tetrahydrofuran, containing formic acid catalyst at 0°C; the reaction is complete within a few minutes. The diol is isolated as a white, crystalline solid, mp 48–58°C, containing much water of solvation (40–50% by weight). The diimine *N,N'*-dibenzyl-1,2-ethanediimine **55** is obtained by simply dehydrating the hydrated diol under reduced pressure (0.1 mm, 25°C) for about an hour. Sufficient formic acid remains in the solvate to assure rapid and complete dehydration of the diol to the diimine. The diol **54** and diimine **55** may readily be distinguished by differences in their ¹H-NMR spectra. The diimine reveals a characteristic vinyl CH signal near δ8.08 in CDCl₃. The benzyl methylene signals appear at δ4.63 and 4.78 for **54** and **55**, respectively. The samples of **54** isolated are rather pure, except for the presence of water and some tetrahydrofuran or ethanol solvent. The diimine samples also contain water, in addition to some oligomers of **55** (¹H-NMR assay).

Diol **54** and diimine **55** are very reactive, unstable substances. At ambient temperature they rapidly change to brown gums within a few days; a low yield (3–5%) of **51a** may be isolated from the gums. However, in solution in acetonitrile solvent containing a small amount of formic acid, both **54** and **55** rapidly produce **51a** (50–60% yield). The diol reacts more slowly than the diimine, indicating dehydration of the diol **55** to be slower than trimerization of **55** to form **51a**. Of the total **51a** formed within 17 hours, 92% of it is formed within the first 30 minutes from diimine **55**, but only 75% from diol **54** during this same time period, under the same reaction conditions. The principal side reaction appears to be polymerization of **55**. Most diimines **53** isolated from other amines and glyoxal are stable materials; they do not polymerize readily nor do they self-react to produce isowurtzitanes. Dibenzyl diimines appear to be unusual in their very reactive behavior to produce **51**.

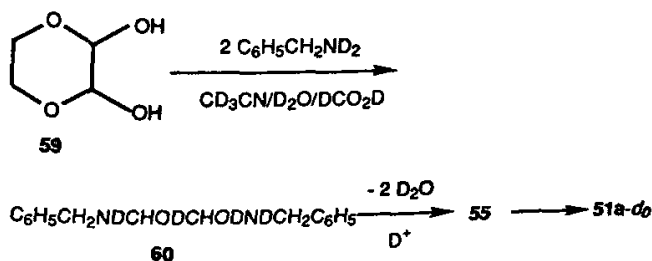
The diimine trimerization to yield **51a** is one of addition of a 1,2-dipole to itself (Scheme 7). The acyclic dimer of a diimine is a dipole, such as **56** which can cyclize and protonate most readily to form a five-membered ring monocyclic dimer (cation **57**). Reaction of **57** with dimer **55** and protonation should lead to the bicyclic trimer **58**. Intramolecular cyclization of **58** leads to **51a** after loss of two protons.

Monoimines derived from most aldehydes and ammonia undergo a related, extremely rapid trimerization to produce 2,4,6-trisubstituted 1,3,5-hexahydrotriazines. These reactions also proceed by additions of an imine 1,2-dipole to itself (Refs. 89,90). The reaction of amines with aldehydes to form *N,N',N''*-trisubstituted-1,3,5-hexahydrotriazines has also been observed; amines include anilines and benzylamine. However, with most amines the reaction is limited to reactions with formaldehyde (Refs. 113–116). Only methylamine and allylamine have been observed to produce

1,2,3,4,5,6-hexasubstituted-1,3,5-hexahydrotriazines, and only when reacting with acetaldehyde (Refs. 114–118). Other amines react with aldehydes to produce imines $RCH=NR'$ that do not cyclize to hexahydrotriazines. Diimine **55** is such an imine.

In the reactions of anilines with aromatic aldehydes to form Schiff bases, the rate-limiting step at neutral or slightly alkaline pH is dehydration of the carbinolamine intermediate $ArNHCHOAr'$ (Ref. 119). The rate of Schiff base formation is slower for electronegatively substituted anilines (Ref. 120). It has been observed in the condensation of benzylamines with glyoxal to form phenylsubstituted hexabenzylhexazaisowurtzitanes **51** that the rate is much slower with benzylamines bearing electronegative substituents (2-Cl, 4-Cl, 4- CH_3O , 3,4- $(CH_3O)_2$) than those with electron-releasing substituents (H, CH_3 , $i-C_3H_7$). Nitro-substituted anilines react with glyoxal to form dicarbinolamines (**52**, $R = 4-NO_2C_6H_4$, $3-NO_2C_6H_4$) of very great stability which do not readily dehydrate to diimines **53**.

To determine the effect of deuterium substitution on formation of **51a**, another method was employed to generate glyoxal. 2,3-Dihydroxy-1,4-dioxane **59**, a hemiacetal derivative of glyoxal, is a very useful precursor that does not require the 40% aqueous solution (Ref. 121). A mixture of **59** and benzylamine- $N,N-d_2$ in CD_3CN/D_2O with formic acid- d_2 as catalyst produced **51a** containing no deuterium. The yield of **51a** was only 30% after 22 hours, compared to 61% when the reaction was conducted in the same manner and the same concentrations with benzylamine/ CH_3CN/H_2O and formic acid catalyst (18-hour reaction time). The reaction is



roughly twice as slow in the deuterated medium, suggesting a proton transfer from the deuterated dicarbinolamine **60** in the rate-limiting step. The protonation of the intermediate anions from the 1,2-dipole self-reaction (**56**, Scheme 7, for example) would be expected to occur at or near the encounter rate. Thus, the observed deuterium isotope effect in the formation of **51a** suggests a rate-limiting step of dicarbinolamine dehydration. In related experiments, the diimine **55** was self-condensed in $CH_3CN/H_2O/HCO_2H$ and in $CD_3CN/D_2O/DCO_2D$ to yield **51a** in 59%

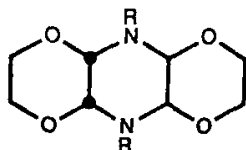
yield in both experiments (17-hour reaction time in each case). These results also indicate that trimerization of **55** to **51a** is not rate limiting.

The absence of deuterium in **51a** isolated from deuterated reactants and solvents discounts mechanisms that require exchange of benzyl α -methylene protons. Certain monoimines derived from benzylamine or α -substituted benzylamines undergo 1,3-dipolar addition with dipolarophiles such as styrene or methyl maleate to form substituted pyrrolidines (Refs. 122,123). These cyclizations require removal of benzyl α -methylene protons. Thus, 1,3-dipolar addition mechanisms of this type may be discounted as a route to **51a**. It has also been observed that the structurally related imine benzylidenebenzylamine, $C_6H_5CH_2N=CHC_6H_5$, does not exchange any of its protons in $CD_3CN/D_2O/DCO_2D$.

The question arises regarding the apparent uniqueness of benzylamines in the condensation with glyoxal, which leads to hexabenzylhexaazaisowurtzitanes. The mechanism depicted in Scheme 7 suggests that the benzyl group is exerting its characteristic stabilizing and activating influence on ionic intermediates. Most N-aryl and N-alkyl groups are much less effective for this purpose. Those groups that are effective, such as *tert*-butyl, are too sterically hindered or perhaps not sufficiently activating. α -Substituted benzylamines yield diimines that fail to trimerize owing to steric effects, known to inhibit imine 1,2-dipole self-reactions (Refs. 89,90,111,112).

The scope of the reaction of amines with glyoxal leading to hexabenzylhexaazaisowurtzitanes **51a** appears to be limited to benzylamine and certain phenyl-substituted benzylamines; it excludes α -substituted benzylamines. The published data indicate that most monoamines react with glyoxal to form diimines **53**. Attempts to convert certain diimines other than **55** into **51a**, under various reaction conditions, including conditions suitable for formation of **51a**, were unsuccessful. Diimines examined included **53**; $R = t-C_4H_9$, $i-C_3H_7$, $C_6H_5CH(CH_3)$, and $(CH_3)_3CCH_2$; the diimines were recovered unreacted. Reactions of mixtures of diimines (**53**, $R = t-C_4H_9$, $i-C_3H_7$, separately) with dibenzyl diimine **55** lead only to **51a** and recovered **53**. Also, mixtures of amines ($t-C_4H_9NH_2$ or $i-C_3H_7NH_2$, separately) with benzylamine and glyoxal lead only to **51a**. Heteroarylmethylamines and allylamines might be expected to produce hexaazaisowurtzitanes. However, efforts to extend the isowurtzitane synthesis to amines of this type were unsuccessful. Amines examined included furfurylamine, 4-pyridylmethylamine, 1- and 2-naphthylmethylamine, 2-aminoethylthiophene, allylamine, cinnamylamine, as well as 2-phenylethylamine and glycine methyl and ethyl esters; most of these reactions lead not to isowurtzitanes or diimines, but to complex, mostly polymeric noncrystalline mixtures. Substitution of 2,3-dihydroxy-1,4-dioxane **59** for 40% aqueous glyoxal in several of the above-mentioned experiments leads to similar results.

The reaction of benzylamine with 2,3-dihydroxy-1,4-dioxane (**59**) in acetonitrile solvent was examined in the presence of one molar equivalent of silver nitrate; no acid catalyst was added. The reaction took a different course. Instead of forming **51**, **54**, or **55**, the dioxane ring remained unopened and a 9,10-diaza-1,4,5,8-tetraoxaperhydroanthracene derivative (**61a**) was obtained (42% yield). This reaction was also observed with 4-pyridylmethylamine, in the absence of either silver nitrate or acid catalyst, to yield **61b** (67% yield). The structures **61a,b** are in agreement with their spectral data. An x-ray crystal structure determination established the structure of **61a**. Both **61** and the related **49** exhibit *cis-transoid-cis* ring stereochemistry.



61a, R = C₆H₅CH₂

61b, R = 4-C₅H₄NCH₂

The three polyazaisowurtzitanes described represent recently discovered ring systems. All have nitrogens at bridges, not bridgeheads. All are prepared by glyoxal-amine condensations. The initial step is more efficient in buffered solutions near pH 9. The polyazaisowurtzitanes are significantly more stable toward acids than the known polyazawurtzitanes.

VI. Summary

Caged nitramines are high-density materials, owing to the presence of structural features characteristic of all caged molecules not found in their acyclic and monocyclic analogues. The known highest energy explosives are those with the highest density (near 2.0 g/cm³). Caged nitramines with a ratio of nitramine to carbon of one or less should have densities near or greater than 2.0. Known methods of synthesizing polycyclic (caged) amines with endocyclic nitrogens in adamantane, wurtzitane, and isowurtzitane cages have been reviewed in this chapter. Most synthetic routes to these materials involve condensation of ammonia, amines, or amides with an aldehyde or ketone or a derivative thereof (acetal, orthoester, animals, etc.). Other less frequently employed methods include olefin additions and halogen-amine displacement reactions.

The desired caged nitramines have nitrogens at bridges to which the nitro group is attached; bridgehead nitrogens are absent. Synthesis of

caged nitramines most frequently involves the more efficient nitration of a preformed polycyclic amine or amine derivative, rather than cyclization of an acyclic nitramine precursor. However, the synthesis of nitramines can involve direct nitration of a polycyclic polyamine with nitrogens at bridge-heads, as in the formation of HMX from hexamine, although in this example the precursor cage is destroyed. Preferred methods include nitration of polycyclic amines, nitrosamines, amides, or trimethyltin-substituted amines. Most known methods of nitramine synthesis should be applicable to the synthesis of caged nitramines, provided destruction of the cage precursor does not occur under the reaction conditions.

REFERENCES

1. A. T. Nielsen. Naval Weapons Center Technical Paper No. NWC TP 5452, February, 1973; *Calculation of Densities of Fuels and Explosives from Molar Volume Additive Increments*; Naval Weapons Center, China Lake, Calif.
2. D. A. Cichra, J. R. Holden, and C. R. Dickinson. Naval Surface Weapons Center Technical Report No. NSWC TR-79-273, February 1980; *Estimation of Normal Densities of Explosives from Empirical Atomic Volumes*, Naval Surface Weapons Center, Silver Spring, Md.
3. (a) L. R. Rothstein and R. Petersen. *Propellants and Explos.* **4**, 56 (1979).
3. (b) L. R. Rothstein. *Propellants and Explos.* **6**, 91 (1981).
4. M. J. Kamlet and S. J. Jacobs. *J. Chem. Phys.* **48**, 23 (1968).
5. J. M. Short, H. F. Eccleston, E. E. Barody, K. F. Mueller, and M. J. Kamlet. *Propellants, Explos., Pyrotech.* **8**, 19 (1983).
6. P. E. Eaton and T. W. Cole, Jr. *J. Am. Chem. Soc.* **86**, 3157 (1964).
7. E. B. Fleischer. *J. Am. Chem. Soc.* **86**, 3889 (1964).
8. L. A. Paquette, R. J. Ternansky, D. W. Balogh and G. Kentgen. *J. Am. Chem. Soc.* **105**, 5446 (1983).
9. J. C. Gallucci, C. W. Doecke and L. A. Paquette. *J. Am. Chem. Soc.* **108**, 1343 (1986).
10. G. C. Hale. *J. Am. Chem. Soc.* **47**, 2754 (1925).
11. W. E. Bachmann and J. C. Sheehan. *J. Am. Chem. Soc.* **71**, 1842 (1949).
12. W. J. Chute, D. C. Downing, A. F. McKay, G. S. Meyers and G. F. Wright. *Can. J. Res.* **27B**, 218 (1949).
13. W. J. Chute, A. F. McKay, R. H. Meen, G. S. Meyers and G. F. Wright. *Can. J. Res.* **27B**, 503 (1949).
14. A. H. Vroom and C. A. Winkler. *Can. J. Res.* **28B**, 701 (1950).
15. T. C. Castorina, F. S. Holahan, R. J. Graybush, J. V. R. Kaufman and S. Helf. *J. Am. Chem. Soc.* **82**, 1617 (1960).
16. J. T. Edward. *J. Chem. Ed.* **64**, 599 (1987).
17. M. R. Crampton, M. Jones, J. K. Scranage and P. Golding. *Tetrahedron* **44**, 1679 (1988).
18. L. Goodman. *J. Am. Chem. Soc.* **75**, 3019 (1953).
19. J. A. Bell and I. Dunstan. *J. Chem. Soc. C* 870 (1966).

20. R. L. Willer and R. L. Atkins. *J. Org. Chem.* **49**, 5147 (1984).
21. N. V. Averina and N. S. Zefirov. *Uspekhi Khimii* **45**, 1077 (1976).
22. T. Sasaki. *Adv. Hetero. Chem.* **30**, 79 (1982).
23. R. Lukes and V. Galik. *Collect. Czech. Chem. Commun.* **19**, 712 (1954).
24. M. S. Newman and H. S. Lowrie. *J. Am. Chem. Soc.* **76**, 4598 (1954).
25. R. Fusco and G. Bianchetti. *Gazz. Chim. Ital.* **86**, 500 (1956).
26. V. Galik, Z. Kafka, M. Safar and S. Landa. *Collect. Czech. Chem. Comm.* **39**, 895 (1974).
27. W. N. Speckamp, J. Dijkink and H. O. Huisman. *J. C. S. Chem. Commun.* 197 (1970).
28. G. D. Georgievskaya, M. D. Boldyrev and L. I. Bagal. *Zh. Org. Khim.* **7**, 1618 (1971).
29. T. Severin, D. Bätz and H. Krämer. *Chem. Ber.* **104**, 950 (1971).
30. V. A. Sokolova, M. D. Boldyrev, B. V. Gidasov and T. N. Timofeeva. *Zh. Org. Khim.* **8**, 1243 (1972).
31. V. A. Sokolova, M. D. Boldyrev and B. V. Gidasov. *Zh. Org. Khim.* **12**, 1525 (1976).
32. B. Delpech and Q. Khuong-Huu. *J. Org. Chem.* **43**, 4898 (1978).
33. G. H. Wahl, Jr. and S. E. Zemyan. *Tetrahedron Lett.* 4545 (1982).
34. H. Stetter, P. Tacke and J. Gärtner. *Chem. Ber.* **97**, 3480 (1964).
35. H. Stetter and K. Heckel. *Chem. Ber.* **106**, 339 (1973).
36. A. R. Gagneux and R. Meier. *Tetrahedron Lett.* 1365 (1969).
37. R. J. Schultz, W. H. Staas and L. A. Spurlock. *J. Org. Chem.* **38**, 3091 (1973).
38. W. H. Staas and L. A. Spurlock. *J. Org. Chem.* **39**, 3822 (1974).
39. J. Bosch and J. Bonjoch. *Heterocycles* **14**, 505 (1980).
40. J. G. Henkel, W. C. Faith and J. T. Hane. *J. Org. Chem.* **46**, 3483 (1981).
41. J. G. Henkel and W. C. Faith. *J. Org. Chem.* **46**, 4953 (1981).
42. J. T. Hane and J. G. Henkel. *Tetrahedron Lett.* **31**, 2949 (1990).
43. F. Galinovsky and H. Langer. *Monatsh. Chem.* **86**, 449 (1955).
44. H. Stetter and H. Henning. *Chem. Ber.* **88**, 789 (1955).
45. V. Galik and S. Landa. *Collect. Czech. Chem. Commun.* **38**, 1101 (1973).
46. J. Kuthan and J. Palecek. *Collect. Czech. Chem. Commun.* **28**, 2260 (1963).
47. W. G. Grot. *J. Org. Chem.* **30**, 515 (1965).
48. S. Welner and D. Ginsburg. *Israel J. Chem.* **4**, 39 (1966).
49. J. Kuthan, J. Palecek and L. Musil. *Z. Chem.* **8**, 229 (1968).
50. J. Kuthan, J. Palecek and L. Musil. *Collect. Czech. Chem. Commun.* **38**, 3491 (1973).
51. T. Sasaki, S. Eguchi, T. Kiriya and Y. Sakito. *J. Org. Chem.* **38**, 1648 (1973).
52. A. I. Kutznetsov, P. F. Yakushev and B. V. Unkovskii. *Zh. Org. Khim.* **10**, 841 (1974).
53. J. Kuthan, J. Palecek and L. Musil. *Collect. Czech. Chem. Commun.* **39**, 750 (1974).
54. P. Scheiber and K. Nador. *Acta Chim. Acad. Sci. Hung.* **84**, 193 (1975); *Chem. Abstr.* (1975) **82**, 124595k.

55. Z. Kafka, V. Galik and M. Safar. *Collect. Czech. Chem. Commun.* **40**, 174 (1975).
56. H. Quast and B. Müller. *Chem. Ber.* **113**, 2959 (1980).
57. L. M. Jackman, T. S. Dunne, B. Müller and H. Quast. *Chem. Ber.* **115**, 2872 (1982).
58. H. Quast, B. Müller, E.-M. Peters, K. Peters and H. G. von Schnering. *Chem. Ber.* **115**, 3631 (1982).
59. A. I. Kuznetsov, E. B. Basargin, M. H. Ba, P. F. Yakushev and B. V. Unkovskii. *Zh. Org. Khim.* **21**, 2607 (1985).
60. O. T. Burdelev, A. I. Kuznetsov and B. V. Unkovskii, U. S. S. R. Patent 376, 359, 1973; from *Otkrytiya, Izobret., Prom. Obraztsy, Tovarnye Znaki* 50, 72; *Chem. Abstr.* **79**, 53353e (1973).
61. H. Stetter and K. Heckel. *Tetrahedron Lett.* 1907 (1972).
62. H. Stetter and K. Heckel. *Chem. Ber.* **106**, 339 (1973).
63. R. E. Portmann and C. Ganter. *Helv. Chim. Acta* **56**, 1986 (1973).
64. R.-M. Dupeyre and A. Rassat. *Tetrahedron Lett.* **29**, 2699 (1973).
65. H. Stetter and W. Böckmann. *Chem. Ber.* **84**, 834 (1951).
66. L. Meurling. *Chemica Scripta.* **7**, 23 (1975).
67. D. A. Durham, F. A. Hart and D. Shaw. *J. Inorg. Nucl. Chem.* **29**, 509 (1967).
68. N. W. Gabel, U. S. Patent 3,301,854 (1967); *Chem. Abstr.* **67**, 21936h (1967).
69. E. B. Hodge. *J. Org. Chem.* **37**, 320 (1972).
70. V. Galik, M. Safar, Z. Kafka and S. Landa. *Collect. Czech. Chem. Commun.* **40**, 442 (1975).
71. M. Safar, V. Galik, Z. Kafka and S. Landa. *Collect. Czech. Chem. Commun.* **40**, 2179 (1975).
72. E. B. Hodge, U. S. Patent 3,904,626, 1975; *Chem. Abstr.* **84**, 5019g (1976).
73. A. T. Nielsen. *J. Heterocycl. Chem.* **12**, 161 (1975).
74. A. F. Farminer and G. A. Webb. *J. Chem. Soc. Perkin I* 940 (1976).
75. A. Edwards and G. A. Webb. *J. Chem. Soc. Perkin I* 1989 (1977).
76. A. I. Kutznetsov, V. A. Kosmakov and B. V. Unkovskii. *Khim. Geterotsikl. Soedin.* 837 (1985).
77. A. Quast and C. -P. Berneth. *Chem. Ber.* **116**, 1345 (1983).
78. H. Quast, C. -P. Berneth, E. -M. Peters, K. Peters and H. G. von Schnering. *Chem. Ber.* **119**, 3842 (1986).
79. H. Stetter, D. Theisen and G. J. Steffens. *Chem. Ber.* **103**, 200 (1970).
80. H. Stetter and J. Bremen. *Chem. Ber.* **106**, 2523 (1973).
81. A. T. Nielsen, S. L. Christian and D. W. Moore. *Synthesis and Chemical Behavior of 2,4,10-Triazaadamantane*; paper presented at Pacific Conference on Chemistry and Spectroscopy, San Francisco, CA, Sept. 28, 1988.
82. A. Butlerov. *Liebigs Ann. Chem., Pharmacie* **111**, 242 (1859).
83. J. F. Walker. "Formaldehyde", Third Edition, Reinhold, New York, 1964, Chapter 19.
84. H. H. Richmond, G. S. Myers and G. F. Wright. *J. Am. Chem. Soc.* **70**, 3659 (1948).
85. A. T. Nielsen, D. W. Moore, M. D. Ogan and R. L. Atkins. *J. Org. Chem.*, **44**, 1678 (1979).

86. (a) C. A. Cupas and L. Hodakowski. *J. Am. Chem. Soc.* **96**, 4668 (1974).
86. (b) D. P. G. Hamon and G. F. Taylor. *Aust. J. Chem.* **29**, 1721 (1976).
87. R. O. Klaus and C. Ganter. *Helv. Chim. Acta* **63**, 2559 (1980).
88. A. T. Nielsen, S. L. Christian, D. W. Moore, R. D. Gilardi and C. F. George. *J. Org. Chem.* **52**, 1656 (1987).
89. A. T. Nielsen, R. L. Atkins, D. W. Moore, R. Scott, D. Mallory and J. M. LaBerge. *J. Org. Chem.* **38**, 3288 (1973).
90. A. T. Nielsen, R. L. Atkins, J. DiPol and D. W. Moore. *J. Org. Chem.* **39**, 1349 (1974).
91. E. M. Smolin and I. Rapoport in *The Chemistry of Heterocyclic Compounds*; A. Weisberger, Ed., Interscience, New York, 1959; Vol 13, Chapter 9.
92. A. R. Katritzky, R. C. Patel and F. G. Riddell. *Angew. Chem. Int. Ed Engl* **20**, 521 (1981).
93. V. T. Ramakrishnan, M. Vedachalam and J. H. Boyer. *Heterocycles* **31**, 479 (1990).
94. S. L. Vail, C. M. Moran and R. H. Barker. *J. Org. Chem.* **30**, 1195 (1965).
95. A. C. Currie, A. H. Dinwoodie, G. Fort and J. M. C. Thompson. *J. Chem. Soc. (C)* 491 (1967).
96. J. M. Edwards, U. Weiss, R. D. Gilardi and I. L. Karle. *Chem. Commun.* 1649 (1968).
97. R. D. Gilardi. *Acta Crystallogr.* **B28**, 742 (1972).
98. H. C. Chitwood and R. W. McNamee, U. S. Patent 2,345,237 1944; *Chem. Abstr.* **38**, 4274 (1944).
99. H. -W. Wanzlick and W. Löchel. *Chem. Ber.* **86**, 1463 (1953).
100. H. Baganz, L. Domaschke and G. Kirchner. *Chem. Ber.* **94**, 2676 (1961).
101. I. J. Ferguson, A. R. Katritzky and R. Patel. *J. Chem. Soc. Perkin II* 1564 (1976).
102. B. Fuchs and A. Ellenweig. *Recl. Trav. Chim. Pays-Bas* **98**, 326 (1979).
103. B. Fuchs, S. Weinman, U. Shmueli, A. R. Katritzky and R. C. Patel. *Tetrahedron Lett.* **22**, 3541 (1981).
104. R. L. Willer. *Propellants. Explos., Pyrotech* **8**, 65 (1983).
105. R. L. Willer, D. W. Moore and D. J. Vanderah. *J. Org. Chem.* **50**, 2365 (1985).
106. R. L. Willer, D. W. Moore, C. K. Lowe-Ma and D. J. Vanderah. *J. Org. Chem.* **50**, 2368 (1985).
107. A. T. Nielsen, R. A. Nissan, D. J. Vanderah, C. L. Coon, R. D. Gilardi, C. F. George and J. Flippen-Anderson. *J. Org. Chem.* **55**, 1459 (1990).
108. J. M. Kliegman and R. K. Barnes. *Tetrahedron* **26**, 2555 (1970).
109. J. M. Kliegman and R. K. Barnes. *J. Org. Chem.* **35**, 3140 (1970).
110. H. tom Dieck and I. W. Renk. *Chem. Ber.* **104**, 92 (1971).
111. M. D. Hurwitz, U. S. Patent 2,582, 128 1952. *Chem. Abstr.* **46**, 8146f (1952).
112. H. tom Dieck and J. Dietrich. *Chem. Ber.* **117**, 694 (1984).
113. A. G. Giumanini, G. Verardo, E. Zangrando and L. Lassiani. *J. Prakt. Chem.* **329**, 1087 (1987).
114. B. Mauzé, J. Pomet, M. -L. Martin and L. Miginiac. *C. R. Acad. Sci. Paris Ser. C*, **270**, 562 (1970).
115. J. Graymore. *J. Chem. Soc.* 1353 (1932).

116. A. G. Giumanini, G. Verardo, L. Randaccio, N. Bresciani-Pahor and P. Traldi. *J. Prakt. Chem.* **327**, 739 (1985).
117. G. B. Carter, M. C. McIvor and R. G. J. Miller. *J. Chem. Soc. C.* 2591 (1968).
118. Y. S. Dolskaya, G. Y. Kondrateva, N. L. Golovina, A. S. Shashkov and V. I. Kadentsev. *Izv. Akad. Nauk SSSR. Ser. Khim.* 1812 (1975).
119. E. H. Cordes and W. P. Jencks. *J. Am. Chem. Soc.* **84**, 832 (1962).
120. E. F. Pratt and M. J. Kamlet. *J. Org. Chem.* **26**, 4029 (1961).
121. M C. Venuti. *Synthesis* 61, (1982).
122. A. T. Kazaryan, S. O. Misaryan and G. T. Martirosyan. *Arm. Khim. Zh.* **31**, 913 (1978); *Chem. Abstr.* **90**, 186707x (1979).
123. R. Grigg and J. Kemp. *Tetrahedron Lett.* **21**, 2461 (1980).

6

Metallacarboranes of the Lanthanide and Alkaline-Earth Metals: Potential High Energy Fuel Additives

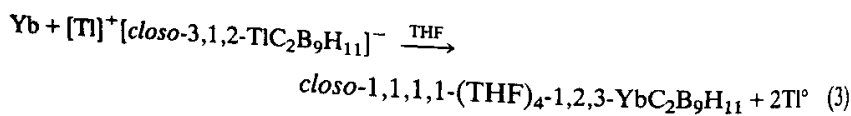
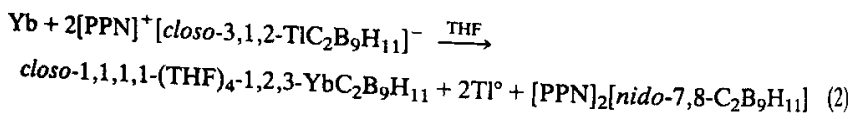
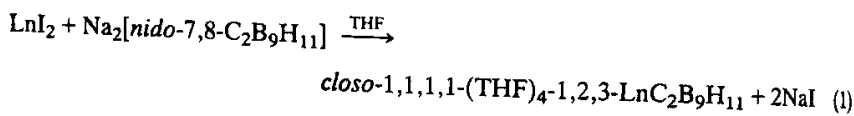
Rajesh Khattar, Mark J. Manning, and
M. Frederick Hawthorne

The organometallic chemistry of lanthanide and alkaline-earth metals has attracted particular attention in recent years. The elegant work of Evans and co-workers has demonstrated that the chemistry of the lanthanides with the cyclopentadienyl ligand is rich and novel [1-10]. The alkaline-earth metals also form similar type of complexes with cyclopentadienyl ligand with beautiful structural arrangements [11]. The isolobal analogy between the cyclopentadienide ligand and dicarbollide ligands [12] led us to explore the chemistry of the latter with the lanthanides. In this chapter, we describe the synthesis and characterization of the first η^5 -bound metallacarborane incorporating the lanthanide metals. We have extended the chemistry of the lanthanide and the alkaline-earth metals to other anionic carborane ligands such as [*nido*-7,9- $C_2B_{10}H_{12}$] $^{2-}$ and isolated corresponding *closo*-metallacarborane species with unusual structural arrangements. These and related metallacarboranes are attractive candidates for use as high energy fuel additives.

1. Lanthanide Element Metallacarboranes

The interaction of $Na_2[nido-7,8-C_2B_9H_{11}]$ with LnI_2 ($Ln = Sm$ or Yb) in THF results in the precipitation of an amorphous solid whose formulation has been established as $Ln(C_2B_9H_{11})(THF)_4$ [$Ln = Sm$ (1) or Yb (2)] on the basis of spectroscopic, magnetic, and complexiometric analyses [13,14]. Both these new complexes are extremely air- and moisture-sensitive and do not melt or sublime up to $200^\circ C$ but can be stored under an

inert atmosphere for extended periods of time. Alternatively, the complex **2** can be prepared more cleanly and conveniently by the direct oxidation of Yb metal with either $[\text{PPN}]^+[\text{closo-3,1,2-TiC}_2\text{B}_9\text{H}_{11}]^-$ or $[\text{Ti}]^+[\text{closo-3,1,2,-TiC}_2\text{B}_9\text{H}_{11}]^-$ in THF at room temperature. The reaction scheme for the synthesis of these divalent lanthanacarborane complexes is given in Eqs. 1–3. The complex with the formulation $\text{Ln}(\text{C}_2\text{B}_{10}\text{H}_{12})(\text{L})_x$ (where $\text{Ln} = \text{Sm}$ or Yb ; $\text{L} = \text{THF}$ or MeCN ; $x = 3$ or 4) can also be synthesized by the interaction of LnI_2 with $\text{Na}_2[\text{nido-7,9-C}_2\text{B}_{10}\text{H}_{12}]$ in a particular coordinating solvent at room temperature [13]. A full report concerning their structural characterization will be published elsewhere.

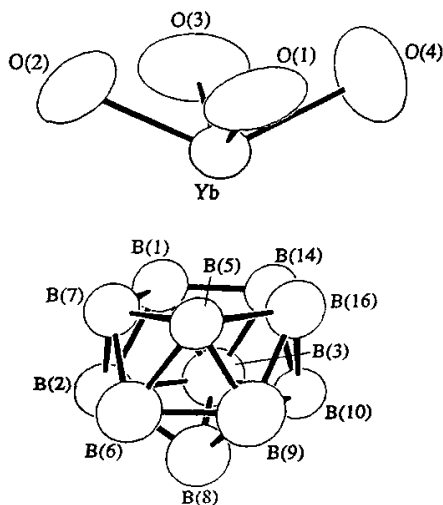


These divalent organolanthanide complexes **1** and **2** are only sparingly soluble in THF but are soluble in other coordinating solvents such as CH_3CN or DMF allowing the THF to be replaced by the solvent ligand. The complex **1** slowly decomposes in coordinating solvents to afford the known monoanion $[\text{nido-7,8-C}_2\text{B}_9\text{H}_{12}]^-$ and as yet an uncharacterized Sm^{3+} species which contains no boron [15]. The complex **2** is stable in the coordinating solvents. The fact that **1** is reactive with solvents in which it is soluble, whereas **2** undergoes ligand displacement reactions with the same coordinating solvents is consistent with the higher reactivity of $\text{Sm}(\text{II})$ versus $\text{Yb}(\text{II})$ [16]. The ionic radius of seven-coordinate $\text{Sm}(\text{II})$ is 0.14 \AA larger than the corresponding radius for $\text{Yb}(\text{II})$ [17], and as a result of it the divalent Sm complexes are less coordinatively saturated and usually more reactive than their ytterbium analogs. The $^1\text{H-NMR}$ spectrum of **2** in THF-d_8 exhibits a broad resonance at $\delta 1.25$ due to carboranyl CH protons along with other resonances due to THF ligands. Since the spectrum was recorded in THF-d_8 , no particular information can be drawn from this spectrum regarding coordinated THF. This problem can be overcome by recording the spectrum of **2** in CD_3CN which shows resonances due to carboranyl CH protons and free THF ligands. Integration of the $^1\text{H-NMR}$ spectrum of **2** in CD_3CN suggests that **2** contains four THF ligands per dicarbollide cage. The $^{11}\text{B-NMR}$ spectrum of **2** in THF displays a pattern

of resonances similar to that found in the spectrum of the known monoanion $[nido-7,8-C_2B_9H_{12}]^-$. The chemical shifts differ slightly from those of the monoanion; a brief exposure of a NMR sample of **2** to air/moisture yields the known monoanion $[nido-7,8-C_2B_9H_{12}]^-$ (as shown by ^{11}B -NMR). The solid-state IR spectra (Nujol mull) of **1** and **2** exhibit a unique split pattern in the region of their B-H stretch. In addition to this, the spectra display absorptions due to coordinated THF (1025 and 876 cm^{-1} for **1**; 1024 and 877 cm^{-1} for **2**). In order to establish the molecular geometry of these complexes, an x-ray diffraction study was carried out [13, 14]. Suitable single-crystals of the DMF derivative of **2** were grown from DMF/Et₂O solution at room temperature over a period of 1 week and the structure was established by x-ray crystallography.

The structure of $Yb(C_2B_9H_{11})(DMF)_4$ (**3**) is shown in Fig. 1. The ytterbium ion symmetrically caps the open pentagonal face of the dicarbollide ligand to generate an icosahedron and the remainder of the coordination sphere about the ytterbous ion is completed by four DMF molecules (only oxygen atoms of the DMF ligands are shown in Fig. 1 for clarity). The four oxygen atoms lie approximately in the same plane with an average O-Yb-O angle close to 90° . The plane defined by the four oxygen atoms is nearly parallel to the plane containing the upper belt (these atoms are capped by the lanthanide) of the dicarbollide cage; the dihedral angle is 7° .

Fig. 1. The molecular structure of **3** showing the atom labeling scheme. Only the oxygen atoms of the coordinated DMF ligands are shown. Due to disorder problems, the carbon and boron atoms in the upper belt of the carborane fragment could not be distinguished.



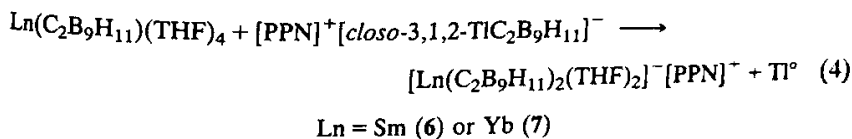
The ytterbium–boron (upper belt) distances range from 2.73 (4) to 2.77 (4) Å with an average value of 2.74 Å and compare very well with lanthanide to ligand distances reported for other structurally characterized divalent organolanthanide complexes. The average Yb–O (DMF) bond distance in **3** is 2.37 Å which is slightly shorter than the Yb–O (THF) distance (2.41 Å) found in the complex $(C_5Me_5)_2Yb(THF)$ [18]. Due to a crystallographic disorder problem, it was not possible to distinguish between carbon and boron on the upper belt of the dicarbollide cage. The disorder was greatly pronounced for the methyl carbons of the coordinated DMF; attempts to collect data at low temperature were unsuccessful.

The molecular structure of **3** raises a number of questions concerning the nature of the interaction of ytterbium atoms and the dicarbollide ligand. In order to obtain additional information concerning the nature of the bonding interaction of the ytterbium atom and the dicarbollide ligand, an IR study was carried out. The solid-state IR spectra of these *closo*-lanthanacarboranes **1** and **2** display two sharp B–H stretching bands (split pattern) separated by about 100 cm^{-1} . This particular kind of split pattern had not been observed before in the IR spectra of other metalla-carborane complexes. In order to elucidate the origin of IR band 'splitting', selectively deuterated lanthanacarboranes, *closo*-1,1,1,1-(THF)₄-1,2,3-LnC₂B₉H₉D₂ [Ln = Sm (**4**) or Yb (**5**)] were prepared [19]. In these deuterated complexes, the two nonadjacent borons [B(4) and B(6)] on the upper belt of the dicarbollide ligand are bound to deuterium [20] and should show a characteristic low frequency B–D stretch in the IR spectrum. The solid-state IR spectrum of both **4** and **5** indeed exhibit an absorption at *ca.* 1839 cm^{-1} which is attributed to a B–D stretch and there is a concomitant decrease in the intensity of the low frequency branch of the terminal B–H absorption. The ratio of ν_{BH}/ν_{BD} (using the low frequency absorption) is 1.32 for both **4** and **5**. A ratio of 1.33 can be calculated for the monoanion precursor $K^+[nido-7,8-C_2B_9H_9D_3]^-$; the same ratio has also been reported for the perdeuterated analogue of the metallaborane $[Cu]^+_2[B_{10}H_{10}]^{2-}$ [21]. When the ratio is calculated using the high frequency B–H absorption a value of 1.38 is obtained for both **4** and **5**. Given the consistency of ν_{BH}/ν_{BD} using the low frequency absorption along with the observed decrease in intensity of this stretch due to deuteration, it seems reasonable to assign the B–H absorption near 2450 cm^{-1} to the upper belt terminal hydrogens. With no other lanthanacarborane complexes available for comparison, it is rather difficult to elucidate the origin of this unique split pattern in the IR spectra. One possible explanation stems from the configuration of the terminal hydrogens of the dicarbollide ligand; these hydrogens are bent "up" out of the C₂B₃ plane by about 28°, and in a similar fashion the terminal hydrogens on the

lower belt are bent "down" out of the B_5 plane by the same amount. It is reasonable to assume that the three hydrogens on the upper belt, by virtue of being close to the capping metal, have a different B-H stretching force constant than that for the lower belt and apical borons. On the basis of these IR correlation studies, it is reasonable to conclude that strong ionic interactions exist between the cationic lanthanide center and the anionic dicarbollide ligand; however, with the data in hand it is impossible to ascertain the relative degree of covalent bonding present. The observation of a split pattern due to the B-H stretching region of the IR spectrum may prove to be a diagnostic test for the presence of ionic bonding in metallacarborane complexes.

II. Preparation and Characterization of Bis-Dicarbollide Complexes of Sm and Yb

The addition of one molar equivalent of $[PPN]^+[closo-3,1,2-TiC_2B_9H_{11}]^-$ to a THF solution of $Ln(C_2B_9H_{11})(THF)_4$ [$Ln = Sm$ (1) or Yb (2)] affords a bis(dicarbollide) lanthanide complex with the composition $[Ln(C_2B_9H_{11})_2(THF)_2]^- [PPN]^+$ [$Ln = Sm$ (6) or Yb (7)] in up to 50% yield according to the reaction given in Eq. 4 [13, 14].



In this reaction, the divalent lanthanide has been oxidized to the +3 oxidation state with the concomitant reduction of thallos ion to thallium metal. The metal in the +3 oxidation state accommodates the high formal negative charge developed by the two dicarbollide ligands. The magnetic spectral data of these complexes also shows these complexes to possess the metal in the trivalent state. The Sm complex 6 has magnetic moment 1.6 BM while the Yb complex 7 has magnetic moment 4.5 BM; both values are well within the reported range observed for other trivalent Sm and Yb complexes [22, 23]. Both these complexes are extremely air- and moisture-sensitive but can be stored for indefinite periods of time under an inert atmosphere of nitrogen/argon. The THF ligands in both these complexes can be displaced by other coordination solvent ligands such as MeCN.

The solid-state IR spectra (Nujol mull) of 6 and 7 exhibit absorption due to coordinated THF ligands along with a broad, but strong absorption centered at 2520 cm^{-1} due to a terminal B-H unit. However, the spectra do not display the unique B-H split pattern observed with the divalent mono

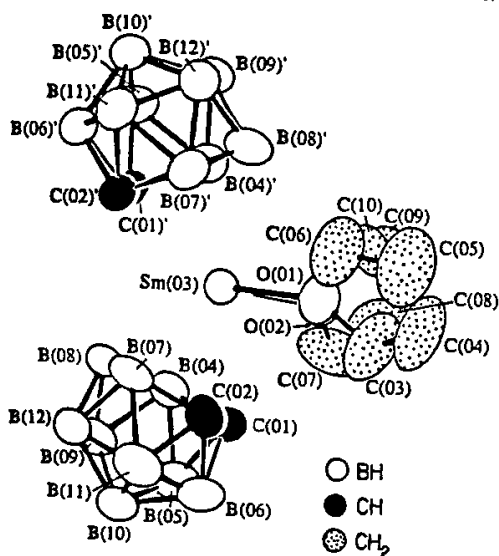


Fig. 2. The molecular structure of $[3,3-(\text{THF})_2\text{-commo-}3,3'\text{-Sm}(3,1,2\text{-SmC}_2\text{B}_9\text{H}_{11})_2]^- [\text{PPN}]^+$ (**6**) showing the atom labeling scheme.

cage lanthanides. The $^1\text{H-NMR}$ spectrum of **6** in CD_2Cl_2 displays two broad resonances at 2.74 and 1.34 ppm due to methylene protons of coordinated THF. The addition of a slight excess of CD_3CN causes these resonances to disappear with the simultaneous appearance of two signals at 3.59 and 1.76 ppm due to free THF. Due to the paramagnetic nature of **7**, it was not possible to interpret the $^1\text{H-NMR}$ spectrum as the signals are weak and broad and are spread over an 80 ppm range (+30 to -50 ppm).

The structure of these new species was established by an x-ray diffraction study [13, 14]. Suitable single crystals of the $[\text{N}(\text{PPh}_3)_2]^+$ salt of **6** were grown from THF/ Et_2O . The molecular structure of **6** is shown in Fig. 2. The coordination geometry about samarium can be best described as a distorted tetrahedron with the two η^5 -bound dicarbollide ligands and the two coordinated THF molecules occupying the coordination sphere about Sm^{3+} . The average ring centroid-Sm-O(THF) angle is 108.2° . There is no evidence for any "slipping" [24] of the dicarbollide ligand relative to the metal. The carbon atoms of the dicarbollide ligands adopt a *transoid* configuration about the samarium ion and in this way the carbon atoms of the dicarbollide ligands lie far apart from each other. A similar structural arrangement has been previously observed in other metallocarborane sandwich complexes [24].

The plane defined by Sm and the two oxygens is nearly normal (89.2°) to the plane defined by Sm and the two ring centroids and is very similar to

the analogous dihedral angle (92.9°) in the complex $(C_5Me_5)_2Sm(THF)_2$ [25]. The angle formed by the two oxygens and the Sm is nearly identical for these two organosamarium complexes: 79.5° for **4** and 82.6° for $(C_5Me_5)_2Sm(THF)_2$ [25]. The ring centroid-Sm-ring centroid angle is $131.9 (5)^\circ$ and is smaller than 137° reported for the complex $(C_5Me_5)_2Sm(THF)_2$. This is not all that surprising because of the larger ionic radius of Sm^{2+} (eight-coordinate, 1.27 \AA) versus Sm^{3+} (eight-coordinate, 1.079 \AA) [17]. The ring centroid-Sm-ring centroid angle found in the cationic trivalent samarium complex $[(C_5Me_5)_2Sm(THF)_2]^+ [BPh_4]^-$ is 134.7° [26], intermediate between the values reported for the complex [25] $(C_5Me_5)_2Sm(THF)_2$ and **4**. A comparison of the ring centroid-Sm-ring centroid angles of these three nearly isostructural complexes provides a good comparison of the bonding abilities of the $[nido-7,8-C_2B_9H_{11}]^{2-}$ and $[C_5Me_5]^-$ ligands and suggest that these two ligands have very similar steric requirements.

The Sm-to-upper belt (these atoms of the dicarbollide ligand are capped by samarium) distances fall in the range $2.693 (10)$ – $2.785 (9) \text{ \AA}$ with an average value of 2.735 \AA . This compares rather well to the Sm–C(C_5Me_5) distances reported in other eight-coordinate trivalent Sm complexes [26, 27] (2.72 and 2.73 \AA for $(C_5Me_5)_2Sm(I)(THF)$, $2.71 (4) \text{ \AA}$ for $[(C_5Me_5)_2Sm(THF)_2]^+$). A close agreement of the metal to ligand distances in these trivalent samarium complexes suggests that the nature of the bonding between a lanthanide and $[nido-7,8-C_2B_9H_{11}]^{2-}$ is predominantly ionic in nature. This is further supported by an application of Raymond's structural paradigm [28] to the metal-dicarbollide distances in **4**. Using the samarium-to-upper belt average distance of 2.735 \AA , the effective ionic radius for the dicarbollide ligand is calculated to be 1.656 \AA (ionic radius for the eight-coordinate Sm^{3+} is 1.079 \AA). This value is very similar to that already determined for the dicarbollide ligand in the complex **3** (1.66 \AA) and is very similar to the average value determined for the cyclopentadienyl ligand ($1.64 \pm 0.04 \text{ \AA}$) [28] and thereby suggests that the bonding in these organolanthanides is similar in nature, that is predominantly ionic.

III. Alkaline-Earth Element Metallacarboranes

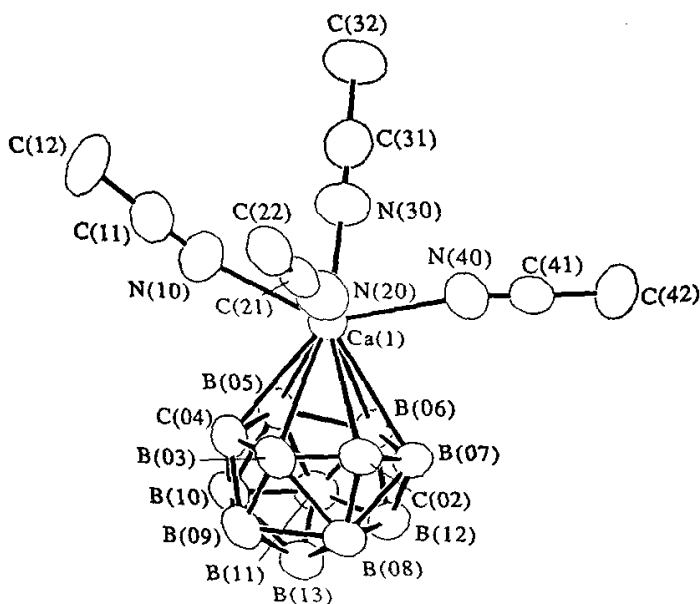
Recently, we have initiated an investigation of the chemistry of carboranes with alkaline-earth metals with a view to incorporate an alkaline-earth metal into a carborane cage. To date, there is no previous report of a discrete metallacarborane complex containing an alkaline-earth metal in its structural framework. These molecules would be interesting from

several points of view. The incorporation of an alkaline-earth into a carborane framework is novel and it would be interesting to see what type of structures these species adopt in the solid state. Secondly, the lower charge/size ratios of Ca^{2+} , Sr^{2+} , and Ba^{2+} suggest that their complexes would be very ionic in nature. Herein, we describe the preparation and structural characterization of calcium and strontium carborane complexes.

Stirring a THF solution of CaI_2 and $\text{Na}_2[\text{nido-7,9-C}_2\text{B}_{10}\text{H}_{12}]$ at room temperature results in the precipitation of a colorless solid. The colorless solid can be washed several times with THF in order to remove any unreacted $\text{Na}_2[\text{nido-7,9-C}_2\text{B}_{10}\text{H}_{12}]$ and NaI which had been formed during the course of the reaction. Recrystallization of the colorless solid from $\text{MeCN}/\text{Et}_2\text{O}$ at room temperature over a period of 3–4 days gives colorless needle-like crystals; the x-ray study showed it to have the formulation $\text{Ca}(\text{C}_2\text{B}_{10}\text{H}_{12})(\text{MeCN})_4$ (**8**) [29]. Due to the delicate nature of this complex, it was necessary to mount the crystal in a glass capillary in a dry box and the capillary was then sealed and the data were collected at room temperature.

The structure of **8** is illustrated in Fig. 3. The calcium atom asymmetrically caps the open hexagonal face of the $[\text{nido-7,9-C}_2\text{B}_{10}\text{H}_{12}]^{2-}$ ligand.

Fig. 3. The molecular structure of *closo*-1,1,1,1-(MeCN)₄-1,2,4-CaC₂B₁₀H₁₂ (**8**). All hydrogen atoms have been omitted for clarity.



The remainder of the coordination sphere about the calcium atom is completed by four acetonitrile ligands. The calcium-carborane distances range from 2.65 to 2.94 Å whereas Ca-N distances range from 2.43 to 2.51 Å. The Ca(1)-C(2) distance is 2.70 Å and compares rather well with that of 2.68 Å [average Ca-C(η^5) distance] reported for the complex $[\text{C}_5\text{H}_3-1,3-(\text{SiMe}_3)_2]_2\text{Ca}(\text{THF})$ [30] and 2.67 Å [average Ca-(η^5) distance] reported for the complex $[(\text{C}_5\text{Me}_5)\text{Ca}(\mu-1)(\text{THF})_2]_2$ [31].

The interatomic distance B(3)...B(8) in **8** is 2.037 (9) Å and is shorter than that found in the complex [32] 1,1-(PPh₃)₂-1-H-1,2,4-RhC₂B₁₀H₁₂ (2.166 Å) but is more comparable to that found in the complex [33] 1-(η -C₅H₅)-1,2,4-CoC₂B₁₀H₁₂ (2.082 Å). The B(9)...C(2) distance is 2.789 (7) Å and is longer than that found in the complex [32] 1,1-(PPh₃)₂-1-H-1,2,4-RhC₂B₁₀H₁₂ (2.720 Å). The C(2)...B(12) distance is 2.814 (8) Å and is nearly the same (2.841 Å) as found in the complex [32] 1,1-(PPh₃)₂-1-H-1,2,4-RhC₂B₁₀H₁₂. The B(3)...B(10) distance is 2.935 (8) Å, nearly identical with the distance 2.938 Å found in the complex [32] 1,1-(PPh₃)₂-1-H-1,2,4-RhC₂B₁₀H₁₂. The four boron atoms in the upper belt (these atoms of the carborane fragment are capped by calcium) of **8** are essentially coplanar (within 0.03 Å) with C(2) lying above (0.277 Å) and C(4) lying below (0.277 Å) this plane. The five boron atoms of the lower belt are coplanar (within 0.07 Å). The planes defined by the upper and the lower belt are nearly parallel (3.4° between their normals).

To our knowledge, the complex **8** is the first structurally characterized example of an alkaline-earth metallacarborane. We have extended this approach to other alkaline-earth metals and obtained a novel species with the formulation $\text{Sr}(\text{C}_2\text{B}_{10}\text{H}_{12})(\text{THF})_3$ (**9**) which displays a beautiful polymeric structural arrangement. The complex **9** can be obtained by the direct interaction of SrI₂ and Na₂[*nido*-7,9-C₂B₁₀H₁₂] in THF at room temperature [34]. The complex **9** is insoluble in THF or Et₂O but is soluble in other coordinating solvents such as MeCN or DMF. Recrystallization of complex **9** from MeCN/Et₂O produces colorless needlelike crystals: x-ray studies show it to have the formulation $\text{Sr}(\text{C}_2\text{B}_{10}\text{H}_{12})(\text{MeCN})_3$ (**10**) [34]. Complex **10** reverts to **9** in the presence of THF. These complexes are extremely air- and moisture-sensitive but can be stored for long periods of time in an inert atmosphere of nitrogen/argon.

The molecular structure of **10** was established crystallographically. Suitable single crystals were grown from MeCN/Et₂O at room temperature over a period of 3-4 days, mounted in a sealed glass capillary and the data were collected at room temperature. The crystal is composed of two crystallographically independent but structurally similar spiral chains. Three units of one of the spiral polymeric chains are shown in Fig. 4. A more detailed view of the metal-to-carborane interactions can be seen in Fig. 5. Each carborane fragment serves as a ligand to two strontium atoms.

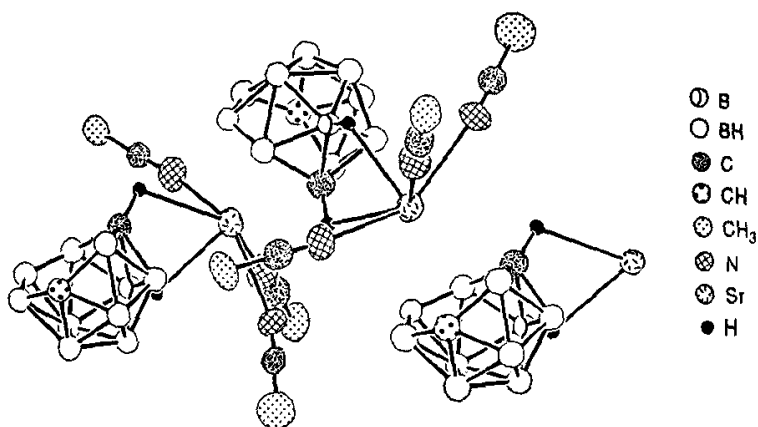
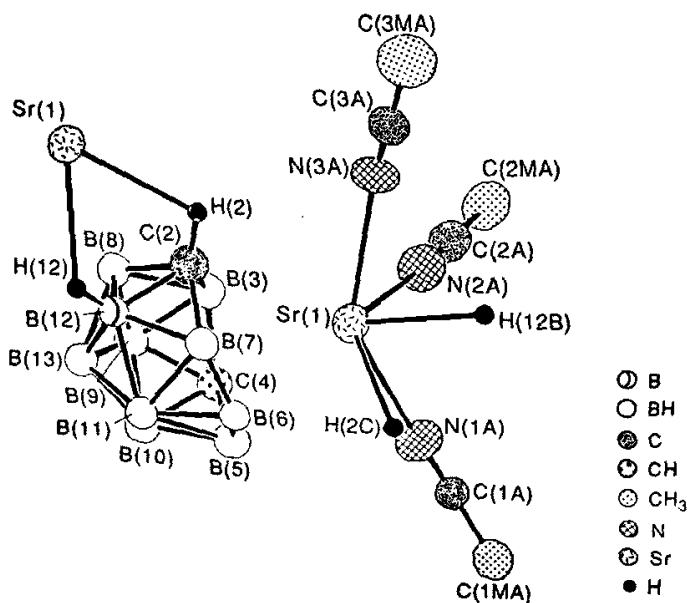


Fig. 4. Three units of one of the spiral polymeric chains of $[\text{closo-1,1,1-(MeCN)}_3\text{-1,2,4-SrC}_2\text{B}_{10}\text{H}_{12}]_n$ (10).

Fig. 5. Closer view of the metal-to-carborane interactions in the polymeric complex $[\text{closo-1,1,1-(MeCN)}_3\text{-1,2,4-SrC}_2\text{B}_{10}\text{H}_{12}]_n$ (10). All terminal hydrogen atoms have been omitted for clarity.



bonded to one through an open hexagonal face and to the other via upper and lower belt M-H-E (where E = B or C) interactions. The coordination geometry about each strontium is completed by three acetonitrile ligands. This arrangement of metal and carborane ligands is repeated to give a polymeric structure. To our knowledge, this is the first structurally characterized example of a polymeric metallacarborane.

The Sr-N distances range from 2.63 to 2.77 Å whereas the strontium-carborane (η^6) distances range from 2.87 to 3.17 Å. The Sr-C (carborane) distance (2.997 and 3.176 Å) is much longer than that found in the complex [30] $[\text{C}_5\text{H}_3\text{-}1,3\text{-(SiMe}_3)_2\text{]}_2\text{Sr(THF)}$ (2.81 Å). In order to accommodate strontium into the carborane cage, the entire upper belt of the carborane ligand in complex **10** is perturbed and is similar to that observed in the complex [32] *closo*-1,1-(PPh_3)₂-1-H-1,2,4-RhC₂B₁₀H₁₂. However, in complex **10**, the C(2) and C(4) lie on the same side in the upper belt of the carborane fragment. This is in contrast to other metallacarboranes [29, 32, 33, 35] containing the C₂B₁₀ fragment where one carbon atom lies above and another lies below the plane defined by four borons in the upper belt. Furthermore, the B(3) and B(6) atoms in the complex **10** lie above the plane defined by C(2), C(4), B(5), and B(7) (max. deviation of defining atoms from the plane is 0.05 Å) in the upper belt. Thus the upper belt adopts a boatlike shape. The carbon atoms C(2) and C(4) interact asymmetrically with the adjacent borons in the upper belt [C(2)-B(3), C(2)-B(7), C(4)-B(3), and C(4)-B(5) distances are 1.716 (14), 1.791 (14), 1.695 (14), and 1.609 (14) Å, respectively] similar to the interaction reported for the complex [35] *closo*-1,1-(PPh_3)₂-1-H-3-OMe-1,2,4-IrC₂B₁₀H₁₁ [C(2)-B(3), C(2)-B(7), C(4)-B(3), and C(4)-B(5) distances are 1.50 (3), 1.62 (3), 1.69 (3), and 1.74 (3) Å, respectively]. In contrast, in the complex [29] *closo*-1,1,1,1-(MeCN)₄-1,2,4-CaC₂B₁₀H₁₂, one carbon atom interacts nearly symmetrically with the adjacent borons [C(2)-B(3) and C(2)-B(7) distances are 1.519 (8) and 1.510 (7) Å] whereas the other interacts asymmetrically with the adjacent borons [C(4)-B(3) and C(4)-B(5) distances are 1.645 (8) and 1.697 (7) Å, respectively].

It is interesting to note that one of the C-H vertices of each carborane fragment interacts with the strontium. Since the B-H vertices of the carborane fragment are certainly more basic than the C-H vertices, one would anticipate that a second M-H-B interaction would be preferred over the observed M-H-C interaction. Consequently, the M-H-C interaction is not yet understood.

The solid-state IR spectra (Nujol mull) of **8** and **10** display a unique split pattern in the terminal B-H stretching region indicative of ionic interactions between an alkaline-earth metal and the carborane cage. Furthermore, the complex **10** exhibits a band at 2390 cm⁻¹ in its IR spectrum

which can be assigned to a M-H-B stretch and compares rather well to that reported for the structurally characterized complex [36] $\text{Ag}(\text{CB}_{11}\text{H}_{12})$ (the Ag-H-B stretching frequency is 2380 cm^{-1}).

It is rather surprising to note that the complex **8** exists as a monomer whereas the complex **10** exists as a polymer in the solid state, even though both were synthesized under similar reaction conditions. The complex **8** may lose a MeCN ligand at higher temperature to produce a polymeric complex with the formulation $\text{Ca}(\text{C}_2\text{B}_{10}\text{H}_{12})(\text{MeCN})_3$. The observed self-assembly of the metal with the carborane unit in the complex **10** may be due to the larger size of strontium compared to calcium. It is believed that the complex **10** exists as a monomer in solution.

ACKNOWLEDGMENTS

We thank the National Science Foundation (Grant CHE 88-06179) for the support of this work. We also thank Dr. Carolyn B. Knobler for her research efforts.

REFERENCES

1. Evans, W. J. *Adv. in Organomet. Chem.* **24**, 131 (1985).
2. Evans, W. J., Hughes, L. A., and Hanusa, T. P. *Organometallics* **5**, 1285 (1986).
3. Williams, A. F., Grandjean, F., Long, G. J., Ulibarri, T. A., and Evans, W. J. *Inorg. Chem.* **28**, 4584 (1989).
4. Evans, W. J., Ulibarri, T. A., and Ziller, J. W. *J. Am. Chem. Soc.* **112**, 2314 (1990).
5. Evans, W. J., and Drummond, D. K. *J. Am. Chem. Soc.* **111**, 3329 (1989).
6. Evans, W. J., and Ulibarri, T. A. *Polyhedron* **8**, 1007 (1989).
7. Evans, W. J., Chamberlain, L. R., Ulibarri, T. A., and Ziller, J. W. *J. Am. Chem. Soc.* **110**, 6423 (1988).
8. Evans, W. J., and Drummond, D. K. *Organometallics* **5**, 2389 (1986).
9. Evans, W. J., Grate, J. W., Hughes, L. A., Zhang, H., and Atwood, J. L. *J. Am. Chem. Soc.* **107**, 3728 (1985).
10. Evans, W. J., and Drummond, D. K. *Organometallics* **7**, 797 (1988).
11. Hanusa, T. P. *Polyhedron* **9**, 1345 (1990).
12. Hawthorne, M. F., Young, D. C., Andrews, T. D., Howe, D. V., Pilling, R. L., Pitts, A. D., Reintjes, M., Warren, L. F. Jr., and Wegner, P. A. *J. Am. Chem. Soc.* **90**, 879 (1968).
13. Manning, M. J., Knobler, C. B., and Hawthorne, M. F. *J. Am. Chem. Soc.* **110**, 4458 (1988).
14. Manning, M. J., Knobler, C. B., Khattar, R., and Hawthorne, M. F. *Inorg. Chem.* submitted for publication.
15. Buchanan, J., Hamilton, E. J. H., Reed, D., and Welch, A. J. *J. Chem. Soc., Dalton Trans.* 677 (1990) and references contained therein.
16. Evans, W. J. *Polyhedron* **6**, 803 (1987).
17. Shannon, R. D. *Acta Crystallogr., Sect. A* **A32**, 751 (1976).

6. Lanthanide and Alkaline-Earth Metallacarboranes

18. Tilley, T. D., Andersen, R. A., Spencer, B., Ruben, H., Zalkin, A., and Templeton, D. H. *Inorg. Chem.* **19**, 2999 (1980).
19. The selectively deuterated monoanion $K^+[9,11-(D)_2\text{-nido-7,8-C}_2\text{B}_9\text{H}_9\text{D}_3]$ with deuterium replacing the bridge hydrogen (verified by ^{11}B FTNMR), can be prepared by stirring previously dried $K^+[\text{nido-7,8-C}_2\text{B}_9\text{H}_{12}]^-$ in 6N DCl/D₂O for 6 h (ref 20). Metathesis with $[\text{HN}(\text{CH}_3)_3]^+\text{Cl}^-$ and subsequent deprotonation with excess NaH in THF yields the selectively deuterated dicarbollide dianion $[9,11-(D)_2\text{-nido-7,8-C}_2\text{B}_9\text{H}_9\text{D}_2]^{2-}$ which was used as before to synthesize the selectively deuterated complexes; *closo*-1,1,1,1-(THF)₄-1,2,3-SmC₂B₉H₉D₂, **4**, and *closo*-1,1,1,1-(THF)₄-1,2,3-YbC₂B₉H₉D₂, **5**.
20. Howe, D. V., Jones, C. J., Wiersema, R. J., and Hawthorne, M. F. *Inorg. Chem.* **10**, 2516 (1971).
21. Paxson, T. E., Hawthorne, M. F., Brown, L. D., and Lipscomb, W. N. *Inorg. Chem.* **13**, 2772 (1974).
22. Tilley, T. D., Andersen, R. A., and Zalkin, A. *Inorg. Chem.* **22**, 856 (1983).
23. Boncella, J. M., Tilley, T. D., and Andersen, R. A. *J. Chem. Soc., Chem. Commun.* 710 (1984).
24. (a) Wing, R. M. *J. Am. Chem. Soc.* **89**, 5599 (1967). (b) Wing, R. M. *J. Am. Chem. Soc.* **90**, 4828 (1968). (c) Mingos, D. M. P., Forsyth, M. I., and Welch, A. J. *J. Chem. Soc., Dalton Trans.* 1363 (1978). (d) Zalkin, A., Templeton, D. H., and Hopkins, T. E. *J. Am. Chem. Soc.* **87**, 3988 (1965). (e) Zalkin, A., Hopkins, T. E., and Templeton, D. H. *Inorg. Chem.* **5**, 1189 (1966). (f) Zalkin, A., Hopkins, T. B., and Templeton, D. H. *Inorg. Chem.* **6**, 1911 (1967).
25. Evans, W. J., Grate, J. W., Choi, H. W., Bloom, I., Hunter, W. E., and Atwood, J. L. *J. Am. Chem. Soc.* **107**, 941 (1985), and references contained therein.
26. Evans, W. J., Ulibarri, T. A., Chamberlain, L. R., Ziller, J. W., and Alvarez Jr., D. *J. Am. Chem. Soc.* (1990) in press.
27. Evans, W. J., Bloom, I., Hunter, W. E., and Atwood, J. L. *Organometallics* **4**, 112 (1985), and references contained therein.
28. Raymond, K. N., and Eigenbrot, C. W. *Acc. Chem. Res.* **13**, 276 (1980).
29. Khattar, R., Knobler, C. B., and Hawthorne, M. F. *J. Am. Chem. Soc.* **112**, 4962 (1990).
30. Engelhardt, L. M., Junk, P. C., Raston, C. L., and White, A. H. *J. Chem. Soc., Chem. Commun.* 1500 (1988).
31. McCormick, M. J., Sockwell, S. C., Davies, C. E. H., Hanusa, T. P., and Huffman, J. C. *Organometallics* **8**, 2044 (1989).
32. Hewes, J. D., Knobler, C. B., and Hawthorne, M. F. *J. Chem. Soc., Chem. Commun.* 206 (1981).
33. Churchill, M. R., DeBoer, B. G. *Inorg. Chem.* **13**, 1411 (1974).
34. Khattar, R., Knobler, C. B., and Hawthorne, M. F. *Inorg. Chem.* **29**, 2191 (1990).
35. Alcock, N. W., Taylor, J. G., and Wallbridge, M. G. H. *J. Chem. Soc., Dalton Trans.* 1805 (1987).
36. Shelly, K., Finster, D. C., Lee, Y. J., Scheidt, W. R., and Reed, C. A. *J. Am. Chem. Soc.* **107**, 5955 (1985).

7

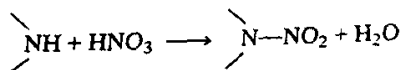
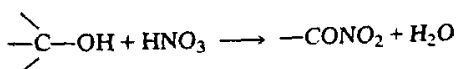
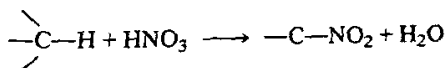
Methods for Preparing Energetic Nitrocompounds: Nitration with Superacid Systems, Nitronium Salts, and Related Complexes

George A. Olah

I. Introduction

Varied nitrocompounds ranging from such C-nitrocompounds as TNT to N-nitrocompounds such as RDX and HMX to O-nitrocompounds such as trinitroglycerol play a most significant role in energetic compounds. Their preparation is thus of substantial importance. This chapter reviews the most frequently used electrophilic nitration chemistry with particular emphasis on the use of superacidic systems, nitronium salts, and related complexes on which my research group for 30 years has continued to carry out intensive research.

Nitration is the reaction of an organic compound with a nitrating agent (generally nitric acid or its derivatives) to introduce a nitro group onto a carbon atom (C-nitration) or to produce nitrates (O-nitration) or nitramines (N-nitration) [1].



The nitro group most frequently substitutes a hydrogen atom, however, other atoms or groups can also be substituted (e.g., halogen atoms). Nitro compounds can also be formed by addition of nitric acid or nitrogen oxides to unsaturated compounds (olefins, acetylenes).

Nitration reactions can be divided into *ionic*, *radical ion*, and *free radical* reactions. Within ionic nitrations one can differentiate the more predominant *electrophilic* nitrations (proceeding through the nitronium ion, NO_2^+ , or some of its polarized $\delta^+\text{NO}_2\delta^- - \text{X}$ carriers) and *nucleophilic* nitrations (displacement reactions of suitable leaving groups by the nitrite ion, NO_2^-). The most widely used nitrations involve the interactions of the electrophilic nitrating agent (i.e., nitronium ion, NO_2^+) with aromatics. The possible role of *electron-transfer* in nitration is of increasing significance. It is becoming evident that in addition to conventional two electron transfer nitration, single electron transfer reactions can also take place. At the same time there are clear limitations to the systems where single electron transfer may be operative. Electrophilic nitrations retain their significance in the plurality of aromatic nitrations. The relationship of ionic and electron transfer nitrations is one of the more fascinating recently emerging aspect of the study of the mechanism of nitration.

II. Protic-Acid-Catalyzed Nitration

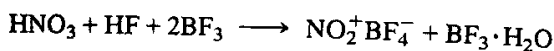
Electrophilic nitrations are carried out by acid-catalyzed reactions of nitric acid and its derivatives. Nitrating agents are of the general formula $\text{NO}_2 - \text{X}$ which serve as sources of the nitronium ion, NO_2^+ , the effective nitrating agent. Ingold called the $\text{NO}_2 - \text{X}$ compounds as carriers of the nitronium ion [2]. From the ease of X-elimination he gave a relative sequence of nitrating activity of different nitrating agents as nitronium ion, NO_2^+ > nitracidium ion $\text{NO}_2 - ^+\text{OH}_2$ > nitryl chloride, $\text{NO}_2 - \text{Cl}$ > dinitrogen pentoxide $\text{NO}_2 - \text{NO}_3$ > acetyl nitrate, $\text{NO}_2 - \text{O}(\text{CO})\text{CH}_3$ > nitric acid, $\text{NO}_2 - \text{OH}$ > methyl nitrate $\text{NO}_2 - \text{OCH}_3$.

The scope of nitrating agents, however, by now is much wider (Table I) [3]. The discussion in this chapter will primarily emphasize reagents and methods developed by the Olah group in its study of nitration chemistry.

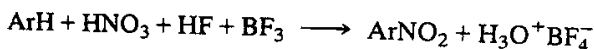
The nitronium ion, NO_2^+ , as established by Ingold's studies in 1940 [2] following an early suggestion by Euler [4], is the reactive nitrating agent in electrophilic nitrations. Forty years of subsequent studies have not changed this. Table I summarizes the most frequently used electrophilic nitrating agents.

Recognizing the limited nitrating ability of the nitric acid-anhydrous hydrogen fluoride system, Olah and Kuhn in 1956 introduced *nitric*

acid—*anhydrous hydrogen fluoride–boron trifluoride* as an extremely effective and safe nitrating agent [5]. Nitric acid ionizes with HF–BF_3 according to



Nitronium tetrafluoroborate can be isolated as a stable salt and used as such as the nitrating agent or the system can be used for *in situ* nitration of aromatics.

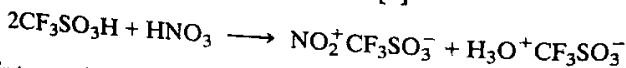


Boron trifluoride can be readily regenerated from its hydrate by distilling it from sulfuric acid (or oleum) and thus the reaction can be made catalytic with recycling of the acid.

Instead of BF_3 , other Lewis acid fluorides such as PF_5 , TaF_5 , NbF_5 , SbF_5 can also be used effectively in related nitrations.

Trifluoromethanesulfonic acid (triflic acid) is one of the strongest known Bronsted acids. H_0 for $\text{CF}_3\text{SO}_3\text{H}$ is -14.5 , comparable to fluorosulfuric acid. Additionally, while fluorosulfuric acid, like sulfuric acid, is also a powerful sulfonating and oxidizing agent, trifluoromethanesulfonic acid does not react with aromatics [6]. It is therefore a most convenient strong acid for nitration with nitric acid, which is completely ionized by it.

During an investigation on the effect of acids on the regioselectivity of nitration of toluene, Coon, Blucher and Hill found that two equivalents of trifluoromethanesulfonic acid react with 100% nitric acid to yield a white crystalline solid, which is a mixture of nitronium trifluoromethanesulfonate and hydronium trifluoromethanesulfonate [7].



The mixture of nitric acid and trifluoromethanesulfonic acid in CH_2Cl_2 , CCl_4 , CF_2Cl_2 , CFCl_3 , and pentane solution is an excellent nitrating agent for benzene, toluene, *m*-xylene, chlorobenzene, nitrobenzene, and benzo-trifluoride (Table II). The reactions were carried out from -110 to 30°C . Mono- or dinitration of toluene can be controlled by specific reaction temperature. Mononitration of toluene is extremely rapid, the reaction being complete in one minute at -110°C . The dinitration is complete in 30 min at 0°C .

The regioselectivity of mononitration of toluene was studied by varying the reaction temperature. At -60° , -90° , and -110°C in halomethane solvents mononitrotoluenes were obtained containing only 0.53, 0.36, and 0.23% *meta*-nitrotoluenes, respectively. The *ortho/para* isomer ratio is also low at -110°C (Table III).

Table II. Nitration of Aromatics with Nitric Acid-Trifluoromethanesulfonic Acid

Substrate	Product	Isomer Distribution, %
Benzene	nitrobenzene	98
	dinitrobenzene	2
Toluene	2-nitrotoluene	50-62
	3-nitrotoluene	0.2-0.5
	4-nitrotoluene	37-44
Nitrobenzene	1,2-dinitrobenzene	10
	1,3-dinitrobenzene	87
	1,4-dinitrobenzene	2
Chlorobenzene	2-nitrochlorobenzene	30
	3-nitrochlorobenzene	0.1
	4-nitrobenzene	70
Benzotrifluoride	2-nitrobenzotrifluoride	14
	3-nitrobenzotrifluoride	85
	4-nitrobenzotrifluoride	0.1

Table III. Mononitration of Toluene with $\text{HNO}_3/\text{CF}_3\text{SO}_3\text{H}$ in Halomethane Solvents

Solvent	Time, Min	Temp, °C	Yield, %	Isomer ratios, %		
				<i>o</i> -	<i>m</i> -	<i>p</i> -
CFCl_3	180	-110	>99	50.5	0.2	49.3
CH_2Cl_2	180	-90	>99	61.3	0.4	38.3
CH_2Cl_2	60	-60	>99	62.1	0.5	37.4
CFCl_3	1	-60	>99	61.9	0.5	37.6
CFCl_3	1	-110	>99	50.8	0.2	49.0

Low *meta* substitution allows favorable regiocontrol in the subsequent preparation of dinitrotoluenes. In general, the nitric acid-trifluoromethanesulfonic acid system shows less *meta* substitution than other nitrating systems at comparable temperatures (Table IV). The major factor, however, effecting low *meta* nitration is the use of extremely low temperatures. Solubility of the formed nitronium salt at low temperature in halomethane solutions is limited and unusual *ortho/para* ratios may be also a consequence of the heterogeneous nature of the reaction mixtures.

Olah *et al.* recently found $\text{CF}_3\text{SO}_3\text{H}-\text{B}(\text{O}_3\text{SCF}_3)_3$ (triflatoboric acid) as a highly efficient new superacid for nitrating aromatics with HNO_3 (Table V). Nitronium tetratriflatoborate $\text{NO}_2^+\text{B}(\text{CF}_3\text{SO}_3)_4^-$ is the reactive nitrating agent [8].

Table IV. Preparation of Dinitrotoluene in Nitrating Mixtures Containing $\text{CF}_3\text{SO}_3\text{H}$

Composition of Nitrating Mixture, wt %				Temp, °C	Yield, %	% Isomer Distribution				Total <i>Meta</i>
$\text{CF}_3\text{SO}_3\text{H}$	H_2SO_4	HNO_3	H_2O			2,6	2,3-2,5	2,4	3,4	%
89.0	0	11.0	0	-5	>98	15.7	0.5	82.8	1.0	1.5
45.5	45.5	6.0	3.0	-20	>98	10.2	0.3	88.7	0.9	1.0
45.5	45.5	6.0	3.0	-20	>99	14.9	0.6	83.4	1.1	1.7
22.7	68.3	6.0	3.0	-20	99.5	12.1	0.4	86.4	1.2	1.6
0	90.6	6.3	3.1	-25	99	11.8	0.5	86.5	1.3	1.8
80	0	10	10	20	99.2	16.8	1.0	81.0	1.3	2.2
65	0	5	30	0	100					

$o-/m-/p\text{-MNT} = 58.86/1.96/39.18$
 $o/p = 1.5$

Table V. Nitration of Aromatics with Nitric-Tetra(trifluoroboric Acid)
($\text{HNO}_3 + \text{H}^+\text{B}(\text{O}_3\text{SCF}_3)_4$)

Aromatic	Rxn. Temp., °C	% Isomer Distribution of Nitro-Product		
		<i>o</i> -	<i>m</i> -	<i>p</i> -
Benzene	-30			
Toluene	-30	55	1	43
Fluorobenzene	-30	52	1	47
Chlorobenzene	-30	1	—	99
Anisole	-30	33	<0.1	67
Naphthalene	-30	58	<0.1	42
		α -97	β -3	

Usual mixed-acid nitrations give water as the byproduct in forming the nitronium ion. The effectiveness of mixed acid is continuously decreased during the progress of the nitration reaction due to dilution of the acid by the water formed.

Coon *et al.* used *nitric acid-fluorosulfuric acid* in the nitration of toluene and compared its effectiveness with that of trifluoromethanesulfonic acid (Table VI) [7]. They found that both acids were effective, but trifluoromethanesulfonic acid is more suitable as it does not cause oxidation or sulfonation.

Olah *et al.* found that a mixture of nitric and fluorosulfuric acid (or $\text{HNO}_3 + \text{HF} + \text{FSO}_3\text{H}$) allows even the trinitration of benzene to 1,3,5-trinitrobenzene at higher temperatures [9]. Water formed in the ionization of nitric acid to the nitronium ion reacts with fluorosulfuric acid (to sulfuric acid and hydrogen fluoride) and thus the nitrating system maintains high acidity. Nitric-fluorosulfuric acid is also a very suitable strong nitrating system for other deactivated aromatics.

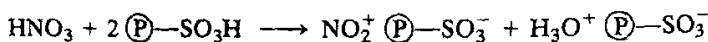
Adding Lewis acid fluorides, such as antimony, tantalum, or niobium pentafluoride to fluorosulfuric acid greatly enhances its acidity. $\text{FSO}_3\text{H-SbF}_5$ (*magic acid*) is one of the strongest known superacids [6]. Nitric-magic acid ($\text{HNO}_3\text{-FSO}_3\text{H-SbF}_5$) is an extremely effective nitrating agent for polynitration of aromatics [8].

Table VI. Comparison of the Nitration of Toluene with $\text{HNO}_3/\text{CF}_3\text{SO}_3\text{H}$ and $\text{HNO}_3/\text{FSO}_3\text{H}$ in CH_2Cl_2 solution at -60°C

Acid	Time, Min	Yield, MNT %	% Isomer Distribution
$\text{CF}_3\text{SO}_3\text{H}$	60	100	$o/m/p = 62/0.5/37$
FSO_3H	120	89	$o/m/p/ = 63/0.7/36$

Nitration with nitric acid in the presence of strong protic acids such as H_2SO_4 , FSO_3H , and $\text{CF}_3\text{SO}_3\text{H}$ or Lewis acids such as boron trifluoride requires subsequent separation of spent acid (due to water formed in the reaction) and neutralization of acid left in the product. One is generally left with a large amount of dilute acid for disposal, which is neutralized in the case of sulfuric-acid-catalyzed nitrations to a mixture of ammonium nitrate and ammonium sulfate. By using a *solid acid catalyst* most of these environmental problems can be eliminated. The solid acid catalyst is simply separated and recycled for subsequent use.

Kameo *et al.* reported [50] the use of polystyrenesulfonic acid as a catalyst in the nitration of aromatics with HNO_3 . Nitration of toluene with 90% HNO_3 over dried sulfonated polystyrene resin (Rohm and Haas amberlite IR-120) was also reported by Wright *et al.* at 65–70°C to give an *ortho-para* isomer ratio of only 0.68, much lower than usual *ortho-para* ratios in acid-catalyzed nitrations [11]. It is considered that the nitronium ion is strongly ion paired to the resinsulfonic acid. The ion-pair salt thus formed is much bulkier than the "free" nitronium ion or such nitronium salts as $\text{NO}_2^+ \text{BF}_4^-$.



This method, however, is of limited use because the catalyst undergoes degradation during the reaction. Polystyrene has benzylic hydrogens that can be abstracted easily by highly reactive species (nitrogen oxides, NO_2^+ , NO^+) present in the reaction medium. The polymer therefore readily undergoes oxidative degradation. In addition, it is likely that the polymer also can undergo nitration, sulfonation, and subsequent degradation under the reaction conditions.

When aromatics are nitrated with mixed acid, the reaction rate slows down with time, because the byproduct water dilutes the acid, thus reducing its reactivity. In preparative nitrations, therefore, a large excess of acid is required with the excess being wasted because of dilution. The disposal of spent acid also represents a significant environmental problem.

In view of these considerations and the limitations of polystyrenesulfonic acids, we studied superacidic Nafion-H[®] perfluorosulfonic-acid-resin-catalyzed nitration of aromatics with nitric acid under conditions of azeotropic removal of water (azeotropic nitration) [12]. The azeotropic removal of water in Nafion-H[®]-catalyzed nitration allows utilization of nitric acid to a significantly greater extent than do conventional conditions of nitration. Both fuming and concentrated nitric acid are effective (Table VII).

The nitrations are carried out by heating the reaction mixture to reflux and azeotropically distilling off the water-aromatic mixture until no nitric

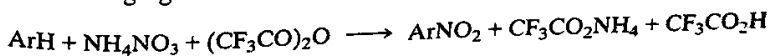
Table VII. Azeotropic Nitration of Aromatics with Nitric Acid over Nafion-H Catalyst

Substrate	Yield, %	Isomer Distribution, %
Benzene	77	
Toluene	80	2-nitro (56) 3-nitro (4) 4-nitro (40)
<i>o</i> -Xylene	47	3-nitro (45) 4-nitro (55)
<i>m</i> -Xylene	68	2-nitro (15) 4-nitro (85)
<i>p</i> -Xylene	60	
Mesitylene	79	
Chlorobenzene	87	2-nitro (38) 3-nitro (1) 4-nitro (61)

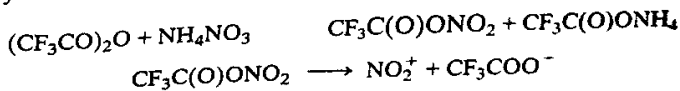
acid is left in the reaction mixture. Part of the nitric acid, however, also distills over in the form of a binary or ternary azeotrope, as do some nitrogen oxides formed under the reaction conditions.

Crivello has shown [13] that alkali metal nitrates can be used with trifluoroacetic anhydride and to a lesser extent with trichloro- and dichloroacetic anhydride. The reaction rate was shown to be significantly affected by the extent of solubility of the inorganic nitrate in the reaction medium. Since ammonium nitrate is reasonably soluble in organic solvents it is particularly successful (*vide infra*). Many metal nitrates have been also shown to be effective nitrating agents in the presence of trifluoroacetic anhydride. Benzene gives nitrobenzene in 90% yield in most cases. The nitration rate is highly solvent dependent, being higher in polar solvents. The reaction is quite general and successful for nitration of aromatics more reactive than nitrobenzene.

Ammonium nitrate in trifluoroacetic anhydride (TFAA) is a particularly good nitrating agent of aromatics [13].

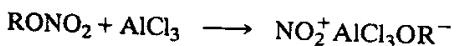
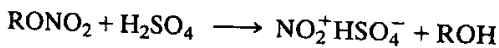


The reaction bears a close resemblance to acetyl nitrate nitration and most probably involves formation of trifluoroacetyl nitrate which subsequently can form nitronium ion.

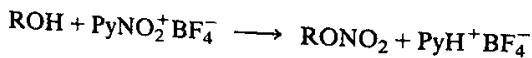


Attempts to isolate trifluoroacetyl nitrate by distillation lead to decomposition. Acetyl nitrate is known to give high ratios of ortho-nitrated products [14]. Similar trends in orientation are seen in the product distributions obtained in TFAA-NH₄NO₃ nitrations. However, in contrast to the rather limited range of substrates that can be nitrated with acetyl nitrate, trifluoroacetyl nitrate is a much more efficient and versatile nitrating agent.

Both protic- or Lewis-acid-catalyzed nitration of aromatics can be carried out with *alkyl nitrates* (i.e., alkyl esters of nitric acid). Acid catalysts are assumed to form nitronium ion from alkyl nitrates or strongly polarized complexes.



Alkyl nitrates must be prepared and stored with care, as particularly in the presence of even traces of acids they can become explosive [15]. They should not be stored over prolonged periods of times. This is particularly the case for nitrates of polyols. The simplest and effective means of their preparation involves reaction of alcohols with nitronium salts in the presence of an acid-binding agent. Transfer nitrations with *N*-nitropyridinium salts are particularly suited for their acid-free preparation [16].



Alkyl nitrates do not nitrate aromatic compounds in the absence of catalysts [17]. However, high yields of nitrated products can be obtained if aromatic compounds and alkyl nitrates react in the presence of sulfuric acid [18-22], poly(phosphoric acid) [23], or Lewis acid halides [24-26].

Alkyl nitrates most frequently used are methyl and ethyl nitrate (bp. 65° and 86-87°C, respectively).

The sulfuric acid-catalyzed nitration of benzene with ethyl nitrate at 78-80°C gives nitrobenzene in only 12% yield [27]. *p*-Fluoroacetanilide is, however, nitrated under similar conditions at 0°C in 85% yield [28].

Recently developed strong solid acid catalysts such as Nafion-H[®] are active in catalyzing nitrations with alkyl nitrates [29]. Benzene and alkylbenzenes are nitrated in excellent yield with *n*-butyl nitrate at around 80°C in the presence of solid Nafion-H acid catalyst. The reaction is generally slow for preparative purposes at lower temperatures and does not proceed at room temperature. The reaction is very selective. Dinitro compounds are not formed in any significant amounts. The steric bulk of the solid-acid-complexed nitrating agent seems to play a significant role in determining the isomer distribution of products. Generally, a decreased amount of the more hindered isomer (*ortho*) is formed compared with conventional electro-

Table VIII. Nitration of Aromatics with *n*-Butyl Nitrate over Nafion-H Catalyst

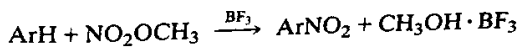
Aromatic	Yield, %	Isomer Distribution (%)
Benzene	77	
Toluene	96	2-nitro (50) 3-nitro (3) 4-nitro (47)
<i>o</i> -Xylene	98	3-nitro (47) 4-nitro (53)
<i>m</i> -Xylene	98	2-nitro (12) 4-nitro (88)
<i>p</i> -Xylene	95	2-nitro (100)
Mesitylene	90	2-nitro (100)
1,2,4-Trimethylbenzene	94	3-nitro (8) 5-nitro (92)
1,2,3,4-Tetramethylbenzene	93	
anisoie	86	2-nitro (32) 4-nitro (68)
Chlorobenzene	15	

philic solution nitrations, thus increasing the selectivity of nitration at the less hindered (*para*) position (Table VIII).

When secondary or tertiary alkyl nitrates are used in the nitration reaction, competing alkylations complicate the system. Consequently methyl or ethyl nitrate are the preferred alkyl nitrates for nitration.

AlCl_3 , SnCl_4 , SbCl_5 and FeCl_3 catalyze the nitration of benzene with ethyl nitrate [30].

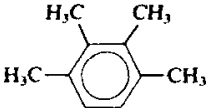
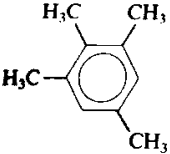
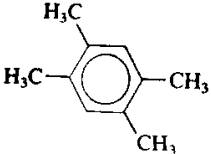
Alkyl nitrates, particularly methyl nitrate, are very effective nitrating agents in the presence of boron trifluoride catalyst [31].



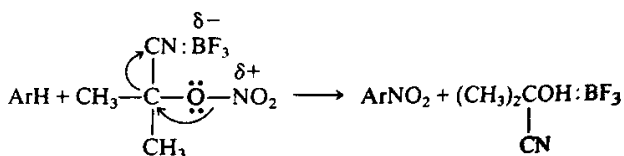
The reaction is useful as a selective and mild nitration method, for example allowing mononitration of durene and other highly alkylated benzenes, which with mixed acid usually undergo dinitration. Methyl nitrate-boron trifluoride can also be used to achieve dinitration of tetramethylbenzenes by using 2- and 3*M* excess of methyl nitrate, respectively. Relative yields of mono- and dinitro product compositions are shown in Table IX.

Other Friedel-Crafts type catalysts can also be used, but boron trifluoride is found to be the most suitable. In the nitration of pentamethylbenzene, aluminum trichloride and titanium (IV) chloride cause formation of significant amounts of chlorinated derivatives (e.g., sulfuric acid leads to nitrodemethylation products).

Table IX. Boron-Trifluoride-Catalyzed Nitration of Tetramethylbenzenes with Excess Methyl Nitrate in Nitromethane Solution

Tetramethylbenzene	$\text{H}_3\text{C}-\text{ONO}_2$: Arene	Total Yield (%) of Nitro Products	Composition	
			Dinitro Product (%)	Mononitro Product (%)
	2:1	93	64.4	35.6
	3:1	90	75.0	25.0
	2:1	94	89.9	10.1
	3:1	94	99.9	0.1
	2:1	95	90.1	9.9
	3:1	92	100	0

Acetonecyanohydrin nitrate (ACN) is found to have enhanced reactivity compared to methyl nitrate in the preparation of various ring-substituted phenylnitromethanes [32]. It was first used by Thompson and Narang [33, 34a] in nitrating aromatics. The boron trifluoride-etherate-catalyzed nitration of alkylbenzenes and anisole [35] gave good yields (Table X). Acetonecyanohydrin nitrate is more reactive than ordinary alkyl nitrates because of the greater ease of O—N bond cleavage in the intermediate O- or N-coordinated (protonated) ACN.



Use of acetonecyanohydrin nitrate has certain practical advantages over other procedures that use alkyl nitrates. It is more stable than CH_3ONO_2 and is stored easily for longer periods of time. BF_3 -etherate is easier to handle than the BF_3 gas used in other methods. Under similar conditions, this method provides cleaner products and higher yields than does a mixture of CH_3ONO_2 and BF_3 -etherate; only small amounts of BF_3 -etherate are required.

Solid superacidic catalysts can also be advantageously applied in nitration with acetonecyanohydrin nitrate [29].

The Nafion-H-catalyzed nitration of deactivated aromatics with alkyl nitrates, such as butyl nitrate, gives only very low yields [29]. Even nitration of chlorobenzene, for example, gives only 15% of chloronitrobenzenes (Table XI). Due to its greater reactivity, nitration of alkylbenzenes with ACN gives the corresponding nitro compounds in good to moderate yield (Table XI). The nitration of chlorobenzene gives 49% yield (as contrasted with 15% with butyl nitrate). The yields increase only modestly with time

Table X. Nitration of Aromatics by Acetonecyanohydrin Nitrate/ BF_3 Etherate

Compound	Yield %	% Isomer Distribution		
		2-Nitro	3-Nitro	4-Nitro
Toluene	77.6	59.8	4.5	35.7
<i>o</i> -Xylene	75.2	0.	60.3	39.7
<i>m</i> -Xylene	78.0	15.3	0	84.7
<i>p</i> -Xylene	90.0	—	—	—
Mesitylene	74.1	—	—	—
Anisole	73.1	72.4	0	27.6

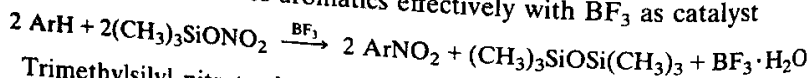
Table XI. Nitration with ACN over Nafion-H[®] Catalyst

Substrate	Yield, %	Isomer Distribution (%)
Benzene	85	
Toluene	79	2-nitro (47) 3-nitro (3)
<i>o</i> -Xylene	60	4-nitro (50) 3-nitro (44)
<i>m</i> -Xylene	61	4-nitro (56) 2-nitro (11)
<i>p</i> -Xylene	61	4-nitro (89)
Meitylene	36	
1,2,3,4-Tetramethylbenzene	69	
Chlorobenzene	49	2-nitro (28) 3-nitro (2) 4-nitro (70)

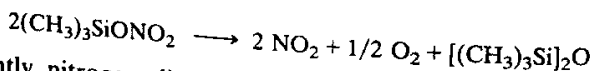
(the isomer ratios remain constant). This may be due to the thermal decomposition of ACN at the needed reaction temperatures necessary for effective catalysis by Nafion-H[®].

The *ortho/para* ratio of nitrotoluenes obtained is lower (0.94) with ACN than with butyl nitrate (1.06), reflecting the somewhat larger bulk of the former reagent.

Trimethylsilyl nitrate, (CH₃)₃SiONO₂, is another interesting but little-studied nitrating agent [33]. It is prepared from chlorotrimethylsilane and silver nitrate and nitrates aromatics effectively with BF₃ as catalyst



Trimethylsilyl nitrate, however, even on standing readily decomposes according to



Consequently nitrogen dioxide formed can also affect nitration in the system. •

III. Lewis-Acid-Catalyzed Nitration

The general Friedel-Crafts acylation principle [36] can be applied to aromatic nitrations involving nitryl halides, dinitrogen pentoxide, and dinitrogen tetroxide (the halides and anhydrides of nitric acid). These should be considered as Friedel-Crafts type reactions, as obviously a very

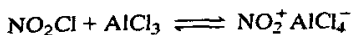
close analogy exists with the corresponding Friedel-Crafts ketone syntheses involving acyl halides and anhydrides [37]. In a generalized sense, nitric acid nitrations catalyzed by protic acids (H_2SO_4 , H_3PO_4 , HF , etc.) or by Lewis acid metal halides (BF_3 , $AlCl_3$, etc.) could be also considered as reactions of Friedel-Crafts type, as an increasing number of Friedel-Crafts ketone synthesis is now known using aliphatic carboxylic acids (acetic, propionic, etc.) as acylating agents.

Friedel-Crafts type nitration using nitryl chloride had been initially reported by Price and Sears [38] who found $AlCl_3$ to be the most suitable catalyst. Deactivated aromatics, however, were nitrated only with difficulty and the method was, therefore, considered to be of limited value. Investigations of Olah and Kuhn [39] have shown that aromatic compounds, including deactivated ones such as halobenzenes and benzotrifluoride, can be nitrated with ease using nitryl halides and a suitable Friedel-Crafts catalyst.

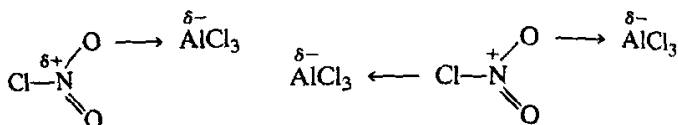


Using nitryl chloride as the nitrating agent, which in the laboratory is conveniently prepared by the reaction of nitric acid with chlorosulfuric acid [40], $TiCl_4$ is found to be the most suitable catalyst. $FeCl_3$, $ZrCl_4$, $AlCl_3$ and $AlBr_3$ are also effective but the reactions are more difficult to handle. With BCl_3 , Olah and Kuhn obtained a smaller amount of nitrated product and considerable ring chlorination; SbF_5 is also an active catalyst for the nitryl chloride nitration of aromatics; BF_3 was found to be inactive as a catalyst. The following yields were obtained upon nitration of the aromatics using $TiCl_4$ as catalyst: benzene, 88%; toluene, 81.5%; ethylbenzene, 79%; fluorobenzene, 91%; chlorobenzene, 41.5%; and benzotrifluoride, 32%. There is always a certain amount of ring-chlorinated by-product formed in the nitrations. Reactions carried out either by using an excess of aromatics as solvent ($TiCl_4$ is miscible with many aromatics) or in carbon tetrachloride solution, always contain chlorinated by-products. The amount of chlorinated by-products can be decreased by using solvents with higher dielectric constants. Tetramethylene sulfone (sulfolane) was found to be a suitable solvent for the $TiCl_4$ and also for most of the other Lewis-acid-catalyzed nitrations. It has excellent solvent properties for aromatics and the catalysts as well as for nitryl halides. It is superior to other solvents that can be used, such as nitromethane. As it is completely miscible with water, the work-up of the reaction mixtures after the reactions are completed is very easy.

In Lewis-acid-halide-catalyzed nitrations with nitryl chloride, are these reactions nitronium salt nitrations according to the ionization



or are they effected by the O-coordinated donor: acceptor complex (1:1 or possibly 1:2 complexes)?



In order to study this problem, Olah and Lin carried competitive studies of nitration of benzene and toluene with nitryl chloride, catalyzed by Lewis acid halides. When carbon tetrachloride or excess aromatics were used as solvent, the data summarized in Table XII were obtained. The data show that the *ortho/para* ratios are smaller than in nitrations with nitronium salts. The observed changes point to the fact that the nitrating agents are the corresponding donor: acceptor complexes and not the nitronium ion itself. The lower *ortho/para* ratios than those obtained in case of NO_2^+ , particularly point to bulkier nitrating agents.

However, when carrying out the reactions in a common polar, ionizing solvent, such as nitromethane, such factors are diminished as shown in Table XII.

Nitryl fluoride is a more powerful nitrating agent than nitryl chloride, but is more difficult to handle. Hetherington and Robinson [42] reported nitration of aromatics with nitryl fluoride in the absence of catalysts. They suggested that in solution, nitryl fluoride dissociates into NO_2^+ and F^- and the intermediate nitronium ion thus formed is the active reagent in the nitrations. Less reactive aromatics such as nitrobenzene were not nitrated and considerable tar formation occurred during the reactions. We found

Table XII. Lewis-Acid-Catalyzed Friedel-Crafts Nitration of Toluene with Nitryl Chloride at 25°C

Lewis Acid Halide	Solvent	% Isomer Distribution			
		<i>ortho</i>	<i>meta</i>	<i>para</i>	<i>o/p</i>
AlCl_3	excess toluene	53.3	1.2	45.5	1.17
TiCl_4		53.1	1.6	45.4	1.17
BF_3		57.1	1.4	41.1	1.40
SbCl_5		56.4	1.4	42.4	1.34
PF_5		57.6	1.6	40.8	1.41
AlCl_3	nitromethane	61.3	3.7	35.0	1.75
TiCl_4		61.1	3.7	35.2	1.74
PF_5		61.6	3.5	34.9	1.76
AlCl_3	CCl_4	42.4	1.7	56.9	0.76
TiCl_4		44.9	1.3	53.7	0.84

that by using a Lewis acid type fluoride catalyst such as BF_3 , PF_5 , AsF_5 , or SbF_5 , simple Friedel-Crafts type nitrations can be carried out with nitril fluoride [39]. Homolytic cleavage of nitril fluoride, which causes most of the side reactions, is considerably suppressed under these conditions in favor of heterolysis, yielding the nitronium ion. The reactions are carried out preferably at low temperatures. Benzotrifluoride is nitrated to *m*-nitrobenzotrifluoride at -50° with 90% yield using boron trifluoride as catalyst. Halobenzenes, including di- and polyhalobenzenes, are nitrated with ease and with yields of over 80%.

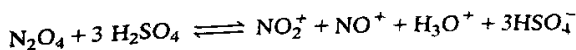
The nitrations are carried out using either (1) an excess of the aromatic as diluent and introducing nitril fluoride and the Lewis-acid-fluoride-catalyst simultaneously at low temperature into the well-stirred reaction mixture or (2) a suitable solvent such as tetramethylene sulfone which can be used advantageously if the fluoride catalyst does not interact with it (SbF_5 , a strong fluorinating agent, attacks the solvent and cannot be used).

Nitril bromide when compared with the chloride and fluoride, is quite unstable. Nitration experiments were carried out with solutions obtained by the halogen exchange of nitril chloride with KBr (not separated from unchanged nitril chloride and decomposition products) in sulfur dioxide solution at -20° , using TiBr_4 as catalyst. Yields of nitrations are lower than those obtained with nitril chloride, due to the formation of more ring-brominated products [39]. This can be attributed partly to free bromine being present from the decomposition of nitril bromide and to the easier hololysis of nitril bromide itself.

It was Schaarschmidt [43] who first investigated the catalytic effect of AlCl_3 and FeCl_3 on the nitration of aromatics with dinitrogen tetroxide, N_2O_4 , the mixed anhydride of nitric and nitrous acid.

Pinck [44] used sulfuric acid to catalyze the nitration of aromatics with N_2O_4 . He observed that only half of the dinitrogen tetroxide was used up in the nitrations, the remainder being present as nitrosylsulfuric acid. Titov [45] dissolved N_2O_4 in sulfuric acid and used this solution as nitrating agent.

Raman spectroscopic [46] and cryoscopic [47] investigations of solutions of N_2O_4 in sulfuric acid gave proof that the effective nitrating agent in the solutions is the nitronium ion (NO_2^+) and also explained the formation of an equimolar amount of nitrosyl sulfuric acid ($\text{NO}^+\text{HSO}_4^-$).



Bachman [48] used the stable $\text{N}_2\text{O}_4 \cdot \text{BF}_3$ complex, prepared as a crystalline salt from the components in aromatic nitrations.

The major difficulty in Friedel-Crafts type nitrations with N_2O_4 was that the N_2O_4 -catalyst complexes were insoluble in the reaction media. This resulted not only in slow reactions and low yields, but in many cases also in undesirable side reactions.

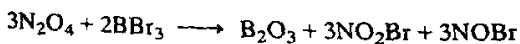
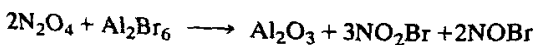
Schaarschmidt reported [43] that when $AlBr_3$ was tried instead of $AlCl_3$ as catalyst, in an unexpected way only ring bromination took place and no nitro product was formed. The use of a fluoride catalyst, such as BF_3 in the work of Bachman [48], eliminated halogenation as side reaction but still dealt with a heterogenous reaction medium.

In the course of Olah's investigation, it was found that homogeneous Friedel-Crafts type nitrations with N_2O_4 and Lewis acid catalysts such as $TiCl_4$, BF_3 , BCl_3 , PF_5 , and AsF_5 can be carried out in tetramethylene sulfone solutions [8,37]. It is not necessary to isolate the catalyst- N_2O_4 complex. Instead, a solution of N_2O_4 and the catalyst is prepared and this solution is added to a tetramethylene sulfone solution of the aromatic to be nitrated.

Nitrobenzene was obtained from the nitration of benzene with yields of 32-67% and fluoronitrobenzenes from fluorobenzene with 28-76% yields; the relative order of activity of the catalysts used was $AsF_5 > PF_5 > BF_3 > TiCl_4 > BCl_3$. With the chloride catalysts, a considerable amount of chlorobenzene was also formed in the reaction, as was the case with $AlCl_3$.

Bromide Lewis acids such as $AlBr_3$, BBr_3 and $TiBr_4$, in agreement with previous observations of Schaarschmidt [43] with $AlBr_3$, gave a high amount of ring bromination but simultaneously about 10% of nitroaromatics were formed.

Subsequent investigations have proven that aluminum, titanium, and boron halides tend to react with N_2O_4 in the following way:



NO_2Br , being unstable, decomposes to $N_2O_4 + Br_2$ and the bromine formed in the presence of the catalyst brominates the aromatic. In a similar manner, but to a lesser extent, chlorination takes place with chloride catalysts.

The use of solid-acid catalysts in aromatic nitration frequently represents substantial advantages over liquid-acid catalyst systems. When alkylbenzenes in the liquid phase were nitrated with N_2O_4 in the presence of Nafion-H[®] at 0°C, nitration was slow [29]. In general, solid-acid catalysts are rather ineffective at such low temperatures. The isomer ratios of nitroarene products (Table XIII), however, show that the products were

Table XIII. Nitration of Aromatics with Dinitrogen Tetroxide over Nafion-H[®] Catalyst at 0°C in CCl₄ Solution

Substrate	% Isomer Distribution
Toluene	2-nitro (49)
	3-nitro (6)
	4-nitro (45)
<i>o</i> -Xylene	3-nitro (41)
	4-nitro (59)
<i>m</i> -Xylene	2-nitro (16)
	4-nitro (84)

obtained via a typical electrophilic aromatic substitution [8]. This sharply contrasted with the nearly statistical isomer distribution observed in the free-radical nitration of toluene with N₂O₄, which is shown in Table XIV, together with typical data of electrophilic nitration with NO₂⁺BF₄⁻ [49].

Nitrations using nitrogen pentoxide, the anhydride of nitric acid, are well known [50]. Most of the work was carried out in solution in the absence of catalyst. Solid nitrogen pentoxide at low temperature is known to be nitronium nitrate, NO₂⁺NO₃⁻. A study of the kinetics and mechanism of nitrogen pentoxide nitrations gave evidence, however, to the fact that other carriers of the nitronium ion may also play a role. Decomposition of N₂O₄ and oxygen should also be considered if the N₂O₅ used is not entirely pure.

Klemenz and Scholler [51] have shown that solutions of N₂O₅ in sulfuric acid are very effective nitrating agents having nitrating properties similar to those of solutions of nitric acid in sulfuric acid.

Millen [52] found the ionization of N₂O₅ in sulfuric acid to be

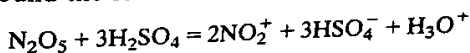


Table XIV. Free Radical Nitration of Toluene

	% Nitrotoluenes		
	<i>Ortho</i>	<i>Meta</i>	<i>Para</i>
<i>N</i> ₂ <i>O</i> ₄ UV Irradiation			
N ₂ O ₄	37.2	38.1	24.7
NO ₂ BF ₄	65.4	2.8	31.8
<i>Tetranitromethane thermal reaction (> 300°C)</i>			
C(NO ₂) ₄	42	39	19
C(NO ₂) ₄ ·BF ₃	64	2	34

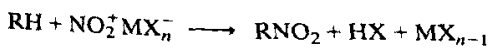
Bachman [53] reported the use of the stable insoluble $N_2O_5 \cdot BF_3$ complex in aromatic nitrations; the active nitrating agent was $NO_2^+ BF_3ONO_2^-$. We have found in our investigations that N_2O_5 can be used as a very effective nitrating agent in Friedel-Crafts type nitrations in the presence of Lewis acid catalysts such as BF_3 , $TiCl_4$, $SnCl_4$, and PF_5 in tetramethylene sulfone solution. It is not necessary to isolate the intermediate N_2O_5 -Lewis acid complexes as the solutions of N_2O_5 and the catalyst can be well controlled in homogeneous solutions. In general, the solution of N_2O_5 and the Lewis-acid-catalyst (in equimolar quantities) is run into the stirred-and-cooled solution of the aromatic in tetramethylene sulfone. After the addition is completed, the mixture is allowed to come to room temperature and is then stirred for another 15 min. Alkylbenzenes (benzene, toluene, xylene, ethylbenzene, propylbenzene, butylbenzene, mesitylene) were nitrated with yields of 87–95%. As the reactions are carried out in homogeneous media, the amount of dinitro products is negligible if an excess of alkylbenzene is used. Halobenzenes (fluoro-, chloro-, bromo-dihalobenzenes, benzotrifluoride) were nitrated with yields of 79–89%.

When the N_2O_5 nitration is carried out in liquid anhydrous HF as solvent (which does not appear to react with N_2O_5 at a temperature below $0^\circ C$) using a catalyst such as BF_3 , SbF_5 , PF_5 , AsF_5 , SiF_4 , NbF_5 , WF_6 , etc., a quantitative formation of the corresponding nitronium salts takes place. As HF also acts as a good ionizing solvent, an extremely active nitration medium is obtained. Nitrobenzene and benzotrifluoride are nitrated with yields of over 90% at temperatures between -20 and $0^\circ C$.

One of the difficulties of using anhydrous HF as solvent (aside from some inconveniences arising from its being handled in laboratories not equipped for fluorine work) is the fact that it is a rather poor solvent for aromatics (solubilities are generally less than 2%) and, therefore, the reactions must be carried out by vigorous stirring of the heterogeneous reaction mixtures. The use of pyridinium polyhydrogen fluoride, a convenient HF-like solvent, overcomes much of these difficulties.

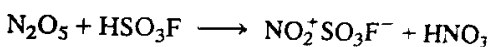
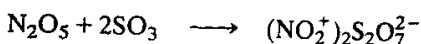
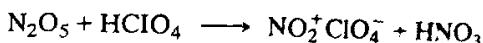
IV. Nitration with Nitronium Salts

Hydrocarbons are efficiently nitrated by nitronium salts under anhydrous conditions as shown by Ingold *et al.* and subsequently developed by Olah *et al.* [54] as a general preparative nitration method



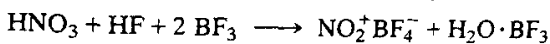
Hantzsch first reported [55] the reaction of HNO_3 with $HClO_4$. He claimed that the product formed was a mixture of nitracidium perchlorate and hydronitracidium perchlorate. It was left to Goddard, Hughes, and Ingold [56], to show that Hantzsch's preparation gave a mixture of nitro-

mium perchlorate and hydronium perchlorate, from which the nitronium salt could be isolated only with difficulty. They themselves developed a preparation of pure nitronium perchlorate and a number of nitronium sulfates were also reported



These and related salts were characterized by Raman spectroscopy and other physical measurements.

A simple and efficient preparation of nitronium tetrafluoroborate was achieved by Olah *et al.* by letting a 2-mol excess of boron trifluoride react with an equimolar mixture of nitric acid and anhydrous HF [54].



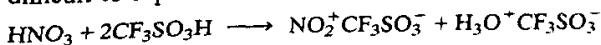
Water formed as byproduct in the reaction is bound by boron trifluoride as a stable hydrate from which BF_3 can be regenerated by distilling with sulfuric acid or oleum. Other nitronium salts (PF_6^- , AsF_6^-) can also be prepared in a similar fashion. The reactions, however, require larger amounts of PF_5 and AsF_5 because of their hydrolytic instability. The method thus can be used to prepare $\text{NO}_2^+\text{BF}_4^-$, $\text{NO}_2^+\text{PF}_6^-$, $\text{NO}_2^+\text{AsF}_6^-$, $\text{NO}_2^+\text{SbF}_6^-$, and $(\text{NO}_2^+)_2\text{SiF}_6^{2-}$. As nitric acid, if not carefully purified, always contains nitrous acid (nitrogen oxides) the nitronium salts obtained generally contain nitrosonium ion (NO^+) salts (*vide infra*).

Kuhn has found that nitric acid can be replaced by alkyl nitrates (free of nitrites) in the preparation of nitronium salts [57].

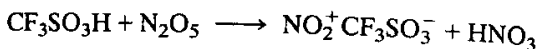
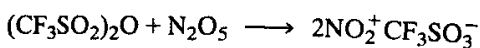


SbF_5 and AsF_5 react explosively with alkyl nitrates. Therefore, the reaction is limited to the preparation of $\text{NO}_2^+\text{BF}_4^-$, $\text{NO}_2^+\text{PF}_6^-$, and $(\text{NO}_2^+)_2\text{SiF}_6^{2-}$. This method provides extremely pure nitronium salts free of nitrosonium ion.

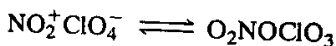
Coon *et al.* [58] have reported the preparation of nitronium trifluoromethane sulfonate based on the analogy of the related preparation of the perchlorate or fluoroborate. Hydronium trifluoromethanesulfonate is, however, difficult to separate from the nitronium salt



Nitronium trifluoromethanesulfonate can also be readily prepared by reaction of N_2O_5 with either trifluoromethanesulfonic anhydride (Yagupolskii, [59a] or trifluoromethanesulfonic acid (Effenberger, [59b]). The former gives pure salt free of nitric acid or hydronium triflate.



Nitronium salts are colorless, crystalline, hygroscopic compounds. Nitronium perchlorate, sulfate, and hexafluoroiodate are unstable. The spontaneous decomposition (explosive nature) of the perchlorate was experienced by Ingold [60]. It is in all probability due to the equilibrium with the covalent unstable nitrate



Consequently, its use is not generally recommended and extreme caution is called for. In contrast, complex fluoride salts such as the tetrafluoroborate and hexafluorophosphate are very stable. Only on heating to higher temperatures ($> 180\text{--}200^\circ\text{C}$) do they decompose into NO_2F and the corresponding Lewis acid fluoride.

Specific conductivity of nitronium tetrafluoroborate varies linearly with concentration. Cryoscopic measurements in sulfolane solution indicate that the nitronium salt is present as ion pairs and the conductance must be due to ion triplets and not separated ions [54].

The nitronium salts have been well characterized by infrared and Raman spectroscopy, ^{15}N NMR, and by x-ray crystallography. All spectroscopic and crystallographic evidence indicates that the nitronium ion has a linear structure. These studies are well reviewed and no further discussion is necessary [1].

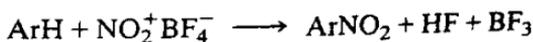
Some nitronium salts with complex fluoride anions are commercially available or can be readily prepared in the laboratory by the procedure of Olah *et al.* from nitric acid [54]. As nitric acid always contains some nitrous acid, the commercial salt generally needs to be purified from nitrosonium ion impurities. This according to Ridd can be readily achieved in case of $\text{NO}_2^+\text{PF}_6^-$ by recrystallization using nitromethane [61]. In the case of $\text{NO}_2^+\text{BF}_4^-$, because of its limited solubility, such purification is difficult. To obtain pure $\text{NO}_2^+\text{BF}_4^-$ free of NO^+BF_4^- starting from nitric acid, it is necessary to purify it from nitrous acid by treatment with urea and immediately convert it into the nitronium ion [62]. Alternatively, alkyl nitrates that can be prepared in pure form can be converted into nitronium salts free of NO^+ [57].

Sulfolane (tetramethylene sulfone) is a relatively good solvent for nitronium salts. $\text{NO}_2^+\text{BF}_4^-$ has about a 7% solubility [63]. Acetonitrile is also applicable for nitrations with nitronium salts but the nitrile group strongly interacts with NO_2^+ and causes acetonitrile to slowly oligomerize even at room temperature. Thus only freshly prepared solutions should be used at low temperature. Nitromethane, nitroethane, and nitropropane can also

be used as solvents for nitrations particularly with remarkably soluble $\text{NO}_2^+\text{PF}_6^-$ (~25%). On the other hand, nitronium tetrafluoroborate has little solubility in nitromethane (<0.5%). All solvents should be thoroughly dried and purified. Although sulfolane has a relatively high melting point for a solvent (+28.9°), its large molar freezing point depression (66.2°) allows nitrations to be carried out in a wide temperature range. Methanesulfonic acid, trifluoromethanesulfonic acid, fluorosulfuric acid, and even sulfuric acid have also been used as solvents especially for deactivated substrates. It is important to choose a solvent which by itself does not react with the nitronium salt and preferably provides homogeneous solutions.

A. Arenes

Nitronium tetrafluoroborate is the most frequently used nitronium salt for nitrating aromatics



The obtained byproducts HF and BF_3 can be readily recycled on an industrial scale and thus the nitration made catalytic.

Results of preparative nitration arenes, haloarenes, and nitroarenes are summarized in Tables XV–XVII. Since HF and BF_3 are the only byproducts of the reaction, nitration with nitronium salts can be carried out under anhydrous conditions. This is advantageous in nitration of aromatics containing functional groups sensitive to hydrolysis. Thus aromatic nitriles, acid halides, and esters can be nitrated in high yield without difficulty (Tables XVIII–XIX).

Nitration of aromatics with nitronium tetrafluoroborate is usually carried out in sulfolane or with the more soluble nitronium hexafluorophosphate in nitromethane solution. Reactions can be carried out in case of reactive aromatics from -20° to room temperature and short reaction times (5–10 min). Deactivated aromatics need higher temperatures and longer reaction times. They are preferentially carried out in strongly acidic solutions ($\text{CF}_3\text{SO}_3\text{H}$, FSO_3H , HF, H_2SO_4). The nitro products are generally formed in very high yield. Mononitrations, with limited (<3%) dinitration, are achieved using an excess of the aromatic substrate. This is different from mixed acid nitrations, where the high solubility of mononitro compounds in the acid layer frequently results in the formation of increased amounts of dinitro byproducts.

The most serious limitation of the use of nitronium tetrafluoroborate is its low solubility in many solvents. As mentioned, the most convenient solvent is sulfolane, in which the tetrafluoroborate is soluble to about 7%.

Table XV. Nitration of Arenes with $\text{NO}_2^+\text{BF}_4^-$

Substrate	Product	% Yield of Mononitro Product
Benzene	Nitrobenzene	93
Toluene	Nitrotoluenes	95
<i>o</i> -Xylene	Nitroxylens	91
<i>m</i> -Xylene	Nitroxylens	90
<i>p</i> -Xylene	Nitro- <i>p</i> -xylene	93
Mesitylene	Nitromesitylene	89
Ethylbenzene	Nitroethylbenzenes	93
<i>n</i> -Propylbenzene	Nitro- <i>n</i> -propylbenzenes	91
Isopropylbenzene	Nitro-isopropylbenzenes	93
<i>n</i> -Butylbenzene	Nitro- <i>n</i> -butylbenzenes	90
<i>s</i> -Butylbenzene	Nitro- <i>s</i> -butylbenzenes	92
<i>t</i> -Butylbenzene	Nitro- <i>t</i> -butylbenzenes	88
Biphenyl	Nitrobiphenyls	94
Naphthalene	Nitronaphthalenes	79
Phenanthrene	Nitrophenanthrene	89
Anthracene	9-Nitroanthracene	85
Fluorene	2-Nitrofluorene	79
Chrysene	6-Nitrochrysene	73
Benzo[<i>a</i>]pyrene	6-Nitrobenzo[<i>a</i>]pyrene	79
Anthanthrene	Nitroanthanthrenes	81
Pyrene	1-Nitropyrene	85
Triphenylene	Nitrotriphenylenes	77
Perylene	3-Nitroperylene	85

Table XVI. Nitration of Haloarenes and Haloalkylarenes with $\text{NO}_2^+\text{BF}_4^-$

Substrate	Product	% Yield of Mononitro Product
Fluorobenzene	<i>o,p</i> -Fluoronitrobenzenes	90
Chlorobenzene	<i>o,p</i> -Chloronitrobenzenes	92
Bromobenzene	<i>o,p</i> -Bromonitrobenzenes	87
Iodobenzene	<i>o,p</i> -Iodonitrobenzenes	90
Benzotrifluoride	<i>m</i> -Nitrobenzonitrifluoride	20
<i>p</i> -Fluorobenzotrifluoride	3-Nitro-4-fluorobenzotrifluoride	85
<i>o</i> -Dichlorobenzene	Nitro- <i>o</i> -dichlorobenzenes	70
<i>m</i> -Dichlorobenzene	Nitro- <i>m</i> -dichlorobenzenes	74
<i>p</i> -Dichlorobenzene	Nitro- <i>p</i> -dichlorobenzene	80
<i>o</i> -Difluorobenzene	Nitro- <i>o</i> -difluorobenzenes	82
<i>m</i> -Difluorobenzene	Nitro- <i>m</i> -difluorobenzenes	79
<i>p</i> -Difluorobenzene	Nitro- <i>p</i> -difluorobenzenes	85
α -Fluoronaphthalene	Nitro- α -fluoronaphthalenes	75
β -Fluoronaphthalene	Nitro- β -fluoronaphthalenes	79
Benzyl chloride	Nitrobenzyl chlorides	52
β -Fluoroethylbenzene	Nitro- β -fluoroethylbenzenes	69
β -Chloroethylbenzene	Nitro- β -chloroethylbenzenes	82
β -Bromoethylbenzene	Nitro- β -bromoethylbenzenes	78

7. Methods for Preparing Energetic Nitrocompounds

140

Table XVII. Nitration of Nitroarenes and Nitrohaloarenes with $\text{NO}_2^+ \text{BF}_4^-$

Substrate	Product	% Yield of Nitro Product
Nitrobenzene	<i>m</i> -Dinitrobenzene	81
α -Nitronaphthalene	Dinitronaphthalenes	85
<i>p</i> -Fluoronitrobenzene	2,4-Dinitrofluorobenzene	78
<i>o</i> -Fluoronitrobenzene	2,4-Dinitrofluorobenzene	84
2,4-Dinitrofluorobenzene	Picryl fluoride	40
<i>p</i> -Nitrochlorobenzene	2,4-Dinitrochlorobenzene	75
<i>o</i> -Nitrochlorobenzene	2,4-Dinitrochlorobenzene	77
2,4-Dinitrochlorobenzene	Picryl chloride	80

Table XVIII. Nitration of Arylcarboxylic Acid Esters and Halides with $\text{NO}_2^+ \text{BF}_4^-$

Substrate	Product	% Yield of Mononitro Product
Methyl benzoate	Methyl <i>m</i> -nitrobenzoate	88
Ethyl benzoate	Methyl <i>m</i> -nitrobenzoate	79
Propyl benzoate	Propyl <i>m</i> -nitrobenzoate	82
Ethyl <i>m</i> -nitrobenzoate	Ethyl 3,5-dinitrobenzoate	60
Benzoyl fluoride	<i>m</i> -Nitrobenzoyl fluoride	69
Benzoyl chloride	<i>m</i> -Nitrobenzoyl chloride	70

Table XIX. Nitration of Aryl and Aralkyl Nitriles with $\text{NO}_2^+ \text{BF}_4^-$

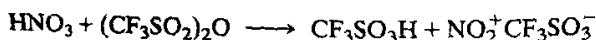
Substrate	Product	% Yield of Nitro Product
Benzonitrile	3-Nitrobenzonitrile	85
<i>o</i> -Toluonitrile	2-Methyl-5-nitrobenzonitrile	90
<i>m</i> -Toluonitrile	Nitrotoluonitriles	85
<i>p</i> -Toluonitrile	4-Methyl-3-nitrotoluonitrile	92
Nitro- <i>o</i> -toluonitrile	3,5-Dinitro- <i>o</i> -toluonitrile	93
Nitro- <i>m</i> -toluonitrile	Dinitro- <i>m</i> -toluonitriles	84
Nitro- <i>p</i> -toluonitrile	3,5-Dinitro- <i>o</i> -toluonitrile	89
<i>p</i> -Fluorobenzonitrile	4-Fluoro-3-nitrobenzonitrile	90
<i>p</i> -Chlorobenzonitrile	4-Chloro-3-nitrobenzonitrile	92
1-Naphthonitrile	Nitronaphthonitrile	91
Benzyl cyanide	Nitrobenzyl cyanides	84

In nitromethane, its solubility is only $\sim 0.2\%$. Therefore, there is a significant need for more soluble and stable nitronium salts.

Nitronium hexafluorophosphate ($\text{NO}_2^+ \text{PF}_6^-$) in contrast to $\text{NO}_2^+ \text{BF}_4^-$ was found to be much more soluble in many solvents. Its solubility in nitromethane for example is $>30\%$. Consequently is a very convenient nitrating agent for aromatics (as well as aliphatics). It can be prepared similarly to tetrafluoroborate by using HF and PF_5 . Lack of ready availability of PF_5 may be, however, a limitation.

Nitration of aromatics with *nitronium trifluoromethanesulfonate* (containing hydronium trifluoromethanesulfonate) formed in the HNO_3 - $\text{CF}_3\text{SO}_3\text{H}$ system have been studied by Coon *et al.* [58]. Selective mono- and dinitration of toluene in 98% yield can be carried out under heterogeneous conditions by varying the reaction temperature. Low reaction temperature (-60 to -110°C) results in the formation of *ortho*- and *para*-nitrotoluenes, with *meta*-nitrotoluene limited to 0.2–0.5%. The very limited *meta*-nitration is probably primarily due to the low reaction temperatures. The heterogeneous nature of these nitrations precludes comparison of data with homogeneous nitrations involving $\text{NO}_2^+ \text{BF}_4^-$.

Nitric acid–triflic anhydride (trifluoromethanesulfonic anhydride) is found by Olah *et al.* to be a very effective nitrating agent [8]. The system can be used in sulfolane or nitromethane solution. $\text{HNO}_3 - (\text{CF}_3\text{SO}_2)_2\text{O}$ acts as nitronium triflate according to



The reactivity of nitronium salts is further enhanced in strong acid such as fluorosulfuric acid. Such solutions can be used to even trinitrate benzene to yield 1,3,5-trinitrobenzene, a reaction which was reported previously only in low yield [64–66]. 1,3,5-Trinitrobenzene is usually obtained only indirectly [67], but can be prepared in good yield by nitration of *meta*-dinitrobenzene with nitronium tetrafluoroborate in fluorosulfuric acid [68]. Optimum reaction conditions require a reaction time of ~ 3 hr at 150°C , to yield 100% pure 1,3,5-trinitrobenzene in 50% yield [41,69]. The data in Table XX show that higher yields can be obtained at shorter reaction times, with mixtures of di- and trinitro products necessitating purification by HPLC. Longer reaction times give pure 1,3,5-trinitrobenzene but also result in oxidative losses and hence lower yield.

Nitronium salts are the most effective electrophilic nitrating agents for nitration of aromatic compounds under very mild conditions. They are also widely applied in the nitration of heterocyclic aromatic compounds. The nitration of heterocyclic compounds by nitronium salts was first studied in the case of pyridine [16,19,70]. N-nitration giving *N*-nitropyridinium ion is followed by ring opening, if excess pyridine is present, yielding glutaconic

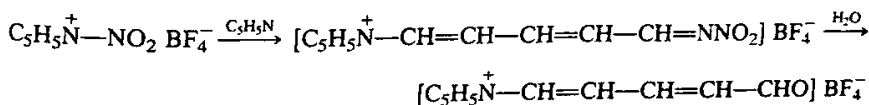
7. Methods for Preparing Energetic Nitrocompounds

143

Table XX. Nitration of *m*-Dinitrobenzene to 1,3,5-Trinitrobenzene with Nitronium Tetrafluoroborate ($\text{NO}_2^+ \text{BF}_4^-$) in Fluorosulfuric acid (FSO_3H) Solution at 150°C .

Reaction Time	Recovery of Nitro Compounds (%)	1,3,5-Trinitrobenzene in Total Nitro Products (%)	Yield of 1,3,5-Trinitrobenzene (%)
0	100	0	0
0.5	95.2	38.0	36.2
1.0	90.3	60.4	54.5
1.7	82.5	80.0	66.2
2.2	77.7	85.0	66.0
3.0	64.8	95.0	61.6
3.4	56.7	98.2	55.7
3.6	52.3	99.4	52.0
3.8	49.3	100	49.3
4.0	44.8	100	44.8
4.2	39.4	100	39.4

aldehyde



Reverse addition of pyridine to excess nitronium salt gives stable *N*-nitropyridinium salts [16]. No *N*-*C* migration of the nitro-group is, however, observed even on heating. On the other hand, alkylnitropyridinium salts are good transfer nitration agents [16,71,72,73].

The preferential *N*-nitration of pyridine would seem to indicate that direct electrophilic *C*-nitration is difficult to achieve expect in sterically crowded systems and when the nonbonded nitrogen electron pair is occupied such as is the case in pyridine-*N*-oxides which are readily nitrated in the 4 position. Pyridinium salts have deactivated rings and are nitrated only with difficulty in the 3 position.

Nitration of pyridine with mixed nitric-sulfuric acid gives a low yield of the 3-nitro product indicating that the nitration is that of the pyridinium ion formed by protonation in the acid medium.

When reacting sterically crowded 2,6-di- and 2,4,6-tri-*tert*-butylpyridine with nitronium tetrafluoroborate, nitration occurred exclusively in the ring. When 2,6-di-*tert*-butylpyridine was reacted with $\text{NO}_2^+ \text{BF}_4^-$ in dry CH_2Cl_2

or CH_2Cl_2 /sulfolane, apart from unreacted starting material, 28% 2,6-di-*tert*-butyl-4-nitropyridine and 6% 2,6-di-*tert*-butyl-3,4-dinitropyridine was formed [74].

Similarly, 2,4,6-tri-*tert*-butylpyridine when reacted with $\text{NO}_2^+\text{BF}_4^-$ in CH_2Cl_2 gave 36% 2,4,6-tri-*tert*-butyl-3-nitropyridine as the only product.

Olah and Kuhn reported that thiophene forms nitrothiophene in 91% yield on nitration with $\text{NO}_2^+\text{BF}_4^-$ [17], while the nitration of furan results in a 14% yield of nitrofuran. 3-Nitro-6-phenyl-2-pyridone has been obtained in 40% yield by the nitration of 6-phenyl-2-pyridone with $\text{NO}_2^+\text{BF}_4^-$ [75].

B. Alkanes

Mixture of nitric and sulfuric acid (mixed acid) used extensively in nitration of aromatic hydrocarbons, is generally unsuitable for nitration of alkanes, since primary nitroalkanes are rapidly hydrolyzed by hot sulfuric acid and secondary and tertiary nitroalkanes form tars (in all probability via rapid alkene-forming elimination and subsequent polycondensation, polymerization, etc.). It is, however, significant to point out that it is not necessarily the lack of reactivity of "paraffins" with mixed acid that makes the nitration of saturated hydrocarbons unsuitable, but that fast secondary reactions of any nitro products formed (as well as oxidative side reactions) can take place. This difficulty can be, at least in part, overcome by using preformed nitronium salts as nitrating agents.

Whereas electrophilic aromatic nitration is one of the most thoroughly studied reactions, electrophilic aliphatic nitration remained long unrecognized. It was only after the development of stable nitronium salts as effective nitrating agents that *bona fide* electrophilic nitration and nitrolysis of alkanes and cycloalkanes was achieved [76]. [The terms are defined as substitution (of hydrogen for the nitro group) and nitrolytic cleavage (of C-C bonds), respectively].

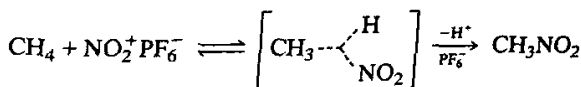
A solution of a stable nitronium salt (generally the hexafluorophosphate $\text{NO}_2^+\text{PF}_6^-$ but also the hexafluoroantimonate $\text{NO}_2^+\text{SbF}_6^-$ or tetrafluoroborate $\text{NO}_2^+\text{BF}_4^-$) in methylene chloride-tetramethylene sulfone solution was allowed to react with the alkane (cycloalkane), with usual precautions taken to avoid moisture and other impurities. Reactions were carried out at room temperature (25°C) in order to avoid or minimize the possibility of radical side reactions and/or protolytic cleavage reactions (tertiary nitroalkanes particularly readily undergo protolytic cleavage, even if the system initially is acid free but nitration forms acid). Data obtained are summarized in Table XXI.

At 25° only 0.1% of nitromethane was obtained in the nitration of methane. Substantially (at least tenfold) increased yields were obtained in

Table XXI. Nitration and Nitrolysis of Alkanes and Cycloalkanes with $\text{NO}_2^+\text{PF}_6^-$ in CH_2Cl_2 -Sulfolane Solution at 25°C

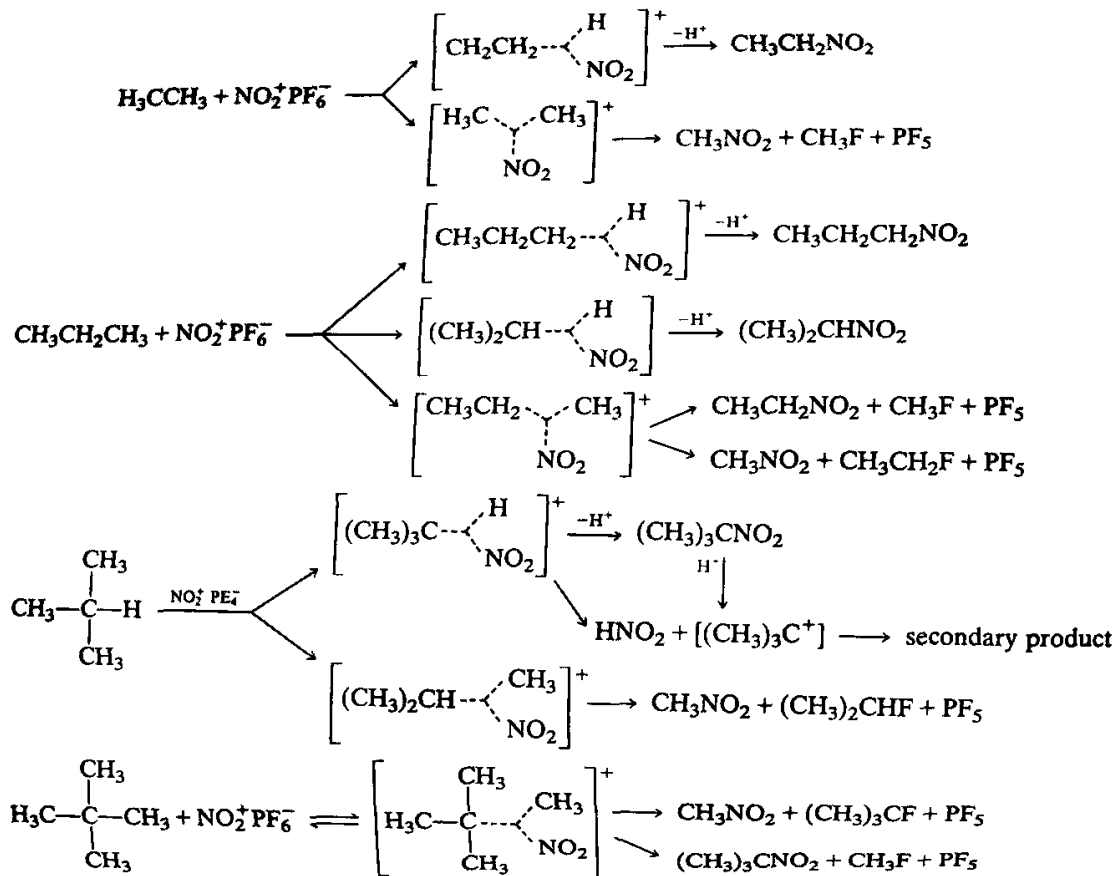
Hydrocarbon	Nitroalkane Products and Their Mol Ratios
Methane	CH_3NO_2
Ethane	$\text{CH}_3\text{NO}_2 > \text{CH}_3\text{CH}_2\text{NO}_2$, 2.9:1
Propane	$\text{CH}_3\text{NO}_2 > \text{CH}_3\text{CH}_2\text{NO}_2 > 2\text{-NO}_2\text{C}_3\text{H}_7 > 1\text{-NO}_2\text{C}_3\text{H}_7$, 2.8:1:0.5:0.1
Isobutane	<i>tert</i> - $\text{NO}_2\text{C}_4\text{H}_9 > \text{CH}_3\text{NO}_2$, 3:1
<i>n</i> -Butane	$\text{CH}_3\text{NO}_2 > \text{CH}_3\text{CH}_2\text{NO}_2 > 2\text{-NO}_2\text{C}_4\text{H}_9 \sim 1\text{-NO}_2\text{C}_4\text{H}_9$, 5:4:1.5:1
Neopentane	$\text{CH}_3\text{NO}_2 > \textit{tert}-\text{C}_4\text{H}_9\text{NO}_2, 3.3:1$
Cyclohexane	Nitrocyclohexane
Adamantane	1-Nitroadamantane $>$ 2-nitroadamantane, 17.5:1

HF and HSO_3F (or other superacid) solutions (see subsequent discussion). Higher alkanes and isoalkanes gave yields of 5–10% and adamantane was nitrated in 30% yield. Data indicate that nitration (nitrolysis) of alkanes with nitronium salts proceeds in accordance with the generalized concept of electrophilic reactions of single bonds [77] involving two-electron, three-center bond carbocationic intermediates (transition states) as illustrated with case of the nitration of methane.



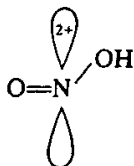
In cases of higher hydrocarbons, nitrolysis of the C—C bond also takes place in competitive reactions (Scheme 1).

The nitronium ion nitration (and nitrolysis) of alkanes and cycloalkanes follows the same pathway as protolytic reactions and alkylations [78] (i.e., the reactions proceed via two-electron three-center bond five-coordinate carbocationic transition states formed by the nitronium ion attacking the two-electron covalent σ bonds, forcing them into electron-pair sharing. It should be remembered that the linear nitronium ion $\text{O}=\text{N}^+=\text{O}$ has no vacant orbital on nitrogen (similar to the ammonium ion) and therefore per se can act only as a polarizable electrophilic nitrating agent. In contrast to π -donor aromatics, σ -donor alkanes are weak electron donors and particularly primary C—H bonds (as those in methane) seem not bring about such polarization. The "reactive" nitronium ion in nitration of methane thus must be somewhat bent (i.e., at least partially rehybridized from sp to sp^2) with a developing empty p -orbital on nitrogen. The driving force for



Scheme 1. NO_2^+ Nitration of Alkanes

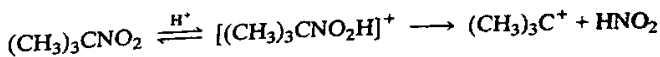
forming the bent nitronium ion must be the ability of the oxygen non-bonded electron pairs to coordinate with the strong acid present in the nitration systems. Protosolvation should result in at least partial bending and development of an empty bonding orbital on nitrogen. If full protonation would be achieved (for which there is yet no direct experimental evidence) the protonated nitronium dication NO_2H^{2+}



would be fully bent with an empty atomic orbital on nitrogen and could be considered as the ultimate electrophilic nitrating agent. The protosolvated nitronium ion indeed may be the reactive species formed in superacidic nitrations (hence the higher reactivity of nitronium salts in these solutions). Whereas reaction at the C—H bond results in substitution of nitro group for hydrogen, reaction at C—C bond causes nitrolysis as shown in the reactions of ethane, propane isobutane, and neopentane.

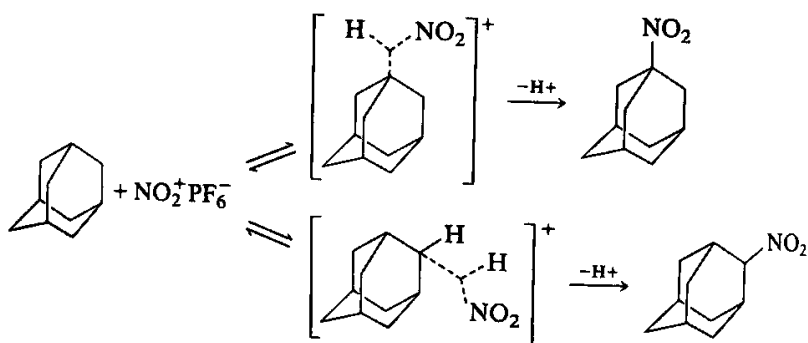
C—C bonds are generally more reactive than secondary or primary C—H bonds, leading to preferential nitrolysis of *n*-alkanes. The nitronium ion, which is linear by itself, does not seem to exercise excessive steric hindrance in the transition state, where it is substantially bent (as indicated also from its behavior in electrophilic aromatic substitutions). Side products of the nitrolysis are methyl, ethyl, and isopropyl fluoride (formed by the reaction of PF_6^- with the cleaved alkylcarbenium ions) or secondary alkylation products, which by themselves are capable of undergoing reaction with the nitronium salt.

Tertiary C—H bonds show the highest reactivity. However, protolytic cleavage of tertiary and secondary nitroalkanes is a major side reaction and can lead to the formation of a variety of byproducts. Protolytic denitration was demonstrated by reacting 2-nitro-2-methylpropane with $\text{FSO}_3\text{H-SbF}_5$, HF-SbF_5 , and HF-PF_5 at -80°C . The protolytic cleavage reaction yields *t*-butyl cation and nitrous acid (or subsequently, nitrosonium ion). No nitronium is formed, as shown by the quenching of the reaction mixtures with benzene and toluene forming no nitroaromatics. At the same time *t*-butylation products were observed.

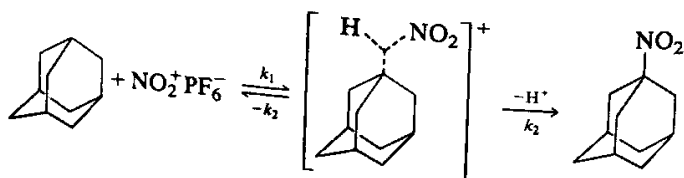


The steric requirements for reaction with tertiary C—H bonds in alkanes are limited, because of the initial linear nature of the nitronium

ion. Adamantane is nitrated with nitronium salts in methylene chloride-sulfolane mixtures, to form 1-nitroadamantane in 10–30% yield. In pure nitromethane or nitroethane solution, yields of 70–80% were obtained. Because of the rigid structure of the adamantyl cage, geometrical constraints allow only front side attack by the nitronium ion. The reaction therefore proceeds via an S_E2 -like electrophilic substitution involving the σ -electron pair of the involved C—H bonds.



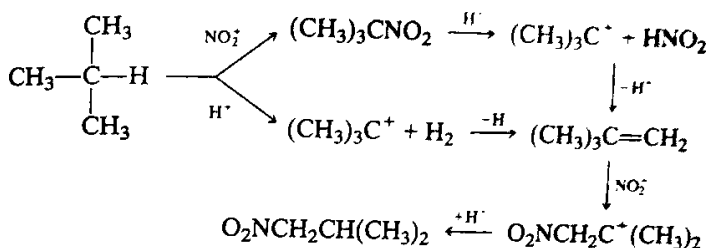
Probing the mechanism of the reaction, a kinetic hydrogen isotope effect study of the rate of nitration of 1,3,5,7-tetradeuterioadamantane compared with that of light adamantane showed a kinetic hydrogen isotope effect ($k_H/k_D = 1.3$). This would indicate a highly unsymmetrical transition state (or high lying intermediate) of carbocationic nature.



Compared to tertiary C—H bonds, C—C bonds are less reactive; primary and secondary C—H bonds have even lower reactivity. Cleavage nitration (nitrolysis of C—C bonds) of *n*-alkanes is the predominant reaction.

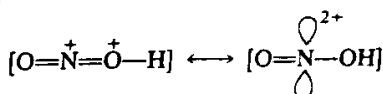
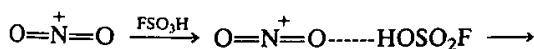
As discussed previously, increased yields of nitromethane can be obtained by carrying out the nitration of methane in anhydrous HF or HSO_3F . As no protolytic reaction of nitromethane occurs in HF under the reaction conditions, no protolytic byproducts are formed. However, during the nitration of isobutane in HF solution, 90% of the nitroalkane obtained consists of 1-nitro-2-methylpropane. Since only traces of this isomer are formed in nitronium salt nitration in methylene chloride-sulfolane solution, this product must be formed from isobutylene, which in turn is

formed either by the direct reaction between isobutane and HF/PF₅ or more probably from the protolytic cleavage of 2-nitro-2-methylpropane.



Nitration of dinitrobenzene to trinitrobenzene and other deactivated aromatics with nitronium salts is greatly facilitated by carrying out the reactions in superacids (FSO₃H, CF₃SO₃H, etc.).

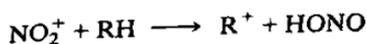
The unexpectedly high reactivity of the nitronium ion in FSO₃H or CF₃SO₃H solution is attributed to its protosolvation.



Fully protonated nitronium dication was found to be unstable by Simonetta's quantum mechanical calculations [79a]. However, recent *ab initio* calculations with 6.31G** basis set indicated a minimum [79b]. Evidence for protosolvation of nitronium ion by fluorosulfuric acid comes also from infrared studies. The O—H stretching frequency of fluorosulfuric acid in AsF₃ is shifted from 3300 to 3265 cm⁻¹ upon addition of 10% w/w NO₂⁺PF₆⁻. Simultaneously, the O—H band broadens. The N=O stretching vibration at 2380 cm⁻¹, however, does not shift or broaden significantly under these conditions.

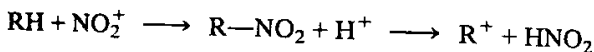
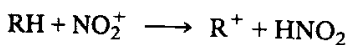
Nitronium salts as discussed react extremely readily with π-donor aromatic compounds as well as with alkenes and alkynes (*vide infra*). They also show high reactivity towards n-donors, such as alcohols, ethers, amines, amides, imides, carbodiimides, oximes, hydrazones, sulfides, sulf-oxides, halides, and phosphines. However, their reactivity towards σ-donors is understandably much lower.

Another reaction mode of the nitronium ion towards σ-donors also exists where NO₂⁺ acts as an oxidant, resulting in the formation of carbocations via hydride abstraction. Rate constants and efficiencies (*k_r*/*k_{collision}*) of the gas phase hydride transfer reactions from alkanes to NO₂⁺ have been measured [80].

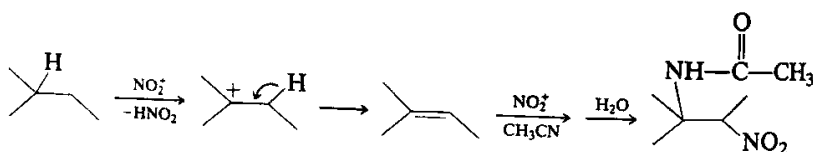


The efficiency of hydride transfer to NO_2^+ is very low. However, gas phase studies indicate disproportionately high efficiency for abstraction of a tertiary hydrogen. The efficiency of hydride abstraction by NO^+ is relatively higher.

It has been demonstrated in solution phase studies that carbenium ions might be formed directly from alkanes via formal hydride abstraction, instead of via nitration followed by protodenitration.

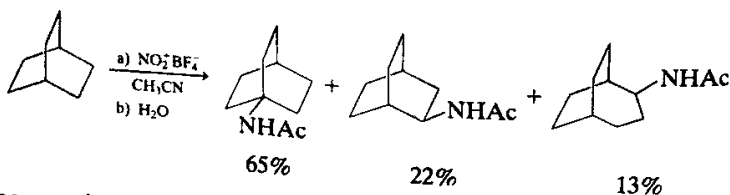


If the reaction is carried out in acetonitrile then the carbocation is converted into the corresponding amide by the Ritter reaction. 2-Methylbutane reacts with nitronium tetrafluoroborate in acetonitrile solution to provide the corresponding amide in moderate yield.



Similarly, bicyclo[2.2.2]octane yields a mixture of acetamides in high yield (75%) on reaction with $\text{NO}_2^+\text{BF}_4^-$ in acetonitrile.

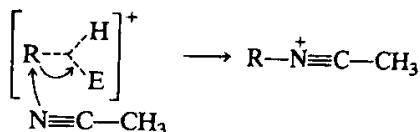
When the nitration of adamantane with $\text{NO}_2^+\text{BF}_4^-$ is carried out in acetonitrile upon aqueous workup *N*-(1-adamantyl)acetamide is obtained in 88% yield. Similarly, norbornane yields *N*-(*exo*-2-norbornyl)acetamide in 77% yield. Bicyclo[2.2.2]octane gives in 73% yield the corresponding amides.



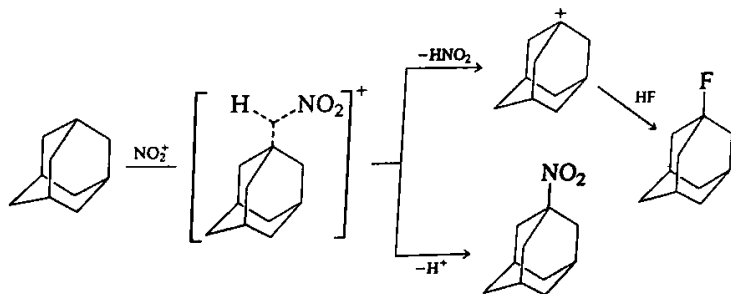
The reaction clearly proceeds via initial formation of bicyclooctyl carbocation, which undergoes subsequent rearrangement. It is striking that the ratio of isomers formed is approximately the same as in the similar isomerization of the carbocation obtained in the solvolysis of bicyclo[2.2.2]octyl-2-*p*-bromobenzenesulphonate, which is in support of the carbocationic mechanism [81,82].

From these studies, it is clear that the reaction medium plays a significant role in the nature of products formed in the reactions of alkanes

with nitronium ion. In nitromethane, methylene chloride-sulfolane, or fluorosulfuric acid, the pentacoordinate transition state leads via deprotonation to nitration. In the more strongly nucleophilic acetonitrile, the solvent reacts with the incipient carbocation.

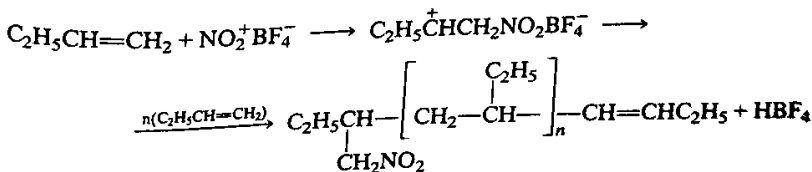


This dichotomy is quite evident in the reaction of cyclooctane with nitronium trifluoroacetate. The products obtained were cyclooctyl trifluoroacetate, cyclooctyl nitrate and nitrocyclooctane. Conversion of adamantane to 1-fluoroadamantane in 95% yield on reaction with nitronium tetrafluoroborate in pyridine polyhydrogen fluoride indicates that formation of adamantyl cation by formal hydride abstraction is a significant alternative to the nitration-protodenitration pathway.

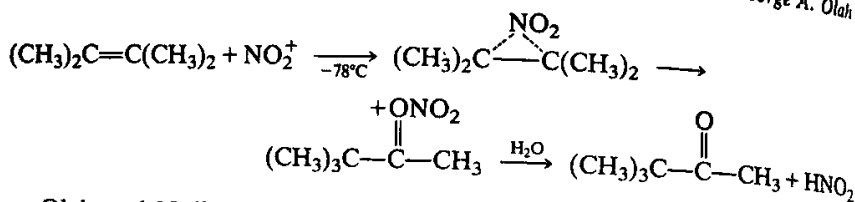


C. Alkenes

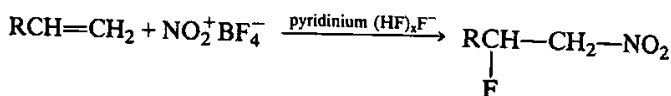
The reaction of nitronium salts with olefins depend on the nature of the alkene and the reaction conditions. When excess alkenes react with nitronium salts, the nitrocarbenium ion formed can initiate polymerization [83].



The nitrocarbenium ion can also be stabilized as a result of an intramolecular rearrangement to a nitrocarboxonium ion. The latter reacts with water to form the corresponding ketone [84].



Olah and Nojima have shown [85] that when alkenes are allowed to react with equimolar nitronium tetrafluoroborate in 70% hydrogen fluoride-pyridine, nitrofluorination takes place.

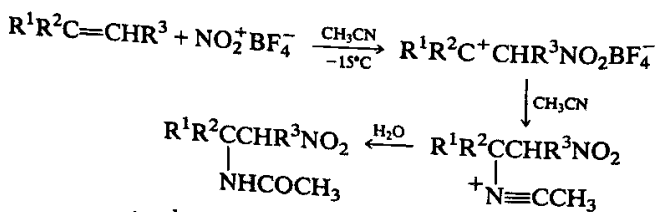


The nitrofluorinated adducts can be obtained in good yield (Table XXII). β -Nitrofluoroalkanes are useful intermediates in the synthesis of β -fluoroalkylamines and give nitroalkanes via dehydrofluorination with bases.

Chloro- and bromoalkenes give less stabilized nitrocarbenium ions and thus do not require HF for the formation of β -nitrofluoroalkanes. With these alkenes, BF_4^- seems to function as an efficient source of F^- .

Extensive studies of the $\text{NO}_2^+\text{BF}_4^-$ nitration of alkenes were reported in the Soviet literature and an excellent review has appeared [86].

If the nitration of olefins by nitronium salts is carried out in acetonitrile, the nitrocarbenium ion intermediates undergo Ritter reaction with the solvent to form nitroacetamides [87].



- $\text{R}^1 = \text{CH}_3$, $\text{R}^2 = \text{R}^3 = \text{H}$, yield 50%
- $\text{R}^1 = \text{R}^2 = \text{CH}_3$, $\text{R}^3 = \text{H}$, yield 23%
- $\text{R}^1 = \text{R}^3 = \text{CH}_3$, $\text{R}^2 = \text{H}$, yield 13%

The mode of the reaction between olefins and nitronium salts depends on the nature of the olefin and the reaction conditions. For example, cyclohexene reacts with $\text{NO}_2^+\text{BF}_4^-$ to form a nitrocarbocation, which leads to the formation of 3-nitrocyclohexene in 40% yield [88,69].

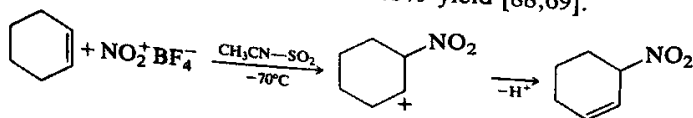
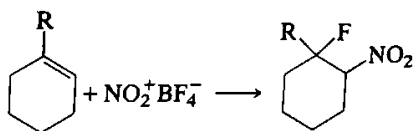


Table XXII. Nitrofluorination of Alkenes with Nitronium Tetrafluoroborate in Pyridinium Polyhydrogen Fluoride

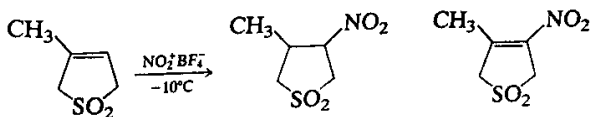
Alkene	Reaction Temperature (°C)	Reaction Time (hr)	Product	Yield (%)
Ethene	20	1	1-fluoro-2-nitroethane	60
Propene	20	1	2-fluoro-1-nitropropane	65
2-Butene	20	0.5	2-fluoro-3-nitrobutane	60
1-Hexene	0	1	2-fluoro-1-nitrohexane	65
Chloroethene	20	2	1-chloro-1-fluoro-2-nitroethane	40
1,1-Dichloroethene	20	2	1,1-dichloro-1-fluoro-2-nitroethane	45
Cyclohexene	0	1	1-fluoro-2-nitrocyclohexane	70
	20	0.3		80

The nitration of 1-substituted cyclohexenes is accompanied by the formation of 2-fluoro-1-nitro-2-*R*-cyclohexanes [90,91].

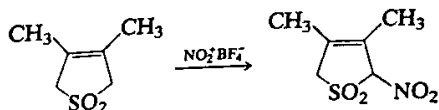


a) $R = \text{CH}_3$, yield 30%; b) $R = \text{Cl}$, yield 60%.

Alkenes with a reduced electron density, for example 3-methyl-2,5-dihydrothiophen 1,1-dioxide, react with $\text{NO}_2^+\text{BF}_4^-$ to give

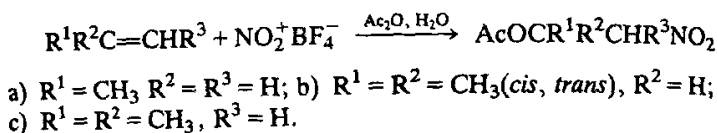


The reaction of 3,4-dimethyl-2,5-dihydrothiophen 1,1-dioxide, in which the double bond is blocked by the methyl groups, apparently proceeds via an electrophilic substitution mechanism [92].



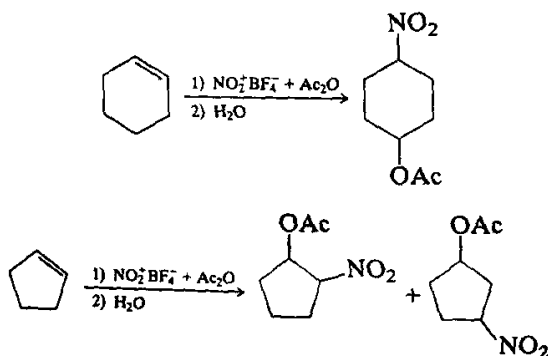
As mentioned, the reaction of nitronium salts with olefins proceeds via the formation of a nitrocarbocation and the decisive factor that determines the success of the reaction is the stabilization of nitrocarbocation and the ease of its conversion into the final product. One of the methods applied

involves nitration in acetic anhydride. It has been suggested that the complex $\text{NO}_2^+\text{BF}_4^- \cdot \text{Ac}_2\text{O}$ reacts and that 2-acetoxy-1-nitroalkane is obtained in 36–60% yield after hydrolysis of the reaction mixture [93]. The reaction involves mainly *cis*-addition:



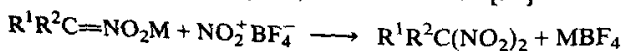
4-Acetoxy-4-methyl-2-pentanone is isolated together with the nitroacetate in the nitration of isobutene, which indicates the formation of an acylium cation in the reaction.

The nitration of cycloalkenes is as a rule accompanied by the formation of the β - and δ -nitroacetates in 18–29% yields [94].



The high degree of stabilization of the nitrocarbocation in the nitration of norbornene in acetic anhydride ensures a high (86%) yield of 2-acetoxy-7-nitrobicyclo[2.2.1]heptane.

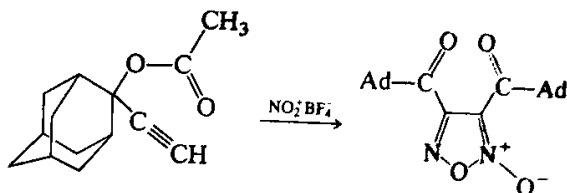
The interaction of nitronium salts with the heteropolar $\text{C}=\text{N}$ double bond in nitroalkane salts is of great interest. Olsen *et al.* showed that *gem*-dinitro compounds are formed in the nitration of 2-nitropropane and nitrocyclohexane salts with $\text{NO}_2^+\text{BF}_4^-$ in acetonitrile [95].



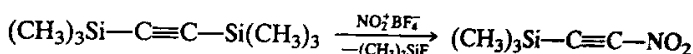
a) $\text{M} = \text{Li}$, b) $\text{M} = \text{Na}$, c) $\text{M} = \text{K}$

D. Alkynes

Britelli and Boswell [96] have shown that nitronium tetrafluoroborate reacts with 2-acetoxy-2-ethynyladamantane in an unusual reaction to yield a furoxan in 89% yield.

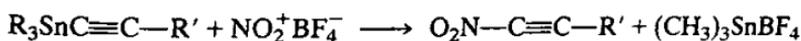


Schmitt *et al.* [97,98] obtained in high yield nitroacetylenes by the nitrodesilylation of trimethylsilylacetylenes.

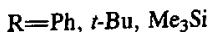
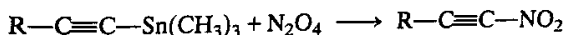


1,2-bis(trialkylsilyl) substituted unsymmetrical acetylenes showed high regioselectivity in the nitro-desilylation reaction. The regioselectivity was determined by the ease of attack of F^- at the less-hindered silyl substituent. Table XXIII summarizes the data.

Nesmeyanov *et al.* [99] and Jäger *et al.* [100] described the synthesis of nitroacetylenes by nitrodestannylation of alkynylstannanes.



Petrov *et al.* reported the nitrodestannylation of trimethylstannylacetylenes with N_2O_4 , albeit in low yield.



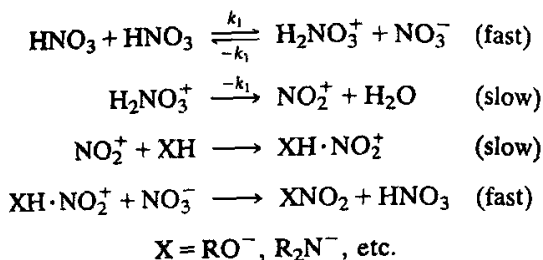
Nitrodestannylation with N_2O_5 also yields the corresponding nitroacetylenes in acceptable yield.

E. O-Nitration

Studying the acid-catalyzed nitration of alcohols Ingold extended his general scheme of aromatic electrophilic C-nitration to the nitration at oxygen (and nitrogen) centers [101].

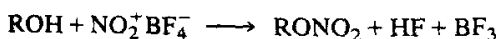
Table XXIII. Nitroacetylenes via Nitro-Detrimethylsilylation with Nitronium Tetrafluoroborate and Hexafluorophosphate

Starting Material	Product	Yield (%)
$(\text{CH}_3)_3\text{SiC}\equiv\text{CSiCH}_3$	$(\text{CH}_3)_3\text{SiC}\equiv\text{CNO}_2$	70
$(\text{CH}_3)_3\text{SiC}\equiv\text{CSi}(\text{CH}_3)_2-\text{CH}(\text{CH}_3)_2$	$(\text{CH}_3)-\text{CH}(\text{CH}_3)_2\text{SiC}\equiv\text{CNO}_2$	34
	$(\text{CH}_3)_3\text{SiC}\equiv\text{CNO}_2$	6
$(\text{CH}_3)_3\text{SiC}\equiv\text{CSi}(\text{CH}_3)_2-\text{C}(\text{CH}_3)_3$	$(\text{CH}_3)_3-\text{C}-(\text{CH}_3)_2\text{SiC}\equiv\text{CNO}_2$	59
	$(\text{CH}_3)_3\text{SiC}\equiv\text{CNO}_2$	29
$(\text{CH}_3)_3\text{SiC}\equiv\text{CSi}[\text{CH}(\text{CH}_3)_2]_3$	$[\text{CH}(\text{CH}_3)_2]_3\text{SiC}\equiv\text{CNO}_2$	57



While studying the O-nitration of alcohols, glycols, and glycerin with excess nitric acid in nitromethane solution, Ingold *et al.* [102] found the reactions to be of zeroth order and identical in absolute rate with one another. For the nitration of methyl alcohol, low concentration of sulfuric acid increased, whereas nitrate ion decreased the rates. When sufficient water was added, the kinetics changed to first order. Clearly the formation of the nitronium ion is rate limiting in nitration in the absence of significant amounts of water. O⁻ (and also studied N⁻) nitrations thus show close similarity to electrophilic aromatic C-nitrations with nitronium ion.

Indeed a significant improvement in the preparation of alkyl nitrates was achieved by Olah *et al.* [103] who applied stable nitronium salts, such as NO₂⁺BF₄⁻ in their preparation.

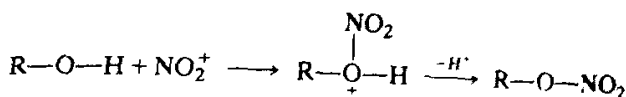


The reaction gives high (frequently nearly quantitative) yields of primary and secondary alkyl nitrates (Table XXIV).

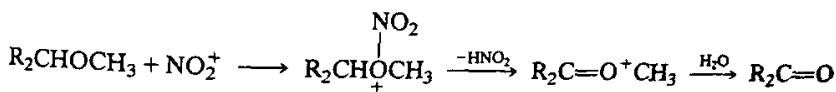
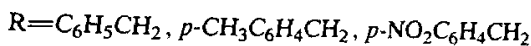
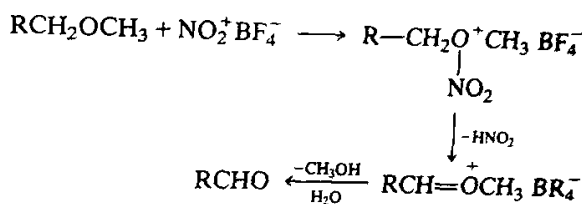
In the conversion of alcohols to alkyl nitrates with nitronium salts, the reaction proceeds via the formation of an *N*-nitrooxonium ion followed by proton loss.

Table XXIV. Preparation of Alkyl Nitrates from Alcohols and NO₂⁺BF₄⁻

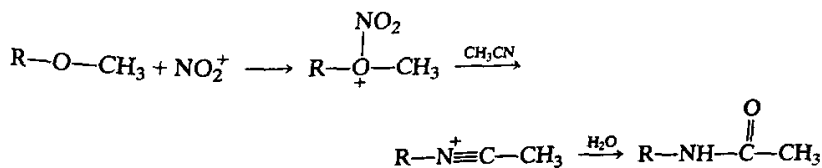
R	% Yield (Isolated)
CH ₃	87
C ₂ H ₅	92
<i>n</i> -C ₃ H ₇	87
<i>n</i> -C ₄ H ₉	94
<i>n</i> -C ₉ H ₁₇	86
C ₂ H ₄ F	88
C ₂ H ₄ Cl	85
C ₂ H ₄ Br	72
CF ₃ CH ₂	72



Nitronium salts also react with the oxygen of the ether linkage. The nitroxonium ion formed in the reaction is readily converted in high yield into the corresponding aldehyde or ketone [104].



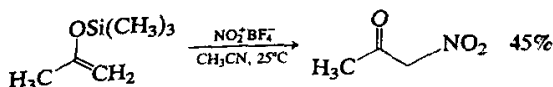
In the presence of other nucleophiles, the nature of the product changes significantly. Thus, methyl ethers of adamantan-1-ol, *t*-butanol, and *exo*-norboran-2-ol react with nitronium tetrafluoroborate in acetonitrile solution to yield the products of a formal Ritter reaction.

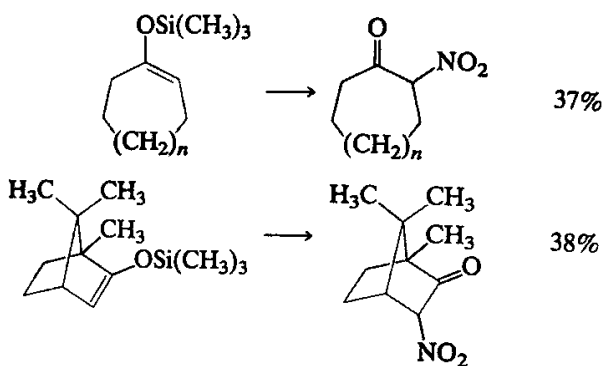


Ethers of secondary alcohols, in general, show poor regioselectivity in the second step, thus yielding mixtures of amides as well as products of oxidation via HNO_2 cleavage (*vide infra*). In an analogous reaction treatment of 1-methoxyadamantane with a 1:1 mixture of acetyl nitrate and HBF_4 resulted in its conversion to 1-acetoxyadamantane in high yield.

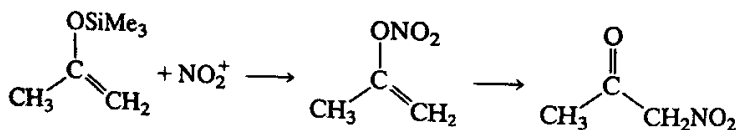
Desilylative nitration of vinyloxysilanes with $\text{NO}_2^+\text{BF}_4^-$ was also studied.

Enol silyl ethers undergo facile nitrodesilylation to yield the corresponding α -nitroketones in moderate yield [105].





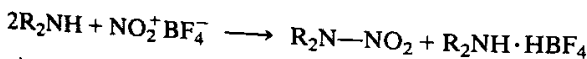
The reaction probably proceeds via O-nitration, a mechanism similar to the reaction with alkoxy-silanes followed by isomerization of the vinyl nitrate.



F. N-Nitration

The first report of the nitration of amines by nitronium salts was by Olah and Kuhn [106].

Primary and secondary amines are nitrated by $\text{NO}_2^+\text{BF}_4^-$ in sulfolane or SO_2 solution to yield nitramines.



The nitration of amines with nitronium tetrafluoroborate to nitramines was studied subsequently by Olsen, Fisch, and Hamel [107].

Satisfactory yields of nitramines were obtained by reacting two equivalents of secondary aliphatic amines with $\text{NO}_2^+\text{BF}_4^-$ in methylene chloride solution (Table XXV).

Table XXV. Nitration of Amines and Their Derivatives with Nitronium Tetrafluoroborate

Compound	Yield of <i>N</i> -Nitro Derivative (%)
Di- <i>n</i> -butylamine	54
Morpholine	72
β,β -bis(cyanoethyl)amine	62
Picramide	85

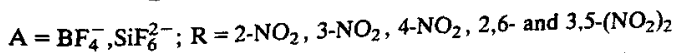
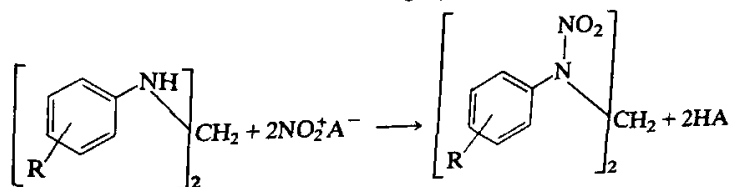
Reaction of a primary aliphatic amine, *n*-butylamine. **however, gave** only a 20% yield of *n*-butyl nitramine. In contrast, picramide gave *N*-2,4,6-tetranitroaniline in 85% yield.

Extensive studies of *N*-nitration were carried out by Soviet investigators and the topic reviewed [86].

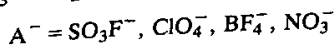
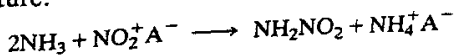
It was shown [108] that the nitration of aromatic amines proceeds differently depending on their basicity. Amines of moderate to low basicity, such as bis(2-cyanoethyl)amine ($pK_a = 5.25$), bis(2,2,2-trinitroethyl)amine ($pK_a = 0.05$) are nitrated by $\text{NO}_2^+\text{BF}_4^-$ to the corresponding *N*-nitramines in acetonitrile or ethyl acetate in yields of 87–98%. The nitration of highly basic dialkylamines ($pK_a = 8.70$ – 11.15) is accompanied by the partial reduction of $\text{NO}_2^+\text{BF}_4^-$ to nitrosonium tetrafluoroborate and the formation of nitrosamines. The content of nitrosamine in the reaction mixture increases with increase of the reaction temperature. Nitronium hexafluorosilicate proved to be a milder nitrating agent; its application makes it possible to reduce greatly the formation of nitroso-derivatives.

The nitration of aliphatic–aromatic amines also proceeds smoothly and the low acidity of the medium makes it possible virtually to avoid the *N*-nitro \rightarrow *C*-nitro rearrangements [108].

Aromatic methylene-bis-amines, which are unstable in an acid medium, were nitrated for the first time with nitronium salts and *N,N'*-diarylmethylenedinitramines were obtained in a high yield [109].



The reaction of nitronium salts and nitrogen pentoxide with ammonia have been investigated [110–113] and nitramine is formed at liquid nitrogen temperature:



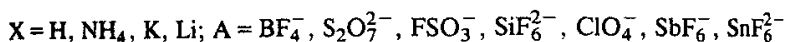
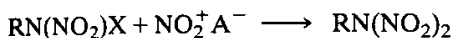
The formation of nitramine is dependent on the nature of the anion; on passing from nitronium chlorosulfate to tetrafluoroborate, the yield increases from 8 to 43%.

Nitronium salts proved to be particularly useful in the synthesis of *N,N*-dinitramines which previously had been difficult to obtain. It was shown [114] that the interaction of primary nitramines (or their salts) with

Table XXVI. N-Nitration of Amides with Nitronium Tetrafluoroborate

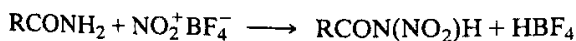
Compound	Yield of N-Nitro Derivative, %	Compound	Yield of N-Nitro Compound, %
Acetamide	13	ethyl <i>n</i> -butylcarbamate	91
2-Chloroacetamide	55	<i>n</i> -butylacetamide	40
2,2,2-Trichloroacetamide	62	succinimide	43
Benzamide	53		

nitronium tetrafluoroborate, (pyrosulphate, fluorosulfate, fluorosilicate, as well as other nitronium salts) leads to the formation of the *N,N*-dinitramines.



Best results are obtained in nitration by nitramine salts in chloroalkanes or acetonitrile. However, the use of more basic solvents, such as ethers and esters, ensures equally high yields in the nitration of both free nitramines and their salts [115].

Amides(acylamines) and urethanes as shown by Olsen [107] gave with one equivalent of $\text{NO}_2^+ \text{BF}_4^-$ in acetonitrile at -30°C the corresponding N-nitro derivatives (Table XXVI).

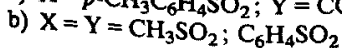
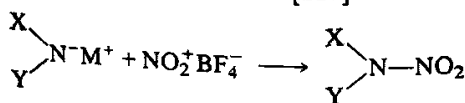


The nitramides of benzoic and chloroacetic acids were obtained in satisfactory yields by the method, but the yield of nitroacetamide was only 12%. This can be explained by the fact that the aliphatic nitramides are readily hydrolyzed even in the presence of potassium acetate.

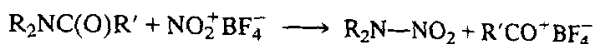
The use of more basic solvents such as ethyl acetate, 1,4-dioxane, or trimethyl phosphate made it possible to obtain various other nitramides of different structure in 40–90% yield [116]. Succinimide is nitrated by $\text{NO}_2^+ \text{BF}_4^-$ in ethyl acetate in 43% yield [107].

It is interesting to note that *N*-methylsuccinimide does not react with nitronium salts and *N*-methylphthalimide undergoes nitration in the aromatic ring exclusively.

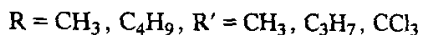
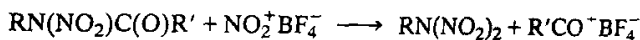
The most convenient synthesis of sulfonic acid nitro-imides consists of the reaction of $\text{NO}_2^+ \text{BF}_4^-$ with imide salts [117].



As discussed, one of the known methods of synthesis of dialkylnitramines involves the reaction of dialkylamides with nitric acid, which leads to the substitution of the acyl group by the nitro group (nitrolysis). However, when nitric acid or its mixtures with acetic anhydride are used, the yield of nitramines is as a rule low and only the use of the $\text{HNO}_3-(\text{F}_3\text{CCO})_2\text{O}$ mixture makes it possible to raise the yield to 90% [118]. For preparative purposes, it is more convenient to nitrate the dialkylamides by nitronium salts [119]. The reaction takes place at 20°C in acetonitrile solution. The dialkylnitramines are formed in yields up to 90% and the acyl group is converted into acylium tetrafluoroborate.

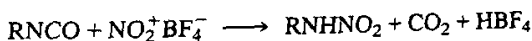


Alkyl-*N,N*-dinitramines were formed in high yields from *N*-alkyl-nitramides [120].

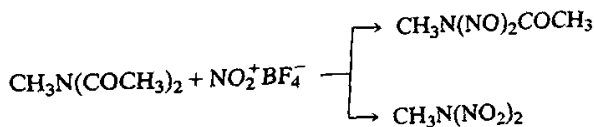


The reaction of $\text{NO}_2^+\text{BF}_4^-$ with *N*-alkylamides has been investigated [107,111] under different conditions, but nevertheless the results permit the conclusion that at a low temperature (-30°C), *N*-butylacetamide and ethyl *n*-butylcarbamate in acetonitrile are nitrated to the *N*-nitro derivatives [107] while at higher temperatures, (up to $+10^\circ\text{C}$) nitrolysis takes place with formation of the corresponding carboxylic acid and alcohol as well as N_2O [121]. The question as to which C—N bond is *N*-nitrated and cleaved in the reactions of *N*-alkylamides with $\text{NO}_2^+\text{BF}_4^-$ requires additional study.

Aliphatic isocyanates react with $\text{NO}_2^+\text{BF}_4^-$ in ethyl acetate or acetonitrile with formation (after hydrolysis) of alkylnitramides [122].

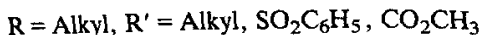
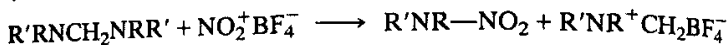


The study of the nitration of a series of *N,N*-diacylmethylamines showed that the acyl group is substituted by the nitro group and, depending on the conditions and the component ratio, methylnitroacetamide or methyl-*N,N*-dinitramine is formed [123].

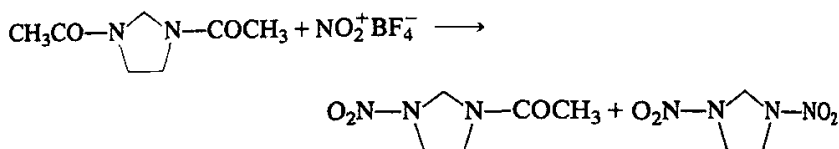


The methanesulfonyl group can also be substituted by the nitro group. The tosyl or an alkoxy-carbonyl group do not enter into this kind of reaction.

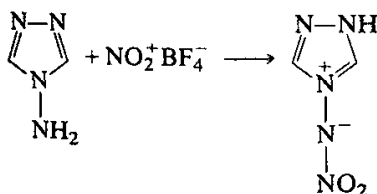
The mode of reaction of $\text{NO}_2^+\text{BF}_4^-$ with substituted methylenediamines depends on the nature of the substituents [123,124]. Alkanesulfonyl, arenesulfonyl, or methoxycarbonyl derivatives undergo nitrolysis at the C—N bond with formation of substituted nitroamines. This reaction pathway is favored by the formation of the carbonium-immonium ion stabilized by the amino nitrogen.



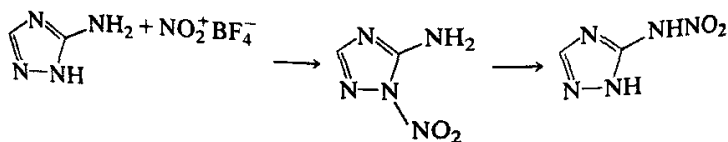
N,N-Diacetylimidazolidine undergoes nitration by nitronium salts to *N*-acetyl-*N'*-nitro- or *N,N'*-dinitro derivatives.



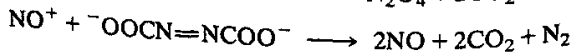
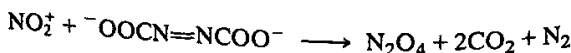
Nitronium salts are convenient nitrating agents for the synthesis of *N*-nitrimines. 4-Amino-1,2,4-triazole reacts with $\text{NO}_2^+\text{BF}_4^-$ in acetonitrile to form 4-nitrimino-1,2,4-triazole in 65% yield [125].



1-Aminobenzimidazole is nitrated analogously and 1,1'-azobenzimidazole is formed as a side product. 3-Amino-1,2,4-triazole reacts with $\text{NO}_2^+\text{BF}_4^-$ in acetonitrile to form *N*-nitrotriazole, which rearranges to the nitroamino-triazole.

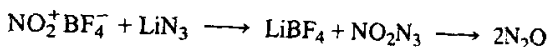


Both nitronium and nitrosonium salts readily react with azodicarboxylate anions in accordance with



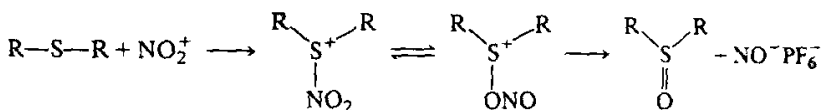
The reaction of alkyl azodicarboxylates depends on the reactivity of the electrophilic species. $\text{NO}_2^+ \text{BF}_4^-$, for example, reacts with ethyl azodicarboxylate, while the weaker electrophile, nitrosonium tetrafluoroborate, does not react.

The reaction of $\text{NO}_2^+ \text{BF}_4^-$ with lithium azide in acetonitrile results in the formation of covalent nitronium azide, which is converted into nitrous oxide above -10°C [126].



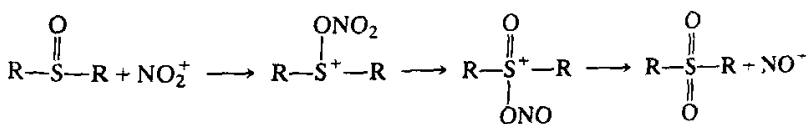
G. S-Nitration

Sulfides react with nitronium hexafluorophosphate at -78°C to form S-nitro sulfonium ions, which isomerize to S-nitrito sulfonium ion on warming to -20°C and subsequently give the corresponding sulfoxides [127a].

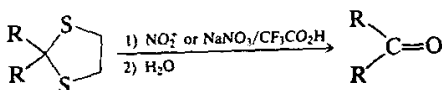


This reaction demonstrates the ambident reactivity of the nitronium ion, in analogy with the ambident reactivity of NO_2 and NO_2^- . The nitro-sulfonium ion intermediate can be observed by ^1H -, ^{13}C -, and ^{15}N -NMR spectroscopy.

In a similar fashion, sulfoxides were oxidized to sulfones [127b].

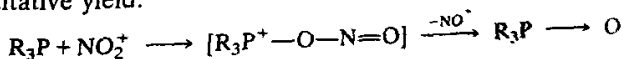


S-nitro or S-nitrito sulfonium ions are similar intermediates in the oxidative cleavage of ethylenethioacetals with nitronium tetrafluoroborate or sodium nitrate-trifluoroacetic acid [127c].



H. Attempted Nitration at Phosphorous

Reaction of nitronium salts with phosphines yields phosphine oxides [127c] in quantitative yield.



Examination of the intermediates by ^{13}C -, ^{31}P -, and ^{15}N -NMR spectroscopy showed the presence of only the P-nitrito phosphonium ion and no P-nitro phosphonium ion $\text{R}_3\text{P}^+-\text{NO}_2$ was observed even at very low temperature.

V. Transfer Nitration

According to Ingold, the reactivity of a nitrating agent NO_2-X is highly dependent upon the electron affinity of X. It is therefore possible to alter the reactivity of the nitronium ion by using different agents of varying electron affinity. If a prepared nitro (or nitrito) onium ion is used as the nitrating agent, transfer of the nitro group to the substrate occurs. These reactions are called transfer nitrations utilizing nitro and nitro onium salts generally derived from suitable O-, S-, or N- containing heteroorganic compounds.

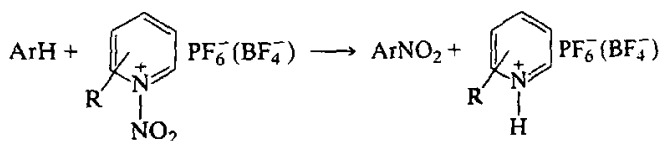
The term *transfer nitration* is thus defined as a nitration carried out by reacting the incipient nitronium ion bound to a suitable carrier (delivery system), in order to modify the reactivity and reaction conditions of nitrations. The term is, however, arbitrary. There is frequently only a fine dividing line between solvated nitronium ions and nitro-onium ions, although in other cases the transfer nitrating agents are stable and well defined.

The regioselectivity of nitration of toluene with nitronium salts has been successfully altered by their prior complexation with crown ethers. Complexation of $\text{NO}_2^+\text{BF}_4^-$ by 18-C-6 crown ether substantially altered the selectivity in nitration of toluene and benzene as reported by Elsenbaumer and Wasserman [128]. Similar effect was observed with polyethylene oxides. Savoie *et al.* reported isolation of the 18-C-6- $\text{NO}_2^+\text{BF}_4^-$ complex and its characterization [129]. Masci carried out the yet most detailed study on the effect of crown ethers on the selectivity of electrophilic aromatic nitration [130].

Equimolar amounts of $\text{NO}_2^+\text{BF}_4^-$ and 21-crown-7 or 18-crown-6 ethers yielded homogeneous solutions in nitromethane and dichloromethane. Using these systems in nitrating benzene and toluene, both substrate and positional selectivities were altered and were dependent upon the nature of the crown ether and (crown ether- $\text{NO}_2^+\text{BF}_4^-$) ratio. The linear nitronium ion obviously forms a complex with the crown ether. However, a guest-host complex with the linear nitronium ion inside the cavity would hardly allow the aromatic access. Therefore, it is more probable that the crown ether complexes the nitronium ion on the outside. The *ortho/para* ratio in nitration of toluene can be varied from 1.5 to 0.3 on changing the (21-crown-6)-($\text{NO}_2^+\text{BF}_4^-$) ratio from 1 to 6. The isomer distribution of the

nitration of toluene with $\text{NO}_2^+\text{BF}_4^-$ in CH_2Cl_2 with 18-C-6 was 53% *ortho*, 4% *meta* and, 43% *para* (*ortho/para* ratio 1.2) and with 21-C-7, 19% *ortho*, 3% *meta*, 78% *para* (*ortho/para* ratio 0.25) showing the much better complexing ability of the latter giving very high preference for *para* nitration. As crown-ether complexation affects the nitronium cation, the high preference for *para*-nitration reflects not only a bulkier reagent but also a much more selective nitration with a weaker electrophile.

Olah *et al.* in 1965 reported the preparation of *N*-nitropyridinium tetrafluoroborate from pyridine and nitronium tetrafluoroborate [71]. The salt showed only limited reactivity in carrying out transfer C-nitration of aromatic hydrocarbons, probably because of the insolubility of *N*-nitropyridinium tetrafluoroborate in the reaction medium. Transfer nitration of *n*-donor heteroorganic substrates (alcohols, etc.) was, however, readily accomplished. Cupas and Pearson subsequently extended the scope of transfer C-nitration by preparation and use of a variety of *N*-nitropyridinium and quinolinium salts [72]. Comprehensive studies by Olah *et al.* [73] allowed the design of reagents of varying reactivity by appropriate choice of the heterocyclic base and also the counter ions (PF_6^- vs. BF_4^-). Nitration with these reagents occurs under basically neutral conditions because the proton eliminated in the aromatic nitration reaction is bound by the heterocyclic base.



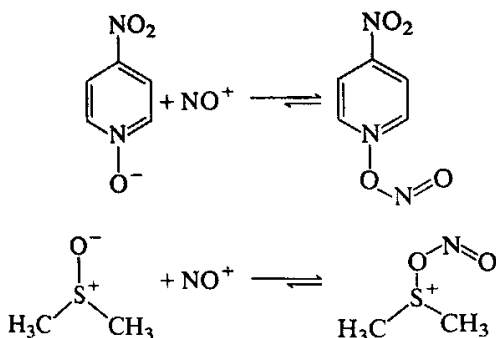
The *N*-nitropyridinium and *N*-nitroquinolinium salts are stable (but moisture sensitive) crystalline reagents, well characterized by spectroscopic methods (NMR, IR, Raman). They are prepared in essentially quantitative yield by the slow addition of the corresponding pyridine to an equivalent amount of the nitronium salt in acetonitrile, nitromethane, or sulfolane solution. It is important to add the pyridine to the solution of the nitronium ion, because excess pyridine present during the reaction can lead to opening of the pyridinium ring. The *N*-nitropyridinium salts can be used as isolated compounds or they can be generated *in situ*.

N-Nitropyridinium hexafluorophosphate does not react with benzene and toluene at room temperature, whereas *N*-nitro-2-picolinium tetrafluoroborate reacts well under similar reaction conditions. This ease of nitration is due to the methyl group causing steric hinderance to resonance with concomitant weakening of the N—N bond. It seems that nonbonded interaction with one α -methyl group is sufficient to completely impede the resonance interaction, since *N*-nitro-2,6-lutidinium salt did not further change the selectivity of the reagent. The steric hinderance to resonance

can also be achieved by utilizing the peri interaction in *N*-nitroquinolinium salts.

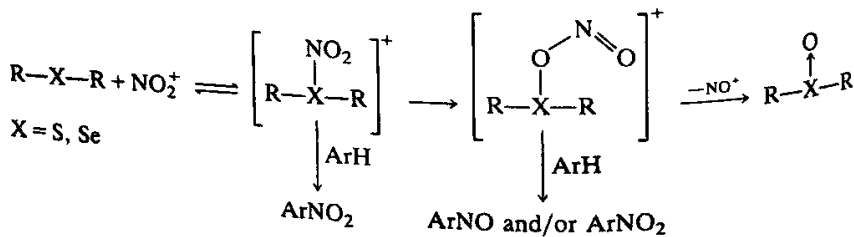
There is generally no significant change of positional selectivity in nitration of aromatics with *N*-nitropyridinium ion. In the case of toluene, the isomer distribution is 62–64% *ortho*-; 2–4% *meta*-; 33–36% *para*-nitrotoluene.

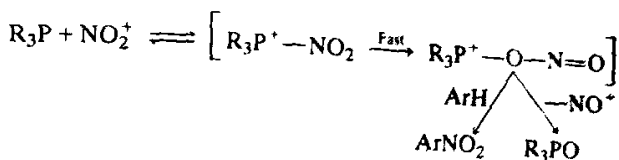
N-Nitrito-4-nitropyridinium salts are isomeric with the previously discussed *N*-nitropyridinium ions. Similarly, dimethylnitritosulfonium salts are isomeric with *N*-nitrosulfonium ions, formed from nitronium salts and dimethyl sulfide. The nitro-onium salts are prepared from nitrosonium hexafluorophosphate with 4-nitropyridine-*N*-oxide and dimethyl sulfoxide, respectively [131].



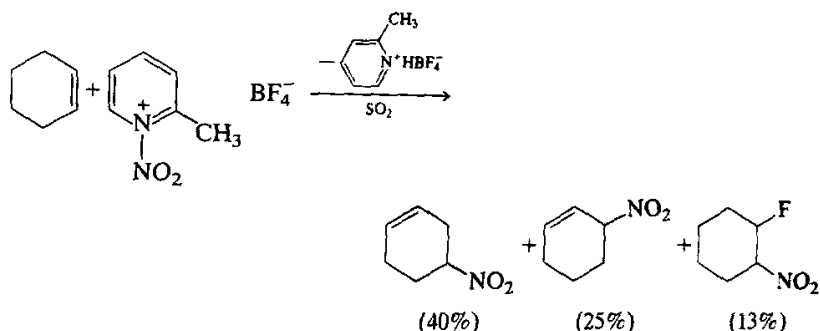
The nitrito-onium salts act as nitrating agents for aromatics that do not undergo nitrosation. Their nitrating ability is, however, considerably less compared to that of the corresponding nitro-onium salts (e.g., toluene is nitrated only at $\geq 60^\circ\text{C}$ whereas the nitro-onium salts nitrate at $\leq 25^\circ\text{C}$).

S-Nitrosulfonium salts isomerize to *S*-nitritosulfonium salts at -20°C . As a consequence dialkylsulfides are readily oxidized to their sulfoxide with nitronium salts. When triarylphosphines are reacted with nitronium salts, only the nitritophosphonium ions are observed spectroscopically (by NMR). They subsequently give the corresponding phosphine oxides and nitrosonium ion. These observations can also be rationalized as a consequence of the ambident reactivity of the nitronium ion reacting not on nitrogen, but on oxygen, and thus acting as an oxidizing agent.

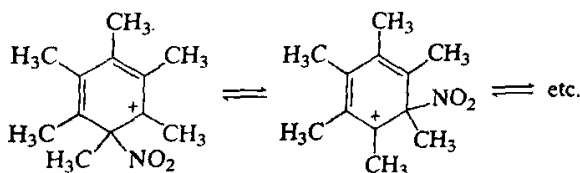




The nitration of olefins, particularly those containing electron-donating substituents, by nitronium salts is complicated by side reactions and does not always lead to the expected result. In many instances nitration with nitronium tetrafluoroborate takes place with higher yields in the presence of α -picoline [91,132]. In this case the nitrating agent is apparently not the nitronium salt but 2-methyl-*N*-nitropyridinium tetrafluoroborate, which is formed rapidly when $NO_2^+BF_4^-$ is mixed with α -picoline [73b].

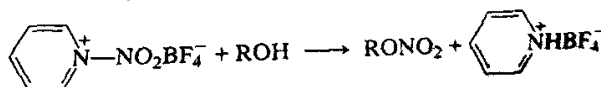


The nitrohexamethylbenzenium ion, prepared from hexamethylbenzene and nitronium salts, was studied by low-temperature NMR spectroscopy [133] showing intramolecular nitro group migration.



Olah *et al.* found that the ion is capable of transfer nitrating benzene and mesitylene [134]. The transfer nitrating ability of the nitrohexamethylbenzenium ion is interesting as addition of hexamethylbenzene as a complexing agent to nitronium salt nitrations of aromatics can affect regioselectivity.

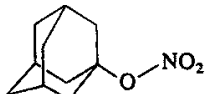
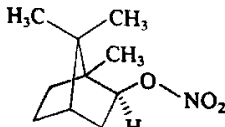
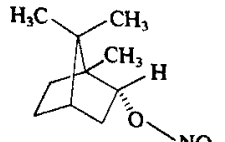
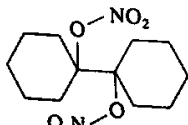
Transfer O-nitration of alcohols with *N*-nitropyridinium tetrafluoroborate was achieved by Olah *et al.* under acid-free conditions [71].

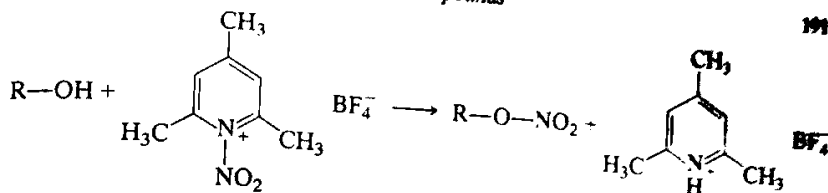


The method was further improved using *N*-nitrocollidinium tetrafluoroborate as transfer nitrating agent for alcohols (polyols) [73].

Alcohols undergo transfer nitration with *N*-nitrocollidinium tetrafluoroborate under essentially neutral conditions. Yields were found to be close to quantitative. Separation of alkyl nitrates by distillation or crystallization gave good-to-excellent preparative yields (Table XXVII).

Table XXVII. Nitrate Esters from Alcohols with *N*-Nitrocollidinium Tetrafluoroborate

Nitrate Ester	Yield (%)
$C_2H_5-O-NO_2$	100
 - CH_2-O-NO_2	78
$n-C_6H_9-O-NO_2$	51
$H_3C-CH_2OCH(CH_3)-O-NO_2$	38
	82
	48
	63
	41
$O_2N-O-(CH_2)_2-O-NO_2$	100
$O_2N-O-(CH_2)_4-O-NO_2$	100
$(O_2N-O-CH_2)_2-CH(ONO_2)$	100



No oxidation of alcohols is observed under the reaction conditions. The *N*-nitrocollidinium salt is generally less reactive than nitronium tetrafluoroborate itself, but gives better control of conditions and superior yields as shown, for example, in the preparation of 1-adamantyl nitrate. Adamantanol gives less than 2% yield of nitrate ester upon treatment with nitronium tetrafluoroborate while the *N*-nitro salt forms the ester in 82% yield.

The nitrate esters are formed with retention of configuration in contrast to the reaction of silver nitrate with alkyl halides. Furthermore, the reaction of benzyl alcohol shows that *O*-nitration of alkylaryl alcohols in transfer nitration is preferred to aromatic *C*-nitration.

1,2-Diols give dinitrates under the reaction conditions. No pinacolone rearrangement was observed. Glycerol gives trinitroglycerin in quantitative yield.

VI. Demetallative Nitration

When toluene is nitrated with conventional electrophilic nitrating agents, the product distribution usually shows 60–65% *ortho*-3–4% *meta*, and 27–30% *para*-nitrotoluene. Only in nitrosative nitrations, in crown ether complexed or transfer nitrations, as well as in heterogeneous solid-acid-catalyzed nitrations is there a significant change in isomer distribution reflecting increased steric hindrance to *ortho* substitution and late arenium-ion-like transition states of highest energy.

One of the most successful approaches for altering the regioselectivity of aromatic nitration involves nitration via metallation [135]. This was discovered as a catalytic nitration which at the same time also provides unusual isomer distribution. The most important metallative nitration reactions involve metallation with mercury, palladium, and thallium salts.

The first report of catalytic nitration via mercuration was a patent issued to Wolfenstein and Boeters [136] at the beginning of the century. They reported a procedure for the synthesis of dinitrophenol and picric acid via oxynitration of benzene with mercuric nitrate and 50–55% nitric acid. The mechanism of oxynitration was delineated by Westheimer *et al.* [137].

Davis *et al.* [138], Tsutsumi *et al.* [139], and Yoshida *et al.* [140] discovered that the *ortho*-*para* ratio of nitrotoluenes can be significantly altered

via mercurative nitration generally increasing *para*-substitution. The *ortho-para* ratio could be changed from 2:1 to 1:2 via mercuration nitration. Stock *et al.* later confirmed and extended these experimental findings [141]. The reaction can be catalyzed by mercuric oxide, mercuric acetate, and mercuric nitrate, and to a lesser extent by mercuric sulfate. The effect of reaction conditions on isomer distribution was examined. The *ortho-para* ratio decreases as the reaction progresses. It was established that nitroluenes are formed via initial nitrosodemercuration followed by oxidation of nitrosotoluenes.

Because of the advantages of using solid superacidic catalysts in electrophilic aromatic nitration and in acid-catalyzed reactions in general, Olah *et al.* have examined the mercury (II)-promoted azeotropic nitration of aromatics using Nafion-H[®] solid superacidic catalyst [142]. Azeotropic removal of water accelerates the rate of reaction by mitigating the dilution of nitric acid in a static reaction system. The yield of nitroaromatics varies from 48–77% (Table XXVIII).

As the water formed is removed azeotropically, the mercury impregnated Nafion-H[®] catalyst can be recovered by filtration without any loss of activity and can be recycled. Comparison of data with nitration in the absence of mercury catalyst shows that formation of less hindered isomeric nitroarenes are favored. It is interesting to note that attempted azeotropic nitration of ethylbenzene with nitric acid/Nafion-H[®] yielded only acetophenone via side-chain oxidation, whereas in the presence of mercury salt under similar reaction conditions, nitroethylbenzenes were obtained in good yield with only 13% of product of side chain oxidation.

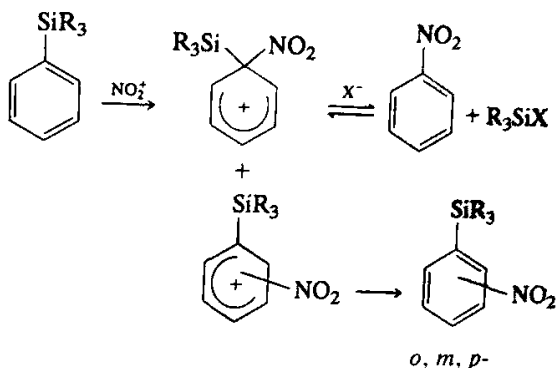
Desilylative nitration of arylsilanes proceeds through *ipso* nitroarenium ion intermediates. In the reactions the major products are, however,

Table XXVIII. Hg²⁺-Promoted Nitration of Aromatics over Nafion-H[®] Catalyst

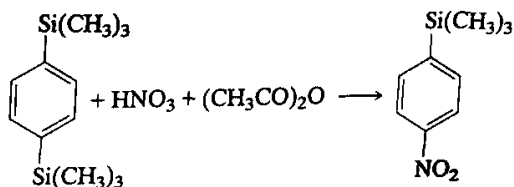
Substrate	Yield (%)	Isomer (Distribution, %)
Benzene	71	
Toluene	67	2-nitro (33), 3-nitro (7), 4-nitro (60)
Ethylbenzene	66	2-nitro (38), 3-nitro (5), 4-nitro (44), acetophenone (13)
<i>tert</i> -Butylbenzene	72	2-nitro (11), 3-nitro (17), 4-nitro (72)
<i>o</i> -Xylene	56	3-nitro (33), 4-nitro (67)
<i>m</i> -Xylene	48	2-nitro (11), 4-nitro (89)
Chlorobenzene	59	2-nitro (37), 3-nitro (2), 4-nitro (61)
Bromobenzene	76	2-nitro (44), 4-nitro (56)
Naphthalene	77	1-nitro (97), 2-nitro (3)

7. Methods for Preparing Energetic Nitrocompounds

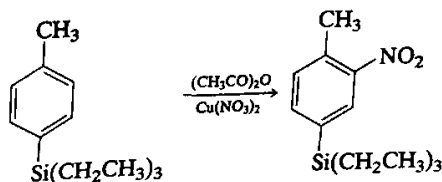
nitrated arylsilanes formed by intact nitration at the *ortho*, *meta*, and *para* positions.



Nitrodesilylation is usually faster than nitrodeprotonation because the nitrosilylbenzenium ion is stabilized by the silyl substituent. Deans and Eaborn showed that 1,4-bis(trimethylsilyl) benzene undergoes nitrodesilylation on nitration with acetyl nitrate [143]. Acetyl nitrate is the reagent of choice, because nitration with a nitric acid/sulfuric acid system will lead primarily to protodesilylation.



Nitrodeprotonation is, however, favored in the nitration of 4-tolyltriethylsilane.

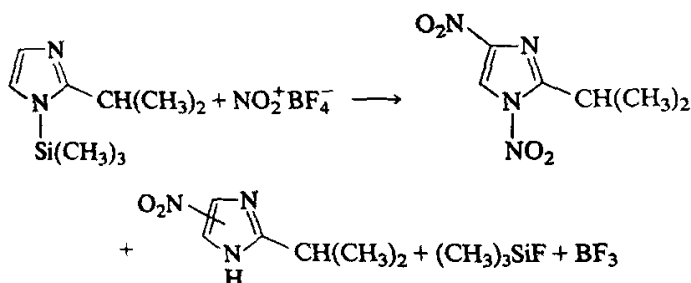


This is perhaps due to the bulkier nature of the triethylsilyl substituent, resulting in steric hinderance to *ipso* attack [144].

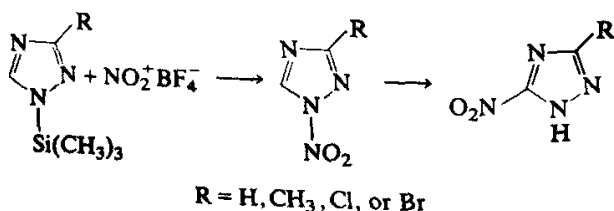
Benkeser [145], Speier [146], and Eaborn [147] have shown that intact ring nitration generally predominates and protodesilylation plays a significant role under the reaction conditions.

Olah and Narang [148] found that reaction of nitronium tetrafluoroborate with phenyltrimethylsilane gives only limited (10%) nitrodesilylation besides intact (predominantly *para*) ring nitration.

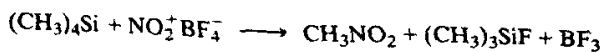
Acid-sensitive systems represent a particularly useful application for desilylative nitration with nitronium salts. Mononitration of imidazoles and triazoles is difficult because acid formed in the reactions even with $\text{NO}_2^+\text{BF}_4^-$ tends to catalyze denitration. However, the nitration of trimethylsilyl derivatives with $\text{NO}_2^+\text{BF}_4^-$ overcomes this difficulty. It has been shown for 2-isopropyl-1-trimethyl-silylimidazole that it is possible to obtain its nitro compounds which could not be obtained previously (e.g., 2-isopropyl-1,4-dinitroimidazole) [149]. Desilylative N-nitration is involved in the reaction.



Similar nitration of *N*-trimethylsilyl-1,2,4-triazoles makes it possible to obtain *N*-nitrotriazoles, which can be converted to the C-nitro derivatives in high yield [150].

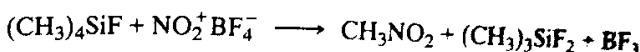


Nitrodesilylation with nitronium tetrafluoroborate is also a mild and efficient way to prepare aliphatic nitrocompounds from readily available alkylsilanes. Olah and Rochin have studied [151] the scope of the reaction. Tetramethylsilane reacts readily with $\text{NO}_2^+\text{BF}_4^-$ in sulfolane solution to give nitromethane in 80% yield.

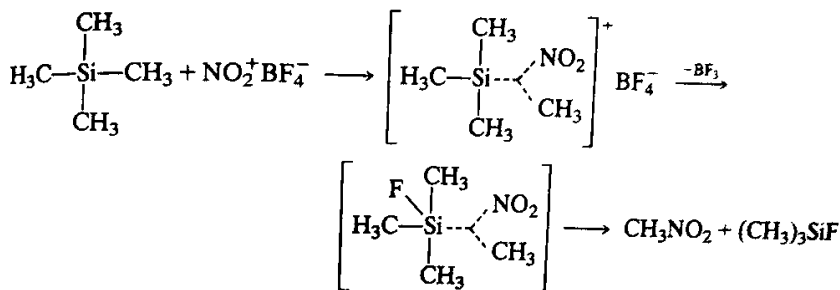


At higher temperature and excess $\text{NO}_2^+\text{BF}_4^-$, two equivalents of nitromethane can be obtained.

7. Methods for Preparing Energetic Nitrocompounds

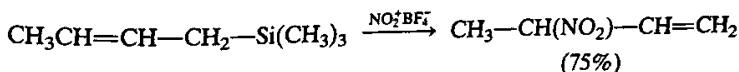
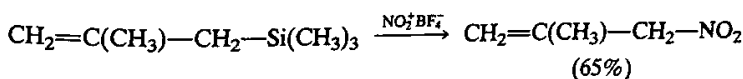
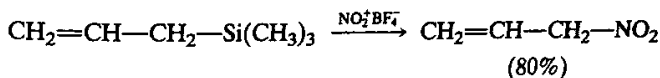


Nitrodesilylation probably proceeds via the pentacoordinate two-electron three-center bonded siliconium ion.

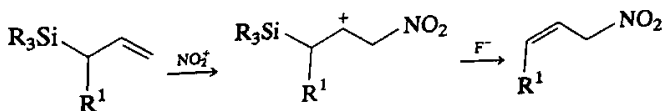


Ethylsilanes react similarly but higher alkylsilanes gave only low yields of nitroalkanes accompanied by products of elimination and subsequent polymerization.

Alkylsilanes react readily with nitronium salts to yield nitroalkenes.

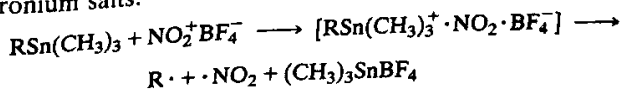


The reactions follow the addition-elimination course.



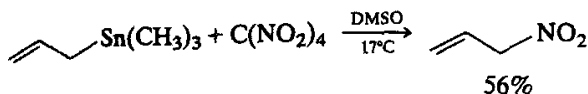
On the other hand, benzylsilanes do not undergo nitrodesilylation, but instead ring nitration takes place.

Although alkylsilanes, as discussed, undergo nitrodesilylation with $\text{NO}_2^+\text{BF}_4^-$, organostannanes in preference undergo one-electron oxidation with nitronium salts.

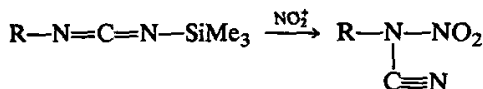


Tetramethylstannane reacts with nitronium salts in dichloromethane, to form chloromethane, chloroethane, methane, and ethane. The products are indicative of the intermediacy of free radicals [152].

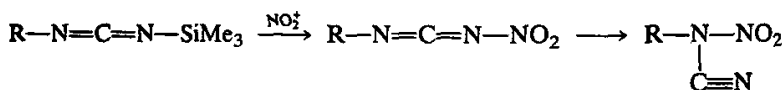
Corey *et al.* have reported [153] facile nitrodestannylation of allyl-trimethylstannane with tetranitromethane in DMSO.



N-Methoxycarbonyl and *N*-methanesulfonyl-*N'*-trimethylsilyl carbodiimides undergo nitrodesilylation, resulting in the formation of *N*-nitrocyanamides.

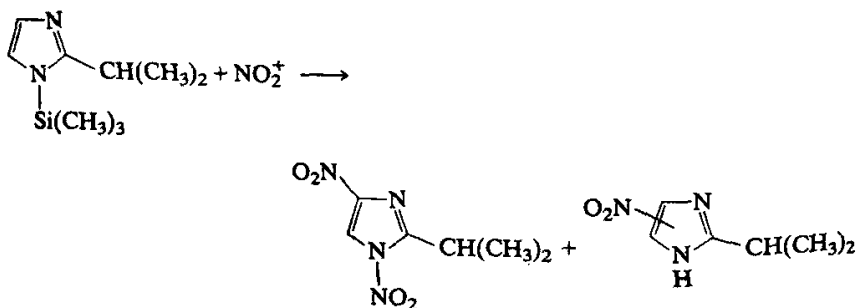


It is not clear whether the *N*-nitrocyanamides are formed via isomerization of the *N*-nitro derivative or not.

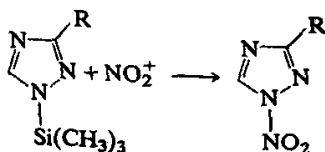


However, direct formation of the *N*-nitrocyanamide seems highly likely.

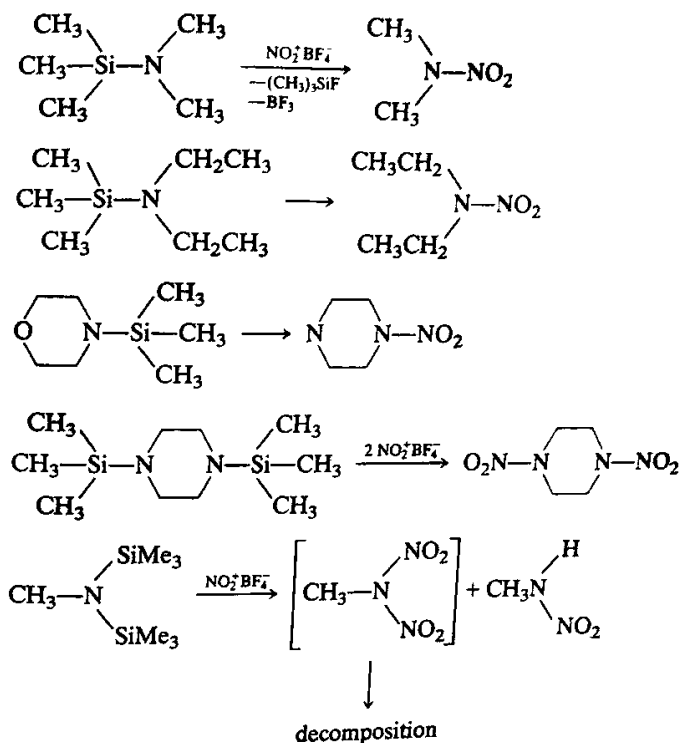
Nitramines can be obtained by nitrodesilylation of silylamines which can provide a route for the synthesis of certain nitramines heretofore unobtainable by conventional nitration methods. 2-Isopropyl-1,4-dinitroimidazole was synthesized by nitration of the corresponding silylated derivative [154].



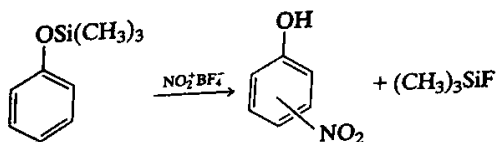
Similarly, *N*-nitrotriazole was synthesized.



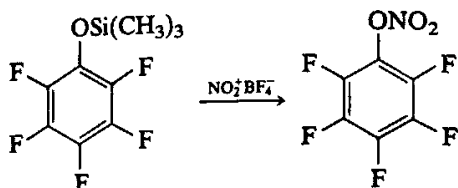
The nitrosilylative N-nitration of a series of amine and diamines was also studied by Olah *et al.* [155].



Phenol silyl ether when reacted with nitronium tetrafluoroborate gives nitrophenols (as well as nitrated silyl ethers).



The desilylative nitration involves initial O-nitration, with phenyl nitrate readily rearranging (catalyzed by the acid formed in the intact ring nitration) to nitrophenols. In case of pentafluorophenyl *O*-trimethylsilyl ether, no rearrangement can occur but there is indication of bimolecular condensation.



ACKNOWLEDGMENT

Support of the nitration work of my group was provided over the years by the U.S. Army Office of Research and subsequently by the Office of Naval Research.

REFERENCES

1. For a detailed discussion of all nitration methods, including conventional mixed-acid nitration, the reader is referred to the monograph: Olah, G. A., Malhotra, R., and Narang, S. C. *Nitration*, VCH Publishers: New York, N.Y. and Weinheim (Germany), 1989, on which this review was in part based.
2. Ingold, C. K. *Structure and Mechanism in Organic Chemistry*, Bell and Sons: London, 1953; 2nd ed. Cornell University Press: Ithaca, N.Y. and London, 1969 and references therein.
3. Seidenfaden, W., and Pawellek, D. in Houben-Weyl, *Methoden der organischen Chemie*, Thieme: Stuttgart, 1971; Vol. XII, pp. 477, 488.
4. Euler, H. *Ann. Chem.* **330**, 280 (1903).
5. Olah, G. A., and Kuhn, S. *J. Chem. Ind.* **98** (1956); Olah, G. A., Kuhn, S. J. and Mlinko, A. *J. Chem. Soc.* 4257 (1956).
6. Olah, G. A., Prakash, G. K. S., and Sommer, J. *Superacids*, Wiley-Interscience: New York (1985). pp. 36-37.
7. Coon, C. L., Blucher, W. G., and Hill, M. E. *J. Org. Chem.* **38**, 4243 (1973).
8. Olah, G. A. *et al.* unpublished results.
9. Olah, G. A., and Lin, H. C. *J. Am. Chem. Soc.* **96**, 549 (1974).
10. Kameo, T., Nishimura, S., and Manabe, O. *Nippon Kagaku Kaishi*, **1**, 122 (1974).
11. Wright, O. L., Teipel, J., and Thoennes, D. *J. Org. Chem.* **30**, 1301 (1965).
12. Olah, G. A., Malhotra, R., and Narang, S. C. *J. Org. Chem.* **43**, 4628 (1978).
13. Crivello, J. V. *J. Org. Chem.* **46**, 3056 (1981); Crivello, J. V. U. S. Pat. 3, 634, 520 (1972), U. S. Pat. 3,715,323 (1973).
14. Dewar, M. J. S., Mole, T., Urch, D. S., and Warford, E. W. T. *J. Chem. Soc.* 3576 (1956).
15. *Methoden der Organischen Chemie (Houben-Weyl)*, Georg Thieme Verlag: Stuttgart, 1971; Vol. X, part 1, p 789.
16. Olah, G. A., Olah, J. A., and Overchuk, N. A. *J. Org. Chem.* **30**, 3373 (1965).

17. Olah, G. A., and Kuhn, S. J. *Friedel-Crafts and Related Reactions*, Olah, G. A., Ed., Wiley: New York, N.Y., 1964; Vol. III, Part II, Chapter 43, 1397.
18. Raudnitz, H. *Chem. Ber.* **60**, 738 (1927).
19. Wright, H. R., and Donalson, W. J. U. S. Pat. 2,416,974 (1947); *Chem. Abstr.* **41**, 3485 (1947).
20. Colonna, H. *Pubbl. Inst. Chim. Univ. Bologna*, **2**, 3 (1943); *Chem. Abstr.* **41**, 754 (1945).
21. Colonna, H., and Andrisano, R. *Pubbl. Inst. Chim. Univ. Bologna*, **3**, 3 (1944); **4**, 3 (1945); *Chem. Abstr.* **41**, 754 (1945).
22. Plazak, E., and Roupuszyński, S. *Rocz. Chem.* **32**, 681 (1958); *Chem. Abstr.* **53**, 3111 (1959).
23. Tsang, S. M., Paul, A. P., and Di Giaimis, M. P. *J. Org. Chem.* **29**, 3387 (1964).
24. Topchiev, A. V. *Nitration of Hydrocarbons*, translated by C. Matthews, Pergamon Press: New York, N.Y., 1959.
25. Bodtker, E. *Bull. Soc. Chim. Fr.* **3**, 726 (1908).
26. Titov, A. I. *J. Gen. Chem. USSR*, **18**, 2190 (1948).
27. Slavinskaya, R. A. *Zs. Obsc. Chim.* **27**, 844 (1957), *Chem. Abstr.* **52**, 2734a (1958).
28. Wilkinson, J. H., and Finar, I. L. *J. Chem. Soc.* 288 (1948).
29. Olah, G. A., Malhotra, R., and Narang, S. C. *J. Org. Chem.* **43**, 4628 (1978).
30. Tronow, B. W., and Ssigba-Aullin, N. C. *Zs. Obsc. Chim.* **62**, 2267 (1930) (Houben-Weyl, XII, p 790).
31. Olah, G. A., and Lin, H. C. *J. Am. Chem. Soc.* **96**, 2892 (1974).
32. Emmons, W. D., and Freeman, J. P. *J. Am. Chem. Soc.* **77**, 4391 (1955).
33. Narang, S. C. Ph. D. Thesis, Flinders University, Adelaide, South Australia, 1975.
34. a) Narang, S. C., and Thompson, M. J. *Austr. Chem.* **28**, 385 (1975);
b) Schmidt, M., and Schmidbauer, H. *Angew. Chem.* **71**, 220 (1959).
35. Olah, G. A., Malhotra, R., and Narang, S. C. *J. Org. Chem.* **43**, 4628 (1978).
36. Olah, G. A. *Friedel-Crafts Chemistry*, Wiley-Interscience: New York, 1973.
37. Olah, G. A., and Kuhn, S. J. *Friedel-Crafts and Related Reactions*, Olah, G. A., Ed.; Wiley-Interscience: New York, N.Y., 1964; Vol. III, pp 1393-1491.
38. Price, C. C., and Scars, C. A. *J. Am. Chem. Soc.* **74**, 3276 (1953).
39. Kuhn, S. J., and Olah, G. A. *J. Am. Chem. Soc.* **83**, 4564 (1961).
40. Dachlauer, K. Germ. Pat. 509,405, (1929); *Chem. Abstr.* **25**, 781 (1931).
41. Lin, H. C., Ph. D. Thesis, Case Western Reserve University, 1972.
42. Hetherington, O., and Robinson, F. L. *J. Chem. Soc.* 3512 (1954).
43. Schaarschmidt, A. *Ber.* **57**, 2065 (1924); *Angew. Chem.* **39**, 1457 (1926).
44. Pinck, L. A. *J. Am. Chem. Soc.* **49**, 2536 (1927).
45. Titov, A. I., and Banyshnikova, A. N. *J. Gen. Chem.* **6**, 1800 (1936); Titov, A. I. *ibid.* **7**, 667 (1937).

46. Goulden, J. D. S., and Millen, D. J. *J. Chem. Soc.* 2620 (1950) Millen, D. J. *ibid.* 2600 (1950).
47. Gillespie, R. J., Graham, J., Hughes, E. D., Ingold, C. K., and Peeling, E. R. A. *ibid.* 2504 (1940).
48. Bachman, G. B., Feuer, H., Bluestein, B. R., and Vogt, C. M. *J. Am. Chem. Soc.* **77**, 6188 (1955); Bachman, G. B., and Vogt, C. M. *ibid.* **80**, 2987 (1958).
49. Olah, G. A., and Overchuck, N. A. *Can. J. Chem.* **43**, 3279 (1965).
50. For an excellent summary, see De la Mare, P. B. D., and Ridd, J. H. *Aromatic Substitution, Nitration and Halogenation*, Academic Press: New York, N.Y. 1959.
51. Klemenz, A., and Scholler, K. *Z. anorg. Chem.* **141**, 231 (1924).
52. Millen, D. J. *J. Chem. Soc.* 2600 (1950).
53. Bachman, G. B., and Dever, J. L. *J. Am. Chem. Soc.* **80**, 5871 (1958).
54. Olah, G. A., and Kuhn, S. J. *Chem. and Ind.* 98 (1956); Olah, G. A., Kuhn, S. J., and Mlinko, A. *J. Chem. Soc.* 4257 (1956); Kuhn, S. J., and Olah, G. A. *J. Am. Chem. Soc.* **83**, 4564 (1961).
55. Hantzsch, A. *Ber.* **58**, 941 (1925); *Z. Phys. Chem.* **149**, 161 (1930).
56. Goddard, D. R., Hughes, E. D., and Ingold, C. K. *J. Chem. Soc.* 2559 (1950).
57. Kuhn, S. J. *Can. J. Chem.* **40**, 1660 (1962).
58. Coon, C. L., Bucher, W. G., and Hill, M. E. *J. Org. Chem.* **38**, 4243 (1973).
59. a) Yagupolskii, L. M., Maletina, I. I., and Orda, V. V. *Zh. Org. Khim, USSR*, **10**, 2226 (1974), Eng. Transl. p. 2240; b) Effenberger, F., and Goke, J. *Synthesis*, 40 (1975).
60. Ingold, C. K. *et al. J. Chem. Soc.* 2559 (1950) and communication to Olah, G. A. in December 1956.
61. Yoshida, T., and Ridd, H. J. in *Industrial and Laboratory Nitrations*, Albright, L. F., and Hanson, C., Eds. American Chemical Society Symposium Series 22, (1976) pp 110-111.
62. Elsenbaumer, R. J. *J. Org. Chem.* **53**, 437 (1988).
63. Olah, G. A., Kuhn, S. J., and Flood, S. H. *J. Am. Chem. Soc.* **83**, 4571 (1961).
64. Radcliff, L. G., and Pollitt, A. A. *J. Soc. Chem. Ind.* **40**, 45T, 90D (1921).
65. Drummond, A. A. *J. Soc. Chem. Ind.* **41**, 338T (1922).
66. Desvergnès, L. *Chim. Ind.* **25**, 291 (1931).
67. Clarke, H. T., and Hartman, W. W. *Organic Synthesis*, Col. Vol. II, John Wiley and Sons: New York, 1943; p 526.
68. Olah, G. A., and Lin, H. C. *J. Am. Chem. Soc.* **96**, 549 (1974).
69. Olah, G. A., and Lin, H. C. *Synthesis*, 494 (1974).
70. Jones, J. *Tetrahedron Lett.* 2177 (1964).
71. Olah, G. A., Olah, J. A., and Overchuck, N. A. *J. Org. Chem.* **30**, 3373 (1965).
72. Cupas, C. A., and Pearson, R. L. *J. Am. Chem. Soc.* **90**, 4742 (1968).
73. a) Olah, G. A., Narang, S. C., Pearson, R. L., and Cupas, A. C. *Synthesis*,

- 452 (1978); b) Olah, G. A., Narang, S. C., Olah, J. A., Pearson, R. L., and Cupas, C. A. *J. Am. Chem. Soc.* **102**, 3507 (1980).
74. Olah, G. A., Laali, K., Farooq, O., and Olah, J. A. *J. Org. Chem.* **55**, 5179 (1990).
75. Shusherina, N. P., and Likhomanova, G. I. *Khim. Geterotsikl. Soed.* 1374 (1972) (quoted by Guk, Y. V., Ilyustrin, M. A., Golad, E. L., and Gidaspov, B. V. *Upspekhi Khimii*, **52**, 499 (1983) (Engl. Transl. **52**(3), 284 (1983))).
76. Olah, G. A., and Lin, C. H. *J. Am. Chem. Soc.* **93**, 1259 (1971).
77. a) Olah, G. A. *J. Am. Chem. Soc.* **94**, 808 (1972); b) Olah, G. A. *Carbocations and Electrophilic Reactions*, Verlag Chemie: Weinheim (Germany), Wiley: New York, 1973; c) *Angew. Chem. Int. Ed.* **12**, 173 (1973).
78. a) Olah, G. A., and Olah, J. A. *J. Am. Chem. Soc.* **93**, 1256 (1971); b) Olah, G. A. *et al.* unpublished results.
79. Cremaschi, P., and Simonetta, M. *Theor. Chim. Acta*, **34**, 175 (1974).
80. Bach, R. D., Holubka, J. W., Badger, R. C., and Rajan, S. Y. *J. Am. Chem. Soc.* **101**, 4416 (1979).
81. Walborsky, H. M., Baum, M. E., and Yossef, A. A. *J. Am. Chem. Soc.* **83**, 988 (1961).
82. Goering, H. L., and Sloan, M. F. *J. Am. Chem. Soc.* **83**, 1397 (1961).
83. Olah, G. A., Quinn, H. W., and Kuhn, S. J. *J. Am. Chem. Soc.* **82**, 426 (1960).
84. Olah, G. A., Schilling, P., Westerman, P. W., and H. C. *J. Am. Chem. Soc.* **96**, 3581 (1974).
85. Olah, G. A., and Nojima, M. *Synthesis*, 785 (1973).
86. Guk, Y. V., Ilyushin, M. A., Golod, E. L., and Gidaspov, B. V. *Russ. Chem. Rev.* **52**, 284 (1983).
87. Scheinbaum, M. L., and Dines, M. *J. Org. Chem.* **36**, 3641 (1971).
88. Smit, V. A., Semenovskii, A. V., and Chernova, T. N. *Izv. Akad. Nauk SSSR, Ser. Khim.* 1681 (1970).
89. Smit, W. A., Semenovskii, A. V., Kucherov, V. F., Chernova, T. H., Krimer, M. Z., and Lubinskaya, O. V. *Tetrahedron Lett.* 3107 (1971).
90. Mursakulov, I. G., and Zefirov, N. S. *Zhur. Org. Khim.* **13**, 1121 (1977).
91. Mursakulov, I. G., Talybov, A. G., Guseinov, M. M., and Smit, V. A. *Zhur. Org. Khim.* **15**, 95 (1979).
92. Speranskii, E. M., Berestovitskaya, V. M., and Perekalin, V. V. Gukkel' [possibly Tiukkel]. "XXVI Gertsenovskie Chteniya, Khimiya, Nauchnye Doklady" (The XXVIth Gertsen Lectures. Chemistry. Scientific reports). Leningrad, No. 2, p 79 (1973).
93. Zlotin, S. G., Krayushkin, M. M. Sevostyanova, V. V., and Novikov, S. S. *Izv. Akad. Nauk SSSR, Ser. Khim.* 2361 (1977).
94. Zlotin, S. G., Krayushin, M. M., Sevostyanova, V. V., and Novikov, S. S. *Izv. Akad. Nauk SSSR, Ser. Khim.* 2286 (1977).
95. Olsen, R. E., Fish, D. W., and Hamel, E. E. in *Sovremennaya Khimiya Raketnykh Topliv* (Modern Chemistry of Rocket Fuels). Atmoizdat: Moscow, 1972; P 55 [*Adv. Chem. Ser.* **54**, 48 (1965)].
96. Britteli, D. R., and Boswell, G. A., Jr. *J. Org. Chem.* **46**, 312 (1981).

97. Schmitt, R. J., and Bedford, C. *Synthesis*, 493 (1986).
98. Schmitt, R. J., Bottaro, J. C., Malhotra, R., and Bedford, C. D. *J. Org. Chem.* **52**, 2294 (1987).
99. Nesmeyanov, A. N., Tolstoya, T. I., and Korol'kov, V. V. *Dokl. Akad. Nauk SSSR*, **241**, 1103 (1978).
100. Jäger, V., Motte, J. C., and Viehe, H. G. *Chimica*, **29**, 516 (1975).
102. Blackall, E. L., Hughes, E. D., Ingol, C., and Pearson, R. B. *J. Chem. Soc.* 4366 (1958).
103. Olah, G. A., Noszko, L., Kuhn, S., and Szelke, M. *Chem. Ber.* **89**, 2374 (1956).
104. Ho, T. L., and Olah, G. A. *J. Org. Chem.* **42**, 3097 (1977).
105. Shvarts, I. I., Yakovenko, V. N., Krayushkin, M. M., Novikov, S. S., and Sevost'yanov, V. V. *Izv. Akad. Nauk SSSR, Ser. Khim.* 1674 (1976).
106. Olah, G. A., and Kuhn, S. J. in *Friedel-Crafts and Related Reactions*, Olah, G. A., Ed.; Wiley-Interscience: New York, 1964; Vol. 3, Chapter 43.
107. Olsen, R. E., Fisch, D. W., and Hamel, E. E. in *Advanced Propellant Chemistry*, Gould, R. E., Ed.; *Advances in Chemistry Series 54*, American Chemical Society: Washington, 1966; Chapter 6.
108. Ilyushin, M. A., Golod, E. L., and Gidasov, B. V. *Zhur. Org. Khim.* **13**, 11 (1977).
109. Ilyushin, M. A., Guk, Yu. V., Golod, E. L., Frolova, G. M., and Gidasov, B. V. *Zhur. Org. Khim.* **15**, 103 (1979).
110. Vast, P. *Rev. Chim. Miner.* **7**, 757 (1970).
111. Barbes, H., and Vast, P. *Rev. Chim. Miner.* **8**, 851 (1971).
112. Vast, P., and Heubel, J. *Compt. rend.* **864c**, 1697 (1967).
113. Vast, P., and Heubel, J. *Compt. rend.* **260**, 5799 (1965).
114. Brit. Pat. 1126591, 1968; U.S. Pat. 3428667, 1969; *Chem. Abst.* **70**, 67584 (1969).
115. Lebedev, B. A., Ilyusin, M. A., Andreev, S. A., and Gidasov, B. V. *Zhur. Org. Khim.* **14**, 2055 (1978).
116. Andreev, S. A., Lebedev, B. A., and Tselinskii, I. V. *Zhur. Org. Khim.* **14**, 2513 (1978).
117. Luk'yanov, O. A., Kozlova, I. K., and Tartakovskii, V. A., "Tezisy VI Vsesoyuznogo Soveshchaniya po Khimii Nitrosoedinenii" (Abstracts of Reports at the VIth All-Union Conference on the Chemistry of Nitrocompounds), Moscow, p 68 (1977).
118. Robson, J. H. *J. Am. Chem. Soc.* **77**, 107 (1955).
119. Andreev, S. A., and Gidasov, B. V. *Zhur. Org. Khim.* **14**, 240 (1978).
120. Andreev, S. A., and Lebedev, B. V. *Zhur. Org. Khim.* **14**, 907 (1978).
121. Andreev, S. A., Lebedev, B. A., and Tselinskii, I. V. *Zhur. Org. Khim.* **14**, 909 (1978).
122. Cherednichenko, L. V., Lebedev, B. A., and Gidasov, B. V. *Zhur. Org. Khim.* **14**, 735 (1978).
123. Luk'yanov, O. A., Mel'nikova, T. G., Seregina, N. M., and Tartakovskii, V. A. "Tezisy VI Vsesoyuznogo Soveshchaniya po Khimii Nitrosoedinenii"

- (Abstracts of Reports at the VIth All-Union Conference on the Chemistry of Nitro-Compounds), Moscow, p 33 (1977).
124. Luk'yanov, O. A., Seregina, N. M., and Tartakovskii, V. A. *Izv. Akad. Nauk SSSR, Ser. Khim.* 225 (1976).
 125. Kartritzky, A. R., and Mitchell, J. W. *J. Chem. Soc. Perkin Trans. (I)*, 2624 (1973).
 126. Doyle, M. P., Whitefleet, J. A. L., Debruyne, D. J., and Wierenge, W. *J. Am. Chem. Soc.* **99**, 494 (1977).
 127. a) Olah, G. A., Gupta, B. G. B., and Narang, S. C. *J. Am. Chem. Soc.* **101**, 5317 (1979); b) Olah, G. A., and Gupta, B. G. B. *J. Org. Chem.* **48**, 3585 (1983); c) Olah, G. A., Narang, S. C., Salem, G. F., and Gupta, B. G. B. *Synthesis*, 273 (1979).
 128. a) Elsenbaumer, R. L., and Wasserman, E. *Abstr. Pap-Chem. Congr. North Am. Cont. 2nd* (1980), *Abstr. 77*; b) Elsenbaumer, R. L., and Wasserman, E. U. S. Patent 4,392,978, 1983.
 129. Savoie, R., Pigeon-Gosselin, M., Rodrigue, A., and Chénevert, R. *Can. J. Chem.* **61**, 1248 (1983).
 130. Masci, B. J. *Chem. Soc. Commun.* p 1262 (1982); *J. Org. Chem.* **50**, 4081 (1985).
 131. Olah, G. A., Lin, H. C., Olah, J. A., and Narang, S. C. *Proc. Natl. Acad. Sci. USA*, **75**, 1045 (1978).
 132. Talybov, A. G., and Mursakulov, I. G. *Azerb. Khim. Zhur.* No. 3, 64 (1978).
 133. a) Olah, G. A., Narang, S. C., Malhotra, R., and Olah, J. A. *J. Am. Chem. Soc.* **101**, 1805 (1979); b) Olah, G. A., Lin, H. C., and Mo, Y. K. *J. Am. Chem. Soc.* **94**, 3667 (1972).
 134. Kim, E. K., and Kochi, J. K. *J. Org. Chem.* **54**, 1692 (1989).
 135. Woelfenstein, R., and Boeters, O. Germ. Pat. 194, 883; *Chem. Abstr.* **2**, 1861 (1980).
 136. Westheimer, F. H., Segel, E., and Schramm, R. *J. Am. Chem. Soc.* **69**, 773 (1947).
 137. Davis, T. L., Worrall, D. E., Drake, N. L., Heimkanys, R. W., and Young, A. M. *J. Am. Chem. Soc.* **43**, 594 (1921).
 138. Tsutsumi, S., and Iwata, E. *J. Chem. Soc. Jpn. Pure Chem. Sect* **72**, 741 (1951); *Chem. Abstr.* **46**, 6604a (1952).
 139. Osawa, T., Yoshida, T., and Namba, K. *Kogyo Kayaku Kyokashi* **27**, 162 (1966).
 140. Stock, L. M., and Wright, T. L. *J. Org. Chem.* **42**, 2875 (1977); *J. Org. Chem.* **44**, 3467 (1979).
 141. Komoto, H., Hoyano, F., Takami, T., and Yamato, S. *J. Polym. Sci. Part A-1*, **9**, 2983 (1971).
 142. Olah, G. A., Krishnamurthy, V. V., and Narang, S. C. *J. Org. Chem.* **47**, 596 (1982).
 143. Deans, F. B., and Eaborn, C. *J. Chem. Soc.* 498 (1957).
 144. Benkeser, R. A., and Landesman, H. *J. Am. Chem. Soc.* **76**, 904 (1954).

145. Benkeser, R. A., and Brumfield, P. E. *J. Am. Chem. Soc.* **73**, 4770 (1951).
146. Speier, J. L. *J. Am. Chem. Soc.* **75**, 2930 (1953).
147. Eaborn, C., Salih, Z. S., and Walton, D. R. M. *J. Chem. Soc. Perkin Trans. II*, 172 (1972).
148. Olah, G. A., and Narang, S. C. unpublished results.
149. Glass, R. S., Blount, J. F., and Butler, D. *Can. J. Chem.* **50**, 3472 (1972).
150. a) Boyer, J. H. "Nitrazoles", VCH Pub.: Deerfield Beach, Fl. 1986; b) Pevzner, M. S., Gidaspov, B. V., and Tartakovskii, V. A. *Khim. Geterotsikl. Soed.* p 550 (1979); c) quoted by Guk, Yu. V., Ilyusin, M. A., Golad, E. L., and Gidaspov, B. V. *Uspekhi Khimii*, **52**, 499 (1983), Eng. Transl. **52** (3), 284 (1983).
151. Olah, G. A., and Rochin, C. *J. Org. Chem.* **52**, 1987 (1987).
152. Kashin, A. N., Bumagin, N. A., Bessonova, M. P., Beletskaya, I. P., and Reutov, O. A. *J. Org. Chem. USSR*, **16**, 1153 (1980).
153. Corey, E. J., and Estreicher, M. *Tetrahedron Lett.* **21**, 1113 (1980) (footnote 9).
154. a) Watanabe, K., Ishikawa, H., and Ando, W. *Bull. Chem. Soc. Jpn.* **51**, 1253 (1978); b) Winer, A. M., Atkinson, R., and Pitts, J. N., Jr. *Science*, **224**, 156 (1984).
155. G. A. Olah, G. K. S. Prakash, and Trivedi, N. unpublished results.

Index

Adamantane

- adamantyladamantane, 19
- hexanitrohexaazaadamantane (HNZADA), 3-6
- nitration of, 170
- 2,4,10-trinitro-2,4,10-triazaadamantane, 5

Alkaline-earth

- calcium complex
 - bond distances, 133
 - coordination sphere, 133
 - molecular structure of, 132-133
 - preparation of, 132
- strontium complex
 - bond distances, 135
 - IR spectra (Nujol mull), 135-136
 - molecular structure of, 133-134
 - preparation of, 133

Bis-dicarbollide complex

- IR spectra (Nujol mull), 129-130
- magnetic spectral data, 129
- NMR spectra, 130
- samarium, 129-131
 - coordination geometry, 130-131
- x-ray diffraction, 130
- ytterbium, 129

Cage compounds, 3-4, 21-22

Caged nitramine explosives, synthesis of

- 1,3-dinitro-1,3-diazacyclopentane, 98
- 1,3,5,7-tetranitro-1,3,5,7-tetraazacyclooctane (HMX), 97-99
- 1,3,5-trinitro-1,3,5-triazacyclohexane (RDX), 97-99

Calcium. *See* Alkaline-earth; Metallacarboranes

closo-metallacarboranes

- bis-dicarbollide lanthanide complex, 129-130
- IR band 'splitting', 128-129
- thallium, oxidation of, 126
- ytterbium, oxidation of, 126

Cubane

- 2-*t*-butylcubylcubane, 16-17
- crystallization of, 16-18
- cubylcubane
 - cocrystallization, 16-17
 - molecular structure, 17
 - packing, 17
- octanitrocubane, 3-5
- phenyltercubyl compound, 18
- strained hydrocarbons, bond lengths, 18
- 1,2-substituted bonds, 21-22
- tetracarboxycubane, 19, 20
- 1,3,5,7-tetranitrocubane, 3-4, 19-20

Energetic materials, structure

background

- applications, 1
- atomic arrangements, determination of, 1
- Cambridge Structural Database, 2
- electron density distributions, 1
- relationship to function, 1
- relation to activity, 2
- structural analysis, 1, 3

cubane and substituents

- 1,4-bis-cubanediammonium perchlorate hydrate, 19, 21
- bond length, 18, 19, 22
- 2-*t*-butylcubylcubane, 16-17
- cage distances, 21
- characteristics, 16-22
- cocrystal packing, 17
- crystallization of, 16-18
- cubylcubane, 16-17
- fusion of, 22
- linkage distance, 18-19
- synthesis of, 19-21
- tetracarboxycubane, 19-20
- 1,3,5,7-tetranitrocubane, 19-20

database

- applications of, 3-4
- cage compounds, 3-5
- energy minimum, calculation of, 4

database (*continued*)

- hexanitrohexaazaadamantine (HNZADA),
 - 4–5
 - illustrations of, 3–4
 - model building, 5–6
 - NO₂ group, 3–5
 - quantum mechanical calculations, 5
 - structure calculation, 3–4
 - target structures, prediction of, 3–6
 - nitramines, bending angles in
 - C-N-C plane, 6–8, 10
 - dimethylnitramine, 8, 10
 - flexibility, 6
 - frequency distribution, 7
 - in-plane, 8
 - nitroaziridine, 8–9
 - N-N vector, 6–8
 - out-of-plane, 6–8
 - nitroolefins
 - bicyclic octanitro compound, 16
 - t*-butylammonium trinitromethanide salt,
 - 15
 - C-C distance, 11, 15
 - characteristics, 11, 15
 - 1,1-diiodo-2,2-dinitroethylene, 11, 13
 - 1,1-dinitro-2,2-di(dimethylamino)ethylene,
 - 11, 13
 - 1,1-dinitro-2,2-di(η -propyl)ethylene,
 - 14–15
 - 1,1-dinitro-2,2-di(phenylamino)ethylene,
 - 14–15
 - out-of-plane rotations, 11, 15
 - spatial crowding, 11–12
 - synthesis intermediates, 11–16
 - synthesis of, 12–15
 - twists, observed and calculated, 12
 - pressure and impulse
 - density, role of, 2
 - hexanitrohexa-aza-adamantane, 3
 - β -HMX, 2, 5
 - octanitrocubane, 3
 - packing models, 3
 - RDX, 2, 5, 6
 - 1,3,5,7-tetranitrocubane, 3
 - Fluorescence decay, temperature dependence of,
 - 61
 - Forward convolution method
 - analysis, 44
 - averaging, 42–43
 - energy distribution, 45–46
 - Newton diagram, 43–44
 - primary channels, 43–44, 47–48
 - primary decomposition step, identification,
 - 44–45
 - secondary channels, 43–44, 47
 - time-of-flight spectra, 42, 44, 45, 47, 49
 - translational energy distribution, 44–48
-
- Haloanthracenes
 - emission decay kinetics, 59, 64
 - fluorescent lifetimes, 58, 64
 - Haloaromatics, photodissociation of. *See also*
 - Molecular dissociation
 - fluorescence data, summary, 58–59
 - fluorescence decay, 61
 - haloanthracenes
 - 9-bromoanthracene, 58–59
 - 9,10-dibromoanthracene, 58
 - 2-iodoanthracene, 59–60, 64
 - 9-iodoanthracene, 59–60, 64
 - halonaphthalenes
 - absorption spectra of, 60, 64
 - emission decay lifetime, 63
 - iodonaphthalene, 56
 - mechanism, 62–63, 65
 - naphthyl radical
 - 2-(bromomethyl)naphthalene, 66
 - 1-(chloromethyl)naphthalene, 65–66
 - emission spectrum, 65–68
 - naphthyl radical
 - detection of, 65
 - streak camera records, 57, 59, 61
 - Halonaphthalenes
 - absorption spectra, 60, 63, 64
 - emission decay, 63–64
 - fluorescence decay, 61
 - Hexanitrohexaazaadamantane (HNZADA), 3–6
 - High-laser fluence excitation, 38–42, 46–49
-
- Lanthanacarboranes. *See also* Lanthanide:
 - Metallacarboranes
 - IR band 'splitting', 128
 - low frequency absorption, 128
 - synthesis of, 126
 - Lanthanide
 - samarium complexes
 - IR spectra (Nujol mull), 127
 - synthesis of, 126
 - ytterbium complexes
 - IR spectra, 128–129

- synthesis of, 126
 $\text{Yb}(\text{C}_2\text{B}_9\text{H}_{11})(\text{DMF})_4$, structure of, 127
 ytterbium-boron distances, 128
 Low-laser fluence excitation, 36-38, 44-46
- Metallacarboranes**
 alkaline-earth, 131-136
 calcium complexes, 132-133
 carborane cage, 131-133
 chemistry of, 131-134
 metal-to-carborane interactions, 133-135
 strontium complexes, 133-136
 anionic carborane ligands, 125-129
 background, 125
 bis-dicarbollide complexes, 129-131
 characterization of, 129-131
 divalent lanthanide, oxidation of, 129
 preparation of, 129-131
 THF, displacement of, 129
closo-species, 125-126, 128, 129, 132, 134
 η^5 -bound, 125, 133
 lanthanide, 125-129
 decomposition, 126
 dicarbollide cage, 126-127
 divalent complexes, synthesis of, 126
 IR spectra, 127, 128
 NMR spectra, 126-127
 oxygen atoms, plane of, 127
 samarium complexes, 125-126
 samarium vs. ytterbium reactivity, 126
 solvent solubility, 126
 Yb and dicarbollide, interaction of, 126
 $\text{Yb}(\text{C}_2\text{B}_9\text{H}_{11})(\text{DMF})_4$, 127-129
 ytterbium complexes, 126-129
 [nido-7,9- $\text{C}_2\text{B}_{10}\text{H}_{12}$], 125-127, 132-133
 Molecular beam apparatus, 33-35
 Molecular dissociation. *See also* Haloaromatics,
 photodissociation of; Picosecond x-ray
 diffraction
 background, 55-56
 bromoanthracenes, 58-59
 bromonaphthalenes, 57, 58
 chloronaphthalenes, 58
 fluorescence decay, temperature dependence
 of, 61
 haloanthracenes, 58-59, 64-65
 haloaromatics, 56-68
 halonaphthalenes, 56, 60-61, 63-64
 halonaphthalenes, transient absorption spectra
 of, 60
 iodoanthracenes, 59-60
 iodonaphthalene, 56
 iodo- vs. bromo-naphthalenes, 56
 kinetics, 59, 60, 62, 68
 mechanism, 62
 methyl iodide, 56
 naphthyl radical, 65-68
 picosecond x-ray diffraction, 69-75
 radicals formed, 55, 65-68
 ring substituent, position of, 58, 62
 Monopropellants, computer-aided design of
 background
 characterization, 77
 components, 77
 evaluation, 77
 specific impulse, 77
 criteria, 92
 perspectives, 91-92
 specific impulse formula
 application of, 80-81
 combustion temperature (T_c), 80-81
 enthalpy of combustion, 80-81
 examination of, 86
 gaseous products, 80
 specific impulse values (I_s)
 aza nitrogens, 89, 91
 calculation of, 81-86
 comparison of, 90
 cubane derivatives, 87-88
 factors determining, 89
 oxidation reactions, 87-88
 relative to HMX, 81-86
 theory
 basis, 77
 kinetics, 78-79
 specific impulse, methods for computing,
 78
- Naphthyl radical, emission spectrum, 65-67
 [nido-7,8- $\text{C}_2\text{B}_{10}\text{H}_{11}$]
 samarium complex, bonding with, 131
 samarium, interaction with, 125-126
 ytterbium, interaction with, 125-126
 [nido-7,9- $\text{C}_2\text{B}_{10}\text{H}_{12}$]
 calcium iodide, interaction with, 132-133
 samarium, interaction with, 125-126
 strontium iodide, interaction with, 133-134
 ytterbium, interaction with, 125-126
- Nitramines
 bending angles in, 6-10
 dimethylnitramine, 8, 10
 1-nitro-3-nitratoozotidine, 8

Nitramines (*continued*)

- 1,3,3-trinitroazetidide, 8–9
- 1,3,5-trinitro-2-oxo-1,3,5-triazacyclohexane, 6–7

Nitration

definition of, 139

Lewis-acid catalyzed

aromatics with dinitrogen tetroxide, 155–156

benzenes, yields, 156

Friedel-Crafts, 152–154, 156, 158

nitrogen pentoxide, 157–158

nitryl bromide, 155

nitryl chloride, 153–154

nitryl fluoride, 154–155

nitryl halides, comparison, 155

ortho/para ratios, 154

protic-acid-catalyzed

acetonecyanohydrin nitrate (ACN), 151–152

alkali metal nitrates, 147–148

alkyl nitrates, 148–149

aromatic, ortho vs. para, 148–149, 152

boron trifluoride, 149–150

electrophilic, 140–141

Lewis acid fluorides, addition of, 145

Nafion-H[®] perfluorosulfonic acid, 146–147, 148–149, 151

nitric acid-fluorosulfuric acid, 145

nitric acid-hydrogen fluoride-boron trifluoride, 142

nitronium ion (NO₂⁺), 140

polystyrenesulfonic acid, 146

scope of, 140–141

triflatoboric acid, 143, 145

trifluoromethanesulfonic acid (triflic acid), 142–144

trimethylsilyl nitrate, 152

reaction types, 140

Nitration, nitronium salts. *See* Nitronium salts

Nitrocompounds, preparation of background, 139–140

Lewis-acid-catalyzed nitration, 152–158

aromatics, 153, 156–158

Friedel-Crafts acylation, 152–153, 154, 156

nitryl halides, 153–156

nitronium salts, nitration with

alkanes, 166–173

alkenes, 173–176

alkynes, 176–177

arenes, 162

aryl and aralkyl nitriles, 163

arylcaboxylic acid esters and halides, 163

demetallative nitration, 191–197

haloarenes and haloalkylarenes, 162

hydrocarbons, 158–166

nitroarenes and nitrohaloarenes, 163

N-nitration, 180–185

O-nitration, 177–180, 197–198

phosphorus nitration, attempted, 185–186

S-nitration, 185

transfer nitration, 186–191

protic-acid-catalyzed nitration, 140–152

aromatics, 142–143, 145, 149

aromatics, azeotropic nitration of, 146–147

dinitrotoluene, preparation of, 143–144

nitrating agents, 140–146

tetramethylbenzenes, 149–150

toluene, mononitration of, 142–143

Nitronium ion (NO₂⁺)

acetonitrile, reaction with, 160–161

alkanes, nitration of, 167–169

as an oxidant, 171–172

cycloalkanes, nitration of, 167

electrophilic nitrating agent, 140–141

ethers, nitration of, 179

hydride transfer, 172

linear, 167, 169, 171

nitrodesilylation, 196

nitryl fluoride dissociation, 154

N₂O₂ in sulfuric acid, solutions of, 155

trifluoroacetyl nitrate dissociation, 147

Nitronium salts

alkanes, nitration of

adamantane reaction, 170, 172

bond reactivity, 167, 169

carbocation formation, 171, 173

electrophilic aliphatic nitration, 166

hydride transfer, 171–172

kinetics, 170

nitronium ion, 168, 169, 171

orbital considerations, 167, 169

protosolvation, 169, 171

reaction pathway, 167–170

steric requirements, 169–170

superacid reactions, 171

alkenes, nitration of

cycloalkenes, 175–176

nitrocarbenium ion, 173, 174

nitrocarbocation, 175

nitrofluorination, 174, 175

Ritter reaction, 174, 179

alkynes, nitration of, 176–177

- characterization of, 160
 demetallative nitration
 mercuration, 191-192
 Nafion-H® catalyst, 193
 nitrodeprotonation, 193
 nitrodesilylation, 192-193, 194-196
 nitrodestannylation, 195-196
 N-nitrocyanamides, 196
 ortho/para ratio, 191-192
 regioselectivity alteration, 191
 hydrocarbons
 general nitration method, 158-159
 nitronium tetrafluoroborate, 159-161
 nitronium trifluoromethane-sulfonate,
 preparation of, 159-160, 164
 nitronium hexafluorophosphate, 164
 nitronium tetrafluoroborate
 aromatic nitration, 161-164, 165
 conductivity of, 160
 preparation of, 159
 reaction of, 161
 N-nitration
 amides (acylamines), 182, 183
 aromatic methylene-bis-amines, 181
 azodicarboxylates, 184-185
 dependence of amine basicity, 181
 isocyanates, 183
 lithium azide, 185
 methylene diamines, 184
 N-alkylamides, 183
 nitramine formation, 180-181
 nitro-imides, 182
 N,N-dinitramine formation, 181-182
 N-nitrimines, 184
 urethanes, 182
 O-nitration
 alcohols, 178, 179
 aldehyde, ketone conversion, 179
 nitrodesilylation, 197
 nitronium ion, 178
 nitrophenols, 197
 N-nitrooxonium ion, 178-179
 reaction order, 178
 vinyloxysilanes, 179-180
 P-nitration, 185-186
 S-nitration, 185
 solvents for, 160-161
 transfer nitration
 alcohols, 189-190
 crown ether complexation, 186
 definition of, 186
 N-nitrocollidinium tetrafluoroborate, 190
 N-nitropyridinium salts, 187-188
 N-nitropyridinium tetrafluoroborate,
 preparation of, 187
 N-nitroquinolinium salts, 187
 olefins, 189
 ortho/para ratio, 186-187
 regioselectivity, 186
 S-nitrosulfonium salts, 188
 Nitronium tetrafluoroborate ($\text{NO}_2^+ \text{BF}_4^-$)
 adamantane nitration, 172-173
 alcohol nitration, 178
 alkane nitration, 166
 alkene nitration, 173-176
 alkyne nitration, 176-177
 amine nitration, 180-185
 aromatic nitration, 161-163, 165
 butyl pyridine, reaction with, 165-166
 characterization, 160
 complexation with crown ethers, 186-187
 cyclohexene reaction, 174-175
 isolation of, 142
 nitroacetylene formation, 177
 nitrodesilylation, 194-195
 nitrofluorination, 175
 nitrophenol formation, 197-198
 preparation of, 159, 160
 silyl ether nitration, 179-180
 solubility, 161-162
 specific conductivity of, 160
 Nitroolefins
 1,1-diiido-2,2-dinitroethylene, 12-13, 15
 1,1-dinitro-2,2-di(dimethylamino)ethylene,
 11, 13
 1,1-dinitro-2,2-di(*n*-propyl)ethylene, 14-15
 1,1-dinitro-2,2-di(phenylamino)ethylene,
 14-15
 synthesis of, 12-15
 twists in, 14
 N-nitro compounds. *See* Nitronium salts.
 N-nitration
 O-nitro compounds. *See* Nitronium salts.
 O-nitration
 Photodissociation. *See* Molecular dissociation.
 Haloaromatics, photodissociation of
 Photofragmentation translational spectroscopy
 dissociation, 30, 31
 excitation, 29-30
 fragment detection, 30

Photofragmentation translational spectroscopy

(continued)

- important features, 29–30
- molecular beam methods, 29–30
- molecular beam velocity, 30–32
- Newton diagram, 30–32
- thermal decomposition, 32–33
- time-of-flight spectrum, 29–30, 33

Picosecond x-ray diffraction (PXR)

- anode, 71
- background, 69–70
- detectors used, 74
- diagnostics, 72–75
- diode, schematic diagram of, 70
- electron bunches, utilization of, 69
- electron emission, 71
- experimental system, 70–72
- experiments, 72–73
- generation of, 69
- Laue diffraction patterns, 71, 72
- metallic surfaces, 70, 71
- photocathode, 70, 71
- pulsed beams, synchronization of, 72, 73
- pulse width, 71
- quantum efficiency, 69, 71
- soft x-ray emission, 69
- source, 69, 70–72
- streak camera traces, 73
- system design, 69–70
- time-resolved, 69, 72

Polyazaadamantanes

- 1-azaadamantane
 - ring substituted derivatives, 100
 - synthesis, 100
- 2-azaadamantane, 100
- 1,3-diazaadamantane, 100–101
- 2,6-diazaadamantane, 101
- hexamethylenetetramine, 104
- triazadamantanes
 - caged orthoamide structures, 102–103
 - synthesis, 101–102

Polyazaisowurtzitanes

- amine reaction with glyoxal, 116, 117–118
- benzylamines, 118–119
- 4,10-dinitro-4,10-diaza-2,6,8,12-tetraazaisowurtzitane, 111
- 2,6-ethylene-8,12-ethylene-4,10-dioxo-2,6,8,12-tetraazaisowurtzitane, 111–112
- hexaazaisowurtzitanes
 - acid stability, 114
 - condensation reactions, 113
 - decomposition products, 114

- deuterium substitution, 117–118
- diimine trimerization, 115–116
- hexabenzyl derivative, 113
- hexabenzyl, mechanism of formation, 115–116
- 4-(methoxybenzyl) derivative, 115
- monoimine trimerization, 116–117
- phenyl substitution, 117

NMR spectra, 115

synthesis, 111–115, 118–119

Polyazawurtzitanes

- 3-azawurtzitane, 104–106
 - endo* substituents, 106
- iceane, 104–105
- 3,5,12-triazawurtzitanes
 - condensation of 1,3,5-triformylcyclohexane, 106–110
 - synthesis of, 106–110
- 1,3,5-triformylcyclohexane, reactions of, 108–110
- triamines, equilibrium with, 108–109

Polycyclic amine chemistry

- background, 95–97
- caged nitramines synthesis
 - 1,3-dinitro-1,3-diazacyclopentane, 98
 - hexanitrohexaazaadamantane, 99
 - hexanitrohexaazaisowurtzitanes, 99
 - hexanitrohexaazawurtzitane, 99
 - HMX, 97–99
 - methods, 98–99
 - nitration process, 98
 - problems, 99
 - RDX, 97–99

density

- caged hydrocarbons, 97
- importance of, 95–96
- maximization parameters, 96
- monocyclic vs. caged compounds, 96
- detonation, chemical energy of (Q), 96
- detonation pressure (P_{C_2}), 95–97, 99
- detonation velocity (D), 95–97, 99
- polyazaadamantanes, 100–104
 - examples of, 100–102
 - nitrogen bridge, 100
 - ring substituted derivatives, 100, 102
 - synthesis, 100–103
- polyazaisowurtzitanes, 110–119
 - known ring systems, 110, 114
 - synthesis, 111–113, 115–119
- polyazawurtzitanes, 104–109
 - examples of, 104–106
 - parent, synthesis of, 104–105

- stability, 108–109
 triimines, equilibrium with, 108–109
 Propellants. *See* Monopropellants
- Samarium. *See* Lanthanide; Metallacarboranes
- S-nitro compounds. *See* Nitronium salts,
 S-nitration
- Specific impulse (I_s)
 background, 77
 formula
 application of, 80–81
 combustion temperature (T_c), 80–81
 enthalpy of combustion (ΔH_{comb}), 80–81
 kinetic energy, 78–79
 methods for computing, 78–79
 relation to thrust, 78
 theory, 78–80
 values
 affect of aza nitrogens, 89, 91
 calculation of, 81–86
 cubane derivatives, properties of, 87–88
 decomposition reactions, 87–88
 factors determining, 89, 90
 heat of formation (H_f), 87–89
 n/M, 87–88
 relative to HMX, 81–86
- Strontium. *See* Alkaline-earth;
 Metallacarboranes
- 1,3,5,7-tetranitro-1,3,5,7-tetraazacyclooctane
 (HMX), 5, 27
 detonation pressure (P_C), 95
 detonation velocity (D), 95
 as energetic material, 2
 heat of formation, 87
 oxidation reaction, 87
 specific impulse value, 81–86
 synthesis of, 97–99
- Translational energy analysis
 C_2H_2 , production of, 49
 energy released, derivation of, 50
 reaction mechanism, 50–51
- 1,3,5-triformylcyclohexane
 amines, condensation with, 106, 108
 ammonia, reaction with, 108–109
 ester formation, 107
 formation of, 107
 formation of triimines, 107–108
 hydrazine, reaction with, 108–109
 phenylhydrazine, reaction with, 108–109
- primary amines, reaction with, 109–110
- 1,3,3-Trinitroazetidine (TNAZ)
 background, 27–28
 cyclic nitroalkyl nitramines, 27
 decomposition
 products of, 29, 32, 33–42
 study of, 29–30
 techniques used in, 29–30
 energetic cyclic nitramines, relation to, 27
 forward convolution method
 center-of-mass velocity, 43
 high-laser fluence, 46–49
 low-laser fluence, 44–46
 primary dissociation, 43–44
 primary vector channels, 43–44, 47, 48
 secondary dissociation, 47–49
 secondary reaction channels, 43–44, 47
 translational energy distribution, 37, 39,
 44–48
 fragment identification, 30–31
 molecular dissociation, 30–31
 NO_2 loss, 28
 photofragmentation translational spectroscopy
 data, interpretation of, 30–33
 molecular beam methods, 29
 Newton diagram, 30–32, 43
 research, areas of, 28
 thermal decomposition of
 bulk studies comparison, 51–53
 data analysis, 35–42
 high-laser fluence excitation, 38–42
 ionization, 36, 39–40
 laser light excitation, 35–40
 low-laser fluence excitation, 36–38
 mass spectra, 35–42, 46–49
 mass-to-charge ratio (m/e), 36–42, 44–45,
 47, 49–51
 methods, 34–35
 molecular beam, 33–34, 51, 53
 reaction summary, 52
 studies, 28, 32–33
 time-of-flight spectra, 30, 35, 37, 39,
 40–42
 unimportant channels, 51
 velocity distribution, 35
 translational energy analysis, 49–51
- 1,3,5-trinitro-1,3,5-triazacyclohexane (RDX),
 5, 27
 decomposition, 32, 34, 46, 51
 as energetic material, 2
 NO_2 loss channel, 48, 52
 specific impulse, 90

1,3,5-trinitro-1,3,5-triazacyclohexane(RDX)*(continued)*

synthesis of, 97-99

translational energy distribution, 46

triple concerted reaction, 51

Ultrafast spectroscopyemission decay kinetics, 59, 60, 62, 63,
66-68

experimental system, 56-57

fluorescence lifetime, 58, 59, 61, 63

gas-phase fluorescence decay, 61

haloanthracenes, 58-59

halonaphthalenes

1-bromonaphthalene, 60-61

singlet-singlet absorption, 60

singlet-singlet transition, 60

transient absorption spectra of, 60-61, 63

materials used, 57

spin-orbit coupling, 62

time-resolved spectra, 57, 59-60, 62

triplet state, 62, 64, 65

Ytterbium. See Lanthanide; Metallacarboranes

Chemistry of Energetic Materials

The study of energetic materials is emerging from a field primarily directed toward practical interests to an advanced area of fundamental research, where state-of-the-art methods and theory are used side by side with modern synthetic methods.

This timely book integrates the recent experimental, synthetic, and theoretical research of energetic materials. Editors George Olah and David Squire emphasize the importance of structure and mechanism in determining properties and performances. They also explore new spectrometric methods and synthetic approaches in this useful reference.

Key Features:

- ▲ *Discusses structural analysis by x-ray crystallography*
- ▲ *Explains chemical dynamics by photofragmentation translational spectroscopy*
- ▲ *Covers kinetic analysis by ultrafast absorption and emission spectroscopy*
- ▲ *Details syntheses of polycyclic caged amines, fuel additives, and polynitro compounds*
- ▲ *Examines computer-aided design of monopropellants*
- ▲ *Includes contributions by two Nobel laureates and five members of the National Academy of Sciences*

Chemistry of Energetic Materials

The study of energetic materials is emerging from a field primarily directed toward practical interests to an advanced area of fundamental research, where state-of-the-art methods and theory are used side by side with modern synthetic methods.

This timely book integrates the recent experimental, synthetic, and theoretical research of energetic materials. Editors George Olah and David Squire emphasize the importance of structure and mechanism in determining properties and performances. They also explore new spectrometric methods and synthetic approaches in this useful reference.

GET IT-SCAN IT-SPREAD IT



Key Features:

- ▲ *Discusses structural analysis by x-ray crystallography*
- ▲ *Explains chemical dynamics by photofragmentation translational spectroscopy*
- ▲ *Covers kinetic analysis by ultrafast absorption and emission spectroscopy*
- ▲ *Details syntheses of polycyclic caged amines, fuel additives, and polynitro compounds*
- ▲ *Examines computer-aided design of monopropellants*
- ▲ *Includes contributions by two Nobel laureates and five members of the National Academy of Sciences*

0-12-525440-7